Geochemistry and geochronology of the Shebandowan greenstone belt in the vicinity of the Moss Lake deposit, NW Ontario

Adrian Perez Avila

A thesis submitted in partial fulfillment of the requirements for the degree of Master of Science

Department of Geology, Lakehead University

Supervisor Dr. Peter Hollings.

Lakehead University.

Thunder Bay, ON

Abstract

This thesis presents a detailed investigation of the geology, geochemistry, and geochronology of the Archean Shebandowan Greenstone Belt (SGB) in the vicinity of the Moss Lake gold deposit in Northwestern Ontario. The Moss Lake property is located in the western part of the SGB and consists primarily of rocks belonging to the Greenwater and Burchell assemblages. The study characterizes the geological attributes, tectonic setting, and timing of magmatism within the belt and provides regional context for ongoing mineral exploration.

The research involved extensive fieldwork, including detailed lithological descriptions and structural analysis, supported by petrographic analysis of thin sections. Whole-rock geochemical analysis was performed on 56 samples to classify rock types, determine magmatic affinities, and evaluate element mobility, revealing distinct geochemical signatures between the Greenwater and Burchell assemblages and various intrusive bodies.

The Greenwater assemblage mafic rocks exhibit tholeiitic affinities with flat HREE, enriched LREE, and negative Nb anomalies. The Burchell assemblage mafic rocks are calc-alkaline, with moderately enriched LREE, flat HREE, and negative Nb-Ti anomalies. Similarly, the felsic and intermediate metavolcanic rocks show distinct geochemical signatures between assemblages. Greenwater rocks are more enriched in LREE and display stronger negative Ti anomalies compared to the less enriched LREE and weaker Ti anomalies observed in Burchell rocks.

U-Pb zircon geochronology on four key samples yielded new ages: 2716.0 ± 0.45 Ma for the Moss Lake syenogranite stock, 2718.34 ± 0.14 Ma for the Obadinaw quartz syenite stock, 2711.80 ± 0.14 Ma for an intermediate metavolcanic rock, and 2707.35 ± 0.14 Ma for the

Greenwater Lake quartz monzonite stock. These ages complement and refine the existing geochronological framework of the SGB.

Neodymium isotope analysis of thirteen samples provided insights into the mantle source and crustal contamination processes. The Greenwater assemblage exhibits consistently positive εNd(t) values in both mafic and felsic-intermediate rocks (+1.6 to +2.7), indicating a dominantly juvenile mantle source with limited crustal involvement. In contrast, the Burchell assemblage shows a broader εNd(t) range (+0.01 to +3.2), suggesting a more heterogeneous source and greater influence from crustal assimilation, despite an overall juvenile magmatic character.

The integration of geological, geochemical, and geochronological data supports models of a complex Neoarchean tectonic evolution involving distinct magmatic pulses and settings for the Greenwater and Burchell assemblages. Geochemical evidence suggested the Greenwater assemblage originated from an oceanic plateau evolving to a primitive arc, whereas the Burchell assemblage formed in a primitive arc environment. Intrusive bodies were classified as tonalite trondjhemite granodiorite, sanukitoids, and Archean hybrid granites, reflecting diverse sources and conditions of formation. The results confirm independent magmatic histories for the two assemblages and highlight a protracted crustal evolution involving juvenile mantle input and crustal assimilation.

Acknowledgments

First, thank God for opening paths and showing me solutions in difficult times. I would especially like to thank my supervisor and mentor, Dr. Peter Hollings, for believing in me, for allowing me to pursue a master's degree at my age and for providing me with the guidance and support necessary to complete it. Thanks to Dr. Tobias Stephan, for his advice, help, counselling, and discussions, which were essential for completing this work. The staff of the Department of Geology at Lakehead University are thanked for their support and assistance.

Thank you to all who supported this project, to Lakehead University, to an Alliance grant from the Natural Science and Engineering Research Council (NSERC), the Institute on Lake Superior Geology and a Mitacs internship. Thanks to Goldshore Resources, especially Michael Henrichsen, Peter Flindell and Jason Pattison and others for providing me with the help and support to complete this study.

Lastly, thank my family for their support and my dear Yamilet and Abraham for their strength and determination.

Table of Contents

List of Figures

List of Tables

1. Introduction

This project was developed in partnership with Goldshore Resources Inc. and Lakehead University and was funded by an NSERC Alliance Grant. The objective was to answer key scientific questions related to the tectonic setting of the Shebandowan greenstone belt to provide context for mineral exploration on the Moss Lake property.

The study area is located in the Shebandowan Greenstone Belt (SGB) of the Wawa-Abitibi terrane. The region consists of approximately 2.7 billion year old plutonic, volcanic, and sedimentary rocks that have undergone metamorphism from lower greenschist to lower amphibolite grade. The belt is bordered by the Quetico Subprovince to the north and the Northern Light-Perching Gull Lakes batholithic complex and Midcontinent Rift to the south. The Moss Lake property is located in the western part of the SGB and consists primarily of rocks of the Greenwater and Burchell assemblages. These rocks include felsic and intermediate volcanic units, thought to have formed in a shallow-water environment influenced by multiple volcanic centers (Osmani, 1997a), with mafic to intermediate intrusions present in the area. Finally, syn-tectonic to late tectonic intrusions, ranging from diorites to syenites, and quartz-feldspar porphyries, are generally present with a lower degree of deformation (Osmani, 1997a).

The Moss Lake deposit holds significant gold resources with a total Indicated Mineral Resource of 1,535 thousand ounces grading 1.23 grams per tonne gold (g/t Au), contained within 38.96 million tonnes and an Inferred Mineral Resource of 5,198 thousand ounces grading 1.11 grams per tonne gold (g/t Au), contained within 146.24 million tonnes (Richards, 2024). The gold

mineralization is hosted in sheared intermediate to felsic metavolcanic rocks, and sheared and fractured diorite, gabbro, or feldspar and quartz-feldspar porphyry bodies within the metavolcanic rocks. The mineralization consists of disseminated sulphides, quartz-albite veining, and alteration minerals like silica, albite, sericite, carbonates, pyrite, and minor chalcopyrite (Poirier et al., 2013).

Gold mineralization in the Moss Lake area was first identified in 1871, prompting a long history of exploration involving multiple companies and methods. Early work included trenching and drilling by the Mining Corporation of Canada, Lobanor Gold Mines, and Airways Exploration between the 1930s and 1950s. More intensive programs resumed in the 1970s with Falconbridge and Camflo Mines revisiting historic showings, followed by drilling and systematic exploration in the 1980s by Tandem Resources, Storimin JV, and others, including regional geophysical and geochemical surveys. Inco/Canico also conducted work at the nearby Span Lake prospect. Moss Lake Gold Mines Ltd. acquired the property in the late 1990s and undertook drilling between 2003 and 2014. In the mid-2010s, Wesdome consolidated ownership of the Moss Lake, Coldstream, and Hamlin blocks before transferring the project to Goldshore Resources.

Despite the extensive history of exploration, there is a limited amount of scholarly research aimed at comprehensively understanding stratigraphic relationships and geochemical evolution in the SGB. A comprehensive regional approach would allow for the identification of key geological features, improve the interpretation of geophysical and geochemical anomalies, and provide a framework for future exploration. Moreover, integrating this knowledge with surrounding areas could contribute to refining metallogenic models for the western area of the Shebandowan Greenstone Belt.

1.1 Location of the study area

The study area is located approximately 150 km west of the city of Thunder Bay. The main access is via Highway 11 to the community of Kashabowie. From here the study area is located approximately 8 km to the south (Fig. 1.1) and is accessible by several secondary roads, as well as a series of forestry roads that cross the area. The area selected for the present study was approximately 455 square kilometers, which includes the Moss Lake deposit.

Figure 1.1. Location of the study area in relation to Thunder Bay. In the figure, the red polygon corresponds to the study area around the Moss Lake deposit. From Google Earth (2024).

1.2 Objectives

The main objective of this thesis was to investigate the stratigraphic, geochemical, and geochronological relationships of the Shebandowan Greenstone Belt in the vicinity of the Moss

Lake deposit, northwestern Ontario. The objective was to establish the tectonic context and the chronology of nearby volcanism and plutonism, to contribute to regional metallogenic models.

To achieve this, specific objectives were: 1) Characterization of the host rocks to the mineralization in the Shebandowan greenstone belt by sampling representative units. 2) Investigate the geologic evolution of the study area utilizing petrology, whole rock geochemistry, and geochronology, to establish the timing and tectonic evolution of the study area. 3) Provide new insights into the tectonic evolution of the study area.

2. Regional Geology

2.1 The Superior Province

The Superior Province comprises about 70% of Ontario's Canadian Shield in the central region of the North American continent (Fig. 2.1). It is surrounded by Paleoproterozoic terranes to the west, north, and east, and by the Mesoproterozoic age Grenville Province to the southeast. The Superior Province was initially segmented into multiple sub-parallel belts known as subprovinces by Card and Ciesielski (1986). Over time, this conceptual framework has undergone several revisions based on new geological and geophysical data (Thurston et al., 1991; Percival et al., 2001; Stott et al., 2007). Recent iterations of this model replace the broad term "subprovince" with the more geologically precise "terrane," defined by Stott et al. (2007) as a tectonically bounded region with internal characteristics distinct from those in adjacent regions prior to Neoarchean assembly of the Superior Province. Terranes dominated by granite-greenstone, such as the Wawa-Abitibi and the Wabigoon, are interspersed with stretches of metasedimentary rocks, migmatites, and S-type granites like those found in the Quetico and English River basins (Williams, 1990).

The lithological diversity of the Superior Province reflects a variety of tectonic settings, including volcanic arcs, continental arcs, back-arc basins, ocean islands, and plateau environments (Thurston et al., 1991; Polat & Kerrich, 2001; Hollings et al., 1999; Whalen et al., 2002). TTG suites, komatiites, basalts, rhyolites, granites, and iron formations record the magmatic evolution of the province. Within volcano-plutonic terranes such as the Wawa-Abitibi, greenstone belts preserve lithostratigraphic associations representing both deep- and shallow-water environments, including komatiite-tholeiite sequences, bimodal successions, and Timiskaming-type fluvial and volcanic rocks (Thurston & Chivers, 1990; Thurston, 2015). These domains host most of the

province's Au, Cu, Zn, and Fe deposits (Card & Ciesielski, 1986). The tectonic assembly of the Superior Province is attributed to a series of accretionary events culminating in the ~2.7 Ga Kenoran Orogeny, subdivided into five orogenies—Northern Superior, Uchian, Central Superior, Shebandowanian, and Minnesotan (Percival et al., 2006).

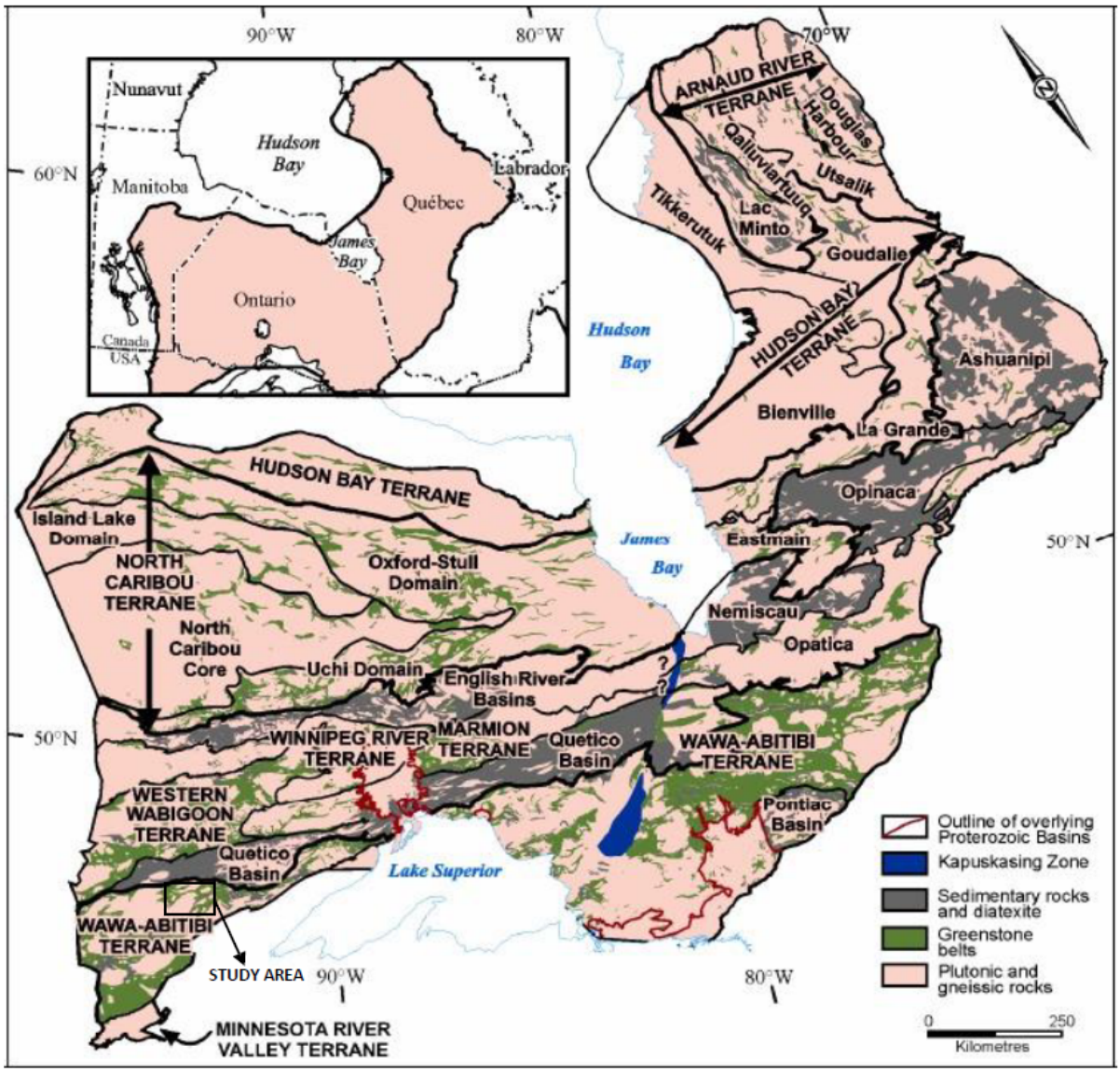

Figure 2.1. Terrane-scale geological map of the Superior Province showing the various terranes. The study area is shown by the black box in the western part of the Wawa-Abitibi terrane. Modified from Stott et al. (2010).

2.2 The Wawa-Abitibi terrane

The Wawa subprovince was initially included within the term "Wawa-Abitibi terrane" by Card and Ciesielski (1986) as part of their proposed subdivision of the Superior Province. This classification was based on cartographic, structural, lithological, metamorphic, geochronological, and geophysical studies (Douglas, 1973). However, this subdivision has recently been refined (Lodge, 2016; Nymoen et al., 2025). Lodge (2016) presented evidence for the contrasts between geodynamic settings and crustal architectures within the Wawa-Abitibi terrane and proposed an Archean microplate tectonic model characterized by complex plate interactions. More recently, Nymoen et al. (2025) provided a zircon U-Pb-Hf-O isotopic perspective for this terrane, concluding that while the Wawa and Abitibi share similarities in lithology, age range (~2.8–2.6 Ga) and geodynamic evolution, key differences include older 2.9 Ga crust, fewer documented volcanic events, and slightly different isotopic signatures in the Wawa subprovince. These differences indicate distinct geological histories, disqualifying them as a single tectonostratigraphic terrane by the formal definition. Therefore, the term "Wawa-Abitibi terrane" may no longer be appropriate (Nymoen et al., 2025; Lodge, 2016).

In the study area, the northern boundary of the western Wawa-Abitibi Terrane is marked by the Quetico Basin. Much of the southern limit is submerged under Lake Superior or concealed by Proterozoic supracrustal rocks of the Animikie Basin (Fig. 2.1). In the southwest, the Great Lakes Tectonic Zone delineates the boundary between the western Wawa-Abitibi Terrane and the Minnesota River Valley gneiss terrane.

The western Wawa-Abitibi Terrane consists of Archean greenstone belts and granitoid rocks. These greenstone belts contain metamorphosed komatiitic to tholeiitic basalt formations,

overlain by iron and magnesium-rich tholeiite, as well as submarine to subaerial calc-alkalic basalts and volcanic rocks ranging from felsic to intermediate compositions (Williams et al., 1991). These can be categorized into two primary concentrations: the first aligns with the northern boundary adjacent to the Quetico Basin, including the Shebandowan Greenstone belt, whereas the other is located in the south-central part of the subprovince near Wawa (Williams et al., 1991). Granitoid intrusions encircle the greenstone belts and additionally occur as intrusions within them. Williams et al. (1991) proposed that the tonalitic formations may exhibit synvolcanic characteristics in relation to the greenstone assemblages of the Wawa-Abitibi Terrane. Williams et al. (1991) observed that komatiites and their associated tholeiitic basalts are located at the basal levels of the volcanic sequences, with tholeiitic and calc-alkaline basalts, andesites, dacites, and rhyolites more frequently encountered at higher stratigraphic positions (Williams et al., 1991).

2.3 The Quetico basin

The Quetico basin is composed of a ~70km wide belt of metasedimentary rocks and migmatitic and anatectic derivatives (Fig. 2.1**)**. Typically, the boundaries of the Quetico basin are delineated by steeply inclined surfaces where there is often a marked contrast in rock composition (Williams et al., 1991). In the Shebandowan area, the boundary between the Wawa and Quetico has been interpreted as either an unconformity between northward-younging sedimentary rocks of the Quetico terrane and overlying volcanic rocks of the Wawa terrane or as a thrust fault along a lithologic contact (Williams et al., 1991**)**.

The Quetico basin primarily consists of metasedimentary rocks originally composed of wacke and siltstone as well as conglomerate and metasedimentary rocks of ultramafic composition.

Igneous formations consist of biotite-hornblende magnetite-bearing granitoid bodies (classified as I-type) with a mixture of mafic and felsic composition and minor associated ultramafic units (Williams et al., 1991). There are also metaluminous to peraluminous leucogranitoids containing one or two micas, some of which originated as metasedimentary material (Williams et al., 1991).

Geochronology of the Quetico subprovince has yielded Rb-Sr and K-Ar dates ranging in age from 2.4 to 2.6 Ga, reflecting regional cooling and metamorphism (Williams et al., 1991). Additionally, U-Pb data on zircons, monazite, and titanite are reported with ages related to igneous crystallization and metamorphic recrystallization (Lodge et al., 2013; Percival & Sullivan, 1988). Detrital zircons from metasedimentary rocks suggest sediment sources ranging in age from 2.698 Ga to >3 Ga (Percival & Sullivan, 1988). These data highlight the complex age relationships within the Quetico terrane and the varied provenance of its sedimentary rocks (Lodge et al., 2013; Williams et al., 1991).

2.4 The Shebandowan greenstone belt

The Shebandowan greenstone belt, ranging in age from 2.75 to 2.65 Ga, has been described as a juvenile island arc sequence formed through horizontal plate tectonics, with its southwards assembly driven by subduction-accretion processes (Stott et al., 2007). The location and boundaries of this greenstone belt have long been a matter of debate, with early models suggesting that it formed independently and then coalesced as allochthons through tectonic forces (Williams et al., 1991).

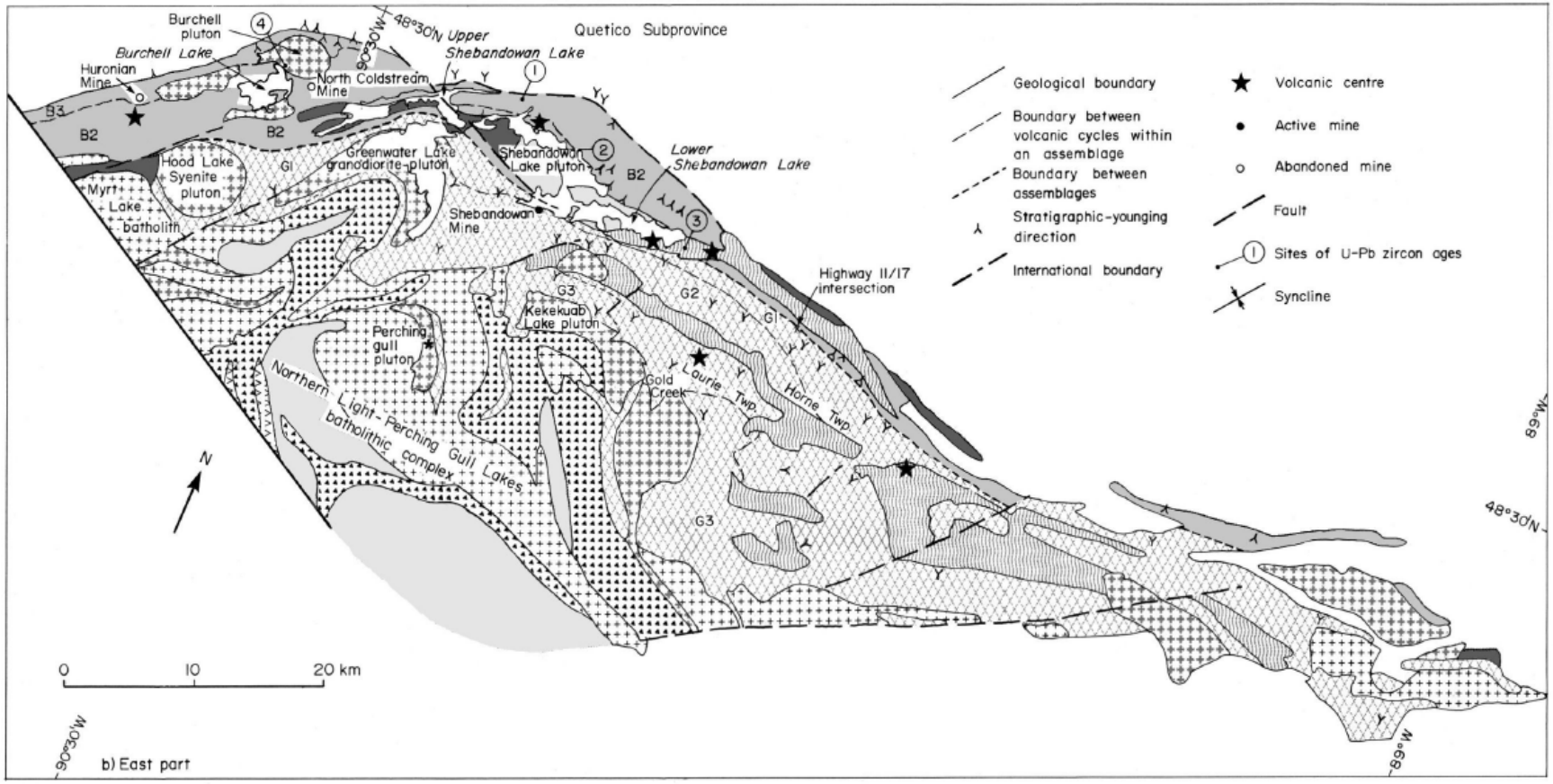

Figure.2.2. Supracrustal assemblages and younging directions of the Shebandowan greenstone belt. Younging directions are taken from Ontario Geological Survey maps and reports cited in the text and from Stott (1986) and Kehlenbeck (1988). Also shown are active and abandoned mines. U-Pb zircon age determinations from Corfu and Stott (1986) are numbered as follows: 1) porphyry sill, 2733± 3 Ma; 2) Shebandowan Lake pluton, 2696± 2 Ma; 3) latite volcanic breccia of the Shebandowan assemblage, 2689 Ma; and 4) posttectonic Burchell pluton 2684 Ma. From Williams et al, (1991).

The Shebandowan greenstone belt extends over about 170 km from Thunder Bay to Shebandowan (Fig. 2.2). Its structural geology reveals distinct episodes of deformation, where Williams et al. (1991) identified three assemblages: the older Greenwater and Burchell assemblages separated by the Knife Lake fault, consist of volcanic cycles generally comprising a sequence of tholeiitic basalt flows, succeeded by a sequence of calc-alkaline andesite, dacite, and rhyolite. The third, younger package is the Shebandowan assemblage, which overlies the two older ones and consists of volcanic and sedimentary rocks (Williams et al., 1991).

Corfu and Stott (1998), through studies of U/Pb geochronology, reevaluated the Shebandowan greenstone belt, leading to the reclassification of the assemblages into three new subdivisions. The first subdivision combines the Burchell and Greenwater assemblages due to their age of 2720 Ma and consistent younging directions. Composed mainly of volcanic cycles, including tholeiitic basalt and an upper sequence of calc-alkaline intermediate to felsic volcanic rocks (Corfu and Stott,1998). The northern part of the Burchell assemblage is further divided into the Kashabowie assemblage with ages of 2695 Ma (Corfu and Stott,1998), which includes 'Timiskaming-type' rocks initially described by Williams et al. (1991) in the overlying Shebandowan assemblage. The third, youngest subdivision was a small sedimentary basin in the northeastern region named the Auto Road assemblage. Lodge (2016) conducted a study of the volcanic assemblages of the Shebandowan Greenstone Belt. In this study, Lodge (2016) reported the presence of komatiites and ultramafic intrusions that are structurally separated from the predominantly intermediate strata, with no clear stratigraphic continuity. He supported his geochemical model with U-Pb zircon ages and isotopic data to conclude that the Shebandowan Greenstone Belt is best subdivided into the Burchell and Greenwater assemblages, as initially proposed by Williams et al. (1991), rather than grouping them into a single unit.

Williams et al. (1991) identified three distinct deformational episodes in the Shebandowan greenstone belt. The D_1 deformation is observable across much of the belt marked by a lineation that plunges towards the west and vertically oriented schistosity that dips to the north (Williams et al., 1991). The subsequent D_2 deformation overlaps with the D_1 deformation. The D_2 deformation also led to the formation of brittle-ductile shear zones, believed to be associated with gold mineralization in the region (Fig. 2.3; Williams et al., 1991). The D3 deformation event produced steeply plunging kink folds, primarily observed in the northern part of the belt (Williams et al., 1991).

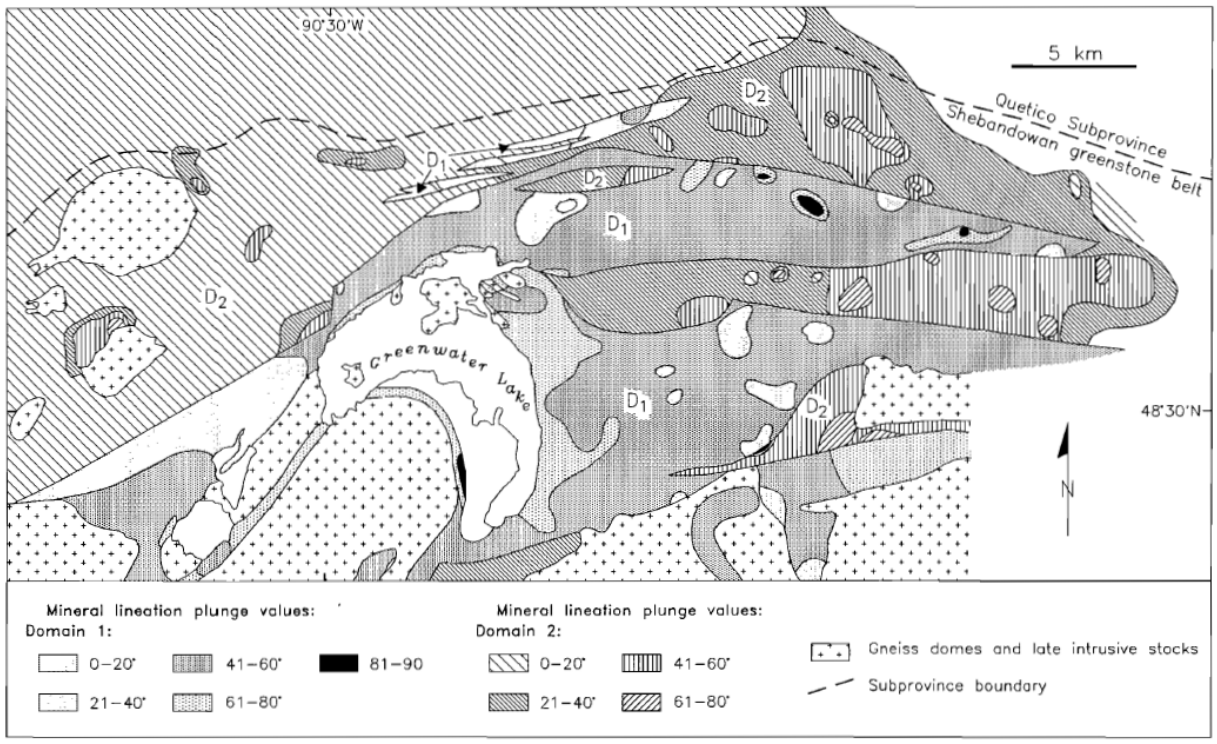

Figure 2.3. Structural domains D_1 and D_2 in the western part of the Shebandowan greenstone belt, characterized by contrasts in plunge directions of mineral and shape lineations. Contoured values of plunges of stretching lineations show lineations plunge westward in D_1 domains and eastward in D_2 domains. The shallowest plunge values occur in the northwestern part of the belt and into the Quetico Subprovince. From Beakhouse et al. (1996).

Corfu and Stott (1986) identified two principal deformation events in the Shebandowan greenstone belt. The D_1 deformation event is seen across the belt with vertical schistosity, west-southwest plunging lineations and upright folds (Corfu and Stott., 1998). The second event, D_2 deformation, only affected the northern section of the belt and extends into the Quetico Subprovince (Corfu and Stott.,1998). This last deformation was likely influenced by significant oblique, subhorizontal compression along a northwest-southeast axis, possibly linked to the closure of the Quetico sedimentary basin (Corfu and Stott., 1998; Lodge, 2016). Metamorphic grades vary across the belt ranging from greenschist to lower amphibolite with greenschist grade rocks prevalent throughout the belt, whereas higher amphibolite grades are only observed near late, post-tectonic felsic intrusions (William et al., 1991).

2.4 Moss Lake property

The Moss Lake property is situated in the western portion of the Shebandowan Greenstone Belt and is largely underlain by rocks of the Burchell and Greenwater assemblages. Geologically, the area is bounded by two major northeast-trending regional fault zones: the Snodgrass Lake Fault (also known as the Wawiag Fault Zone) and the Knife Lake Fault, which delineate key lithotectonic domains (Fig. 2.4; Osmani, 1997; Poirier et al., 2013). The Knife Lake Fault, mapped over a 60 km strike length, separates felsic metavolcanic rocks to the northwest from mafic metavolcanic units to the south, while the Snodgrass Lake Fault transects the principal target area of exploration (Osmani, 1997).

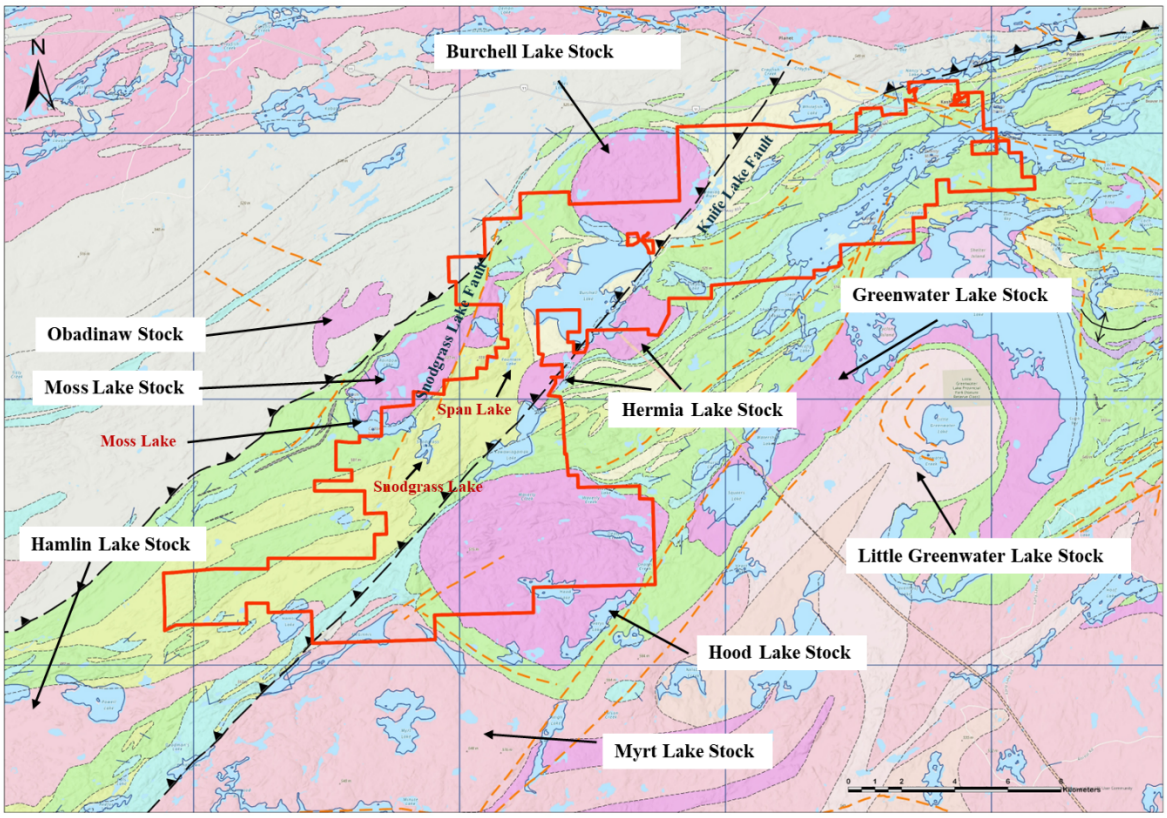

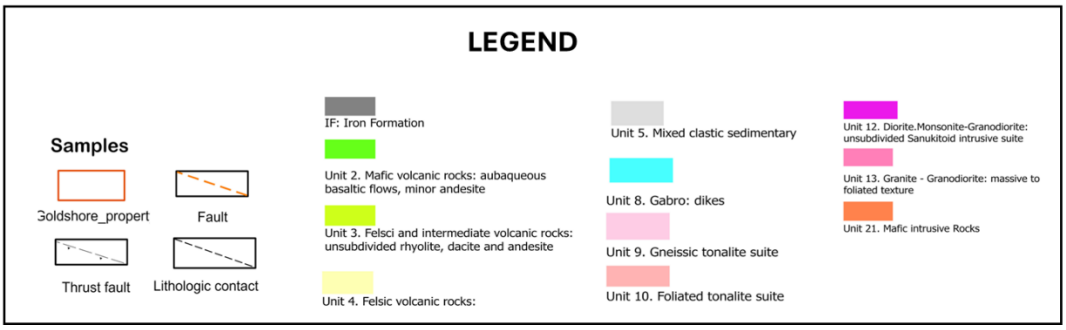

Figure 2.4. Areas of interest in the geological map of the Moss Lake property with the most relevant locations, detail of the geology of the Moss Lake deposit. Modified from Hunt. (2010), Osmani (1997) Osmani (1997) Poirier et al. (2013) and Santaguida (2001).

The lithological setting is dominated by andesitic to dacitic-rhyolitic volcanic rocks, lapilli tuffs, fragmental units, and localized chemical sediments such as iron formation. These units are intruded by lenticular diorite to gabbro sills and narrower, elongated intrusions of syenite, as well

as intermediate to felsic feldspar and quartz-feldspar porphyries. To the northwest and southeast, the property is flanked by syenitic intrusions, namely the Moss Lake Stock and the Hood Lake Stock (Fig. 2.4; Osmani, 1997). In the central region of the property, the dominant rock types include aphanitic to fine-grained massive or porphyritic felsic metavolcanic flows and autoclastic breccias containing plagioclase and quartz phenocrysts (Osmani, 1997; Poirier et al., 2013). Pyroclastic rocks such as tuffs, pyroclastic breccias, and lapilli tuffs are well developed in areas east-southeast of Pearce Lake, west-southwest of Fountain Lake, and in the vicinity of Snodgrass Lake. This package is bounded to the north and south by the Snodgrass Lake and Burchell Lake faults, respectively (Fig. 2.4; Osmani, 1997; Poirier et al., 2013).

The structural framework of the property is defined by foliation, shearing, and faulting oriented northeast, subparallel to the regional stratigraphy. These structures exhibit steep to vertical dips and locally define small-scale folds. Additionally, subhorizontal lineations dipping southwest (10–30°) have been recorded on the edges of outcrops (Hunt, 2000). Numerous schistose zones and minor faults aligned with the regional trend exhibit evidence of both brittle and ductile deformation, accompanied by intense hydrothermal alteration (Hunt, 2010; Poirier et al., 2013). Alteration assemblages include silicification, carbonatization (calcite and ankerite), chloritization, hematization, sericitization, albitization, sulphidation (pyrite), and potassic alteration, all of which are commonly observed in outcrop and drill core (Hunt, 2010; Poirier et al., 2013).

Gold mineralization at the Moss Lake deposit is hosted by sheared intermediate to felsic metavolcanic rocks and by sheared and fractured intrusive bodies, including diorite to gabbro and feldspar to quartz-feldspar porphyries emplaced within the volcanic sequence (Hunt, 2010; Poirier et al., 2013). Additional anomalous gold values have been reported from fractured diorite, sheared

feldspar porphyry, and a moderately deformed, pink-weathering quartz-amphibole-phyric intrusion. The latter closely resembles syenogranitic rocks of the Moss Lake Stock in hand sample, suggesting a possible genetic link (Poirier et al., 2013). Similar lithologic assemblages, structural patterns, and alteration styles associated with gold mineralization are also observed in the northeastern extensions of the Moss Lake deposit (Poirier et al., 2013).

3. Methods

3.1 Field campaign and sample collection

The initial field campaign, conducted in October 2022, focused on sampling and structural assessment across a designated area of approximately 455 square kilometres. A total of 96 samples were collected during this phase. A second campaign was carried out in June 2023 to target areas where data gaps had been identified during the initial campaign, resulting in the collection of an additional 45 samples. Field data was collected, using an iPad with Strabo Spot software (Walker et al., 2019). Sample descriptions followed a systematic approach, starting with an analysis of the geomorphology, followed by a detailed examination of outcrops, and concluding with sampling. The outcrop analysis involved documenting lithological details (rock type, texture, shape, composition, colour, thickness, etc.), capturing structural data, such as faults and folds, taking photographs, and collecting samples.

3.2 Petrography

Thirty-nine samples were selected for petrographic analysis with thin sections prepared at the Lakehead University lapidary facility. Thin sections were analyzed using an Olympus BX51 microscope for transmitted and reflected light minerals. For the photographs, a Zeiss Axioscope 7 microscope was used, which allows high-quality photographs and has motorized components that allow the taking of composite photographs. The description of the sections included textural associations and compositional classification in terms of modal mineralogy. For the classification of igneous rocks, the Le Maitre (1989) system was used. Streckeisen (1976) was used as a

reference for intrusive rocks, Streckeisen (1978) for volcanic rocks and Schmid (1981) for volcano-sedimentary rocks.

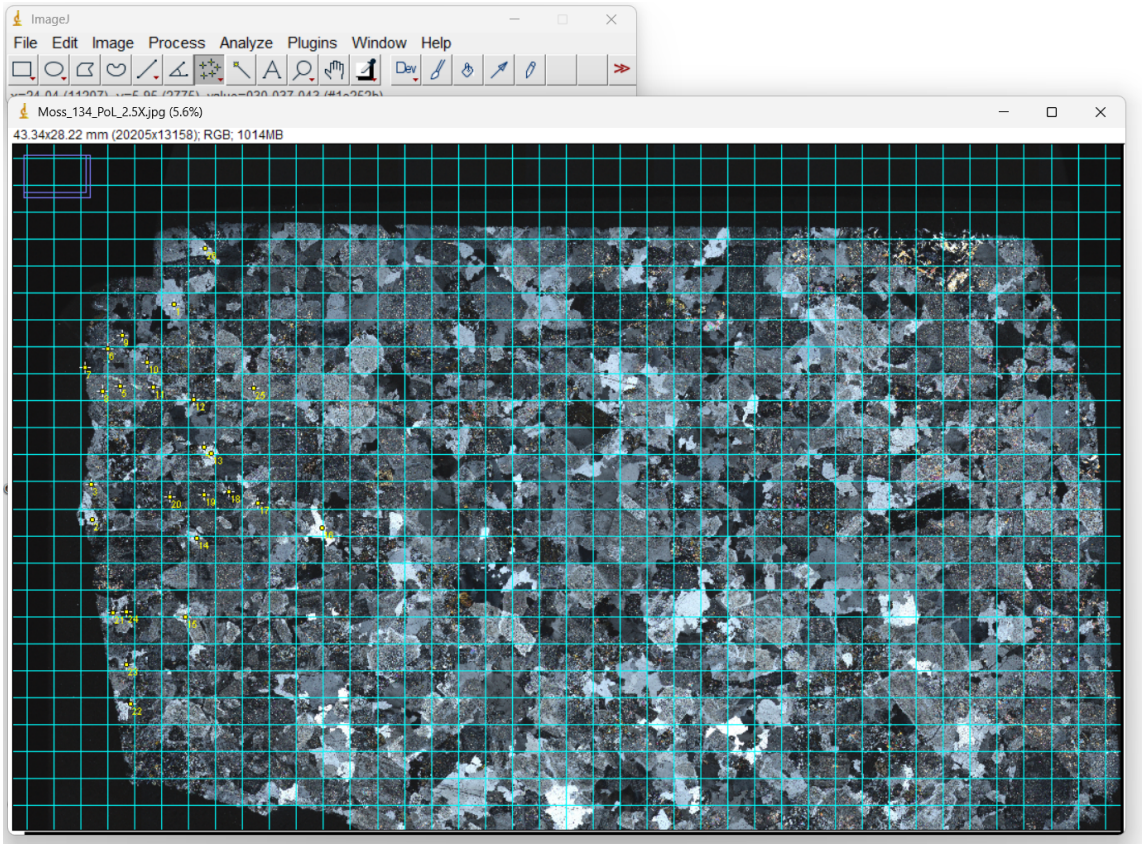

Figure 3.1. Digital image analysis of the thin section of Moss-134, in a photograph taken with a 2.5 X lens, resolution 300 dpi. The photograph shows the blue grid of 1 mm by 1 mm and the yellow points of the plagioclase count.

Quantitative analyses were performed using digital image analysis to determine the size and shape of the crystals (textural classification). For these determinations, photographs taken with a Zeiss Axioscope 7 microscope were used, with a resolution of 300 dpi and a clearly defined photographic scale. The digital image analyses were performed using the ImageJ image processing program (Rasband, 2024). The methodology for each thin section consisted of calibrating the

image scale, determining the grids to count the crystals, and performing modal counts of the crystals according to the population and the type of specimens identified. The crystals were then measured, and their shapes were determined (Fig. 3.1). Finally, a textural classification was carried out with the information obtained, presented in the petrographic descriptions of each thin section.

3.3 Whole rock geochemistry

Fifty-seven samples were selected for whole-rock geochemistry. These were analyzed by ALS Laboratory Group in Thunder Bay using commercial packages including CCP-PKG01, ME-MS42, QA-GRA05, TOT-ICP06, ME-4ACD81, ME-ICP06, C-IR07, S-IR08 and ME-MS8 (ALS, 2023) table 1.

Table 3.1. Techniques used in the analytical determination of rock samples from this thesis.

Method ALS	**Element analytes**	**Description preparation and technique.**
ME-ICP06	SiO_2; Al_2O_3; Fe_2O_3; CaO; MgO; Na_2O; K_2O; Cr_2O_3; TiO_2; MnO; P_2O_5; SrO, and BaO	Fusion decomposition followed by ICP-AES measurement
OA-GRA05	LOI	Loss on Ignition at 1000ºC after the sample is pre-dried at 105ºC.
C-IR07	C (Total)	Total carbon by induction furnace/IR.
S-IR08	S (Total)	Total sulfur by induction furnace/IR.
ME-MS81	Ba, Ce, Cr, Cs, Dy, Er, Eu, Ga, Gd, Ge, Hf, Ho, La, Lu, Nb, Nd, Pr, Rb, Sm, Sn, Sr, Ta, Tb, Th, Tm, U, V, W, Y, Yb, and Zr	Lithium borate fusion before acid dissolution followed by ICP-AES measurement
ME-MS42	As, Bi, Hg, In, Re, Sb, Se, Te, and Tl	Aqua regia digestion followed by ICP-MS measurement
ME-4ACD81	Ag, Cd, Co, Cu, Li, Mo, Ni, Pb, Sc, and Zn	Four acid digestion followed by ICP-MS measurement
Au-AA25	Au	Fire assay followed by AAS measurement

These packages include a comprehensive analysis of complete rock samples under various analytical techniques, including Plasma Mass Spectrometry (ICP-MS), Atomic Emission Spectrometry (ICP-AES), the total sulphur and carbon content were determined by infrared spectroscopy (IR), with Atomic Absorption Spectroscopy (AAS) used for the gold content. The digestion media were the most appropriate, including aqua regia for volatile trace elements and major elements, four acids for base metals, and lithium borate fusion for trace elements (ALS, 2023).

3.2.1. Analytical quality control

Analytical quality control of the geochemical data included the evaluation of the precision factors using duplicates, accuracy using certified reference materials, and the level of contamination that some samples could present in their analysis process using blanks.

Precision is used to quantify the random errors that affect analytical measurements. This allows the evaluation of the repeatability and reproducibility of the analytical data obtained. A graph of relative error of less than or equal to 20% was used to evaluate precision. Pairs (duplicate-original) that present a value higher than the established control limit are considered failures. The percentage of failures allowed corresponds to 10% of the total pairs.

Four pairs of duplicates were used for the analysis of duplicates, representing 7% of the data set. For all the variables presented, the duplicates have a relative error less than or equal to 20%, except for some Th pairs (Fig. 3.2), which show a relative error of 22%. Figure 3.2 presents the elements with the highest relative values; the graphs of the other elements are not included since they do not have significant relative error values.

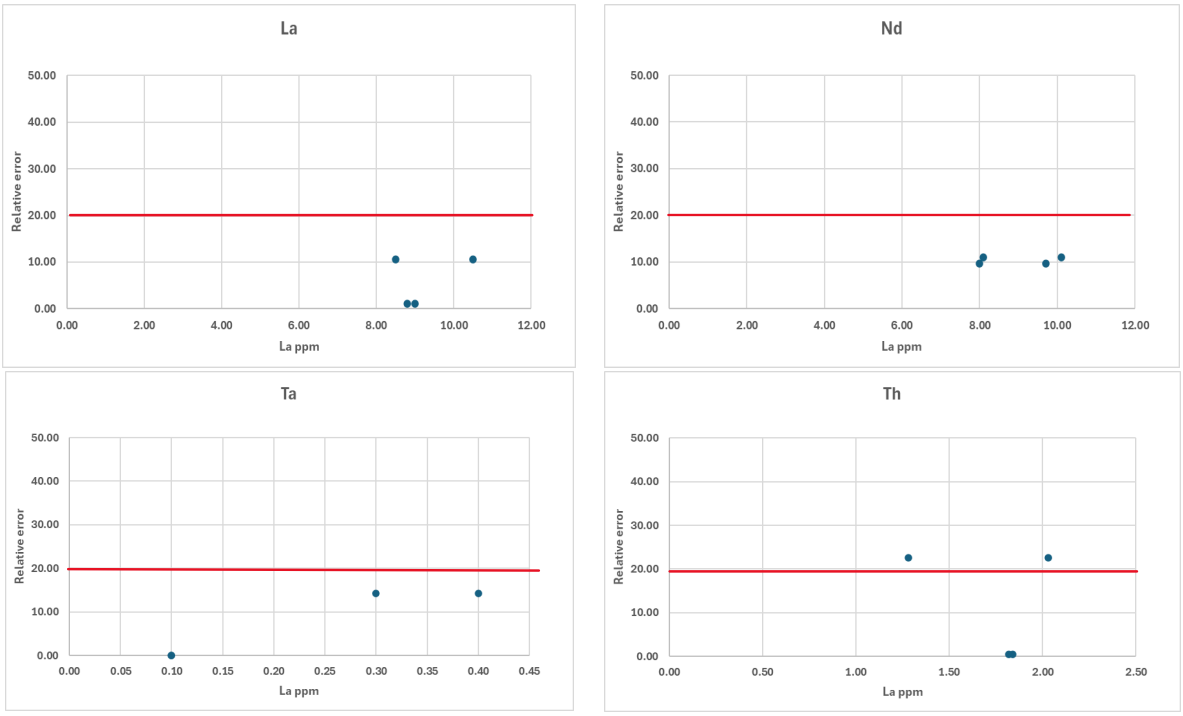

Figure 3.2. Accuracy evaluation graphs using % Relative error for La, Nd, Ta, and Th in rock samples. The red line indicates a relative error of 20%.

Contamination involves the inadvertent transfer of material from a sample or the environment to another sample. It can occur during any stage of the preparation, analysis or, in general, during the sample handling process (Méndez, 2011). For the evaluation of contamination, control charts for preparation blanks were used; the control limit used was three times the Detection Limits (DL) according to each analytical technique. Values higher than the established control limit (·3 DL) are failures; when the number of failures is higher than 4% of the total samples, it is considered that a significant level of contamination of an element has occurred. Nine blank samples were used to analyze contamination, representing 15 % of the data set. According to the control charts made with the preparation blanks, it was observed that no blank exceeded the acceptance (4%) /rejection level corresponding to 3DL. Figure 3.3 presents the elements with the highest relative values. The graphs of the other elements are not included since they do not have

significant relative error values. Figure 3.3 presents the elements with the highest contamination values.

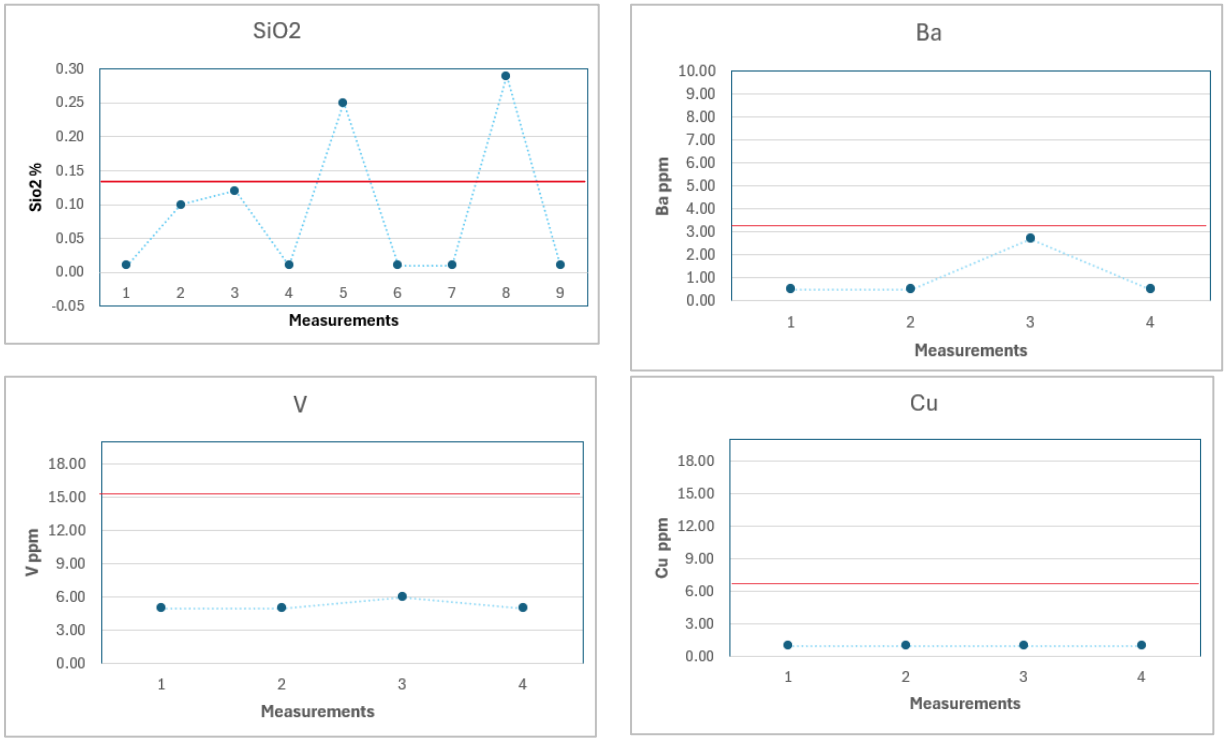

Figure 3.3. Control charts for evaluating blanks in rock samples for SiO_2, Ba, V and Cu. The red line corresponds to the 3-detection limit LD and is the criterion for rejecting or accepting the blank.

Accuracy is understood as the degree of agreement between the result of a test and the accepted reference value of an analyte (Miller & Miller, 2002), allows us to evaluate the certainty in analytical determinations, using certified reference materials and contrasting their recommended values against the results obtained by applying analytical methodologies, while allowing the assessment of the error in the measurements, covering the present systematic and random errors inherent to the applied method. Accuracy assessment was performed using certified CRM reference materials used by the laboratory.

The data obtained were plotted with the upper and lower control limits represented by red lines, and the data are plotted as black dots. Those samples outside the established control limits are considered erroneous.

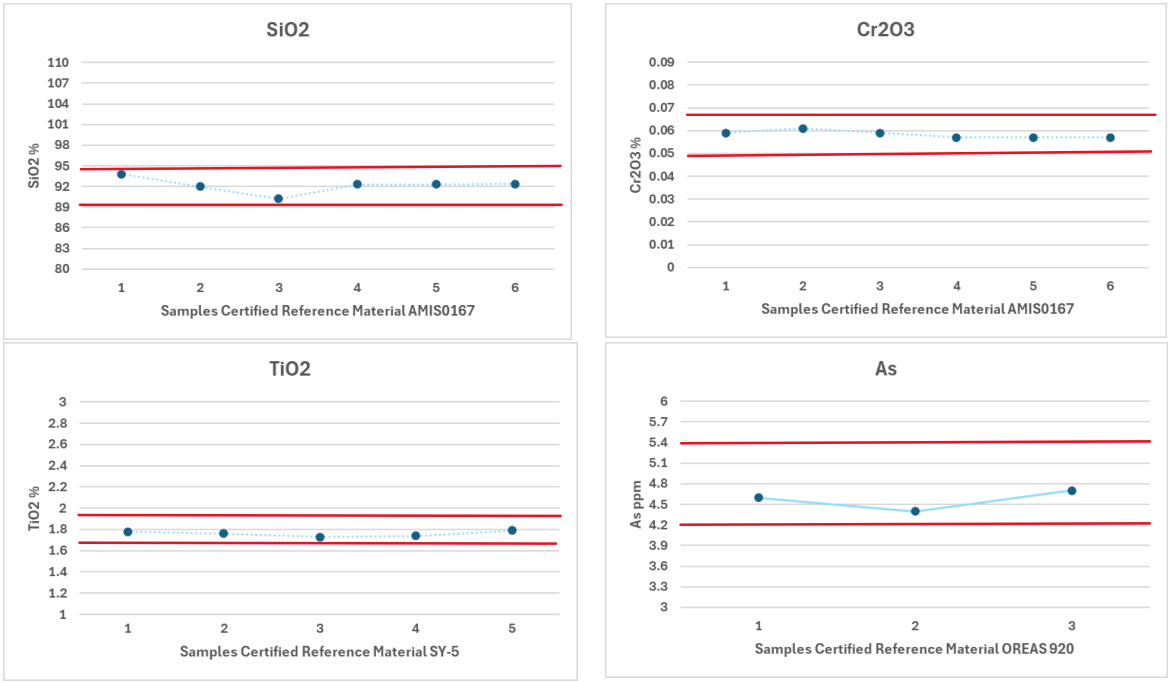

Figure 3.4. Control charts for evaluating certified material for SiO_2 (AMIS0167), Cr_2O3 (AMIS0167), TiO_2 (SY-5) and as (OREAS920). The red line corresponds to upper and lower control limits.

The ALS laboratory used sixteen reference materials, which considered the elements analyzed, the digestion, and the instrumental technique. Some reference materials were used for different analytical methods, so graphs were made to examine element by element according to each reference material. The upper and lower limits were taken from the analysis certificates of each reference material, as well as the recommended concentrations. In general terms, the control graphs show symmetrical data dispersion patterns and optimal precision; no CRM presented values outside the control limits (Fig. 3.4).

3.3 Scanning Electron Microscope/ Energy Dispersive Spectrometer (SEM/EDXA)

The Scanning Electron Microscope/Energy Dispersive Spectrometer (SEM/EDXA) facility at Lakehead University was used to measure the elemental composition of some minerals. This Scanning Electron Microscope (SEM) equipment has a Hitachi Su-70 Schottky Field Emission with an X-Ray spectroscopy (EDXA) Oxford Aztec 80mm/124ev, which enables a resolution of 1.0nm @15kv/ 1.5 nm at 1kv with a working distance of 15mm. At the beginning of each analysis session, standards were calibrated according to the type of mineral to be identified, and results were compared to ensure accuracy within 5% of the total value of the mineral.

3.4 Neodymium Isotopes

Neodymium isotope analyses were conducted on thirteen samples. These samples were selected using rare-earth element patterns normalized to primitive mantle, which revealed distinct trends across different lithologies. Additionally, it was considered that the selected samples covered the study area well.

The samples were prepared at the Isotope Geochronology and Geochemistry Research Centre (IGGRC) at Carleton University (Carleton University, 2025). Rock powders underwent doping with a mixed spike of ^{148}Nd-^{149}Sm before their dissolution in a solvent comprising concentrated HF and HNO_3. The resultant sample solutions were subsequently evaporated to dryness, and the resultant residues were systematically dissolved in 7M HNO_3 followed by 6M HCl, ultimately being dried to a completely dry state. The residues derived from the samples were then dissolved in 1.5 ml of 2.5 M HCl and subjected to loading onto 14-ml Bio-Rad borosilicate glass chromatography columns containing 3.0 ml of Bio-Rad AG50W-X8 cation exchange resin.

Neodymium (Nd) was eluted using 0.26M HCl, followed by samarium (Sm) elution using 0.5M HCl. The neodymium isotope ratios were determined using the Thermo-Finnigan Neptune MC-ICP-MS at IGGRC. The Nd ratios were normalized to $^{146}Nd/^{144}Nd = 0.7219$. To correct instrumental drift, $^{143}Nd/^{144}Nd$ values were adjusted using bracketed JNdi-1 standards, referenced against an average JNdi-1 value of 0.512100 measured on IGGRC's Thermo-Finnigan Triton TIMS. The average values of standard reference materials over ten months for this analysis are JNdi-1 $^{143}Nd/^{144}Nd = 0.512096 \pm 0.000013$ (2SD, n=104), along with total procedure blanks for Nd <50 pg.

3.5 Geochronology

Eleven samples were submitted for geochronology analysis to the Pacific Center for Isotopic and Geochemical Research of the University of British Columbia (PCIGR, 2023). The methodology applied was that of Mattinson (2005) that was adapted for the Pacific Centre for Isotopic and Geochemical Research (PCIGR) at the University of British Columbia (PCIGR, 2023).

For zircon extraction, the zircons were separated using a Wilfley wet vibrating table with a precision machined Plexiglas surface (PCIGR, 2023). Sequentially, conventional magnetic and heavy liquid separation techniques were implemented using a Frantz magnetic separator, after which the zircon particles were meticulously selected by visual inspection with a binocular microscope (PCIGR, 2023). The extracted zircons were mixed with hydrofluoric acid and nitric acid in a ratio of 10:1 into the liner, which was subsequently positioned within the jacket (Scoates and Scoates, 2013), sealed, and subjected to a temperature of 240°C for a duration of 40 hours to

achieve complete dissolution. The resultant solutions were then evaporated on a hot plate maintained at 130°C. The fluorides were subsequently solubilized in 3.1 N hydrochloric acid (HCl) within a high-pressure apparatus for a period of 12 hours at 210°C (Scoates and Scoates, 2013).

The methodologies for the separation and purification of lead (Pb) and uranium (U) utilized ion exchange column techniques that were slightly modified from the procedures delineated by Parrish et al. (1987), wherein Pb and U were eluted sequentially into a singular receptacle (Scoates and Scoates, 2013).

Zircons were analyzed using chemical abrasion thermal ionization mass spectrometry using a VG354S or VG54R thermal ionization mass spectrometer (TIMS) instrument, which employs an EARTHTIME ET535 tracer or a UBC ^{205}Pb-$^{233\text{-}235}$U isotope tracer (PCIGR, 2023). The concordia diagrams were constructed with the IsoplotR software (Ludwig. 2003) from the ^{206}Pb/^{238}U and ^{207}Pb/^{235}U data provided by the laboratory.

4. Results

4.1 Fieldwork and petrography

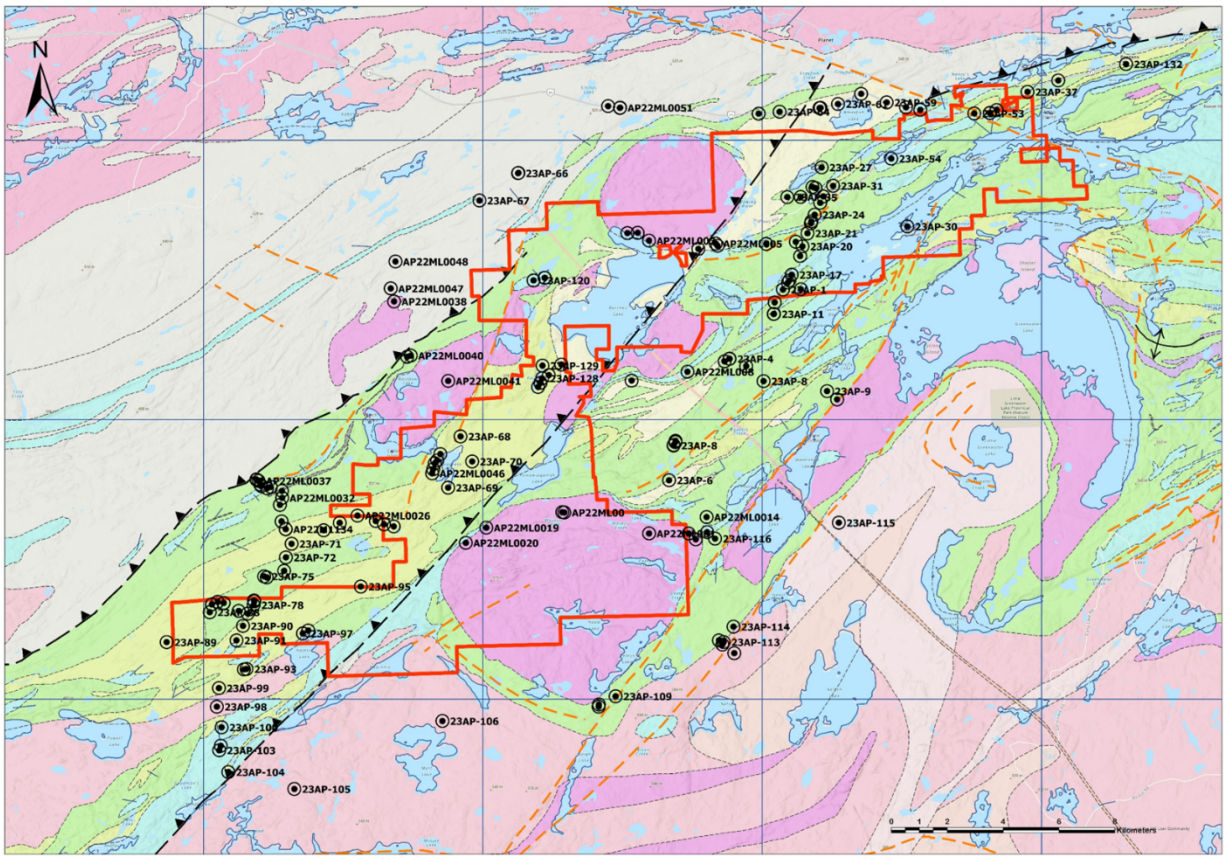

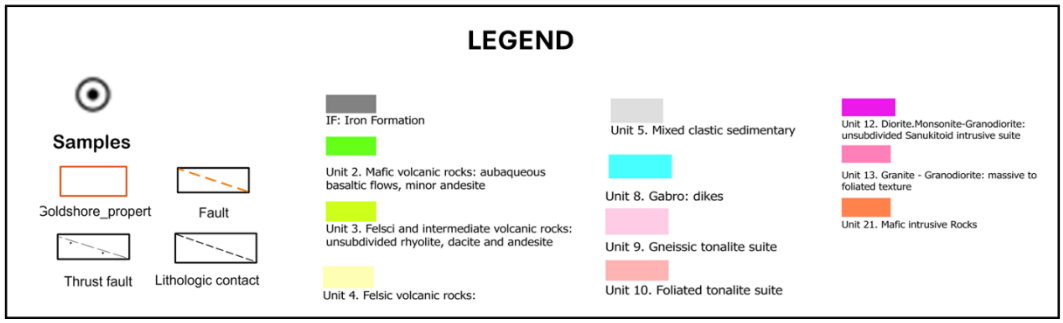

Figure 4.1. Spot location map. A black icon represents the spots. See appendix E for a higher resolution version of this figure.

This section presents the lithological descriptions of the rocks observed in the field. The fieldwork was conducted during the summers of 2022 and 2023, with 177 control points (Appendix F) taken (Fig. 4.1). Field observations are supported by petrographic descriptions of 40 polished thin-section samples (Appendix A).

The geological observations are categorized according to the rock group and were not differentiated by assemblage (Williams et al., 1991), as this will be addressed in the discussion. All samples exhibit a certain degree of metamorphism, nonetheless, protolith rock names were used throughout the fieldwork and petrographic analysis for better discrimination, with the prefix "meta" dropped. In some cases, the rocks had undergone more intense metamorphism, thereby warranting the use of metamorphic nomenclature.

4.1.1 Mafic metavolcanic rock

This type of rock is the most abundant and is distributed throughout the study area. They generally occur in elongated bodies with a predominantly NE direction (Fig. 2.4).

Contacts with other units were rarely exposed but were seen in some outcrops (Fig. 4.2). The outcrops are characterized by vertical fractures predominantly oriented towards the northeast, which align with the prevailing regional deformation. The rocks are fine to medium-grained, dark green to black on fresh surfaces, and commonly weather to a lighter greenish tone. The rocks comprise fine-grained dark green to black basalts, exhibiting aphanitic to porphyritic textures. Generally, chlorite and epidote are present, implying a low-grade metamorphic history, a green hue, and subtle schistosity. Well-preserved pillow structures were observed at some locations, suggesting subaqueous emplacement (Fig. 4.3).

Outcrops of pillow lava were also observed in this unit, located in the northeastern part of the work area (Moss 108). The pillow lavas are well preserved and show the classic pillow structures. The pillows vary from 30 to 60 cm in diameter with a dark green to black rim and a fine-grained crystalline interior (Fig. 4.3). The cooling margins are approximately 3 cm thick, consistent with rapid cooling during submarine extrusion, with radial and concentric cooling fractures filled with carbonate. The pillows are elongated along a NE-SW axis, with way-up indicators such as bulbous tops, and flattened bases indicating that the stratigraphic top is to the west or NW (Fig. 4.3).

Figure 4.2. Outcrop 23AP-MOSS111. The photograph shows rocks belonging to the mafic metavolcanic unit in contact with the Hamlin Lake stock.

Figure 4.3. Outcrop 23AP-MOSS034. The photograph shows the pillow lavas, note the cooling margins and the radial cooling fractures.

Petrographically, the rocks are composed of orthoclase phenocrysts (5 - 10%) with skeletonized textures 0.65 – 2.5 mm in size and altered to carbonates (10%). Tabular biotite (10 - 15%) with 0.6 – 1 mm in size and epidote (1%). The dark groundmass (60%) is generally altered to sericite (5%) and tremolite actinolite crystals (8%); opaque minerals (2%), mainly pyrite, were observed (Fig. 4.4).

Petrographically, the pillow lava was classified as a chlorite-altered basalt. It has a relict, microcrystalline aphanitic, holocrystalline aphyric texture (Fig. 4.5). It is composed of subhedral quartz (7%) with particle sizes of 0.08 mm, plagioclase (80%) with subhedral to anhedral shapes less than 0.006 mm, and pyroxenes (10%) that are tabular and less than 0.003 mm. Other minerals produced by alteration include actinolite-tremolite (2-4%) and chlorite (1-2%) with particles less than 0.004 mm. Additionally, amygdaloid structures with microfractures were observed (Fig. 4.6).

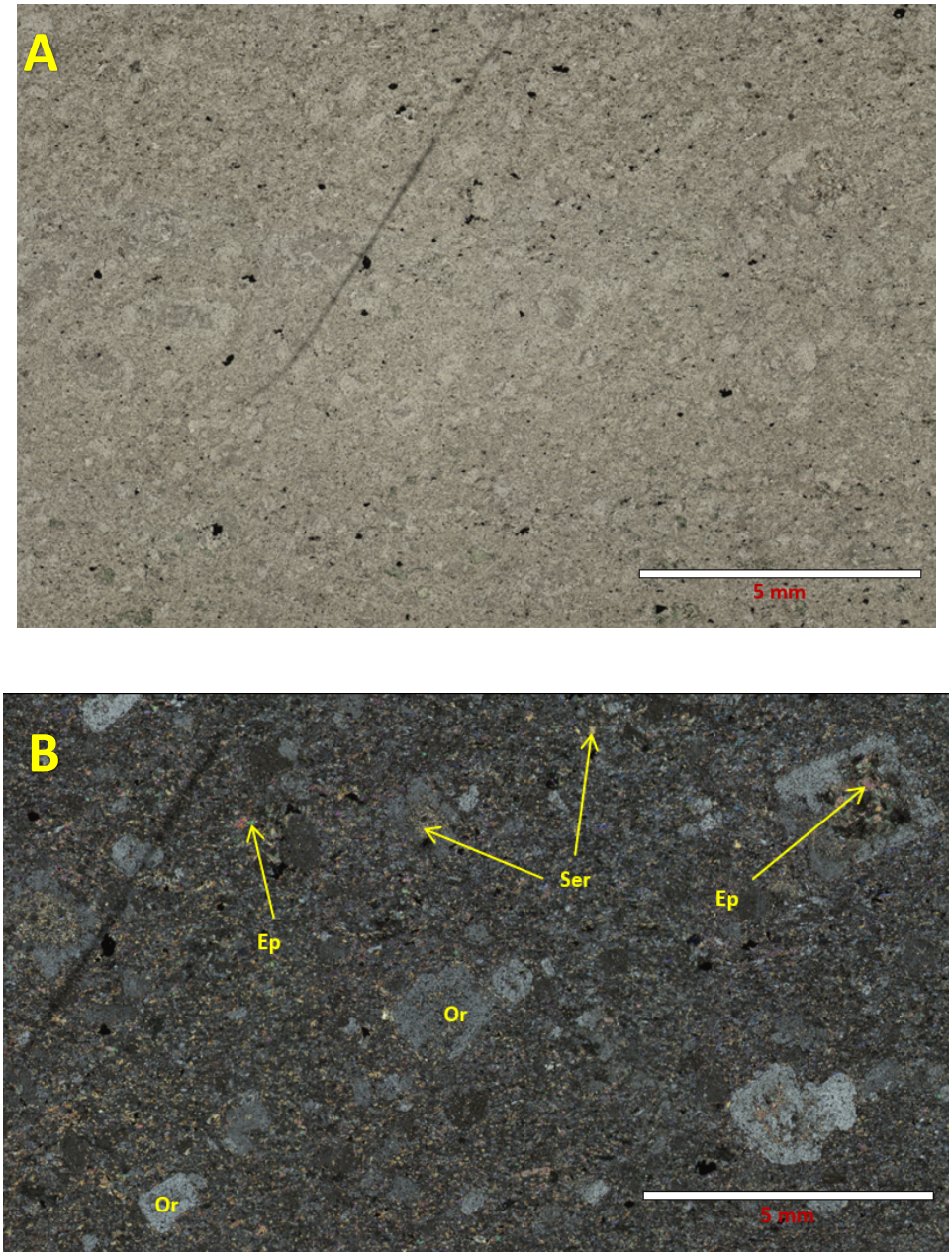

Figure 4.4. Photomicrograph of sample MOSS 107. A. Image in cross-polarized light (XPL). B. Image in Cross-Nicols (NX) showing tabular crystals classified as orthoclase (Or) altered to sericite (Ser) and epidote (Ep). The groundmass is aphanitic and altered to sericite and epidote.

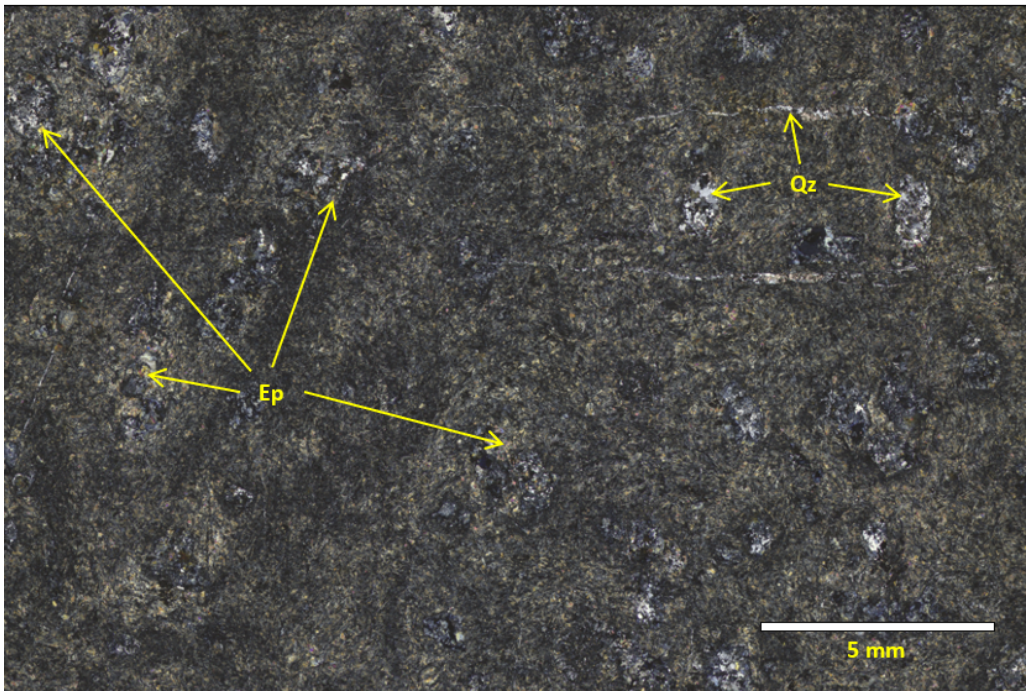

Figure 4.5 Photomicrograph of sample MOSS 108. Cross-Nicols (NX) image showing alteration to epidote (Ep) as well as filling of vesicles and microfractures with quartz (Qz).

Figure 4.6. Photomicrograph of sample MOSS 108. Details in XPL (Scale 500 µm) of a large amygdule composed of quartz (Qz) can be seen in the micro fractures of carbonates.

4.1.2 Felsic and intermediate metavolcanic rocks

This unit was observed at forty-six control points (Fig. 2.4). The best-exposed regions are found in the Snodgrass and Fountain Lakes areas. The unit is bound by fault contacts with the Knife Lake fault to the east and to the west by the Snodgrass Lake fault (Fig. 2.4).

Figure 4.7. Outcrop 23AP-MOSS096. The photograph shows the interdigitated contact between rhyolites and pyroclastic flows.

The felsic to intermediate metavolcanic rocks are fine- to medium-grained and range in colour from light grey to pink on fresh surfaces, typically weathering to pale grey. The different lithologies observed in the unit are usually interbedded, and the differentiation between lithologies is challenging; they exhibit a variety of volcanic textures, including massive, flow-banded, and locally fragmental features indicative of pyroclastic activity. Aphanitic to weakly porphyritic

textures are common, suggesting a volcanic origin. These rocks have been metamorphosed under greenschist facies conditions, as shown by widespread sericite, chlorite, epidote, and secondary quartz replacing the primary groundmass. Despite the metamorphism, primary volcanic textures, such as welded tuff structures, are locally preserved, as well as rhyolite flows (Fig. 4.7). Foliation is variably developed. Generally, it aligns in a northeast direction, often marking zones of increased strain and development of joint zones.

Basaltic andesites

This rock type was only identified in one greenish-black outcrop ~50 × 50 cm (Moss 57) in the southern part of Snodgrass Lake. The sample has massive to weakly porphyritic and intergranular to subophitic textures. The small phenocrysts are plagioclase (2-4 mm, subhedral), weak mineral alignment, occurring in a fine-grained groundmass of plagioclase, pyroxene and opaque minerals (Fig. 4.8).

Figure 4.8. Detail of sample MOSS 057. The sample shows intergranular to subophitic texture and plagioclase phenocrysts.

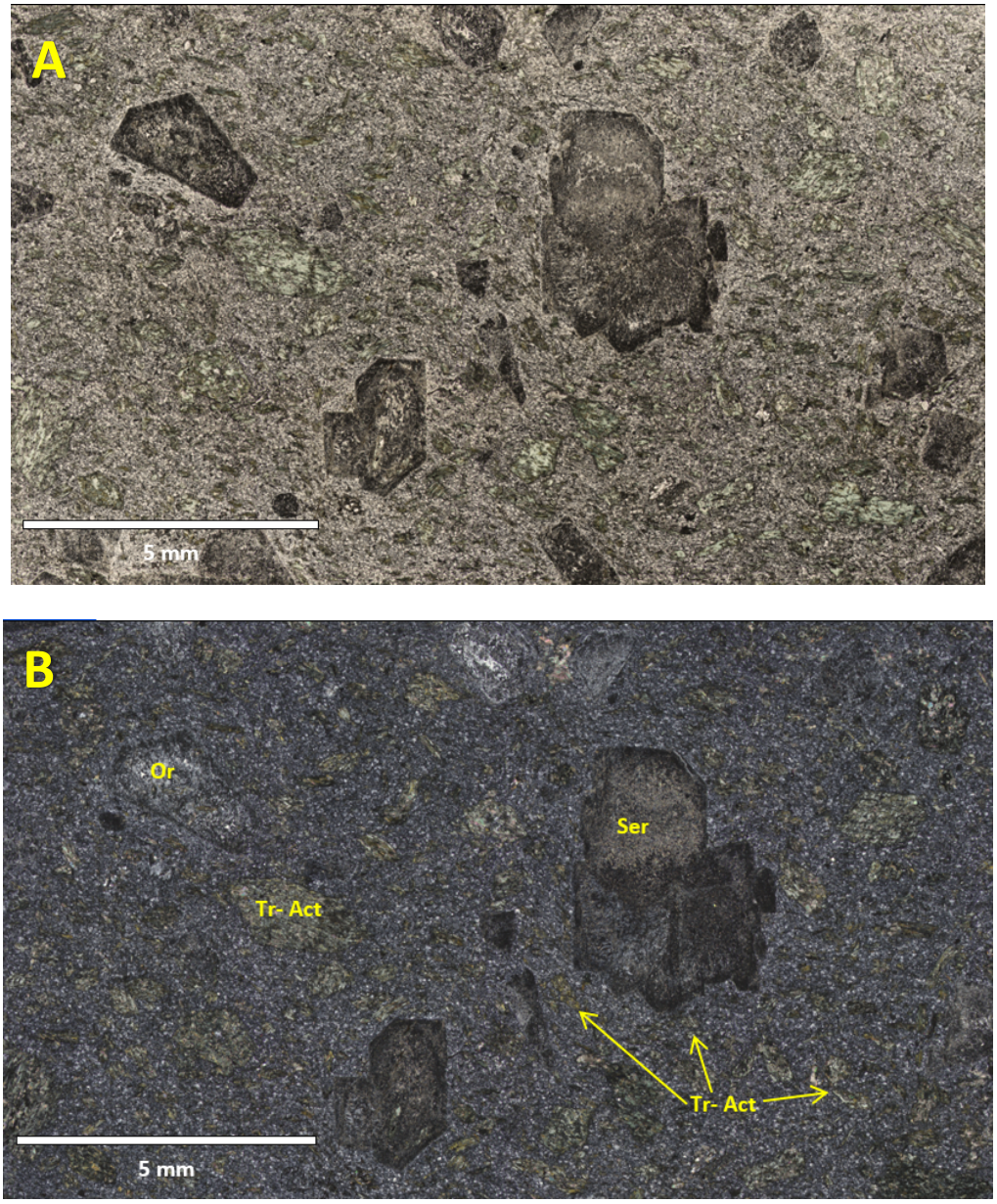

Figure 4.9. Photomicrographs of sample MOSS 057. A. (XPL) Microphotograph shows the phenocrysts originally formed by feldspars and amphiboles, as well as the matrix exhibiting alteration. B. (NX) Photomicrograph shows phenocrysts originally of hornblende altered to tremolite-actinolite (Tr-Act), feldspar phenocrysts altered to sericite (Ser), orthoclase phenocrysts (Or).

Petrographically, two types of plagioclase were observed. The first type of plagioclase phenocrysts (20%) with 2.3 – 4.5 mm size are subhedral with actinolite-tremolite within the

crystals. A second type of plagioclase (40%) is smaller, with sizes of 0.06 mm occurring in the chloritized groundmass. Quartz (10%) is also present in the groundmass. Actinolite tremolite (15%) is distributed throughout the sample, mainly in plagioclase and hornblende phenocrysts (5%) with subhedral shapes and 0.3 mm in size. Alteration minerals include calcite (5%), sericite (2%) and chlorite (2%). Additionally, opaque minerals such as magnetite (1%) were observed (Fig. 4.9).

Andesites

The outcrops range from black to light grey to dark green. In some localities, foliation is well developed (Fig. 4.10), likely reflecting regional deformation, and is accompanied by parallel and perpendicular carbonate-filled fractures. The outcrops show massive to weak porphyritic textures, with plagioclase phenocrysts up to 1 mm, dark green chlorite-rich groundmass and fine silt-sized crystals.

Figure 4.10. Outcrop 22AP-MOSS11, showing dark green (chloritized) andesite and perpendicular fractures filled with carbonates; note the characteristic foliation in the outcrops.

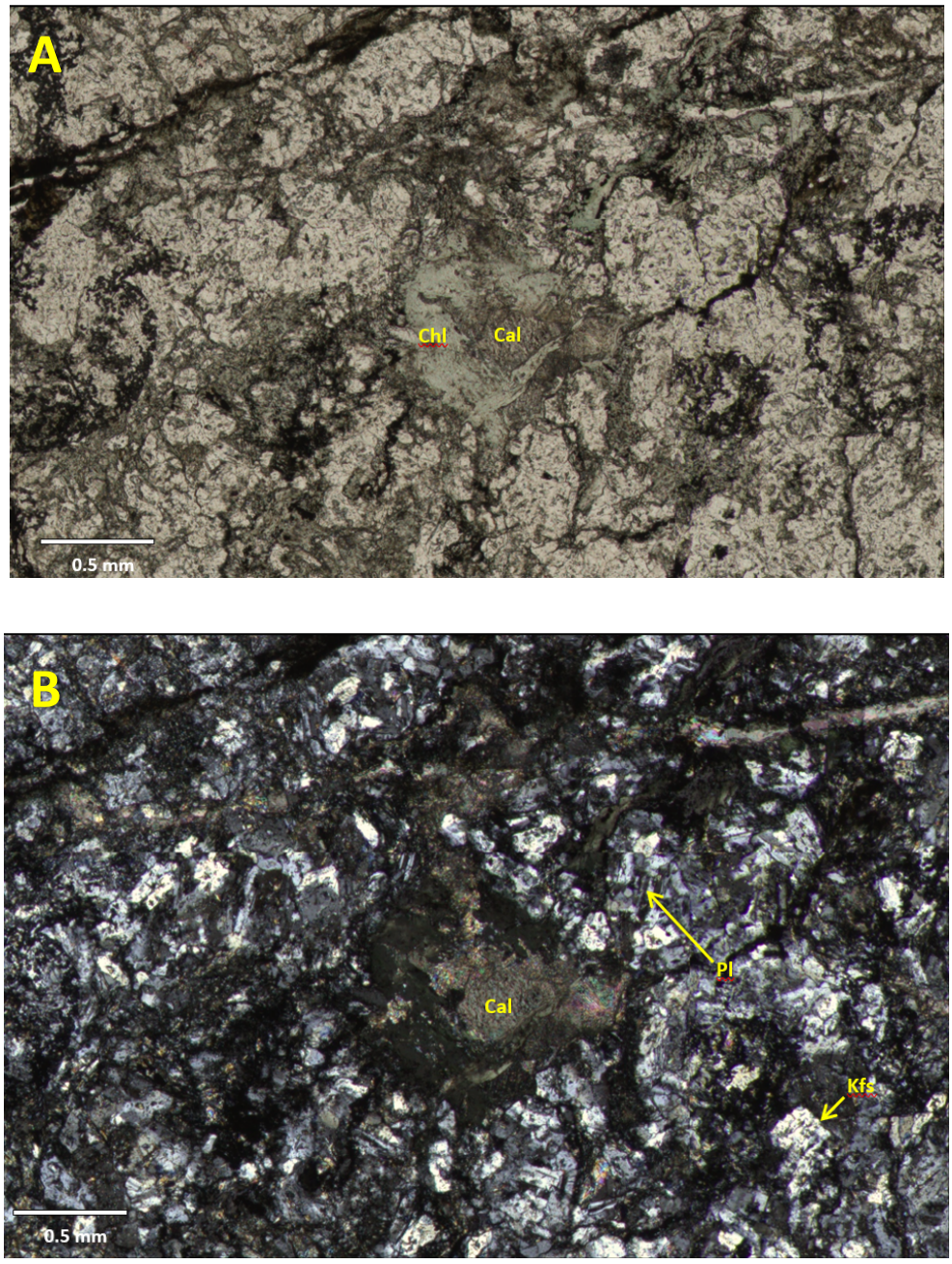

Figure 4.11. Photomicrograph of sample MOSS 025. A. XPL Image of alteration minerals such as chlorite (Chl) and calcite (Cal) can be observed, preferentially located in microfractures that cut the rock. B. NX image. The aphanitic texture of the host rock formed mainly by orthoclase (Kfs) and plagioclase (Pl) crystals can be observed, with alteration minerals (Cal) along microfractures.

Petrographically, the rocks contain subhedral to euhedral crystals plagioclase (50 - 70%) of 0.3 mm size, predominantly albite; some crystals are porphyritic and altered. Anhedral orthoclase (10 - 15%) 0.3 mm in size are deformed and occur with plagioclase. Quartz (10 - 15%) is generally subhedral between 0.1 – 0.3 mm size, with carbonates (2 - 10%), chlorite (2-3%) and < 0.08 mm sericite comprising between 3 – 5%, as well as pyrite – chalcopyrite (<1%) in veins (Fig. 4.11).

Rhyolites

The outcrops are generally light grey to pale greenish grey, with flow-textures and lithic fragments up to 5 mm in size. Texturally, they are massive flows with a porphyritic texture, with 3 mm subhedral to euhedral plagioclase phenocrysts and quartz in minor amounts. In some outcrops, up to 5 cm quartz amygdules were observed, deformed in the flow direction (Fig. 4.12). In general, relict volcanic textures are locally well preserved, allowing a clear distinction from other types of rocks.

Petrographically, the rocks comprise feldspars (55%) with anhedral to subhedral shapes with crystals between 80-310 μm. Quartz (25%) sizes less than 1900 μm and euhedral plagioclase (5%) with crystals between 50 – 90 μm size mostly andesine (Michel-Levy method). Alteration minerals, including alunite (5%), are pervasive and distributed in feldspar crystals. Flaky chlorite (5%) and sericite (1%) occur in veinlets. Calcite (1%) occurs as well-developed prismoid at crystals at the edges of the veinlets. Opaque minerals (3%), including pyrite and chalcopyrite, are distributed throughout the sample (Fig. 4.13).

Figure 4.12. Outcrop 23AP-MOSS095. The photograph shows quartz amygdules, deformed in the direction of lamination.

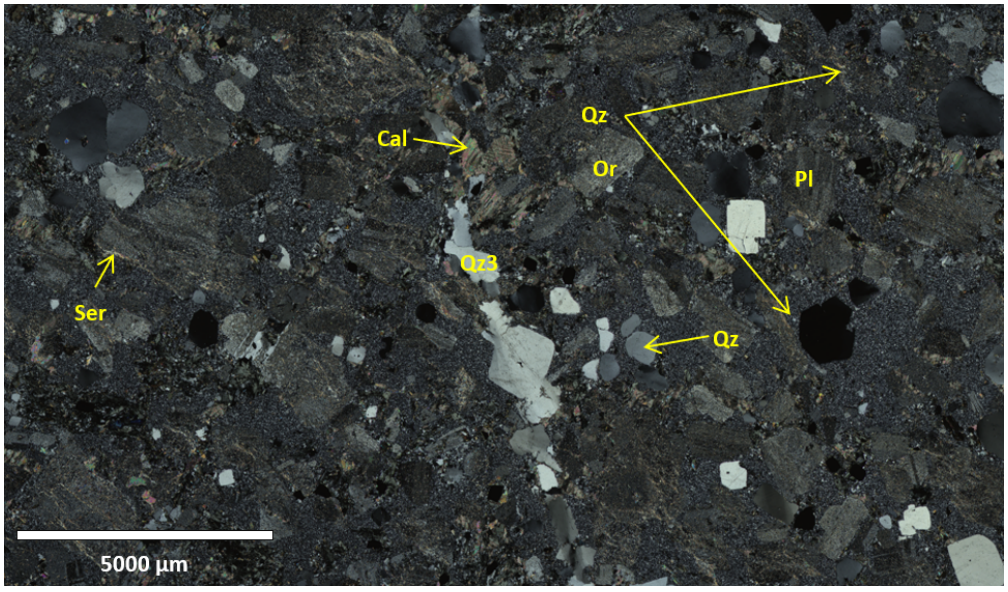

Figure 4.13. Photomicrograph of sample MOSS 003 in NX. a) quartz 1 (Qz1) and quartz 2 (Qz2) grains in the matrix. The tabular habit crystals are plagioclase (Pl) and orthoclase (Or) feldspar types affected by alteration to sericite (Ser); in addition, there is the presence of calcite (Cal) as a replacement mineral in the groundmass.

Ash tuff

The rocks in outcrop are pale grey to light greenish grey, with a slightly friable surface. A stratification is preserved in some outcrops, with layers that vary from 1 to 10 cm thick, with internal lamination < 0.5 cm. The outcrops contain fractures, many of which are filled with quartz-carbonate veins. The rock comprises fine-grained particles with laminar flows, erosion surfaces (Fig. 4.14), and flattened shards. Pyroclastic textures can be inferred locally, represented by lamination and fragments, supporting its interpretation as ash tuffaceous material that may have been reworked. In thin section, the samples are massive to finely banded, with oriented polycrystalline quartz and spherulitic quartz ~200 μm across (Fig. 4.15). Sericite, carbonates, and chlorite strongly alter the samples, the latter associated with opaque minerals, including pyrite (Fig. 4.16).

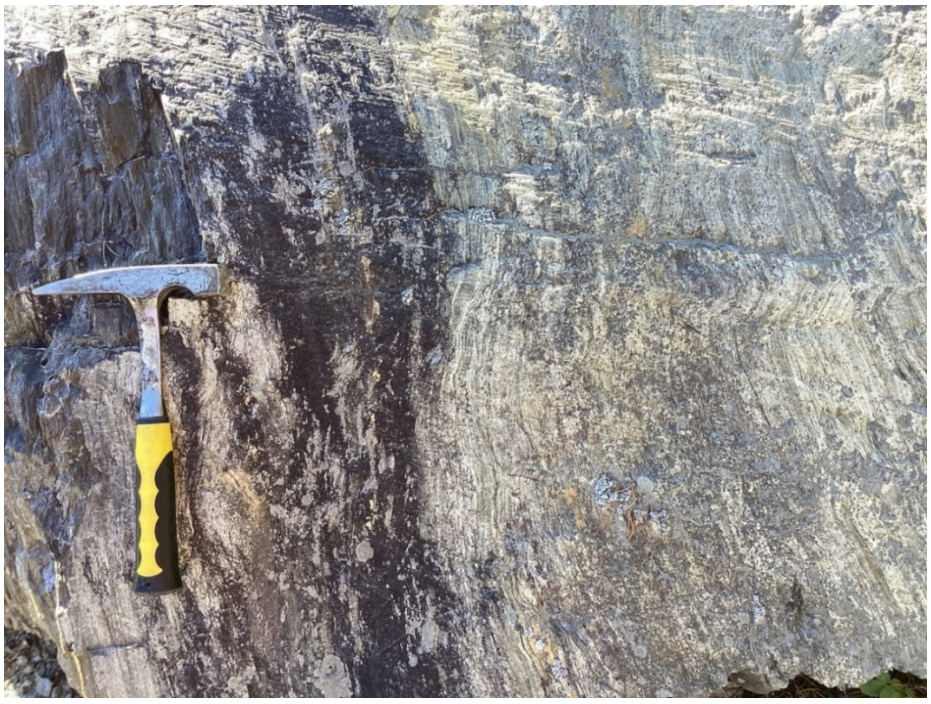

Figure 4.14. Outcrop 22AP-MOSS009, the photograph shows the plane-parallel lamination with laminae less than 0.5 cm.

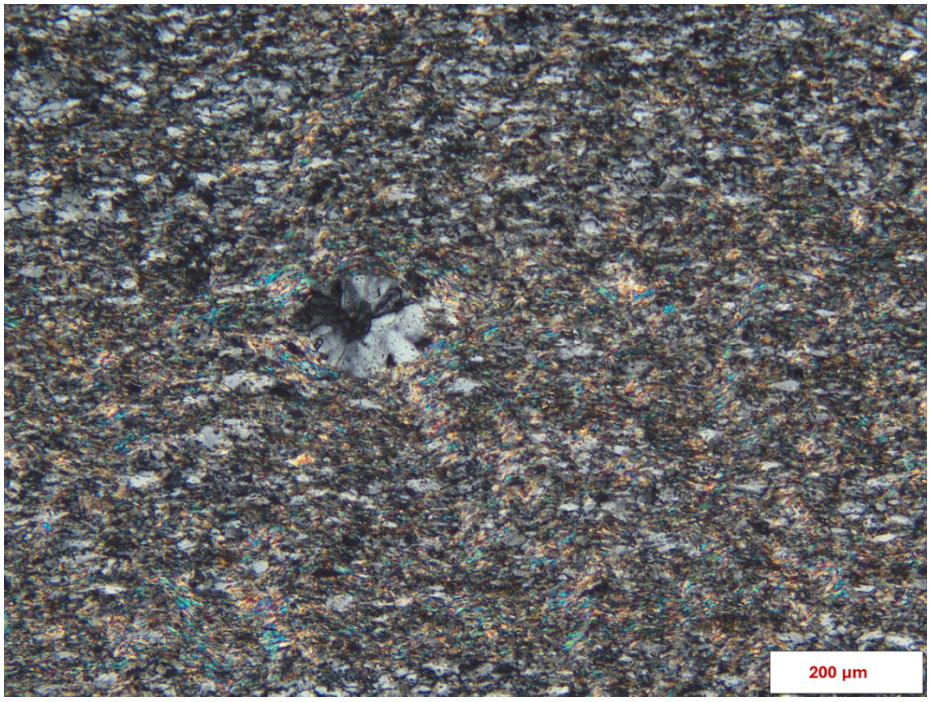

Figure 4.15. Photomicrograph of sample MOSS 028. Image in NX (scale 200 µm) showing detail of spherulite in volcanic rock.

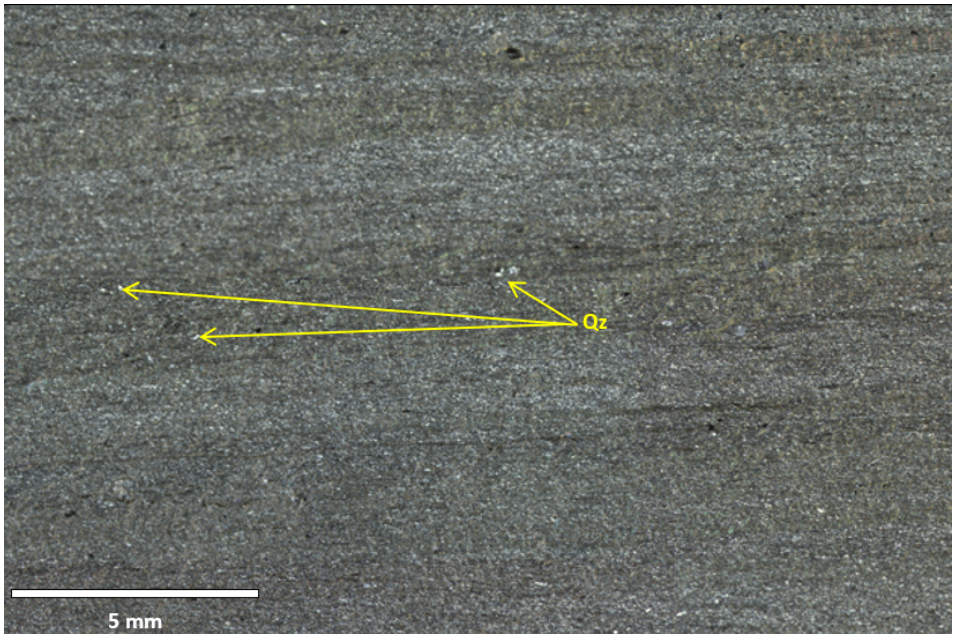

Figure 4.16. Photomicrograph of sample MOSS 028 (NX) details of lamination with quartz (Qz) between the layers.

Massive flows

This unit occurs mainly in the Burchell Lake and the Hermia Lake areas and has been largely interpreted from airborne magnetic data and drill holes (Osmani, 1997). However, several outcrops were identified during geological reconnaissance work. These were very weathered and poorly exposed. The outcrops are generally light cream and grey, competent, with quartz veinlets (Fig. 4.17). with plagioclase phenocrysts that were aligned with quartz in the groundmass, which can represent flow textures.

Figure 4.17. Detail of sample 22AP-MOSS 14. The sample shows plagioclase phenocrysts, which are aligned with quartz in the groundmass.

Petrographically, deformed layers were observed, some layers with polycrystalline quartz. Between the layers, some epidote crystals with irregular and tabular habits were observed as

granular aggregates filling fractures and associated with opaque minerals (Fig. 4.17). Some sectors contained tremolite-actinolite of high relief and prismatic habit oriented to lamination. Composed of tabular plagioclase (30 - 50%) <4µm size with quartz (3 - 5%) less 4µm. Alteration minerals such as tremolite actinolite (5-8%), chlorite (12 - 15%) and epidote (15%) with 30 µm size are present (Fig. 4.18).

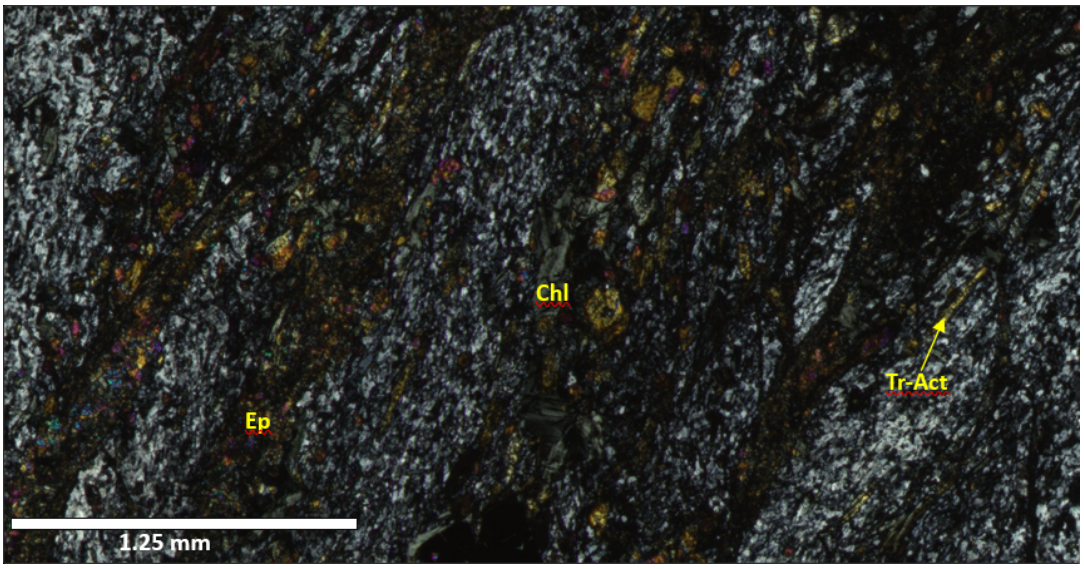

Figure 4.18. Photomicrograph sample MOSS 014. (NX) image showing chlorite (Chl) with late first-order interference colours disseminated in the rock and oriented in the direction of lamination, epidote (Ep), which appears irregular and tabular in habit, as granular aggregates filling fractures and associated with opaque minerals, tremolite-actinolite (Tr-Act) with a high degree of relief and prismatic habit oriented in the direction of lamination.

4.1.3 Clastic sedimentary rocks.

This unit is limited to the westernmost part of the study area, bordered by the Quetico fault, with a predominant NE trend (Fig. 4.1). Ten control spots were taken in the field. Due to surface oxidation, the outcrops are brown to reddish in colour but medium to dark gray on fresh surfaces. The predominant rocks are fine- to medium-grained clastic metasedimentary rocks with plane-

parallel laminations (Fig. 4.19). These rocks show similarity in outcrop with ash tuff. However, it was possible to differentiate them due to the clasts' size (fine to medium-grained) and the absence of flow textures or erosion surfaces, characteristic of ash tuff. Additionally, petrography was used to improve discrimination (Fig. 4.19), allowing for corroboration of field observations.

Figure 4.19. Outcrop AP22 – MOSS4, showing the characteristic lamination of sedimentary rocks and brown to reddish colors resulting from alteration.

Petrographically, the samples are metagreywacke, with a framework of quartz particles (25 - 45%) of angular to sub-rounded shape of medium sand grain size. The quartz fragments are of two types, monocrystalline and polycrystalline, with 5 - 10% of fine grain angular grains of plagioclase. The matrix comprises quartz (10%) made up of sub-rounded grains of silty size, with hematite (2%) and biotite (13%), some samples contain carbonates (10-20%) and sericite (up to 10%; Fig. 4.20).

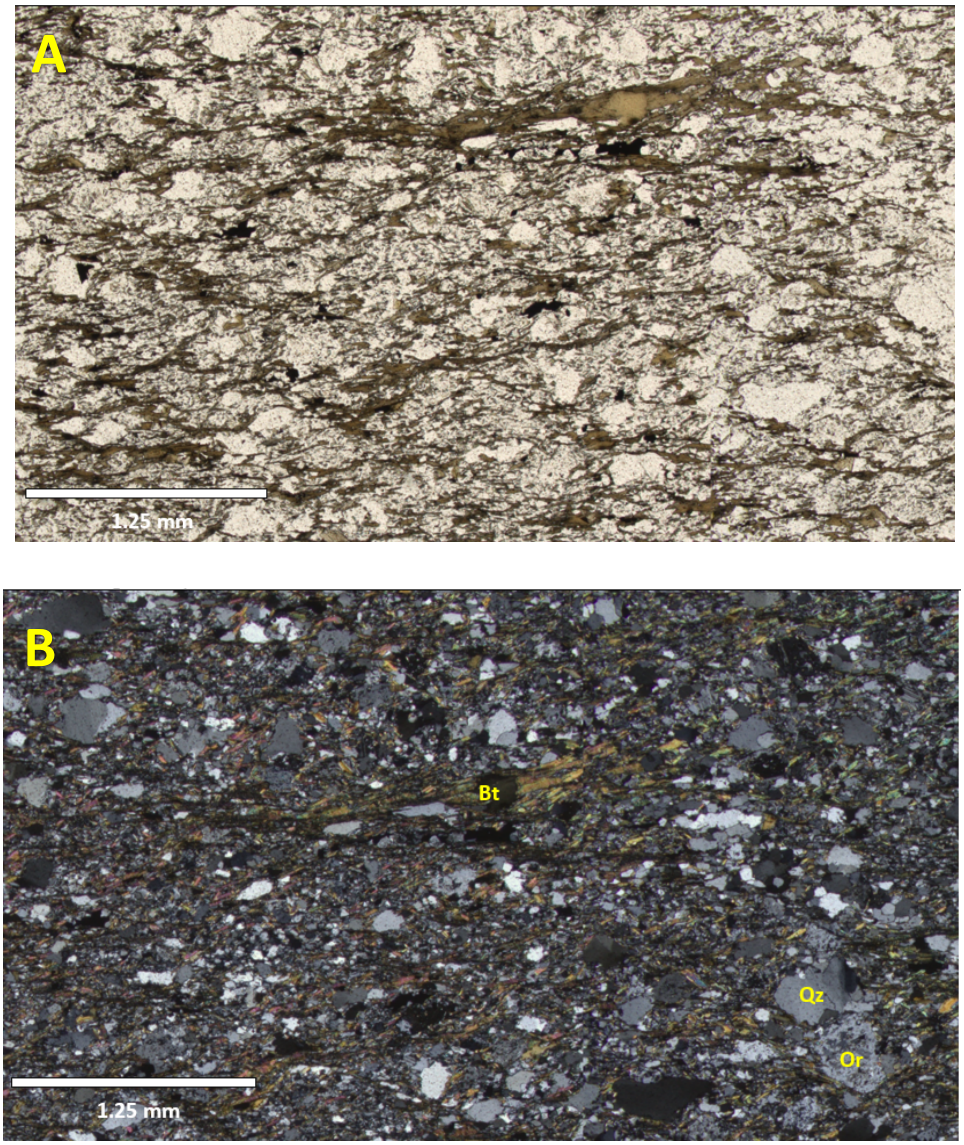

Figure 4.20. Photomicrograph of sample MOSS 059. A. Image (XPL) showing the lamination of the particles. B. Image (NX) showing the foliation characterized by the orientation of biotite (Bt) in the cleavage domains and the presence of quartz aggregates (Qz) and detrital grains probably from plutonic lithics in the microliths.

4.1.4 Mafic and ultramafic intrusive rocks

Twenty outcrops of foliated competent rock were observed, with dark green to grey and black colours (Fig. 4.21). In some outcrops, foliation and joints were observed, mainly oriented NE and NW (Fig. 4.1). The rocks are predominantly gabbros, with plagioclase, pyroxene, though

altered to chlorite (Fig. 4.22). In addition, sulphides (pyrite, chalcopyrite) and accessory minerals such as magnetite were observed.

Figure 4.21. Outcrop 22AP-MOSS012. The photograph shows an outcrop of an ultramafic intrusive dike. Two directions of joints are visible.

Petrographically, the rocks are gabbros. They have a holocrystalline texture, predominantly panidiomorphic and locally hypidiomorphic. With euhedral to subhedral hornblende phenocrysts (25-80%) 0.50 mm in size, with skeletal structures. In some samples, the epidote (30-40%) is 0.02 mm in size and has a subhedral shape. The groundmass is actinolite (10 - 20 %) with pyroxenes – augite (1 – 3%) less than 0.02 mm in size. Alteration minerals sericite (4%) and chlorite (1 - 8 %) were observed, filling microfractures and between the hornblendes. The opaque minerals comprise less than 1% and were mainly chalcopyrite-pyrite (Fig. 4.23).

Figure 4.22. Detail of sample MOSS 024. Example of mafic and ultramafic intrusive rock.

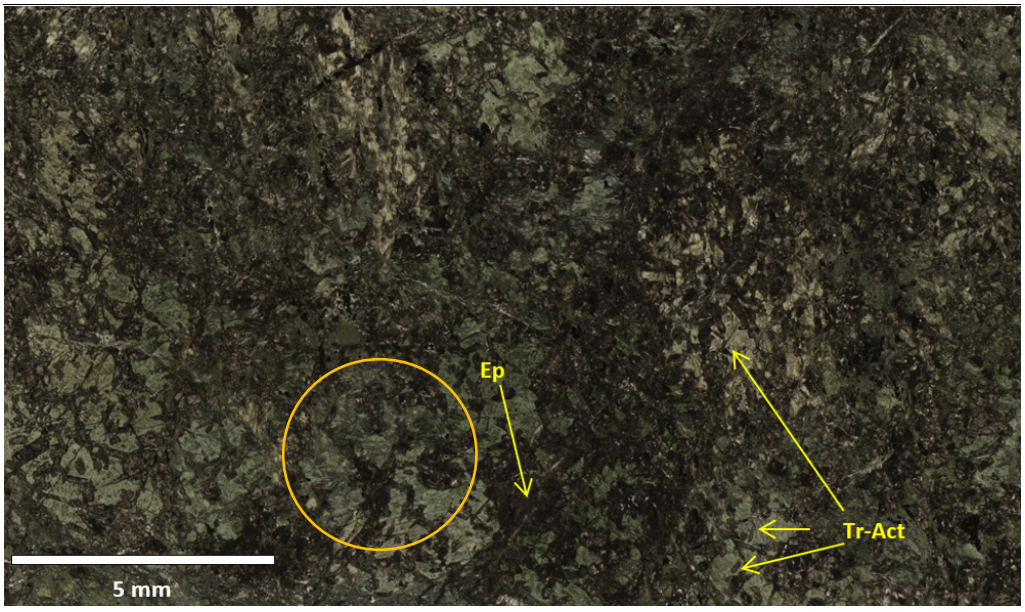

Figure 4.23. A. Photomicrograph of sample MOSS 020 (XPL) showing the strong alteration and mineral aggregates of very fine size and acicular and granular by tremolite-actinolite (Tr-Act) and epidote (Ep). Skeletal structure in the orange circle.

4.1.5 Gneissic tonalite suite

Two control spots were from this unit, which is restricted to the Little Greenwater Lake stock (Fig. 4.1). This is delineated on aeromagnetic maps by diffuse low-intensity anomalies, with linear and oval anomalies of greater intensity that suggest metavolcanic and mafic gabbroic enclaves (Osmani, 1997).

Figure 4.24. Outcrop 23AP-MOSS115. Bands can be identified, mainly of quartz and plagioclase. Note the folding of the rocks; they could be classified texturally as gneissic.

The outcrops are predominantly altered and poorly exposed, white and grey, with weak foliation in various orientations. Medium- to coarse-grained bands of quartz and plagioclase with equigranular textures were identified. Despite the deformation in the outcrops and their high degree of weathering (Fig. 4.24), the rock type was identified as granodiorite, which was corroborated by geochemical data.

4.1.6 Late felsic to mafic intrusive rocks

Six stocks of deformed granite are found in the study area (Fig 4.1). The bodies are distributed throughout the study area and form topographic highs. They have distinctive colours that vary from pink when fresh to white when weathered. These intrusions are predominantly granite to monzodiorite, with equigranular to porphyritic textures, with potassium feldspar, plagioclase, and quartz as the main phases. The felsic plutons generally display undeformed to weak foliation and intrude earlier volcanic assemblages, suggesting their emplacement during late or post-tectonic stages.

Moss Lake Stock

This intrusion is located in the western part of the area and borders the Goldshore property (Fig. 2.4). The Snodgrass Lake Fault cuts the intrusion with a NE orientation, displaying undeformed to weak foliation. Four control points were taken with samples collected for petrography, geochemistry and geochronology from the central part of the body (west of the Snodgrass Lake Fault; Fig. 4.1).

The stock mainly comprises granites and monzogranites with fine- to medium-grained phaneritic equigranular textures and ranges from pink to light pink (Fig. 4.25). It is composed predominantly of quartz, K-feldspar, and plagioclases in roughly equal proportions, with hornblende and biotite as the main mafic minerals.

Figure 4.25. Outcrop 22AP-MOSS041. The photograph shows the degree of weathering of the Moss Lake Stock outcrops, note the distinctive pinkish colour of the stock.

Petrographically, the samples comprise equigranular holocrystalline textures with fine to medium grain size. It consisted of anhedral orthoclase (60 - 70%) 1.5 – 3 mm in size and anhedral sanidine - microcline (1 - 4%) crystals 2 mm in size. Quartz (15%) is 0.3 – 1.9 mm in size and polycrystalline, the subhedral plagioclase (3 - 8%) is oligoclase that exhibits polysynthetic twinning 0.5 mm in size, subhedral hornblende (7%) is between 0.6 - 1.4 mm in size, biotite (1%) and pyroxenes (1 - 7%) possibly aegirine euhedral and 0.8 mm in size. Alteration minerals include actinolite-tremolite (1%) epidote (1%), sericite (1%), and clay minerals (1%). Opaque minerals include titanite <1%, and magnetite-hematite (<1%) generally associated with hornblende and biotite (Fig. 4.26).

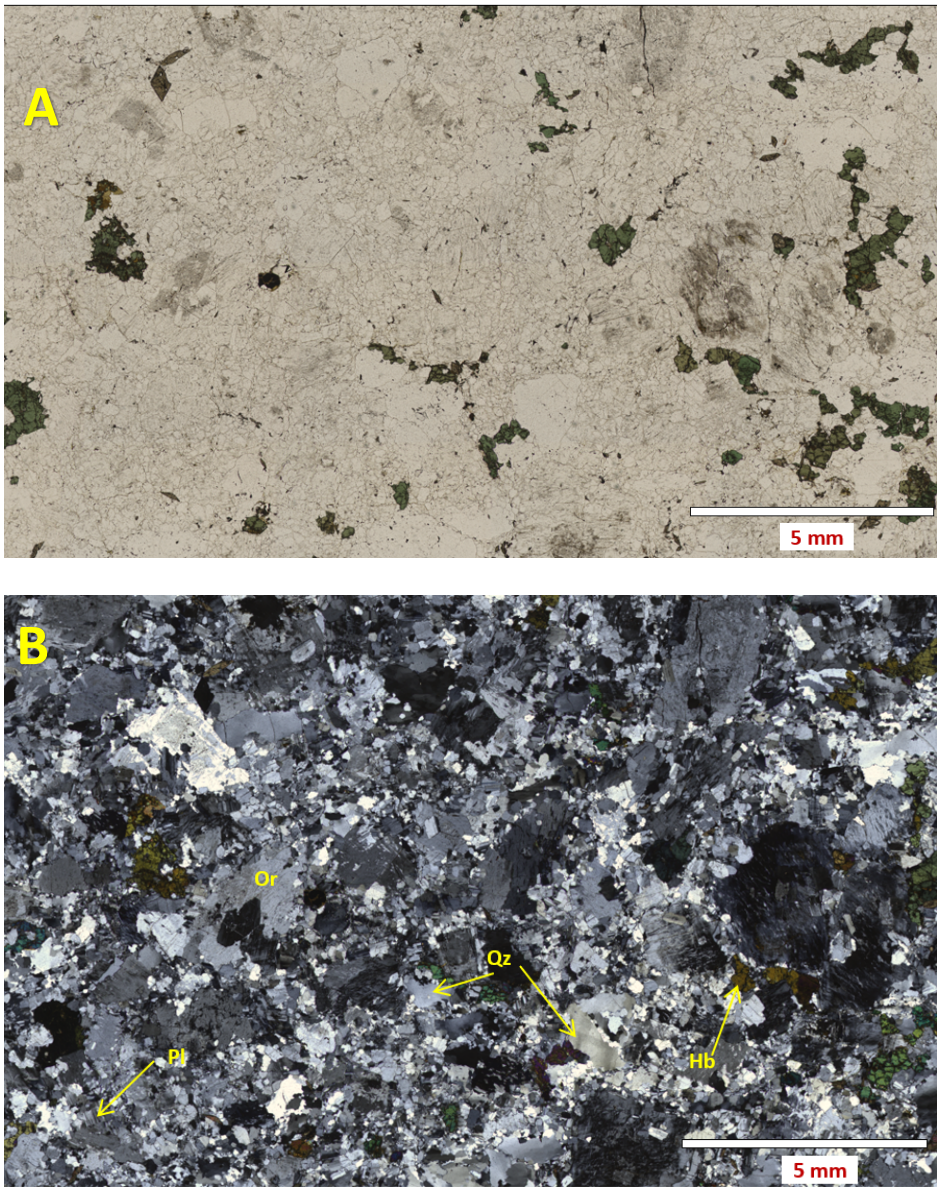

Figure 4.26. Photomicrograph of sample MOSS 053. A. Image (XPL), the inequigranular texture and the presence of amphiboles. B. Image (NX) showing the predominantly inequigranular texture and the mineralogy of the rock formed by quartz (Qz), hornblende (Hbl), orthoclase (Or), plagioclase (Pl).

Hermia Lake Stock

This body is located in the southeastern part of Burchell Lake and is cut by the Knife Lake Fault with NE orientation (Fig. 4.1). Ten outcrops were examined mainly on the shores of Burchell Lake or small islands within it (Fig. 4.27). These are light pink to white due to weathering. The outcrops are mainly of syenites, medium- to coarse-grained, inequigranular holocrystalline texture, with porphyritic plagioclase and little to no quartz (<5%). The K-feldspar commonly occurs as large subhedral to anhedral grains.

Figure 4.27. Outcrop 23AP-MOSS048. The photograph shows an outcrop of Hermia Lake Stock on the shores of Burchell Lake.

Petrographically, the samples comprise equigranular holocrystalline textures with fine to medium grain size. It consisted of anhedral orthoclase (60 - 70%) 1.5 – 3 mm in size and anhedral sanidine - microcline (1 - 4%) crystals 2 mm in size. Quartz (15%) is 0.3 – 1.9 mm in size and polycrystalline, the subhedral plagioclase (3 - 8%) is oligoclase that exhibits polysynthetic

twinning 0.5 mm in size, subhedral hornblende (7%) is between 0.6 - 1.4 mm in size, biotite (1%) and pyroxenes (1 - 7%) possibly aegirine euhedral and 0.8 mm in size. Alteration minerals include actinolite-tremolite (1%) epidote (1%), sericite (1%), and clay minerals (1%). Opaque minerals include titanite <1%, and magnetite-hematite (<1%) generally associated with hornblende and biotite (Fig. 4.26).

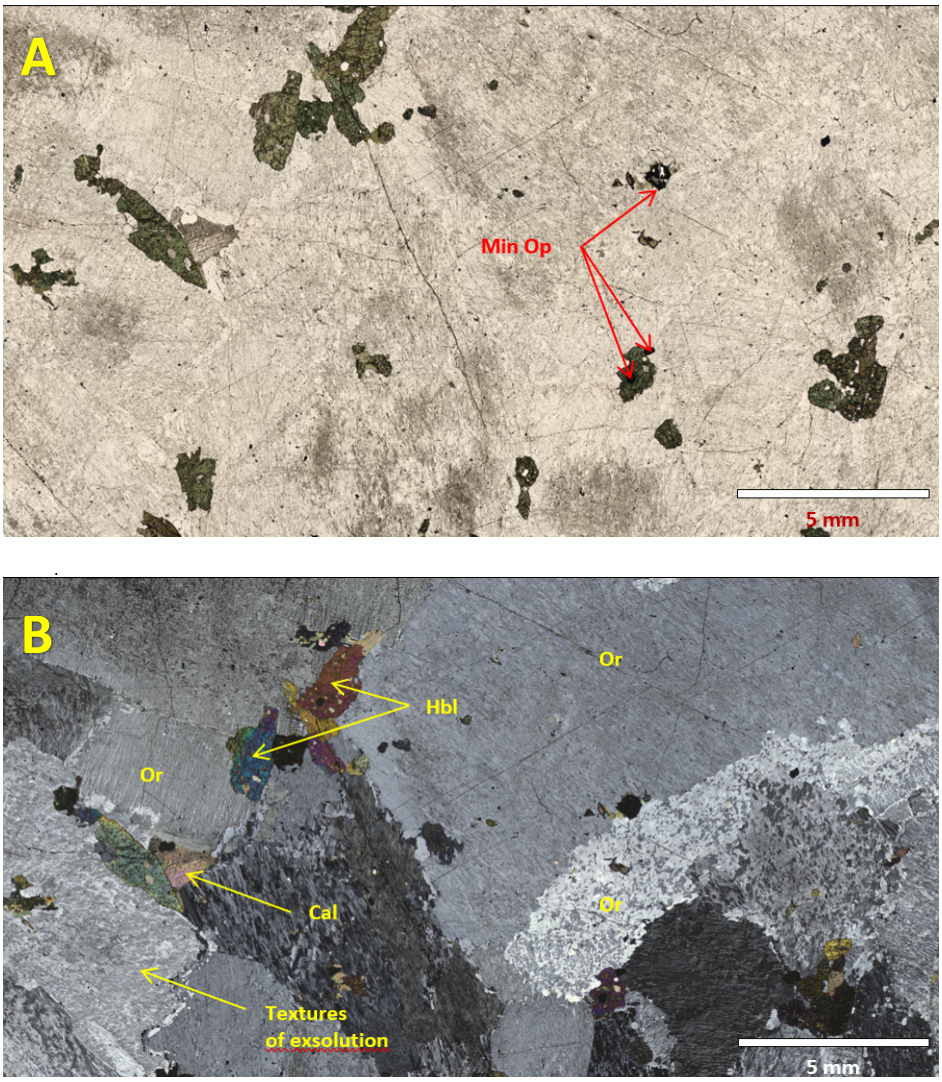

Figure 4.28. Photomicrograph of sample MOSS 114. A. Image (XPL), showing the inequigranular texture characterized by the presence of small crystals of amphibole and opaque minerals (Min Op) surrounded by large feldspar crystals. B. Image (NX), showing crystals of hornblende (Hbl), calcite (Cal), opaque minerals (Min Op) and orthoclase (Or).

Burchell Stock

The stock is located north of Burchell Lake, is bounded to the east by the Knife Lake Fault (Fig. 4.1) and was observed at nine control points. The stock is predominantly monzogranite to diorite, with a porphyritic to inequigranular texture of medium-grained crystals (Fig. 4.29). It is composed predominantly of quartz, K-feldspar, and plagioclase, with biotite as the principal mafic mineral. Only one dioritic sample (Moss-91) was observed, consisting of medium- to coarse-grained, dark grey colour, composed of plagioclase and mafic minerals such as hornblende and biotite, with minor quartz and K-feldspar.

Figure 4.29. Outcrop 22AP-MOSS001. The photograph shows the colour of the weathered Burchell Lake stock.

Petrographically, the samples present an inequigranular holocrystalline phaneritic texture, although some samples had porphyritic phenocrysts. It comprises anhedral orthoclase (25-45%)

0.4 – 1 mm in size with diffuse edges due to alteration to clay minerals, microcline (5 -8%) in 0.6 mm size occurs as subhedral-anhedral crystals in zoned phenocrysts with inclusions of hornblende and plagioclase. Quartz (18 - 40%) is <4 mm in size and is monocrystalline, whereas plagioclase (5 - 20%) is subhedral and 0.3 mm in size. Biotite - muscovite (1-2%) and amphiboles such as hornblende (1%) usually occur together. Alteration minerals, including chlorite (1 - 3%) and clay minerals (1%), typically replace orthoclase and plagioclase. Opaque minerals (1%) are mainly pyrite and chalcopyrite and are generally associated with hornblende and biotite (Fig. 4.30).

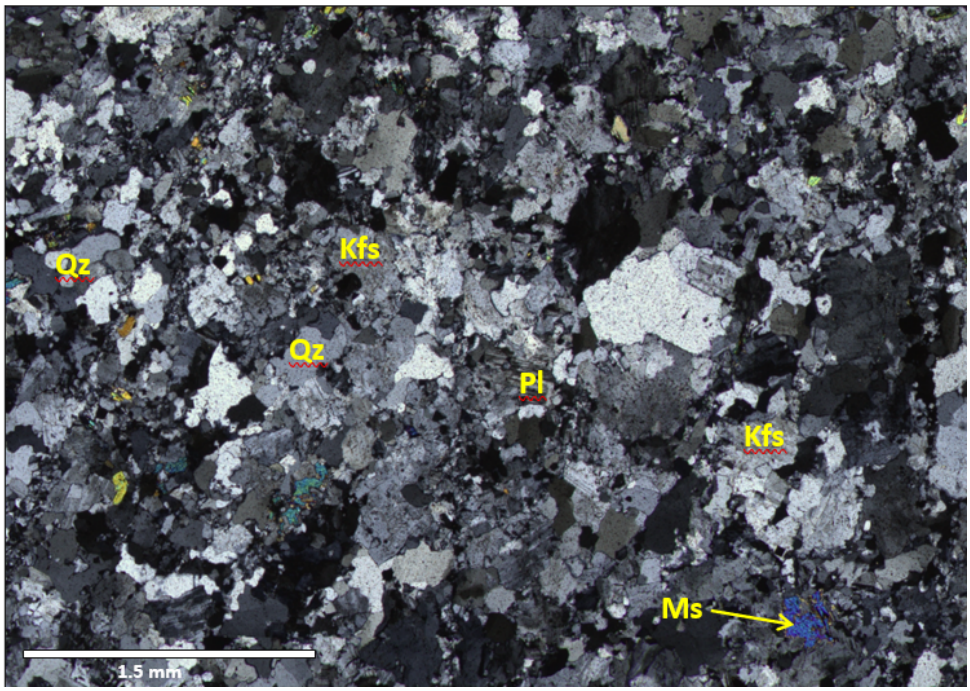

Figure 4.30. Photomicrograph of sample MOSS 090. The photograph (NX) shows the presence of quartz crystals (Qz), plagioclase (Pl), orthoclase (Kfs) and muscovite (Ms).

Greenwater Lake Stock

The Greenwater Lake Stock is a crescent-shaped intrusion (Fig. 4.1). Three outcrops were observed. The outcrops were light grey to pinkish grey colored and, in general, were very

weathered and covered with vegetation. The hand samples correspond to medium-grained equigranular granites and granodiorites (Fig. 4.31), displaying an equigranular to weakly porphyritic texture and are composed of quartz, plagioclase, K-feldspar and biotite.

Figure 4.31. Outcrop 23AP-010. The photograph shows the orientation of the amphiboles and pyroxenes in the Greenwater stock.

Petrographically, the samples are granodiorites with a holocrystalline, hypidiomorphic texture. Quartz (20 - 30%) is monocrystalline with a size of 0.5 - 1 mm, subhedral to anhedral plagioclase (40 - 55%) and microcline (5%) with a size of 1 to 2.5 mm. Hornblende (2 - 5%) is anhedral with 0.3-0.6 mm in size, the anhedral clinopyroxenes (4 - 10%), subhedral diopside that is augite 0.4 - 1 mm in size. Accessory minerals include epidote (<1%), titanite (<1%), zircons (<1%) and opaque minerals (<1%), mainly magnetite (Fig. 4.32).

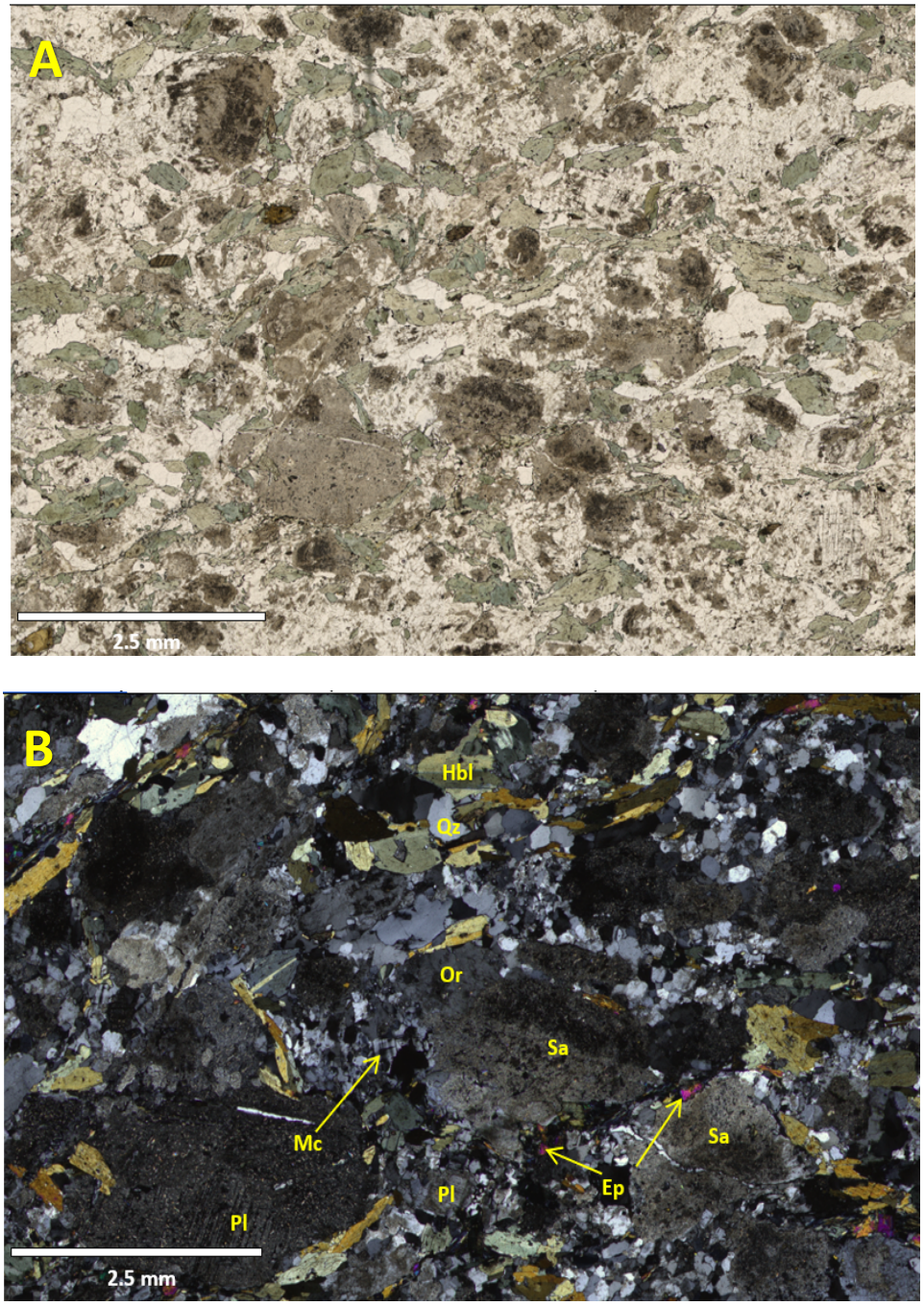

Figure 4.32. Photomicrograph of sample MOSS 100. A. Image (XPL) note the holocrystalline, hypidiomorphic texture. B. Crossed Nicol image. In the photograph, hornblende (Hbl), orthoclase (Or), sanidine (Sa), plagioclase (Pl), quartz (Qz), microcline (Mc) and epidote (Ep).

Hood Lake Stock

This body is located in the southern part of the study area and is bounded to the west by the Knife Lake fault (Fig. 4.1). It forms a rounded topographic high. Seven light pink to white outcrops were described. The outcrops are mainly syenites, with inequigranular holocrystalline to porphyritic textures, with well-developed K-feldspar as large subhedral to anhedral crystals, up to 6 cm across (Fig. 4.33). These crystals have an orientation that is observable at the outcrop scale (Fig. 4.33).

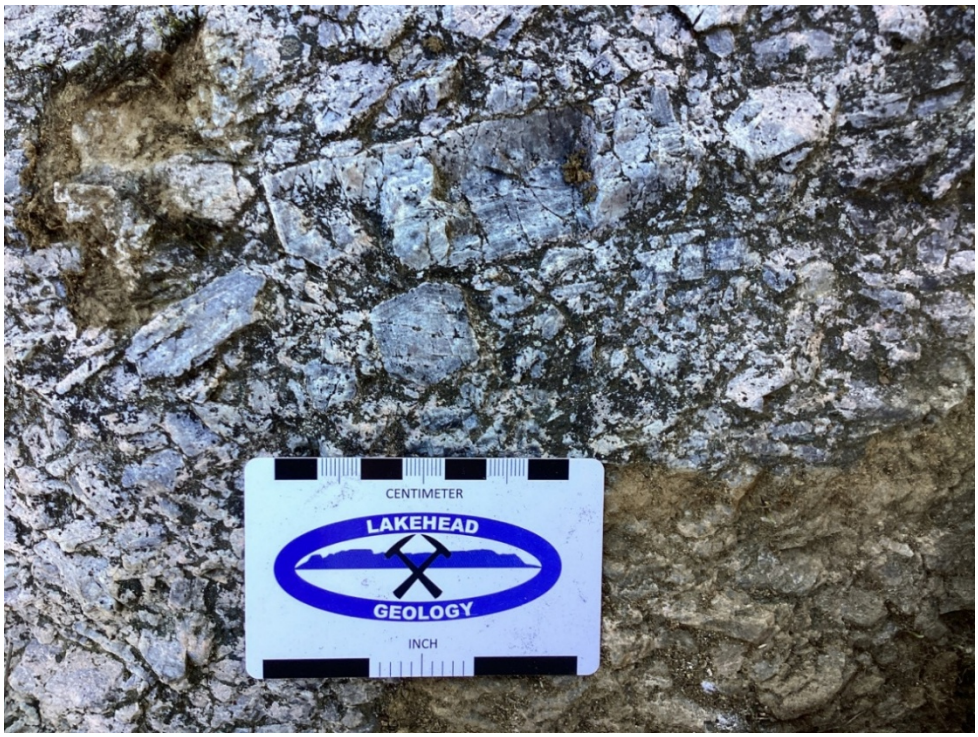

Figure 4.33. Outcrop 22AP-021. The photograph shows the porphyritic texture with well-developed feldspar phenocrysts of up to 6 cm in the Hood Lake stock.

The samples are an alkaline quartz feldspar syenite with an equigranular holocrystalline texture with phenocrysts. They comprise orthoclase (50 - 35%), sanidine (2%), and microcline (2%), with sizes between 0.5 and 15 mm oriented with well-developed crystalline forms. Monocrystalline quartz (5 - 10%) is restricted to sizes between 0.2 - 0.7 mm and is preferably

located between orthoclase. Hornblende (20%) is associated with clinopyroxene (8%), biotite (3%) and epidote (1%), as well as zircons of sizes less than 0.6 mm and opaque minerals (1%), mainly rutile and magnetite (Fig. 4.34).

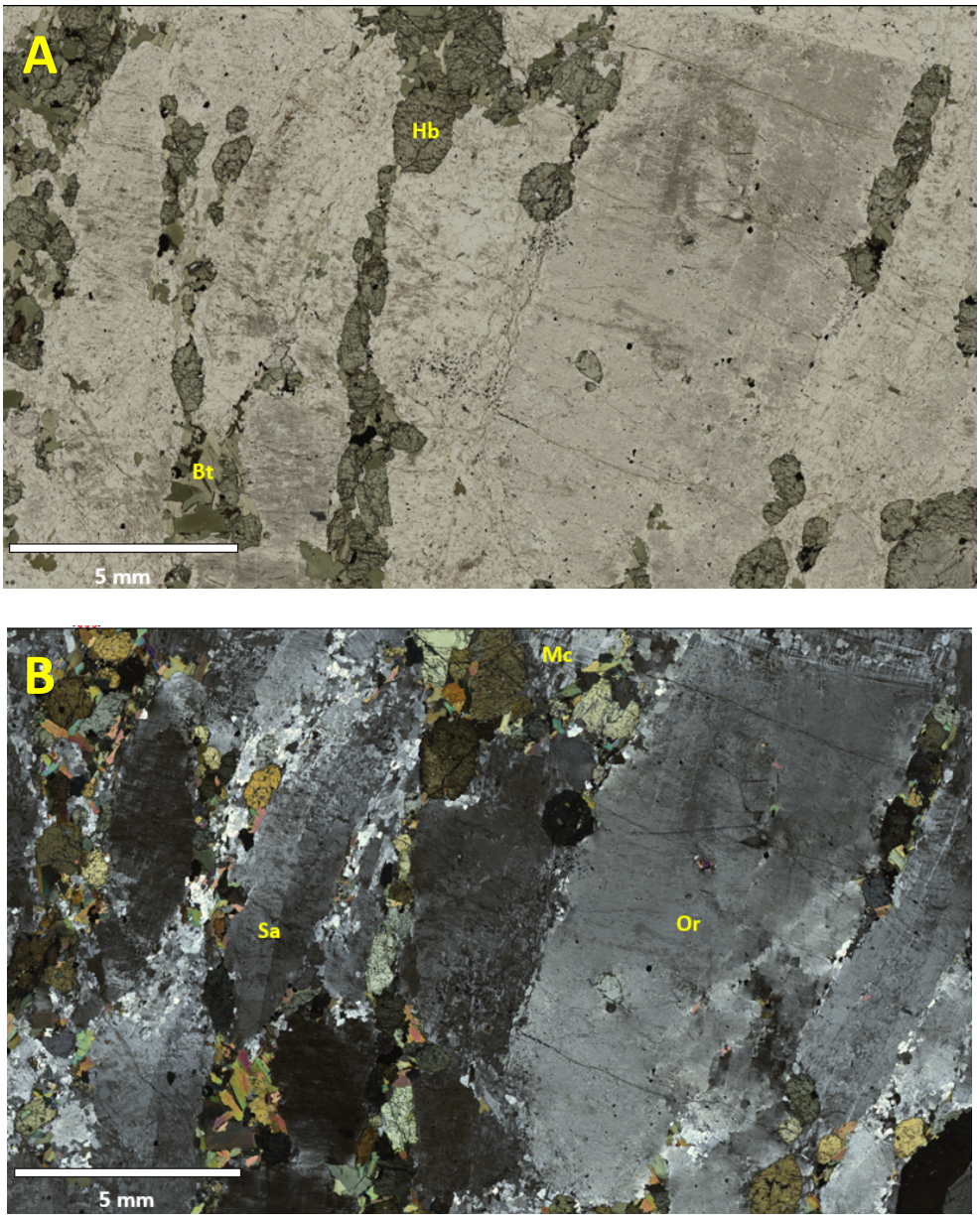

Figure 4.34. Photomicrograph of sample MOSS 032. A. XPL, shows the orientation of the hornblende (Hbl) and biotite (Bt). B. NX, orthoclase (Or), sanidine (Sa) and microcline (Mc).

Obadinaw Stock

The Obadinaw stock is located west of the study area and is elongated NE (Fig. 2.4). The Obadinaw stock was examined at two locations, where it was emplaced in Quetico-type metasedimentary rocks. Outcrops are small and pink on fresh surfaces. Texturally, medium- to coarse-grained equigranular, composed of quartz, plagioclase, and K-feldspar, with biotite and hornblende mafic minerals (Fig. 4.35).

Figure 4.35. Outcrop of Obadinaw stock at spot 22AP-038.

Petrographically, the samples correspond to quartz alkali feldspar syenite with an equigranular holocrystalline texture. Compositionally anhedral orthoclase phenocrysts (80%) of perthitic texture with sizes between 2 – 4.5 mm. Polycrystalline quartz (10%) is located between the orthoclase crystals with sizes between 0.2 – 0.7 mm. Plagioclase (3%) with polysynthetic,

twinning and euhedral crystals between 0.2 -0.5 mm in size, tabular biotite (2 - 4%) and associated with carbonates (<1 – 2%). Opaque minerals (1%), including magnetite and pyrite, have a size of less than 0.01 mm (Fig. 4.36).

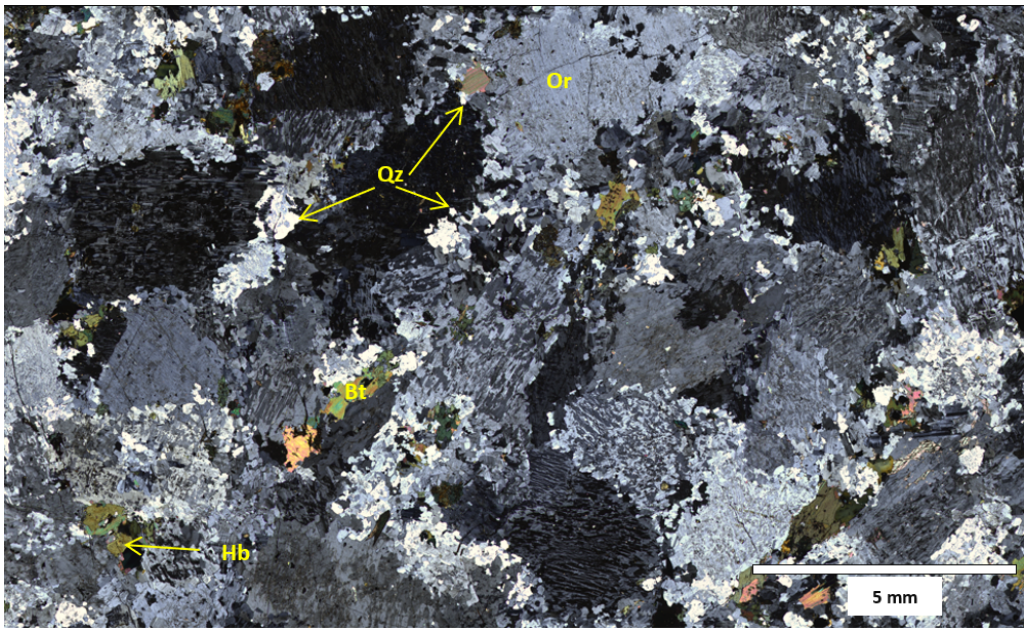

Figure 4.36. Photomicrograph of sample MOSS 051 from the Obadinaw stock, photograph (NX), shows the presence of orthoclase (Or), biotite (Bt), hornblende (Hbl), quartz (Qz), and exsolution and intergrowth textures.

4.1.7 Granodiorite.

This unit is located in the southernmost part of the study area and was observed at eight locations. It occurs near the Hamlin Lake and Myrt Lake stocks, separated by the Knife Lake fault (Fig. 4.1). Outcrops are poorly preserved and rarely exposed. The hand samples are pink to light reddish with a granitic equigranular texture of medium- to fine-grained crystals, mainly quartz, K-feldspar and plagioclases in roughly equal proportions with hornblende (Fig. 4.37).

Figure 4.37. Outcrop of granodiorite 23AP-MOSS105.

Samples have an inequigranular holocrystalline texture with fine to medium-grain size. Consists of monocrystalline quartz (25%) with 0.4 – 1 mm size and euhedral orthoclase (25%) 2.5 – 1 mm in size with sericite alteration. Plagioclase (10%) has been altered to clay minerals and sericite. Euhedral microcline (5%) is 0.5 mm in size, whereas euhedral sanidine (5%) is 0.5 – 1 mm size. Accessory minerals include sphene-titanite (1%), tabular biotite (1%), hornblende (0.5%), apatite (1%), chlorite (<1%) and zircon (<1%). Additionally, opaque minerals (1%), include pyrite and magnetite (Fig. 4.38).

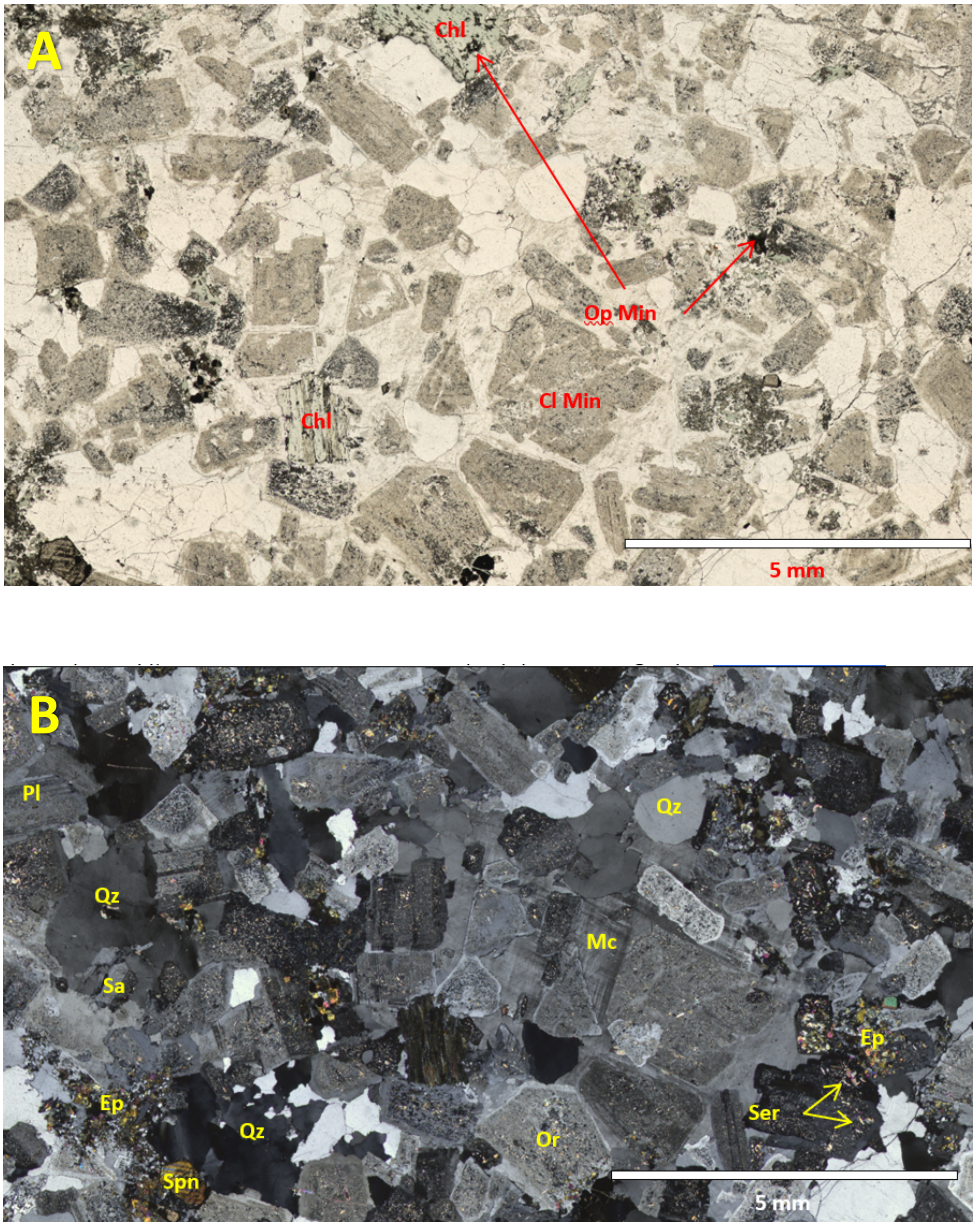

Figure 4.38. Photomicrograph of sample MOSS 134. A, Image (XPL), the photograph shows the alteration of feldspars to clay minerals (Cl Min), the presence of opaque minerals (Op Min), as well as the alteration to chlorite (Chl) B. Image (NX) showing quartz (Qz), orthoclase (Or), plagioclase (Pl), microcline (Mc), epidote (Ep), sericite (Ser), sanidine (Sa) and sphene-titanite (Spn).

4.2 Whole rock geochemistry.

A total of 56 samples were collected for whole-rock geochemical analysis. The coverage and location of the samples are shown in Figure 4.39, and the complete data set is presented in Appendix B. Major element analyses are reported in wt% and trace elements in parts per million (ppm), including gold (Au).

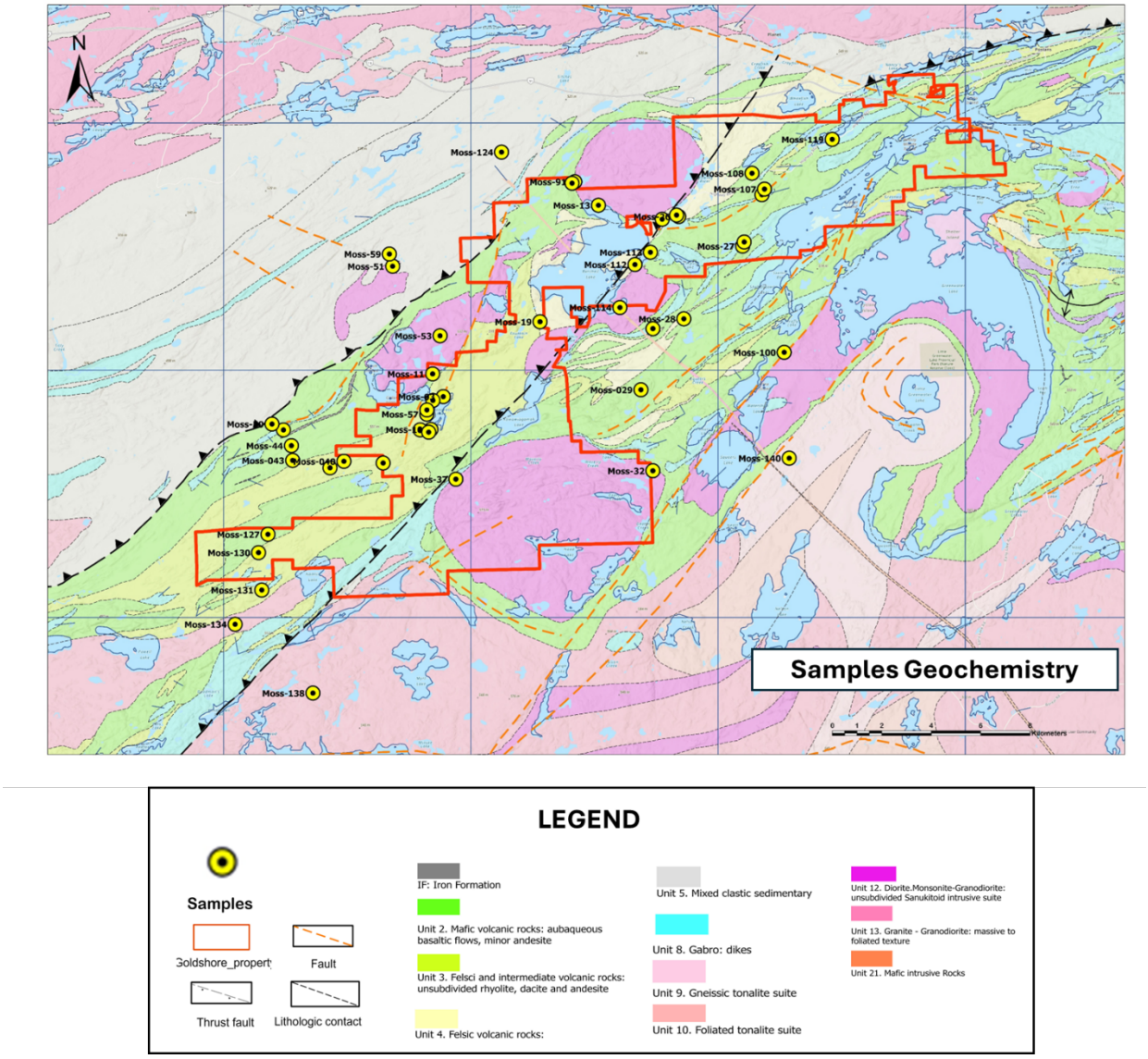

Figure 4.39. Location of samples for whole for rock geochemistry. See appendix E for a higher resolution version of the figure.

The dataset was used to classify lithological units and interpret their genesis and tectonic setting. Given that the greenstone belt rocks have undergone deformation, metamorphism, and hydrothermal metasomatism (Santaguida, 2001; Osmani et al., 1991; Osmani, 1997), interpreting geochemical data requires caution, as these processes can obscure original geochemical signatures (Pearce, 1996). Major elements were primarily used to identify alteration trends, while immobile elements—such as aluminium (Al), titanium (Ti), phosphorus (P), and high field strength elements (HFSE) including thorium (Th), zirconium (Zr), niobium (Nb), hafnium (Hf), yttrium (Y), and rare earth elements (REE)—were used to preserve the primary geochemical character and reduce the influence of alteration (MacLean & Barrett, 1993; Pearce, 1996; Rollinson & Pease, 2021). Although generally considered immobile, light rare earth elements (LREE) and Y may exhibit slight mobility during metasomatic alteration (Rollinson & Pease, 2021).

To evaluate the mobility of elements before the application of classification diagrams that typically incorporate either mobile or immobile elements, bivariate diagrams illustrating the relationships of Al_2O_3, MgO, K_2O, Na_2O, SiO_2 (Fig. 4.40) and P_2O_5 against TiO_2, as well as diagrams depicting Nb about La, Th, Y, Yb, TiO_2, and Zr (Fig. 4.41). Elements that exhibit a linear correlation within the diagrams are classified as immobile, whereas those demonstrating substantial dispersion are categorized as mobile (MacLean & Barrett, 1993). The considerable dispersion noted in K_2O and Na_2O, along with a lesser degree in SiO_2 and Al_2O_3, indicates that these elements experienced mobility during hydrothermal metamorphism and metasomatism (Fig. 4.40). On the other hand, Figure 4.41 illustrates narrower, more linear trends that align with the relatively immobile characteristics of La, Th, Y, Yb, Ti, and Zr. Therefore, these elements will be employed to classify rocks and draw inferences regarding tectonic environments. Since the rocks

in the study area show deformation and alteration the Pearce's classification diagram for volcanic rocks was used (Pearce, 1996; Rollinson & Pease, 2021; Fig. 4.42).

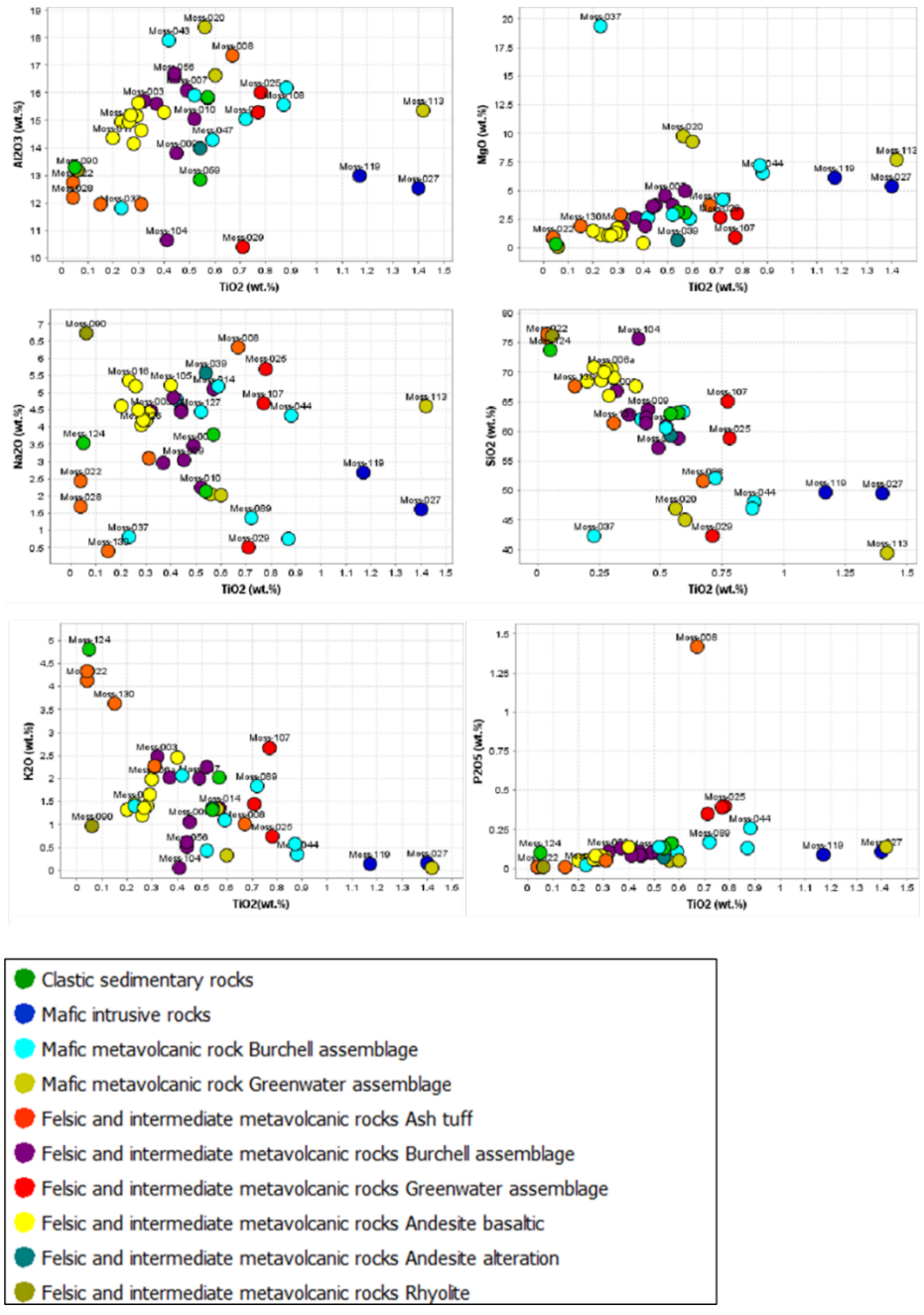

Figure 4.40. Bivariate variation diagrams of TiO_2 vs major element in oxides.

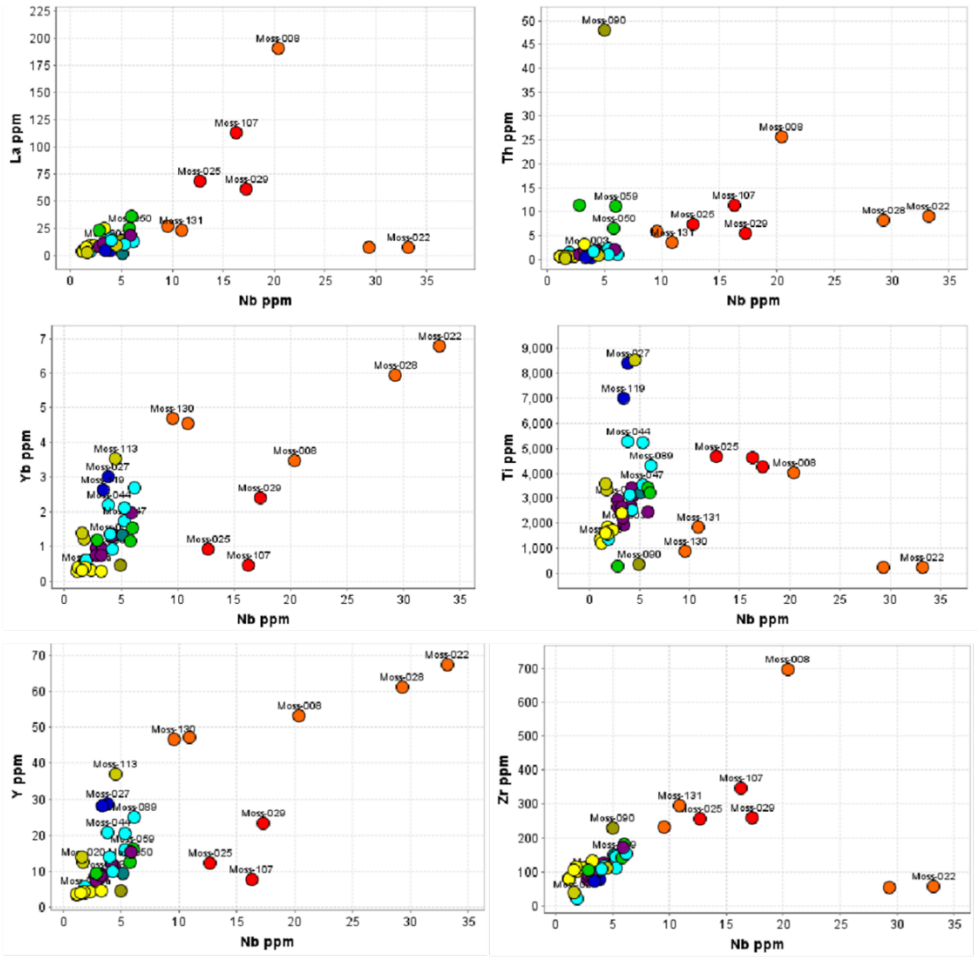

Figure 4.41. Bivariate variation diagrams of Nb vs trace elements.

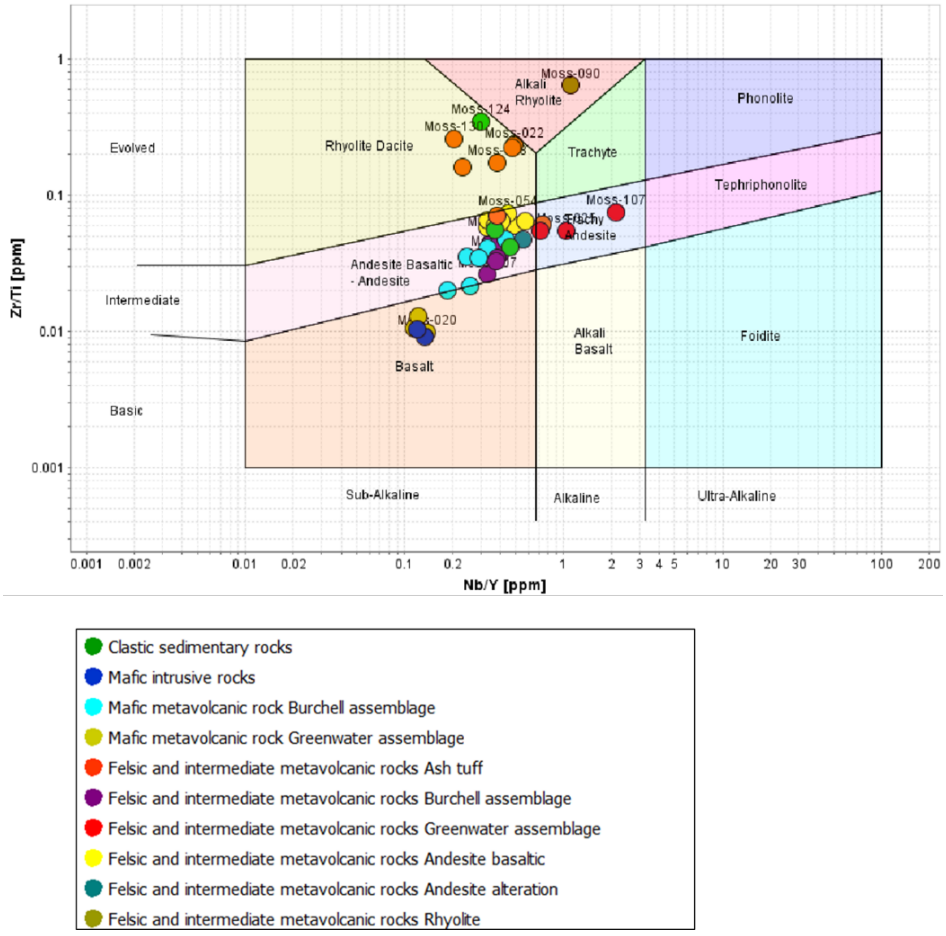

Figure 4.42. Zr/Ti versus Nb/Y diagram by Pearce 1996. The diagram shows the classification of the samples according to their geochemical affinity.

To determine the magmatic affinity of the rocks, the Jensen Cation Plot diagram (Jensen, 1976) was used as it uses the cations Al_2O_3, FeO -*- Fe_2O_3 + TiO_2 and MgO, which are relatively immobile (Fig. 4.43A). However, as major elements can sometimes be mobile magmatic affinities were corroborated using the AFM diagram (Fig. 4.43B).

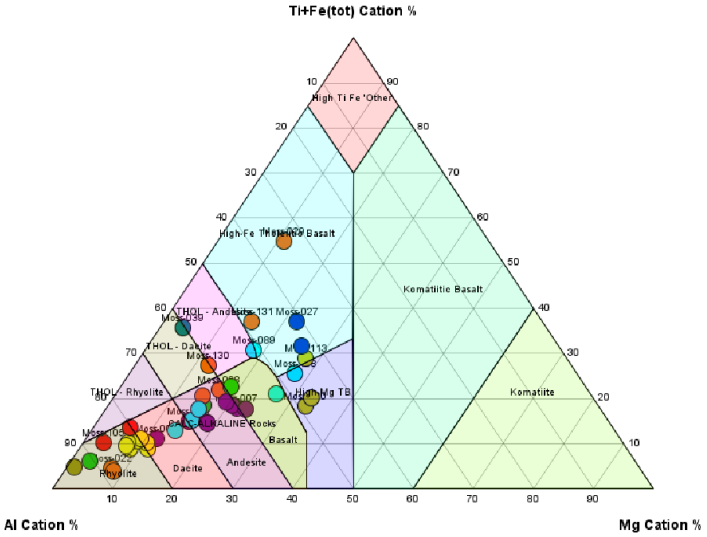

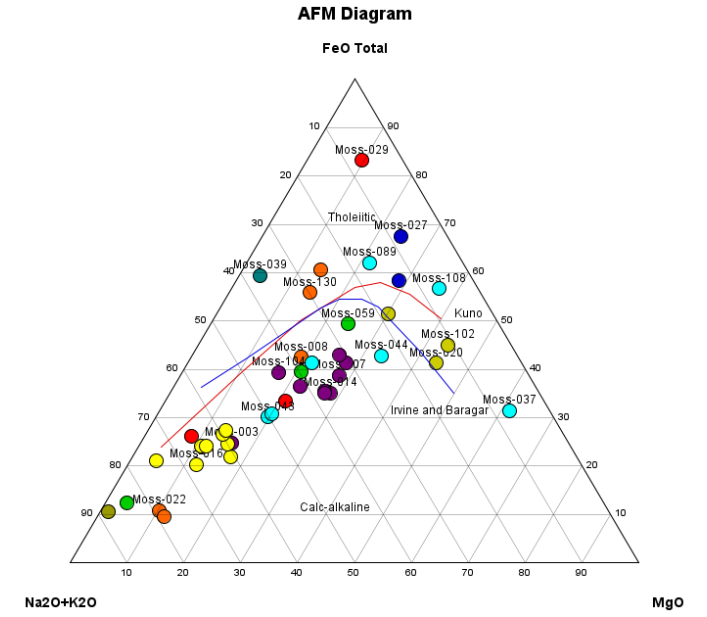

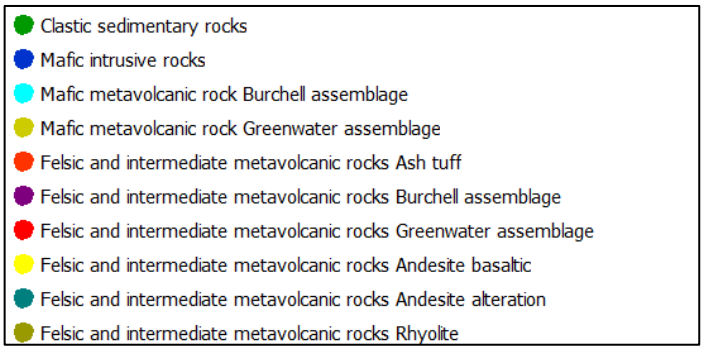

*Figure 4.43. **A**. Jensen Cation Plot diagram (Jensen, 1976). **B**. AFM pot diagram.*

Additionally, the Ross and Bedard (2009) diagram was used only for mafic rocks, which uses the geochemical ratios of immobile elements Th/Yb vs Zr/Y (Fig. 4.44), reducing the uncertainty in the classification.

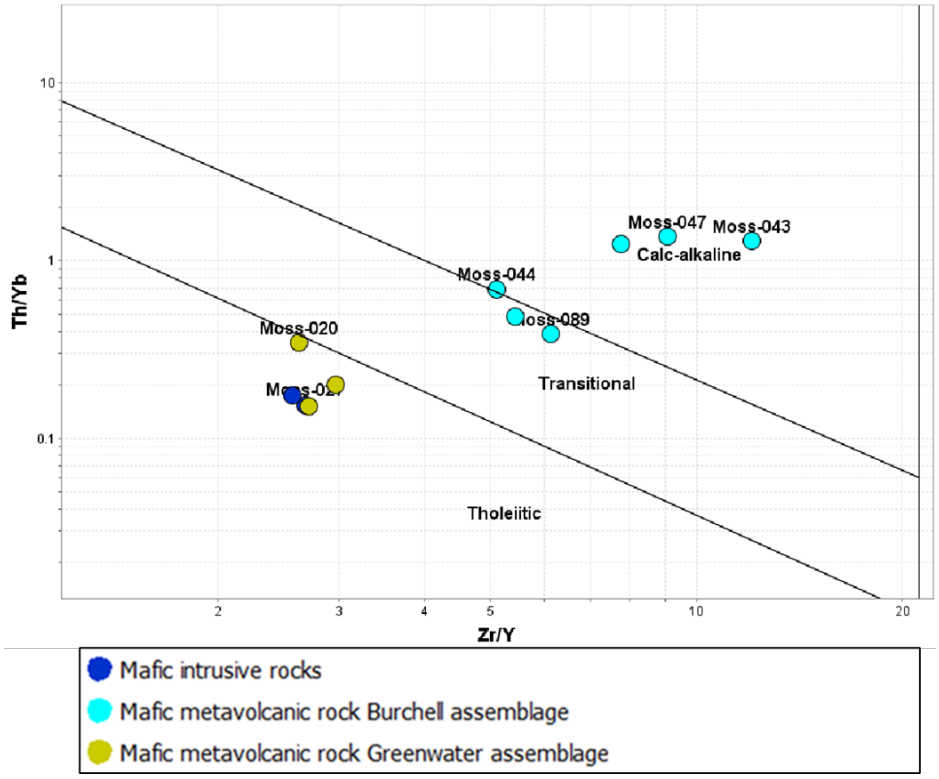

Figure 4.44. Th/Yb versus Zr/Y diagram by Ross and Bedard (2009). The diagram shows the mafic and ultramafic rocks.

4.2.1 Mafic intrusive rocks.

The mafic intrusive rocks are located east of the Knife Lake fault (Fig. 2.4) These rocks have 5 – 7 % MgO, Ni concentrations of 37 - 65 ppm and Cr concentrations of 20 - 72 ppm (Fig. 4.45). They plot within the basaltic field in a Zr/Ti versus Nb/Y diagram (Fig. 4.42). The magmatic series would correspond to a tholeiitic series, as observed in the Th/Yb vs Zr/Y diagrams (Figs. 4.43A, B and 4.44). The samples present flat LREE (La/Sm = 0.81 – 0.99) and flat to slightly

fractionated HREE (Gd/Yb = 1.15 - 1.28; Fig. 4.45). A slight negative anomaly is observed in Nb (Th/Nb = 0.92) and Ti.

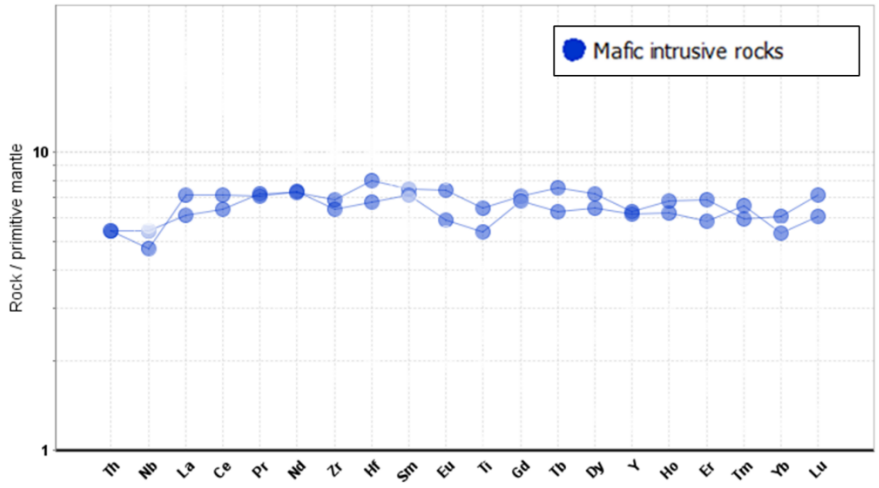

Figure 4.45. Primitive mantle normalized for mafic intrusive rocks. Normalizing values from Sun and McDonough (1989).

4.2.2 Mafic metavolcanic rocks.

Mafic metavolcanic rocks they can be divided into two geochemical units bounded by the Knife Lake fault (Fig. 2.42). One unit corresponds to rocks located in the Greenwater assemblage (Williams et al., 1991), and a second geochemical unit represented by rocks located in the Burchell assemblage. The mafic metavolcanic rocks of the Greenwater assemblage are located within the basaltic field of the Zr/Ti versus Nb/Y diagram (Fig. 4.42). In contrast, mafic metavolcanic rocks of the Burchell assemblage plot within the basaltic/andesitic field (Fig. 4.42). The mafic rocks of the Greenwater assemblage correspond to a tholeiitic series whereas the rocks belonging to the Burchell assemblage are transitional to calc-alkaline (Fig. 4.44). Normalized spider diagrams also distinguish between the two types of mafic metavolcanic rocks (Fig. 4.46). The mafic metavolcanic rocks of the Greenwater assemblage with weaking enriched the LREE (La/Sm =1.24

– 1.75) with negative Nb anomalies. The HREE shows a flat to slightly fractionated (Gd/Yb =1.06 – 1.27; Fig. 4.48).

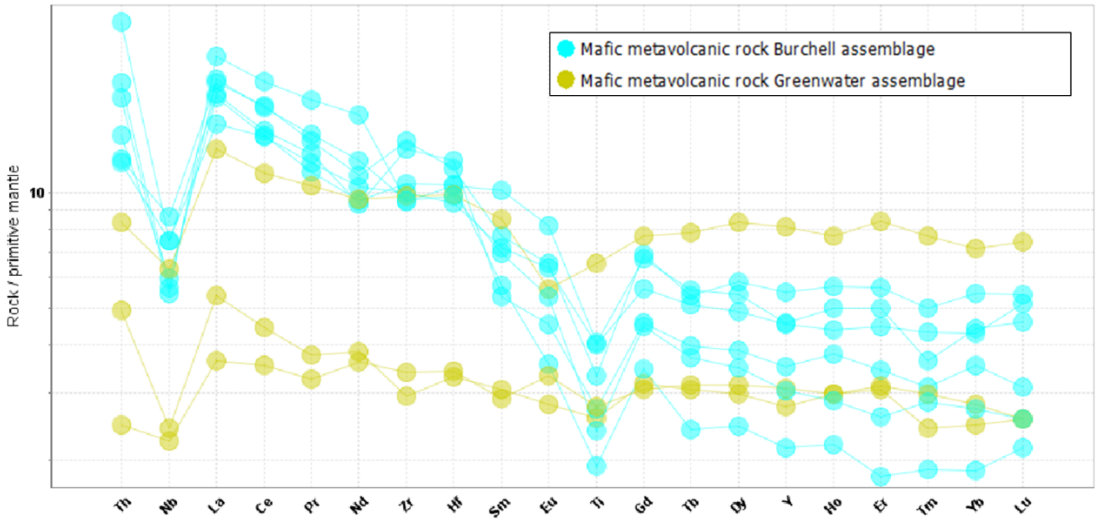

Figure 4.46. Primitive mantle normalized for mafic metavolcanic rocks. Normalizing values from Sun and McDonough (1989).

Mafic and ultramafic metavolcanic rocks Burchell assemblage show a steeper trend, marked by enriched the LREE (La/Sm = 2.10 – 3.36) and negative Nb anomalies with flat to slightly fractionated HREE (Gd/Yb = 1.25 – 1. 14) and a marked negative Ti anomaly (Fig. 4.46).

4.2.3 Felsic and intermediate metavolcanic rocks

Felsic and intermediate metavolcanic rocks are composed of ash tuff, basaltic andesite, andesite and rhyolite, ranging from basaltic andesite-andesite to alkaline rhyolite and trachy-andesite (Fig. 4.42). Intermediate felsic and metavolcanic rocks show SiO_2 contents ranging from 50-77.5 wt%, with significant scatter of major elements such as Al_2O_3, MgO and Na_2O and a linear

trend in P_2O_5, SiO_2 and K_2O (Fig. 4.40). Bivariate diagrams of trace elements versus Nb suggest the presence of three geochemical units (Fig. 4.41). The first unit is intermediate comprising andesitic and diorite rocks (Fig. 4.42). The second geochemical unit corresponds to dacitic rhyolites and petrographically are classified as ash tuffs (Fig. 4.42). The third geochemical unit are felsic and intermediate metavolcanic rocks (Fig. 4.42). All samples plot within the calc-alkaline andesite to rhyolite fields, except for sample Moss 39, which is altered and plots in the tholeiitic dacite field (Fig. 4.47).

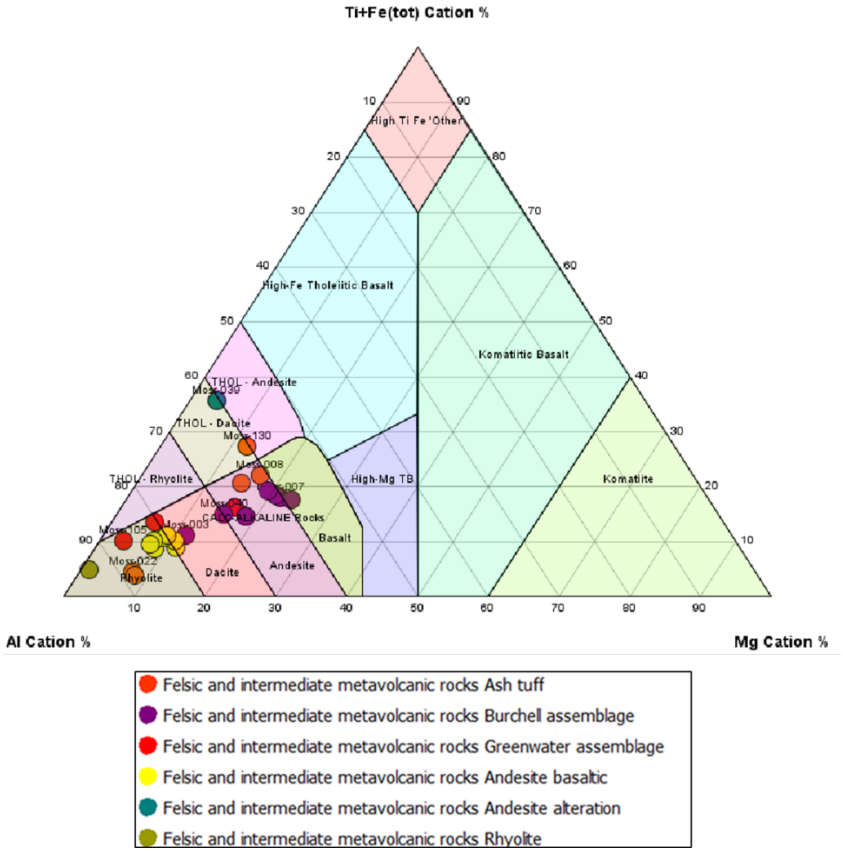

Figure 4.47. Jensen Cation Plot diagram (Jensen, 1976) for felsic and intermediate metavolcanic rocks.

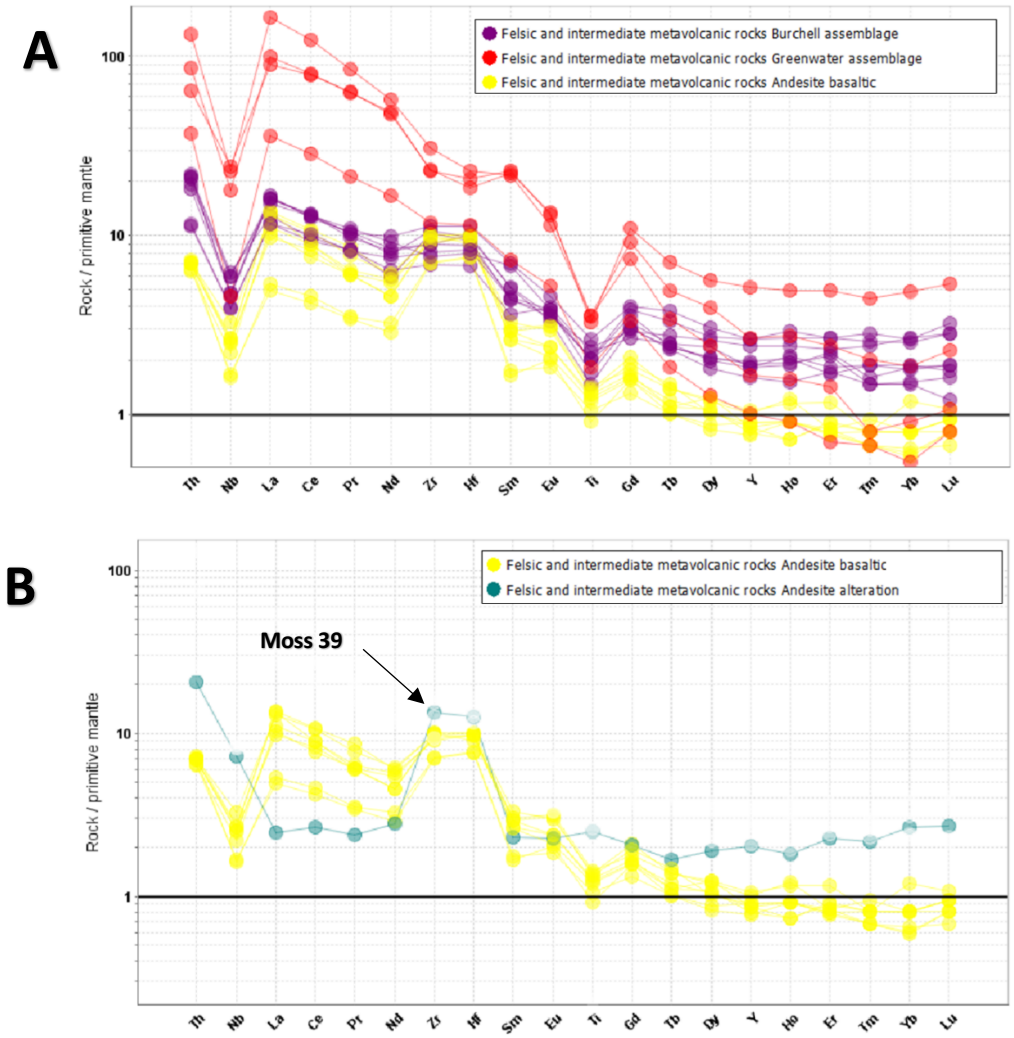

*Figure 4.48. Primitive mantle normalized plot for **A:** for felsic and intermediate rock by assemblages and felsic and intermediate rock andesite basaltic **B:** felsic and intermediate rock andesite basaltic and Moss 39 sample. Normalizing values from Sun and McDonough (1989).*

The first geochemical unit of intermediate felsic and metavolcanic rocks can be divided into groups. The first group related to the Greenwater assemblage show a strong enrichment in LREE (La/Sm = 4.31 - 7.62) and fractionated HREE (Gd/Yb = 4.90 - 8.11). The second group is related to the Burchell assemblage presents less enriched LREE (La/Sm = 2.15 - 4.36) in comparison to the Greenwater assemblage and flat HREE (Gd/Yb = 1.11 - 1.94; Fig. 4.48A). Additionally, a third group, petrographically classified as basaltic andesites, is characterized by

enriched LREE (La/Sm = 2.96 – 5.09) and fractionated HREE (Gd/Yb = 1.49-3.17; Fig. 4.48 B); these samples are found scattered throughout the study area (Fig. 4.1). The Moss 39 sample can be distinguished, which is altered with a value of 12.5% in Fe_2O_3 and pyrite and chalcopyrite in hand sample.

A second unit of intermediate felsic composition group was identified and associated with ash tuff. These are characterized by enriched LREE (La/Sm = 2.37 - 4.28) with flat HREE (Gd/Yb = 1.20 – 1.24). The samples show strong negative anomalies of Nb and Ti, the latter with values below one (Fig. 4.49).

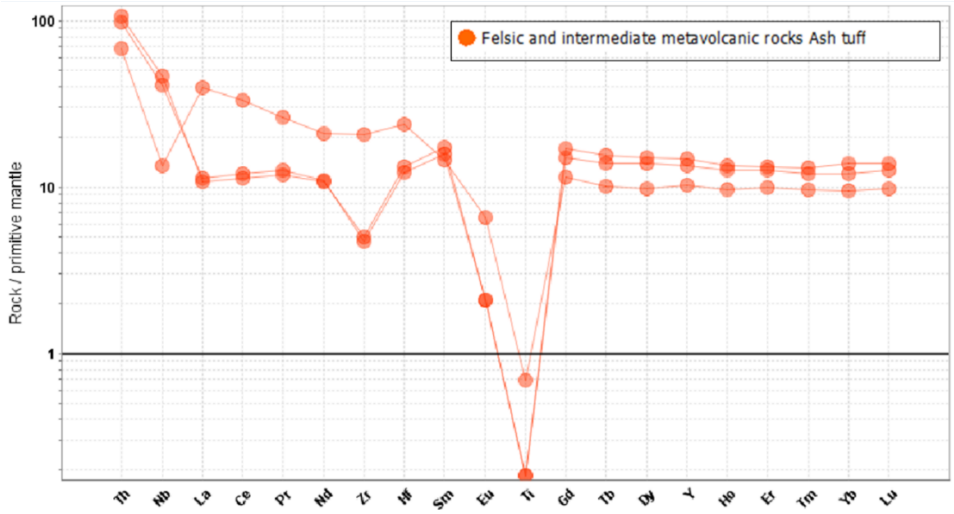

Figure 4.49. Primitive mantle normalized plot for felsic and intermediate metavolcanic ash tuffs. Normalizing values from Sun and McDonough (1989).

The third group corresponds to a sample of felsic and intermediate rhyolite metavolcanic rocks (Fig. 4.50). This has enriched LREE (La/Sm = 6.78) with fractionated HREE (Gd/Yb = 1.53). The sample has strong negative anomalies of Nb and Ti, the latter with values below one (Fig. 4.50).

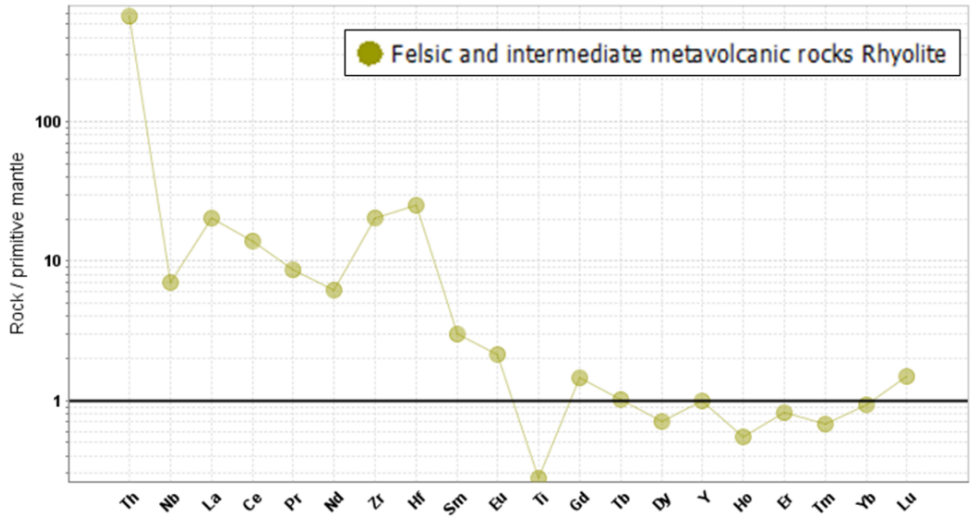

Figure 4.50. Primitive mantle normalized plot for felsic and intermediate metavolcanic rocks rhyolite. Normalizing values from Sun and McDonough (1989).

4.2.4 Clastic sedimentary rocks

The sedimentary rocks were classified by petrography and field observations. The normalized spider diagrams are LREE enriched (La/Sm = 4.02 – 4.22) with flat HREE (Gd/Yb = 1.57 - 2.25) and negative Nb and Ti anomalies (Fig. 4.51).

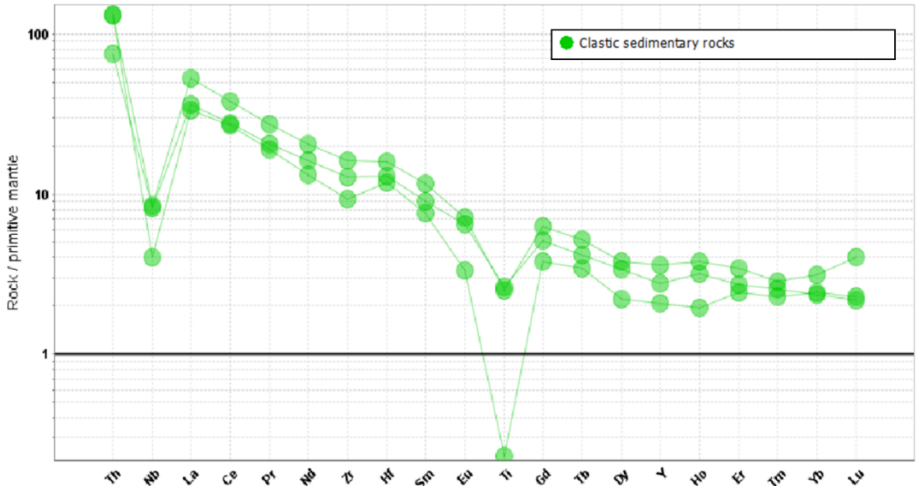

Figure 4.51. Primitive mantle normalized plot for sedimentary rocks. Normalizing values from Sun and McDonough (1989).

4.2.5 Late felsic intrusive rocks and granodiorite.

The intrusive bodies in the study area are represented by six stocks. These are the Greenwater Lake Stock, Moss Lake Stock, Burchell Stock, Obadinaw Stock, Hood Lake Stock and Hermia Lake Stock (Fig. 2.4). The stocks show linear patterns for SiO_2, Fe_2O_3, MgO, CaO and P_2O_5 versus TiO_2 (Fig. 4.54) and scattered patterns for Al_2O_3, K_2O and Na_2O versus TiO_2 (Fig. 4.52), which suggests mobility of some of the major elements.

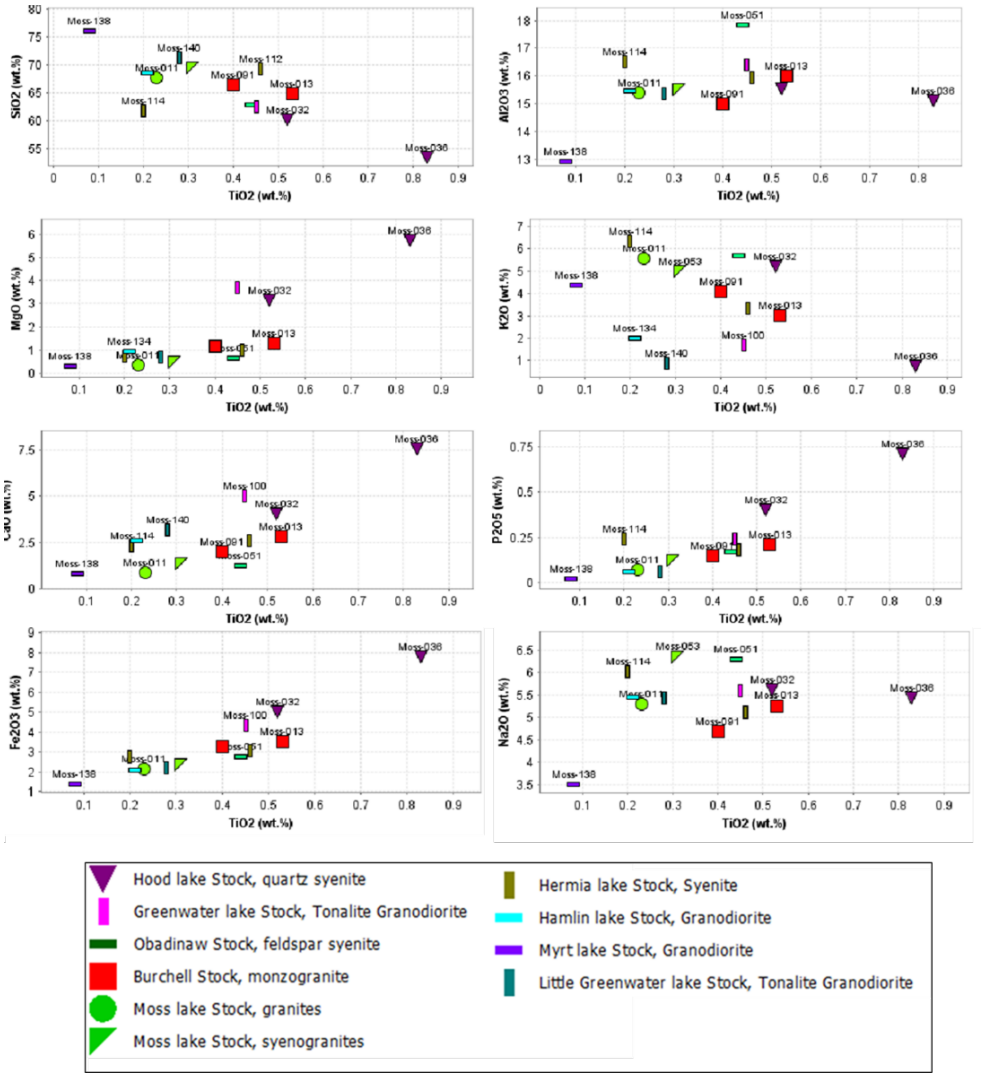

Figure 4.52. Bivariate variation diagrams of TiO_2 vs major element in oxides for late felsic to mafic intrusive rocks and granodiorite.

The stocks were plotted on the TAS diagram modified by Middlemost (1994), with the samples corresponding to monzodiorites, quartz monzonites and syenites (Fig. 4.53). However, this diagram presents some limitations due to the mobility of the major elements since metamorphism or hydrothermal activity can generate changes in composition (Rollinson & Pease, 2021). Therefore, the use of petrography was essential for their classification. All samples correspond to a calc-alkaline series, as shown in the AFM diagram (Fig. 4.54).

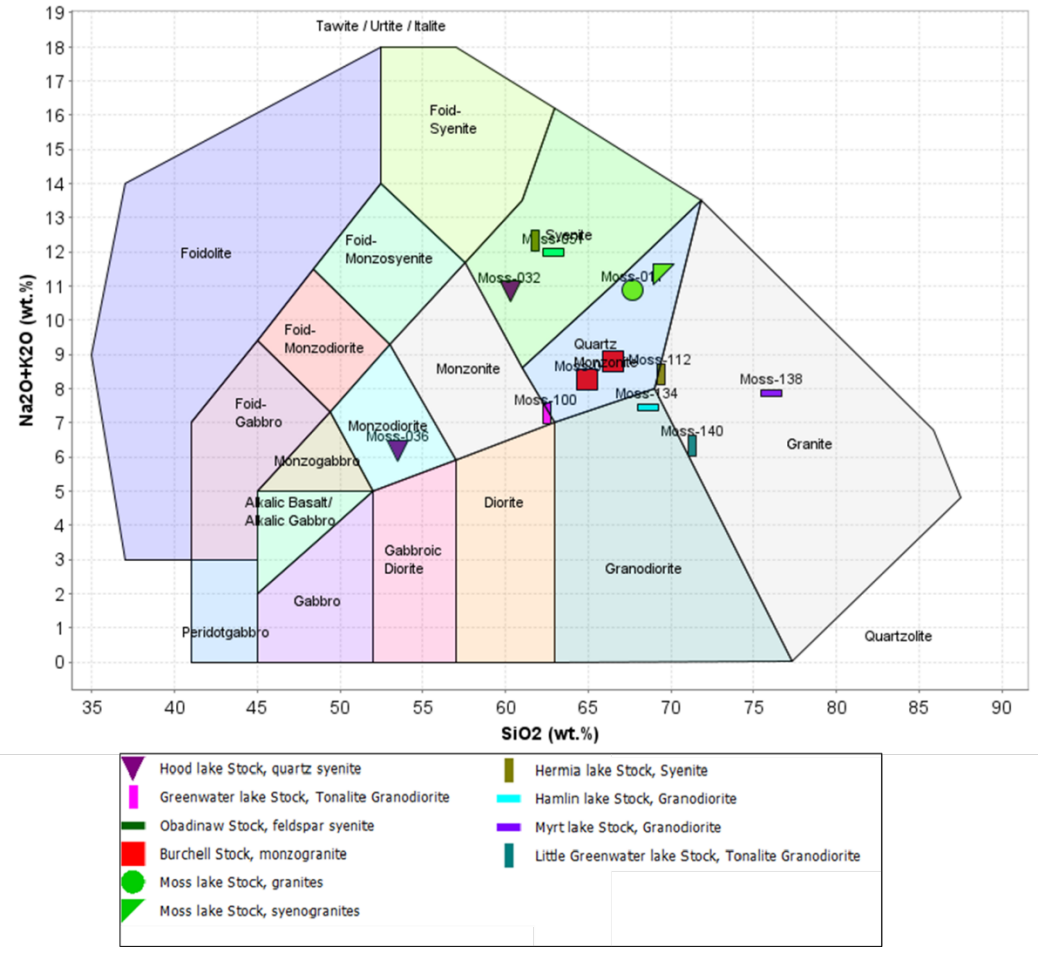

Figure 4.53 TAS diagram modified by Middlemost (1994) for felsic to mafic intrusive rocks and granodiorite.

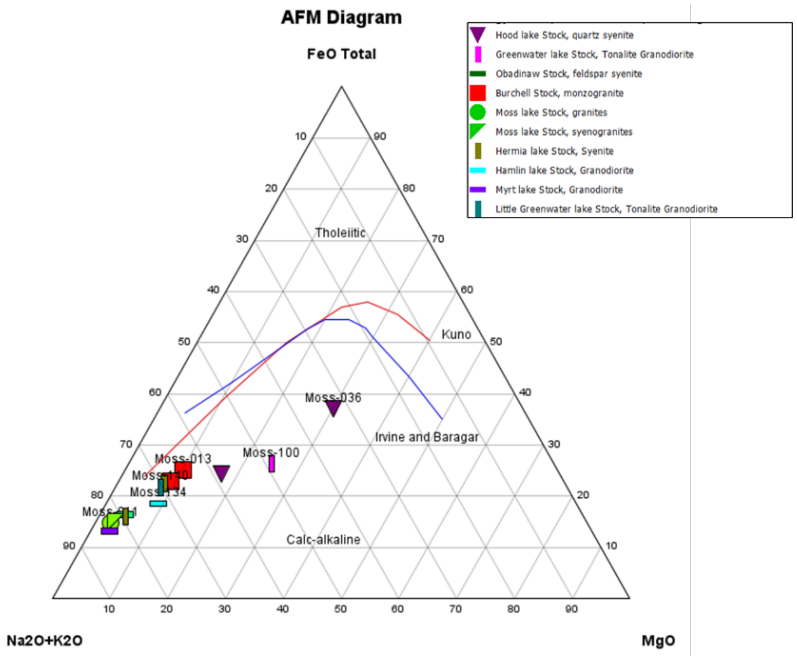

Figure 4.54. AFM diagram for late felsic to mafic intrusive rocks and granodiorite.

All samples show similar trace element patterns on a normalized spider diagram (Fig. 4.55). They are characterized by enriched LREE (La/Sm = 3.16 – 5.74) and fractionated HREE (Gd/Yb = 3.06 – 6.22), with strong negative anomalies of Nb and Ti (Fig. 4.55).

Granodiorite

In the study area, a group of intermediate to felsic intrusive bodies was observed, composed mainly of granodiorites. These correspond to Hamlin Lake Stock, Myrt Lake Stock and Little Greenwater Lake Stock. The samples are composed of granodioritic rocks, with similar major element trends to those observed in the felsic to mafic intrusive rocks (Fig. 4.52). This group of rocks has a clear difference in the element on normalized spider diagrams compared to the late felsic to mafic intrusive rocks (Fig. 4.56). They are characterized by enriched LREE values (La/Sm

= 3.45 – 7.08) and fractionated HREE (Gd/Yb = 2.03 – 2.74) with negative Ti and Nb anomalies (Fig. 4.56)

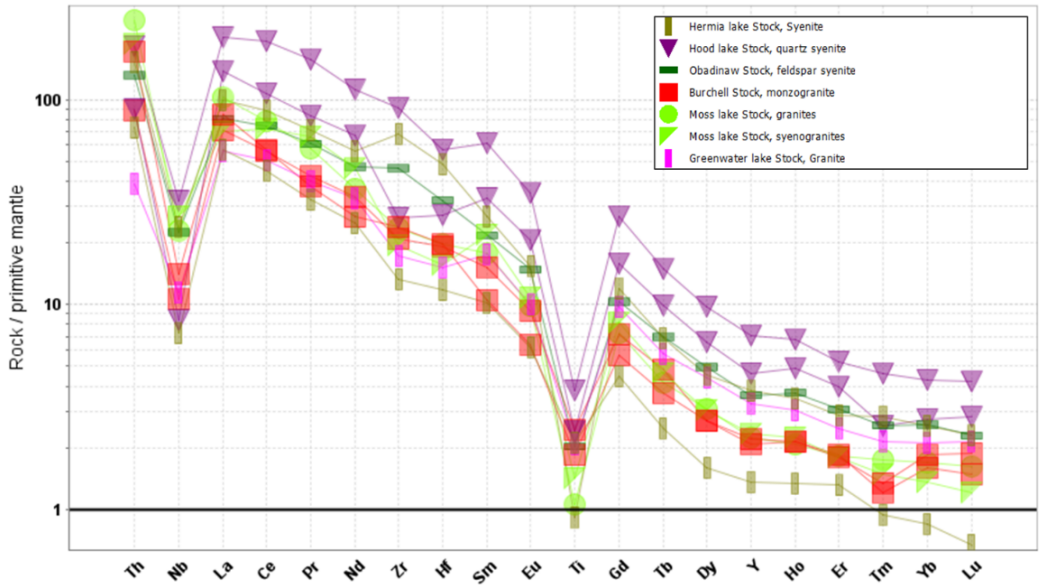

Figure 4.55. Primitive mantle normalized plot for late felsic to mafic intrusive rocks. Normalizing values from Sun and McDonough (1989).

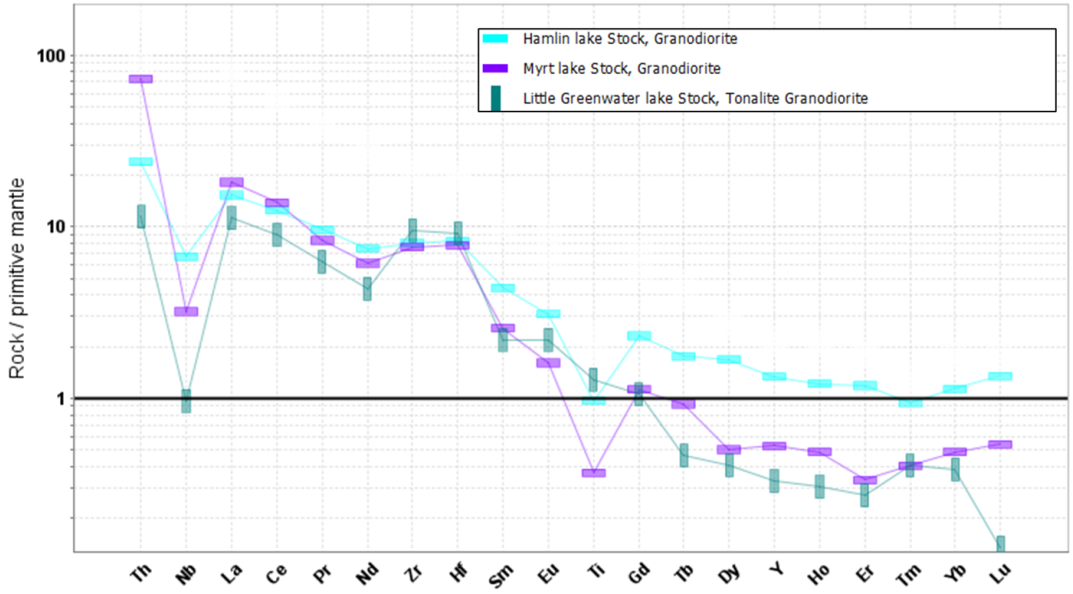

Figure 4.56. Primitive mantle normalized plot for granodiorite rocks. Normalizing values from Sun and McDonough (1989).

4.3 Neodymium Isotopes

Thirteen samples were analyzed for radiogenic Nd isotopes. Sample coverage and location are shown in Figure 4.57, and analytical results are found in Appendix C.

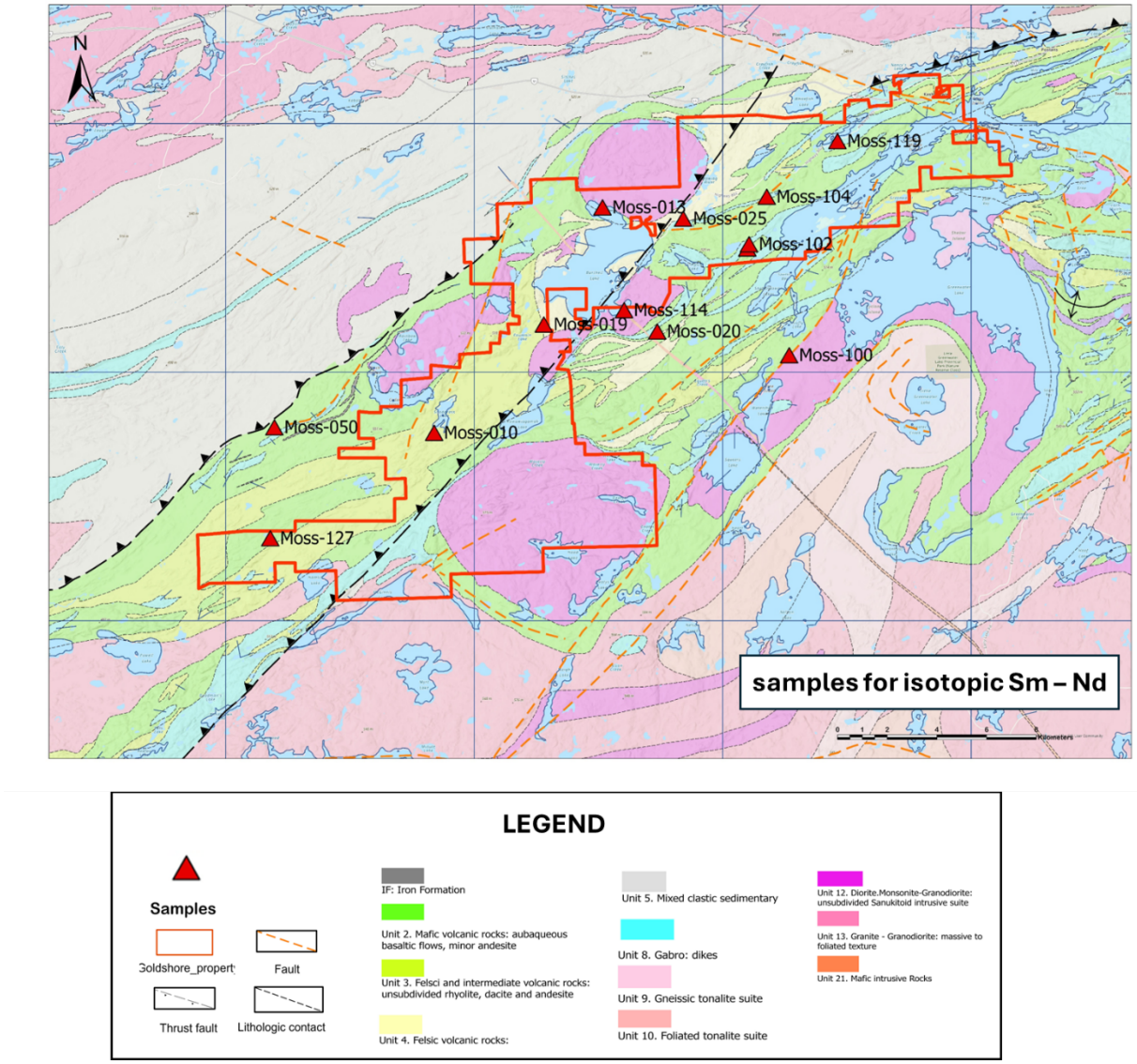

Figure 4.57. Location map of samples for neodymium isotopes. See Appendix E for a higher resolution version of the figure.

Neodymium isotopes were analyzed to identify the magmatic source and assess crustal contamination, as Nd remains relatively immobile during alteration, preserving the primary isotopic signature. This makes Nd isotopes a reliable tracer of crustal inheritance during petrogenesis, with implications for magmatic evolution and tectonic setting. The calculations used an age of 2700 Ma and a CHUR value of 0.512638 to determine εNd(t), summarized in Table 4.2. The dataset includes three intrusive rocks, four mafic metavolcanic rocks, one ultramafic rock, three felsic metavolcanic rocks, one intermediate metavolcanic rock, and one metasedimentary sample.

Table 4.2. Nd isotope results. εNd(t) calculated with age of 2700 Ma.

Sample	Rock Type	Assemblage	$^{143}Nd/^{144}Nd$ (current)	$^{143}Nd/^{144}Nd$ (initial)	εNd(t)
Moss-010	Felsic metavolcanic	Burchell	0.51152	0.50914	0.21
Moss-013	Diorite	Burchell Lake stock	0.51083	0.50917	0.98
Moss-019	Mafic metavolcanic	Burchell	0.51127	0.50922	1.98
Moss-020	Mafic metavolcanic	Greenwater	0.51229	0.50921	1.65
Moss-025	Intermediate metavolcanic	Burchell	0.51086	0.50949	1.74
Moss-027	Ultramafic intrusive	Greenwater	0.51272	0.50921	1.51
Moss-050	Metasedimentary	Burchell	0.51104	0.50912	0.02
Moss-100	Monzonite	Greenwater Lake stock	0.51119	0.50924	2.34
Moss-102	Mafic metavolcanic	Greenwater	0.51263	0.50922	1.71
Moss-104	Felsic metavolcanic	Greenwater	0.51127	0.50924	2.43
Moss-114	Syenite	Hermia Lake stock	0.51087	0.50916	0.91
Moss-119	Mafic metavolcanic	Greenwater	0.51257	0.50923	1.87
Moss-127	Felsic metavolcanic	Burchell	0.51138	0.50919	1.37

4.3 Geochronology

Eleven rock samples were selected for geochronological analysis, which corresponded to intermediate to felsic metavolcanic rocks and felsic intrusive bodies.

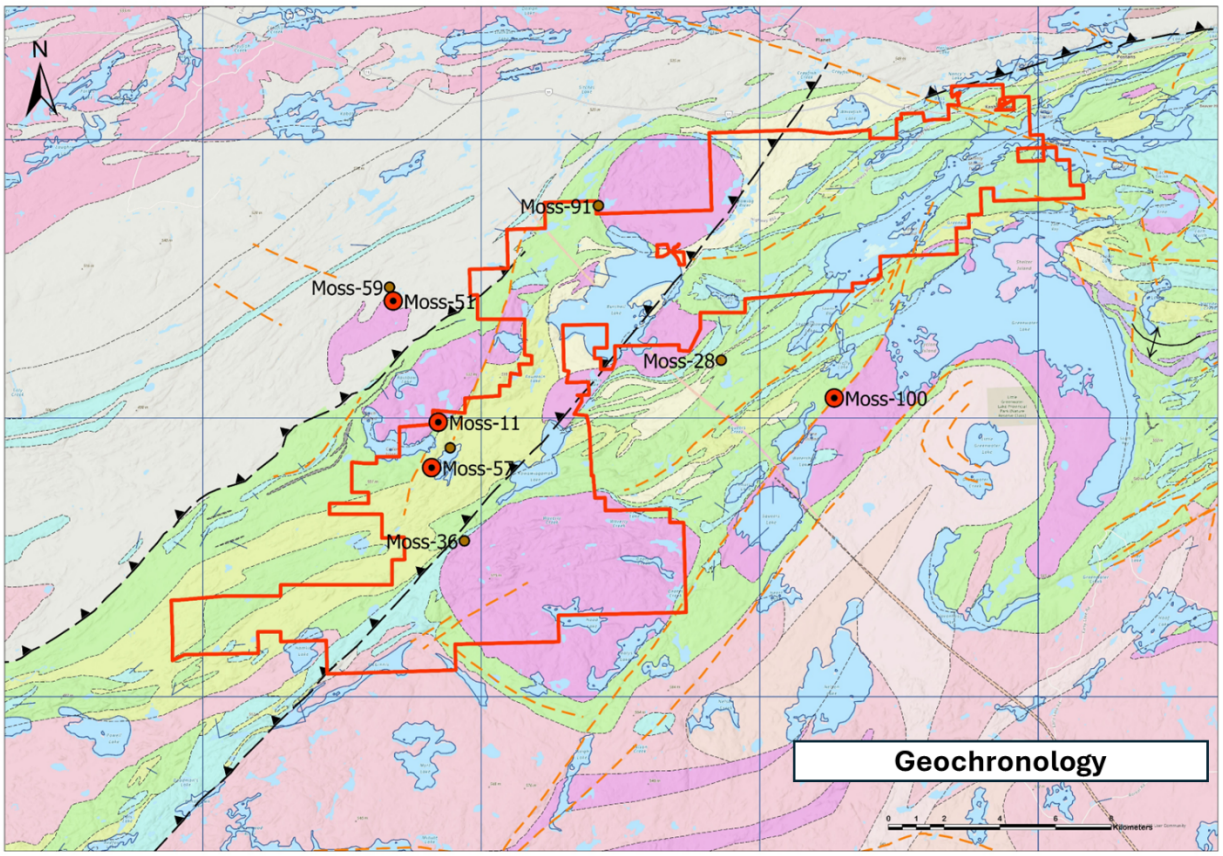

Figure 4.58. Location map of samples for geochronology. Samples with geochronological data are represented by red icons, while samples without data are represented by brown icons. See appendix E for a higher resolution version of the figure.

However, due to the complexity of the geology and the type of rocks found in the work area, sufficient zircon was only recovered from four samples (Moss-11, Moss-51, Moss-57 and Moss-100). The location of the samples taken and analyzed can be seen in (Fig. 4.58). The complete results are presented in Appendix D.

Analyzed zircons were characterized by a Th/U ratio greater than one consistent with an igneous origin for the zircons (Fig. 4.59; Harley et al., 2007).

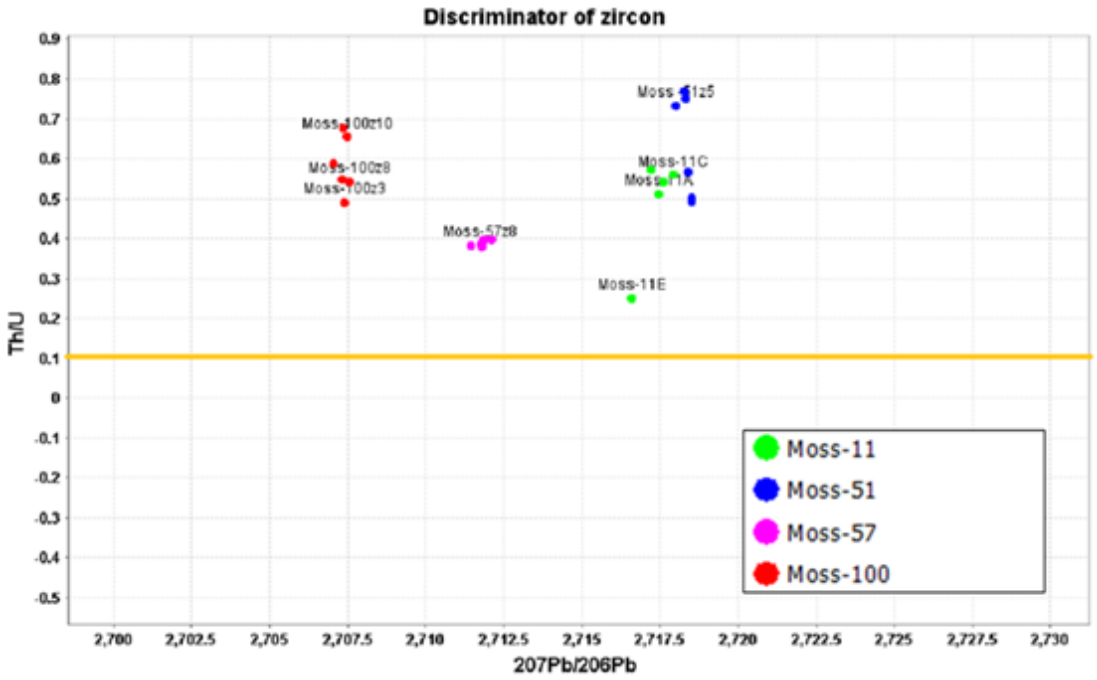

Figure 4.59. Th/U vs $^{207}Pb/^{206}Pb$ diagram for discrimination of zircons igneous or metamorphic origin. The diagram shows twenty-three zircons belonging to the samples from this study, above the yellow line with a ratio 0.1 Th/U value.

Sample Moss 11. The sample corresponds to a felsic intrusive rock with inequigranular holocrystalline texture and fine to medium grain size, and is a syenogranite of the Moss Lake Stock. It consists of orthoclase (70%) and sanidine (1%) of anhedral-type shape crystal. The quartz (15%) is restricted to 100 - 190 sizes polycrystalline; plagioclase (3 %) which exhibits

polysynthetic twinning, biotite (1%) and amphiboles such as hornblende (1%) and zircon (<1%). Alteration minerals included actinolite-tremolite (1%) and epidote (1%). Sericite (1%) and minerals clays (1%) are preferentially located where there is orthoclase. Opaque (5%) minerals are generally associated with hornblende and biotite. Five zircons were extracted and dated, yielding a concordant age of 2716.09 ± 0.45 Ma interpreted to be the crystallization age of the Moss Lake stock (Fig. 4.60)

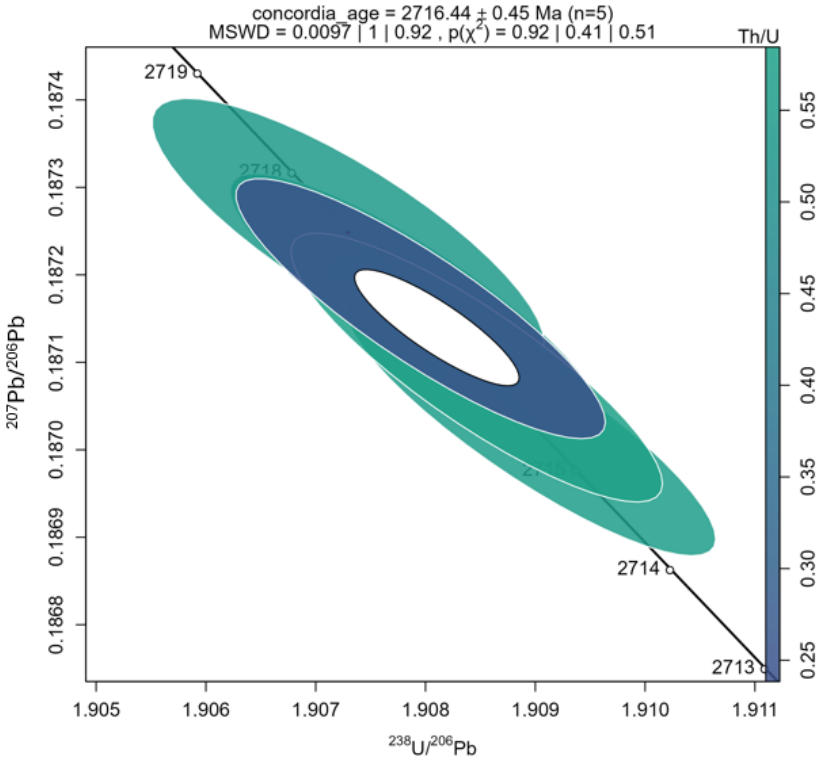

Figure 4.60. Concordia diagrams of the zircon U/Pb samples of Moss 11 sample.

Sample Moss 51 The sample is a felsic intrusive rock with an inequigranular holocrystalline texture and is a quartz syenite from the Obadinaw Stock. Petrographically, the sample consists of orthoclase (80%) with a perthitic texture and anhedral crystals. The polycrystalline quartz (10%) is located between the orthoclase crystals with sizes between 0.2 -

0.7 mm. Plagioclase (3%) presents polysynthetic twinning; the crystals are between the orthoclase crystals like quartz. Biotite (2%) is associated with carbonates, possibly due to alteration. Amphiboles such as hornblende (3%) are aligned with the biotites. Alteration minerals such as carbonates are associated with biotite and calcite (2%), with a well-developed crystalline habit with its characteristic twining, opaque minerals (1%), including magnetite and pyrite, with a size equal to or less than 0.01 mm. Six zircons were extracted and dated yielding a concordant age of 2718.34 ± 0.14 Ma interpreted to be the crystallization age of the Obadinaw Stock (Fig. 4.61)

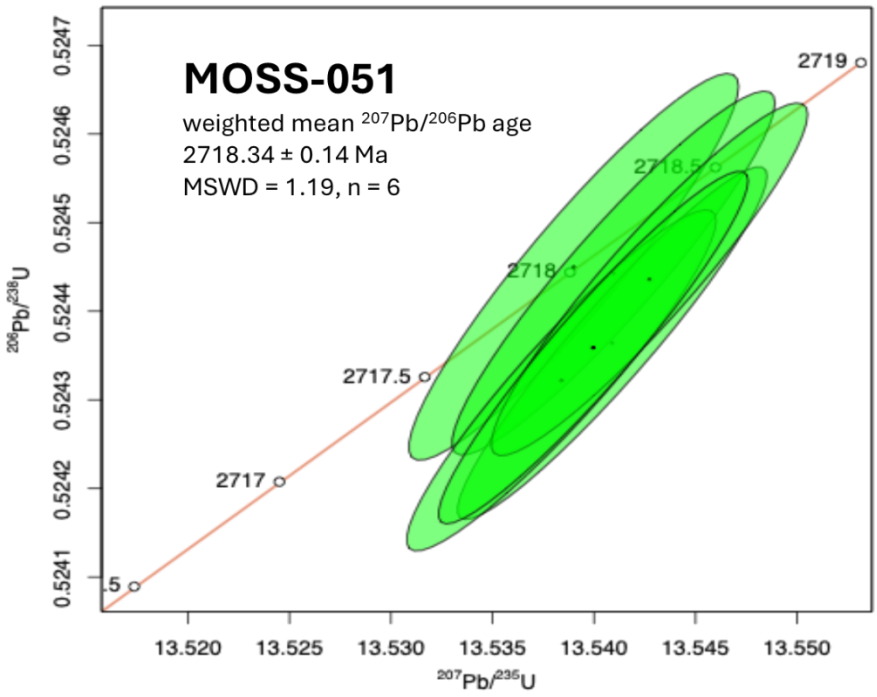

Figure 4.61. Concordia diagrams of the zircon U/Pb from sample Moss 51.

Sample Moss 57 The sample corresponds to a strongly chloritized intermediate porphyritic metavolcanic rock, with hyalocrystalline groundmass. The sample consists of subhedral crystals of plagioclase (20%), and hornblende phenocrysts (5%) with actinolite tremolite within the crystals. Actinolite tremolite (15%) is distributed throughout the sample but is located mainly in

the phenocrystals. The groundmass comprised plagioclase (40%) with sizes 0.06 mm, which is chloritized. Subhedral quartz (10%) is also presented in the groundmass. Alteration minerals included calcite (5%), sericite (2%), and chlorite (2%) which is present throughout the sample. Opaque minerals are magnetite (1%), which is 0.1 mm in size or smaller. Six zircons were extracted and dated yielding a concordant age of 2711.80 ± 0.14 Ma, interpreted to be the crystallization age of the porphyritic metavolcanic rock (Fig. 4.62).

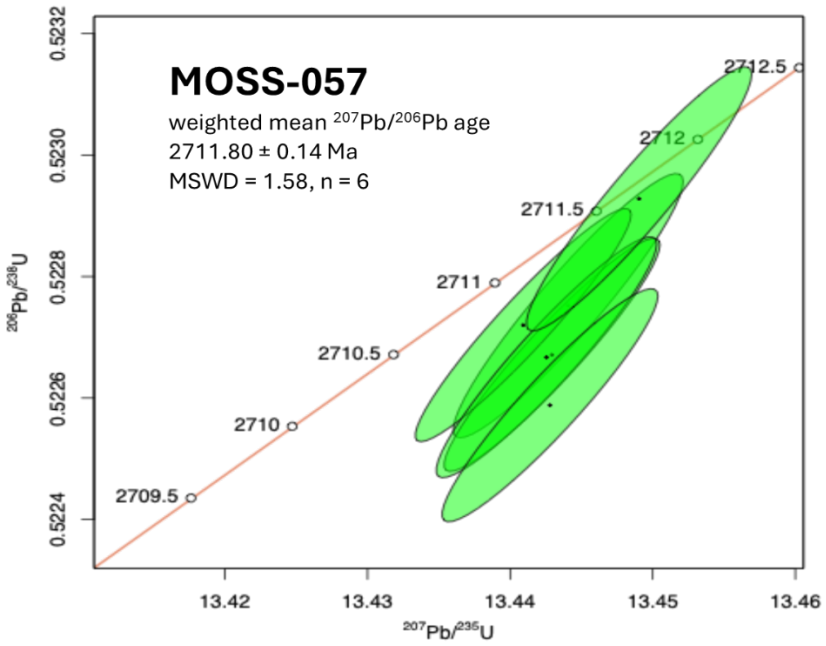

Figure 4.62. Concordia diagrams of the zircon U/Pb sample of Moss 57.

Sample Moss 100

The sample is a felsic intrusive rock with holocrystalline and hypidiomorphic texture, it is classified as quartz monzonite from the Greenwater Lake Stock. Petrographically, the sample is composed of two types of quartz: monocrystalline quartz 1 (10%) 0.5 – 1 mm in size, anhedral quartz 2 (30%) between 0.1 – 0.2 mm. Plagioclase (10%) and microcline (5%) are present as well

as hornblende (2%) and clinopyroxenes (4%), possibly diopside and augite. Accessory minerals are titanite and zircons (<1%) and opaque minerals (<1%), mainly magnetite. Six zircons were extracted and dated, yielding a concordant age of 2707.35 ± 0.14 Ma, interpreted to be the crystallization age of the Greenwater Lake Stock (Fig. 4.63).

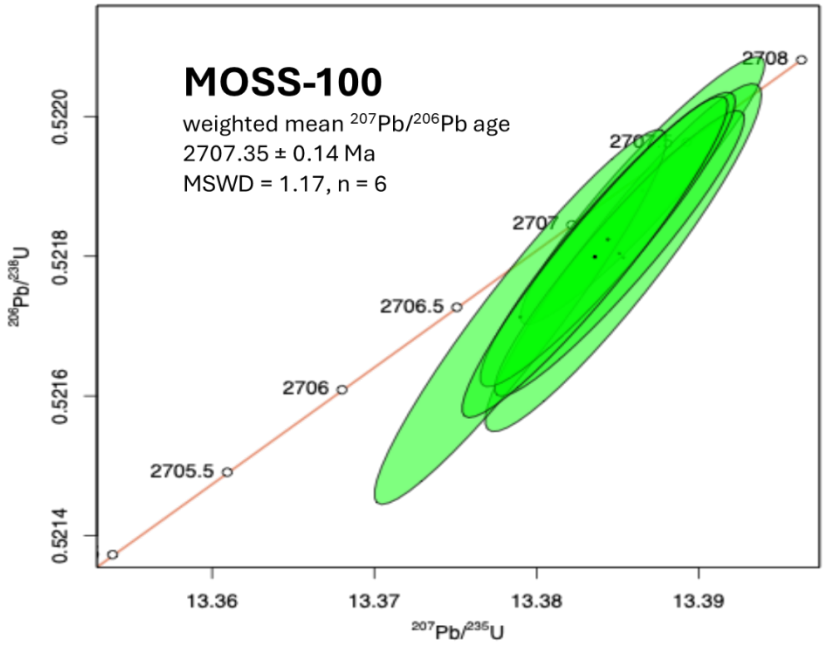

Figure 4.63. Concordia diagrams of the zircon U/Pb from sample Moss 100.

5. Discussion

The results of this study provide insight into the tectonic and magmatic evolution of the Shebandowan Greenstone belt. Several key interpretations and implications emerge by integrating geochemical, petrographic, and geochronological data.

5.1 Geochronology

The ages obtained in the present study range from ~2718 to ~2707 Ma. All zircons analyzed are characterized by Th/U values greater than 0.1, consistent with an igneous origin (Fig. 4.58; Harley et al., 2007). Ages were obtained from the Moss Lake syenogranite stock (Moss 11) which yielded an emplacement age of 2716.09 ± 0.45, the Obadinaw quartz syenite stock (Moss 51) with an age of 2718.34 ± 0.14, an intermediate metavolcanic rock (Moss 57) yielded an age of 2711.80 ± 0.14 (Fig. 5.1) and a quartz monzonite from the Greenwater Lake stock (Moss 100) with an age of 2707.35 ± 0.14. A compilation of volcanic and intrusive lithologies throughout the study area was also used (Corfu, 1986; 1998; Hart, 2007, Stephan et al., in review; Fig. 5.2).

The compilation of age dates suggests a history of magmatic activity spanning from ~2723 Ma for felsic and intermediate metavolcanic rocks (Corfu, 1998, Hart, 2007) to ~2683 Ma for the intrusive rocks of the Burchell Lake stock (Corfu, 1986; 1998; Hart, 2007). The new ages obtained in the present study fit well with the existing geochronological framework (Fig. 5.2).

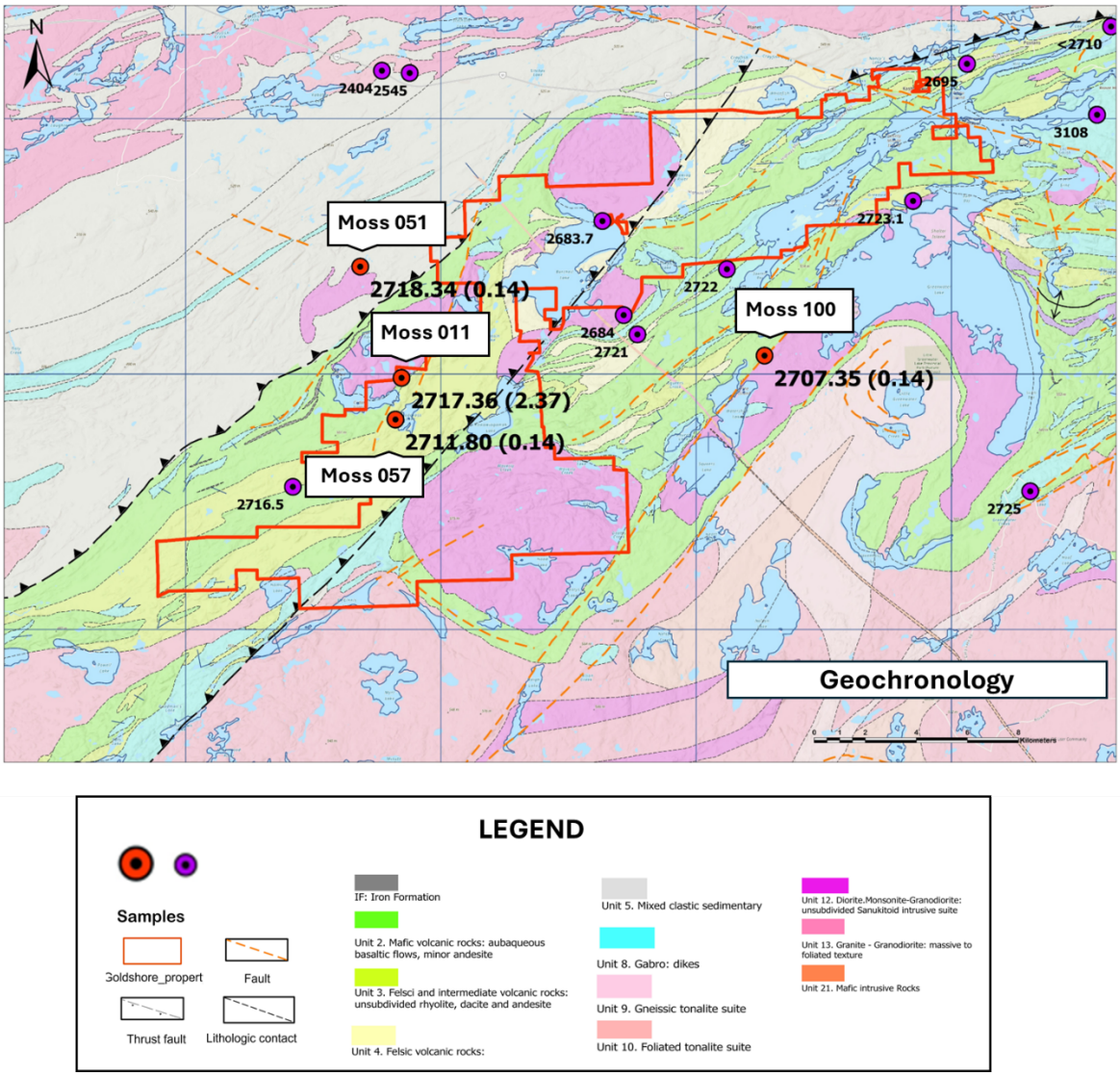

Figure 5.1. Location map of samples used for geochronology. The purple icon samples correspond to the compilation, whereas the red icon samples are from this study. (See Appendix E for a higher resolution version of the figure).

The Burchell assemblage displays intrusive ages (~2718 to ~2683 Ma). Published ages for early felsic and intermediate metavolcanic rocks in this assemblage reach up to ~2723 Ma (Corfu, 1986, 1998; Hart, 2007). The ages obtained in this study for the Obadinaw syenite (2718.34 Ma) and the Moss Lake syenogranite (2716.09 Ma), as well as an intermediate metavolcanic rock

(2711.80 Ma) are within the initial part of the main Burchell volcanic pulse (Corfu et al. 1986; 1998), suggesting significant synvolcanic plutonism contemporaneous with the ongoing arc activity (Fig. 5.2).

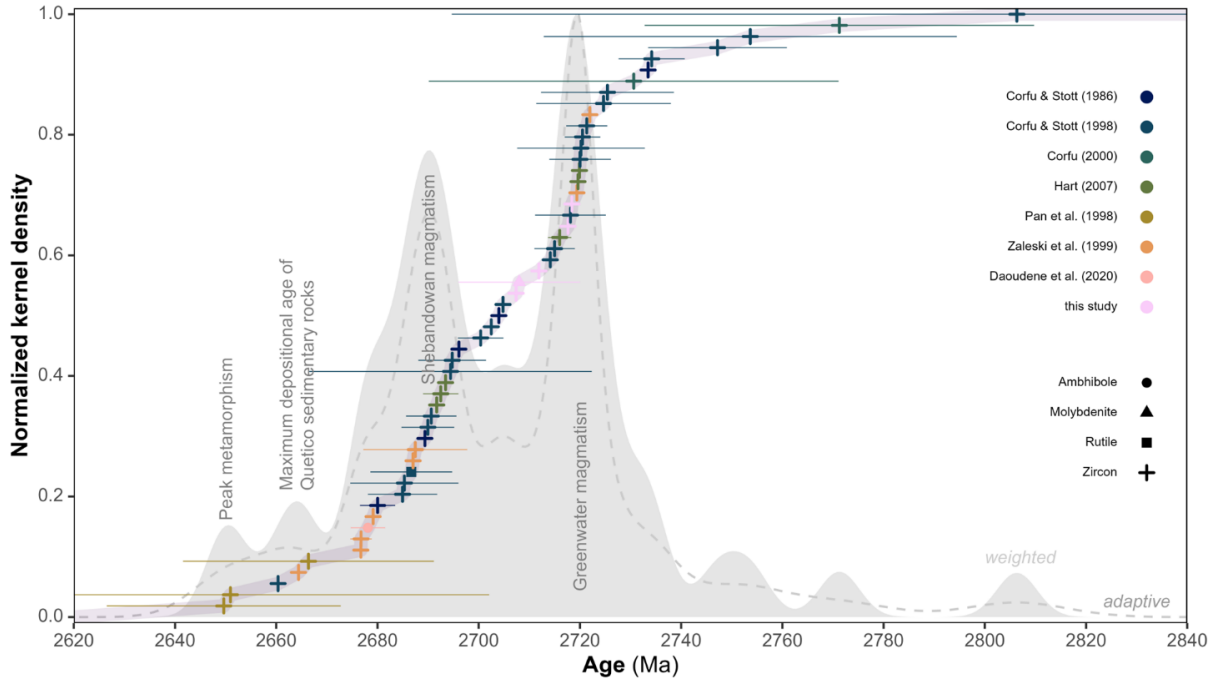

Figure 5.2. Age distribution from rocks from the Shebandowan greenstone belt (Stephan et al., under review). The diagram shows the distribution of ages determined for rocks in the vicinity of the Moss Lake deposit; the normalized density plot shows the age range with the highest density, which is inferred to be the peak age of magmatic activity.

The Greenwater magmatic pulse (Corfu & Stott, 1986; 1998) lies directly within a distinct, slightly younger magmatic pulse, as observed in the ages of the Greenwater Lake stock (2707.35 Ma) and identified in the age distribution diagram (Fig. 5.2). This confirms that significant intrusive activity occurred at this time, independent of the main volcanic peak of the Burchell assemblage and distinct from the later ~2680 Ma intrusion of the Burchell Lake stock. This observation supports an independent magmatic history for the two assemblages. The new accurate

U-Pb zircon ages for the Obadinaw quartz syenite (2718 Ma), the Moss Lake syenogranite (2716 Ma), intermediate metavolcanic unit (2712 Ma), and the Greenwater Lake quartz monzonite (2707 Ma) helping to better define the chronology of magmatism in the region. These data identify specific intrusive and volcanic events, confirm distinctive pulses of magmatism within the Burchell and Greenwater assemblages, and provide crucial temporal markers connecting the main phase of volcanism with later intrusive episodes.

It is important to note that the Moss Lake deposit is located within the Burchell Assemblage, with a reported Re-Os molybdenite age of 2708 ± 12 Ma for the gold mineralization (Nwakanma, 2024). This mineralizing event corresponds to the beginning of the Greenwater magmatic pulse, so the gold mineralization mechanism was likely formed post the emplacement of the intrusions related to the Burchell Assemblage.

5.2 Neodymium Isotopes

The Sm-Nd isotopic system is an effective tool for assessing the mantle origin of igneous rocks and tracing crustal contamination (Rollinson, 2021). Therefore, the Sm-Nd isotope data obtained from this thesis were integrated with the Lodge and Chartran (2013) dataset, which covers a significant portion of the study area (Fig. 5.3). To interpret the Sm-Nd isotope values, εNd(t) values were calculated from both our data and those of Lodge and Chartran (2013), with a CHUR value of 0.512638 (DePaolo, 1981), and an εNd(t) vs. La/Sm plot was created (Fig. 5.4).

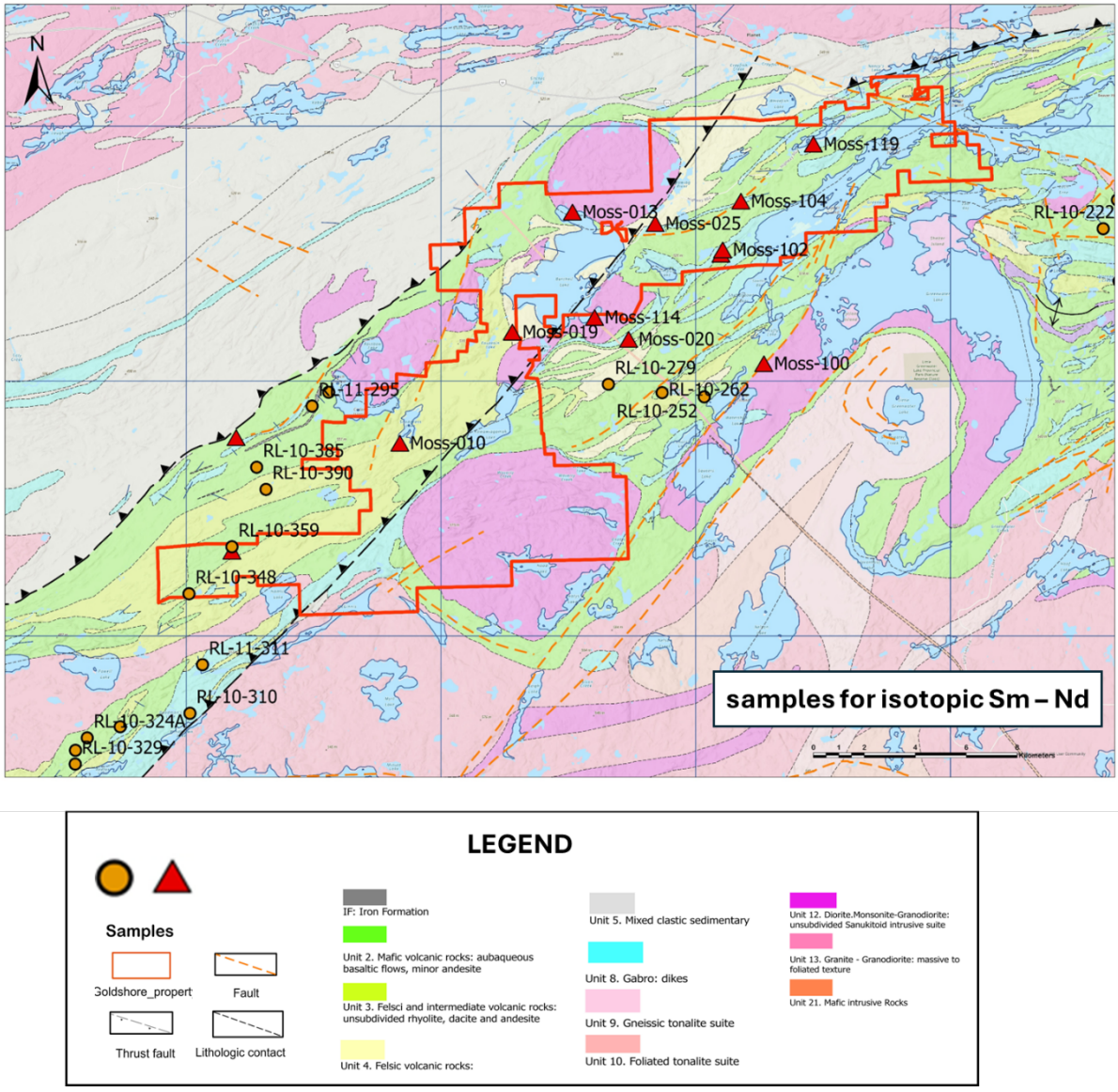

Figure 5.3. Location map of samples chosen for isotopic Sm – Nd work. The red triangle icon samples correspond to this thesis, and the orange circle icon samples correspond to the Lodge and Chartrand (2013). See appendix E for a higher resolution version of the figure.

The samples belonging to the Greenwater assemblage have all their εNd(t) values over +1 (+1 to +2.7; Fig. 5.4), which suggests derivation from depleted mantle sources with minimal participation of older continental crust. The Burchell assemblage generally have positive εNd(t) values (+0.01 to +3.3; Fig. 5.4), however two samples present values lower than one, sample Moss-

10, which corresponds to a volcanic ash tube, and sample Moss-50 which corresponds to greywacke, these εNd(t) values are consistent with the petrographic and geochemical descriptions of the samples, and suggest a partial mixing with older and slightly enriched crustal components. The other samples present values greater than +1 likely reflecting a juvenile magma source derived from the mantle. The felsic intrusive bodies of Hermia Lake (Moss-114) and Burchell Lake (Moss-019) exhibit εNd(t) values less than +1 (Fig. 5.4) and have been texturally classified as diorites and syenites, respectively. These two intrusive bodies are located within the Burchell assemblage and exhibit the youngest ages (~2683 Ma) of the felsic intrusive bodies in the entire study area (Fig. 5.2). This suggests possible partial mixing with older, enriched crustal components. On the other hand, the Greenwater Lake stock (Moss-100), located within the Greenwater assemblage, exhibits εNd(t) values of +2.34 (Fig. 5.4), which could indicate derivation from depleted mantle sources.

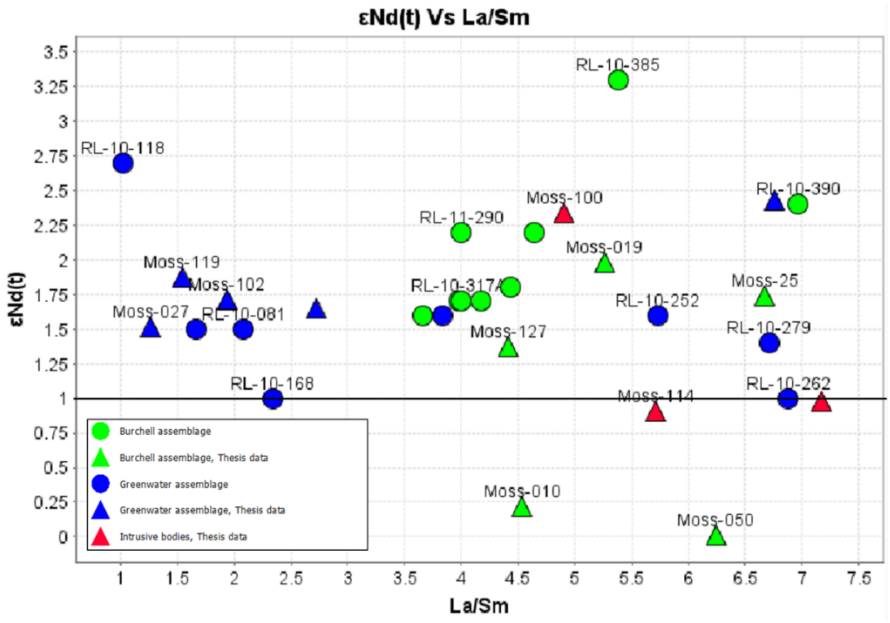

Figure 5.4. Binary diagram of εNd versus La/Sm from samples in the study area. The triangle icon samples correspond to this thesis, and the circle icon samples correspond to the Lodge and Chartrand (2013)

The Sm-Nd isotope data from the study area fall within the range characteristic of depleted mantle sources in the western Superior Province at 2.7 Ga, with εNd values ranging from +1 to +3 (DePaolo, 1981; Shirey & Hanson, 1986; Lodge et al., 2015; Henry et al., 1998, in Tomlinson et al., 2004). Tomlinson et al. (2004) interpreted the lower εNd (+1) values in the western Superior Province to reflect derivation from a less depleted mantle source, such as the asthenospheric plume mantle or arc mantle modified by endogenous contamination, which might correspond to the samples with lower εNd (+1).

5.3 Geochemistry

This section discusses the geochemical results from the Burchell and Greenwater assemblages and integrates data from previous studies (Osmani, 1997; Lodge & Chartrand, 2013), in order to identify and evaluate the tectonic setting as well as possible crustal assimilation or heterogeneity of mantle sources.

5.3.1. Mafic extrusive and intrusive rocks.

The extrusive mafic rocks of the Greenwater assemblage are characterized by flat HREE with enriched LREE and negative Nb anomalies (Fig. 5.5). The LREE enrichment and negative Nb anomalies could reflect either formation in a subduction zone or contamination by continental crust. The εNd(t) values of +1 to +2.75 (Fig. 5.4) are not conclusive, lying at the lower end of the range for depleted mantle at this time and permissive of either model. This is also seen in the diagram of Pearce (2008), where the mafic rocks of the Greenwater assemblage plot outside the

mantle range, with a possible contamination signature (Fig. 5.6), since oblique trends to the mantle array imply mixing or assimilation of crustal source (Pearce, 2008; Lodge, 2016).

During field work, pillow lavas belonging to the Greenwater group were observed (Figs. 4.3 and 4.6), which suggests an oceanic environment. Williams et al. (1991), Osmani (1997), and Corfu et al. (1998) and Londge (2016) reported the presence of rocks with tholeiitic affinity ranging from basaltic komatiite to tholeiitic basalt, located in the eastern part of the Greenwater assemblage. The presence of komatiites within the assemblage suggests involvement of a mantle plume (Williams et al., 1991; Osmani, 1997; Corfu et al., 1998) and is more consistent with an oceanic plateau setting for the mafic rocks rather than an arc source. The absence of inherited zircons suggests a juvenile mantle-derived magma with slight partial mixing with older, slightly enriched crustal components, as argued by Lodge (2016).

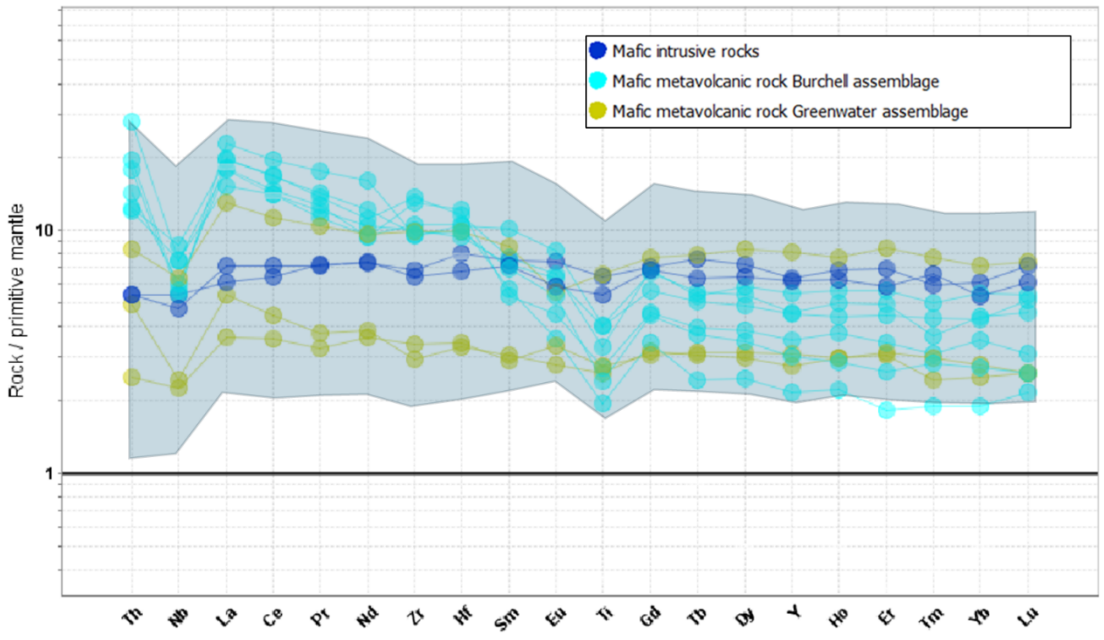

Figure 5.5. Primitive mantle normalized diagram for mafic intrusive rocks and mafic metavolcanic rocks. Normalizing values from Sun and McDonough (1989), In blue shade, reference work values from Lodge and Chartrand, (2013).

The mafic intrusive rocks show flat patterns on primitive mantle normalized diagrams (Fig. 5.5). Hollings et al. (1998) interpreted rocks with these patterns to come from an oceanic plateau environment and they fit most of the diagnostic geochemical and geological features of oceanic plateaus defined by Kerr (2003) making this interpretation plausible for the mafic intrusive rocks of the Greenwater assemblage

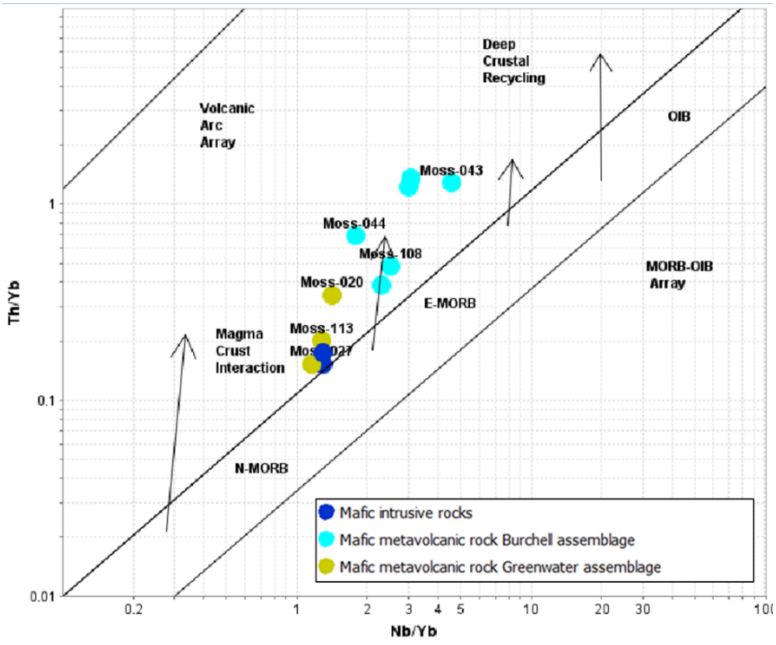

Figure 5.6. Diagram from Th/Yb vs Nb/Yb for mafic and ultramafic rocks (Pearce 2008).

On the other hand, the mafic metavolcanic rocks of the Burchell assemblage are characterized by moderate to enriched LREE and relatively flat HREE, with negative Nb and Ti anomalies (Fig. 5.5). They belong to the calc-alkaline series (Fig. 4.44), with negative niobium and titanium anomalies, consistent with formation in a primitive arc environment or assimilation of metasomatized amphibolitic crust (Smith et al., 1997; Pearce & Stern, 2006). Additionally, they have weak positive Eu anomalies, indicating plagioclase fractionation (Fig. 4.46). The

geochemistry of the mafic rocks is consistent the work of Osmani (1997) for the Burchell assemblage, who observed a trend of calc-alkaline basalts with patterns ranging from flat to slightly enriched LREE (Fig. 5.7). These observations suggest that the mafic rocks of the Burchell assemblage would correspond to a primitive arc environment, unlike the mafic rocks of the Greenwater assemblage, which correspond to an oceanic plateau.

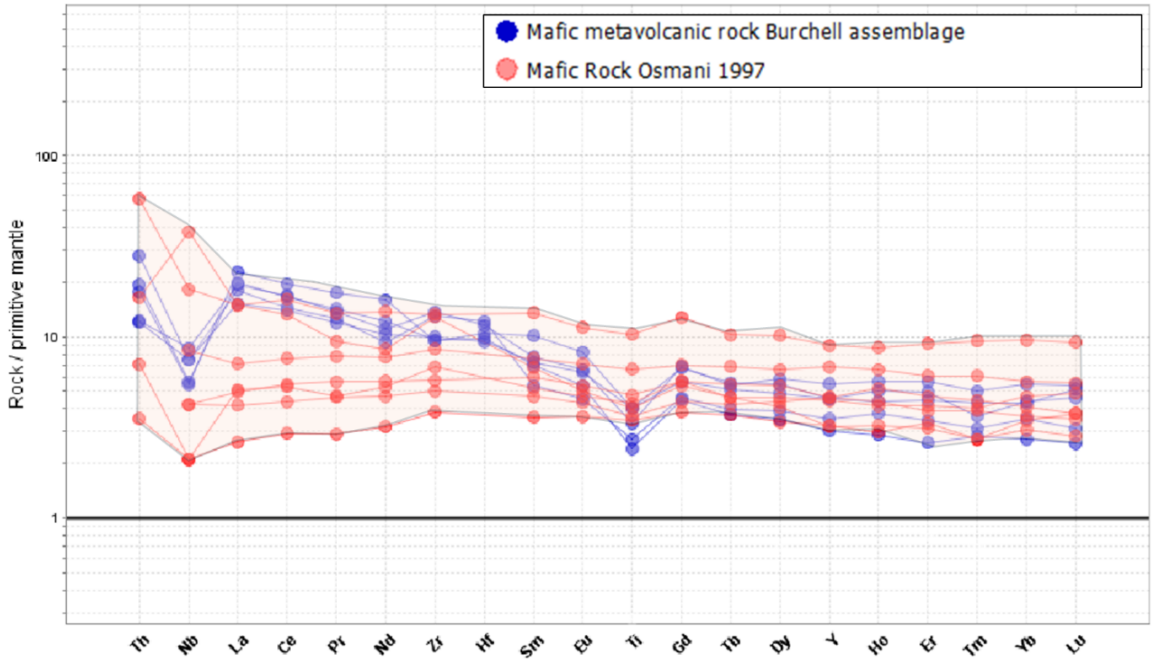

Figure. 5.7. Primitive mantle normalized diagram for the Burchell assemblage mafic rock suites. Normalizing values from Sun and McDonough (1989).

5.3.2. Felsic and intermediate metavolcanic rocks

The felsic and intermediate metavolcanic rocks of the Greenwater assemblage are geochemically subdivided into three distinct units. The first unit is characterized by LREE enrichment coupled with flat HREE patterns (Fig. 4.49). A second unit, exclusive to the Greenwater assemblage, comprises andesitic to dioritic compositions that exhibit enriched LREE,

fractionated HREE, and pronounced negative Nb and Ti anomalies (Fig. 4.48A). The third unit consists of porphyritic basaltic andesites featuring a holocrystalline groundmass; these rocks display moderately sloped REE patterns and are distinguished by positive Zr and Hf anomalies (Fig. 5.8).

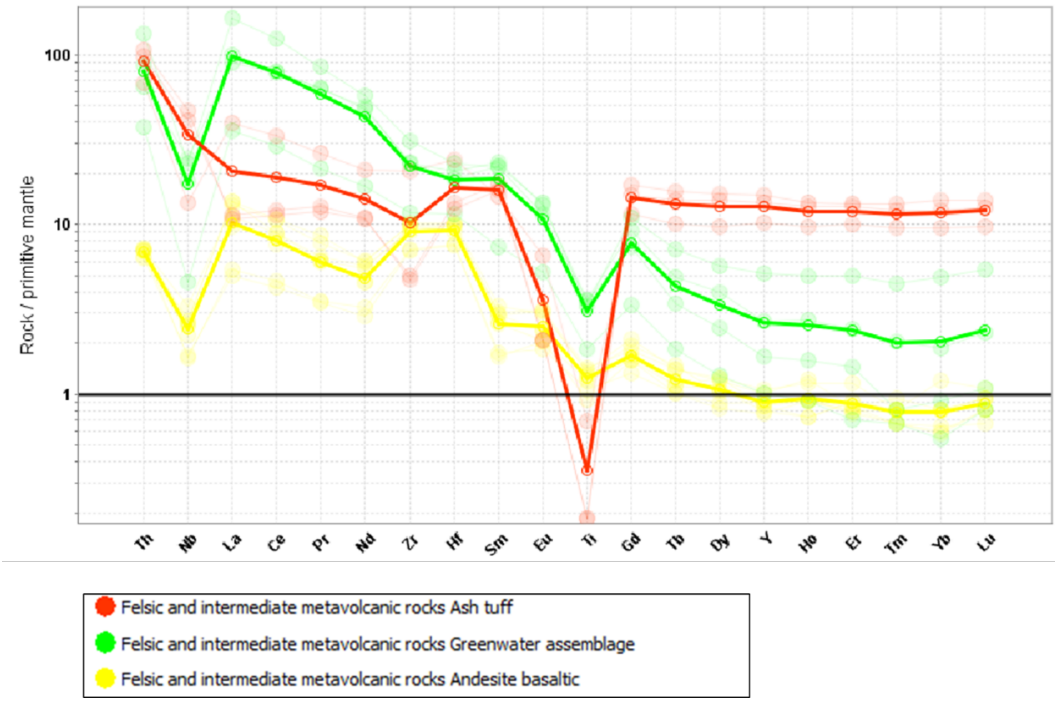

Figure. 5.8. Primitive mantle normalized diagram for the Greenwater assemblage felsic and intermediate rock suites. Normalizing values from Sun and McDonough (1989). Note the highlighted lines representing the average for each of the three units.

Similarly, the felsic and intermediate metavolcanic rocks of the Burchell assemblage are categorized into four geochemical units (Fig. 5.9). The first unit consists of ash tuffs and fine-grained volcaniclastic rocks, showing LREE enrichment and moderately fractionated HREE (Figs. 4.16, 4.49). The second unit is composed of basaltic andesites, with moderate LREE enrichment, flat HREE, and positive Zr and Hf anomalies (Fig. 4.48B); sample Moss-39 likely belongs to this unit, though its lower Thorium (Th) values, less REE fractionation, and high Loss on Ignition

(LOI) suggest alteration may have influenced its signature. A third unit, exclusive to the Burchell assemblage, includes andesitic to diorite rocks with moderately sloped REE patterns and no Zr or Hf anomalies (Fig. 4.48A). Finally, the fourth unit comprises rhyolites marked by strong LREE enrichment, flat HREE, high Th values, and negative Ti anomalies (Fig. 4.50).

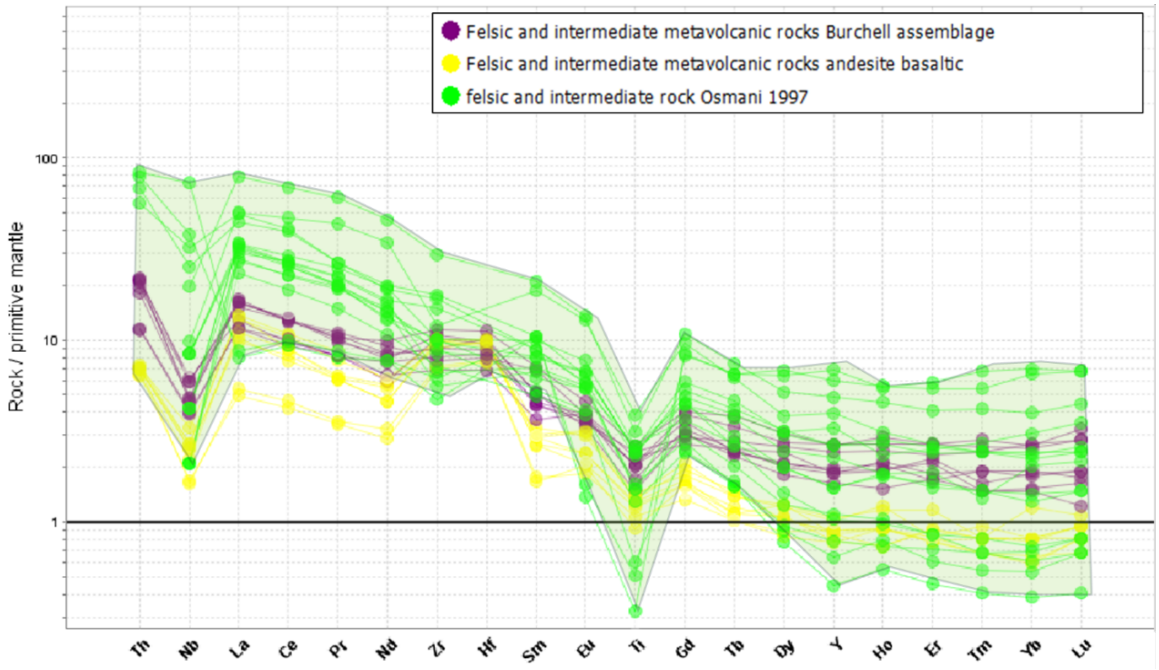

Figure. 5.9. Primitive mantle normalized diagram for the Burchell assemblage felsic and intermediate rock suites. Normalizing values from Sun and McDonough (1989).

Regardless of geochemical subdivisions within each assemblage, the felsic and intermediate metavolcanic rocks from the Greenwater and Burchell assemblages share a number of characteristics. These include enriched LREE, relatively flat HREE patterns, and negative Nb and Ti anomalies. Furthermore, these rocks exhibit a calc-alkaline affinity, with compositions ranging from andesite to rhyolite, which would indicate a subduction-related magmatic environment, consistent with Smith et al. (1997) and the interpretations of Pearce and Stern (2006).

Notably, the flatter HREE patterns (Fig. 5.8) could represent shallower melts. These patterns suggest an arc system that would generate melts from low-grade partial melts from a mafic source with minimal fractionation (Hart et al., 2004). However, HREE characteristics only provide information on the depth of melting and do not reliably distinguish between arc and back-arc.

5.3.3. Clastic sedimentary rocks, Quetico basin

The sedimentary rocks are predominantly greywacke and are part of the Quetico basin. The samples show a positive slope in the LREE and relatively flat HREE, with negative Nb and Ti anomalies (Fig. 4.51). One sample has a greater slope in the Ti and HREE values (Fig. 4.51), which could indicate more than one source for the sediments. This is consistent with models for the Quetico terrane, where different sources are proposed for the formation of sedimentary rocks (Williams, 1991; Corfu et al., 2007).

5.3.4. Intrusive rocks

The felsic and granodiorite intrusive rocks in the study area can be divided into two groups: the first group is composed mainly of granodiorites and includes the Hamlin Lake, Myrt Lake and Little Greenwater Lake stocks (Fig. 2.4). The second group consists of granites, syenogranites, mozogranites and syenite; and includes the Greenwater Lake, Moss Lake, Burchell, Obadinaw, Hood Lake and Hermia Lake stocks (Fig. 2.4). On a TAS diagram, there is a clear tendency for the first group to plot in the granite and granodiorite field whereas the second group plot in the syenite to monzodiorites field (Fig. 4.53). The intrusive bodies show two geochemical trends that coincide with the initial classification of granodiorites (first group) and granites (second group).

The granodiorites have a moderate slope for LREE (La/Sm = 3.45 – 7.08) and flat HREE (Gd/Yb = 2.03 – 2.74), with primitive normalized mantle values close to or less than 1 (Figs. 4.55 and 4.56). In contrast, the granites are characterized by steep LREE (La/Sm = 3.16 – 5.74) and HREE (Gd/Yb = 3.06 – 6.22), with values greater than or close to 1 for HREE (Fig. 4.56).

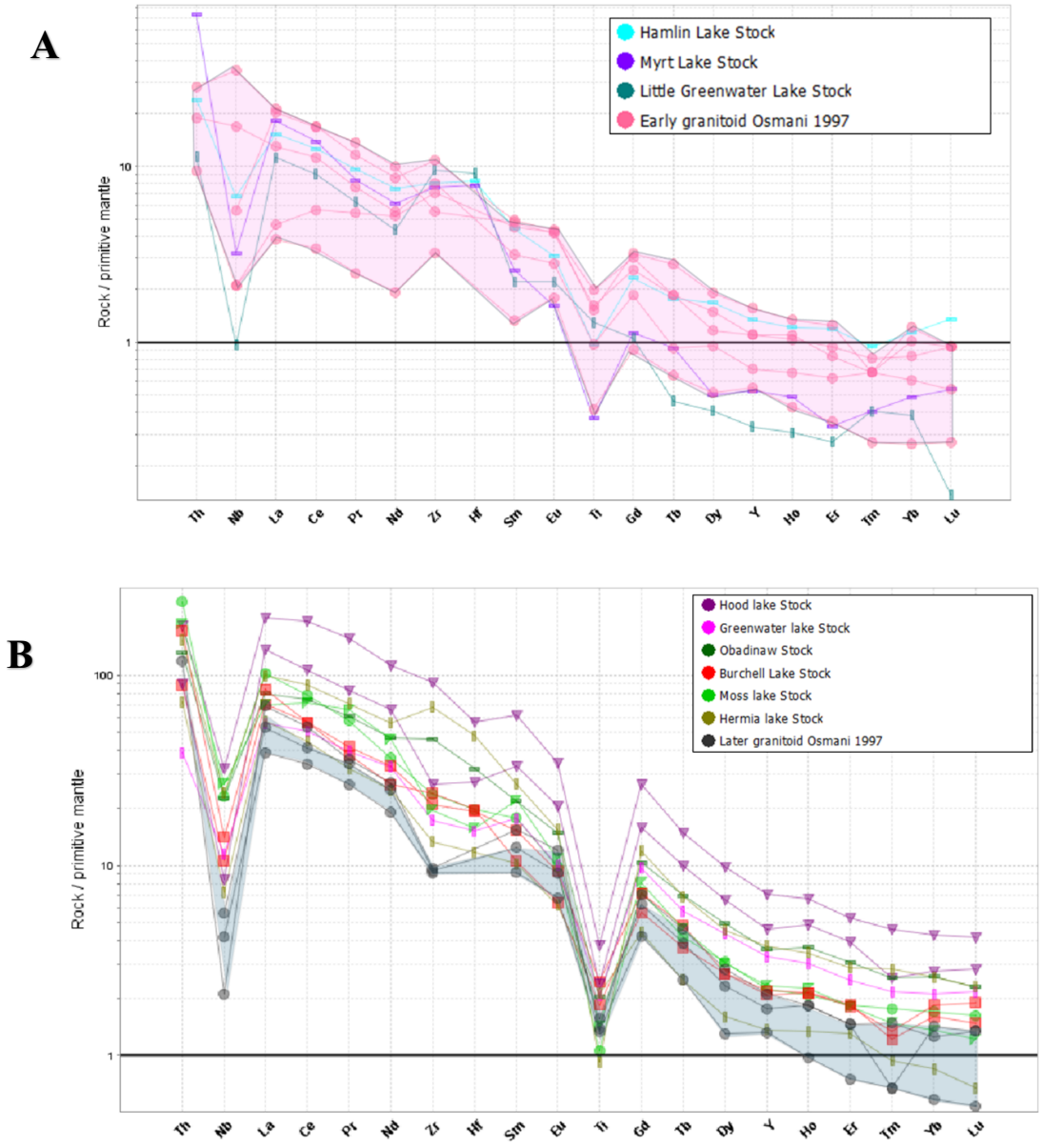

Figure. 5.10. Primitive mantle normalized diagram based on data from intrusive body rock suites. Normalizing values from Sun and McDonough (1989). ***A****. Early Archean granodiorite rocks (Osmani, 1997).* ***B****. Late Archean granodiorite rocks (Osmani, 1997)*

These two geochemical trends were also observed in the work of Osmani (1997), who highlighted the difference between intrusive bodies and proposed that the granodiorite bodies were early Archean (Fig. 5.10A), whereas the granitic intrusions were late Archean in age (Fig. 5.10B; Osmani, 1997). An important aspect is that all intrusive rocks present negative Nb and Ti anomalies, consistent with formation in a subduction environment.

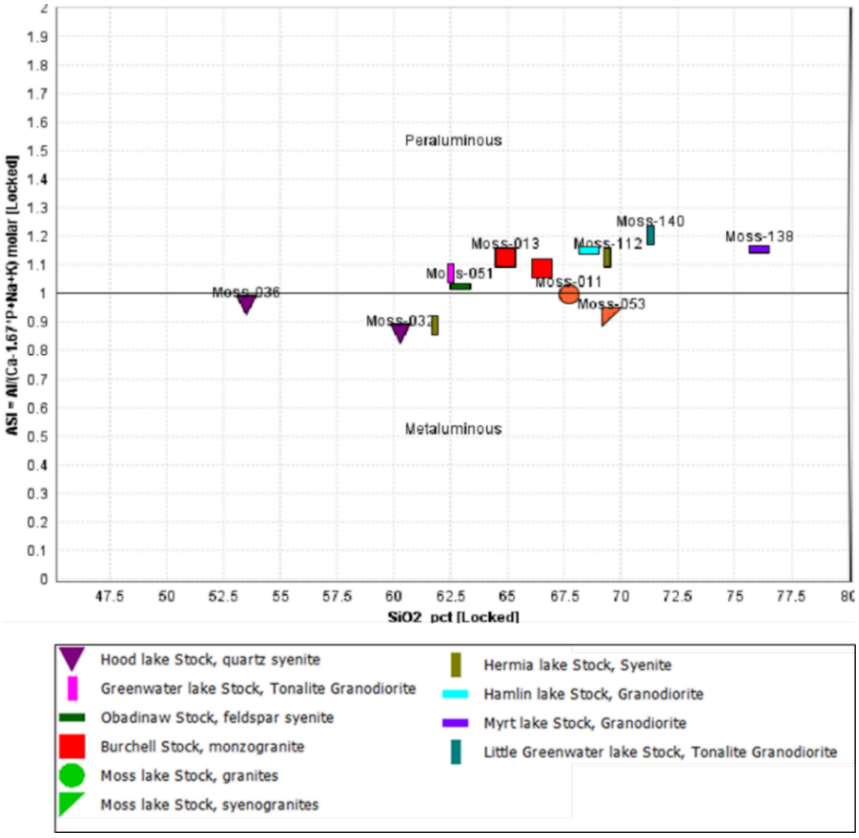

Figure 5.11. Plot of aluminum saturation index vs SiO_2 modified after Frost & Frost (2008) for felsic intrusive rocks and granodiorite.

The granodiorite bodies show enriched LREE (Fig. 4.56) and negative Nb and Ti anomalies. They also have strong negative Y and Yb anomalies (Fig. 4.56) and peraluminous ASI values of the very close and more than 1 (Fig. 5.11). These geochemical trends suggest partial

melting of hydrous amphibolite rocks with pressures between 12 and 15 kbar and depths greater than 40 km, as well as moderate temperatures between 700 and 900 degrees (Condie, 1993; Rapp & Watson, 1995; Martin & Moyen, 2002). However, the Myrt Lake stock and Hamlin Lake stock exhibit a moderate slope for HREE in the spider diagrams (Fig. 4.56), with normalized mantle values greater than 1. This suggests shallow melting depths with the general characteristics of an Archean hybrid granite as classified by Laurent et al. (2014).

In contrast, the granite bodies show a steep slope for LREE and HREE, with values greater than or close to 1 for HREE (Fig. 4.56) and slightly peraluminous or very close to the ASI value of 1 (Fig. 5.11). This suggests they were formed at depths between 10 to 30 Km and moderate temperatures between 650 to 750 degrees (Condie, 1993; Rapp & Watson, 1995; Martin & Moyen, 2002).

All intrusive bodies plot in the calc-alkaline rock field (Fig. 4.54), and the molar ratio Aluminum Saturation Index (ASI; Frost & Frost, 2008) indicates that the samples are slightly peraluminous (<1.3 ASI; Fig. 5.11). This suggests moderate aluminum enrichment, potentially reflecting partial melting of metasedimentary sources or crustal assimilation during magmatic evolution (Frost & Frost, 2008). In contrast, samples from the Hood Lake and Hermia Lake stocks, which include quartz syenites and syenites, are metaluminous but very close to the ASI value of 1 (Fig. 5.11), which could indicate an igneous source with limited crustal interaction (Frost & Frost, 2008). The variation in ASI among different stocks points to heterogeneous regional magmatic sources and processes. The methodology proposed by Laurent et al. (2014) was used to determine a better classification of the felsic intrusive rocks. This methodology proposes a classification of Archean granite bodies based on the nature of their sources, classifying Archean felsic intrusive

bodies into TTG, sanukitoid, biotite-mica granites, and hybrid granites (Laurent et al., 2014; Fig. 5.12).

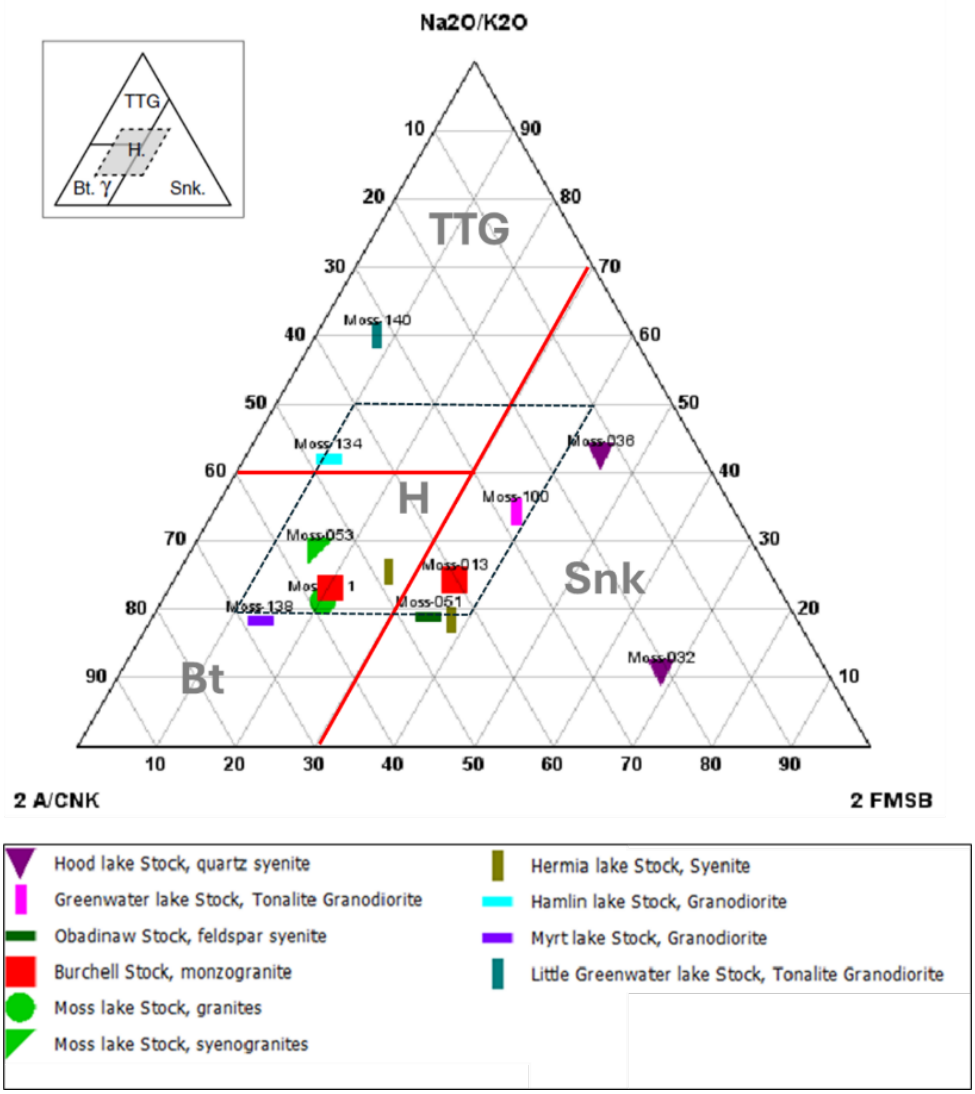

Figure 5.12. Ternary classification diagram of Laurent et al. (2014) showing the felsic intrusive rock affinity. Ternary classification diagram for late-Archean granitoids: 2 ∗ A/CNK (molar $Al_2O_3/[CaO + Na_2O+K_2O]$ ratio); Na_2O/K_2O ratio; 2 ∗ (FeOt + MgO)wt.% ∗ (Sr + Ba)wt.% (=FMSB; Laurent et al., 2014). TTG = Tonalite trondhjemite granodiorite, Snk = Sanukitoids, Bt = Biotite- two mica granites, H= Hybrid granites.

Based on geochemical discrimination and the methodology proposed by Laurent (2016), the intrusive felsic bodies were divided into three groups. The first group of felsic intrusive rocks

are granodiorites that exhibit enriched LREE and fractionated HREE trends with low Eu values (<0.5 ppm), consistent with tonalite-trondhjemite-granodiorite (TTG; Moyen, 2011). The TTG rocks are generally composed of calc-alkaline magmatic rocks with slightly peraluminous characteristics (Fig. 5.11). The TTG rocks are rich in silica and have a low content of ferromagnesium oxides (FeOt + MgO + MnO + TiO_2) less than or equal to 5 wt%, values that are consistent with this first group of felsic intrusive rocks in this study (Fig. 5.13).

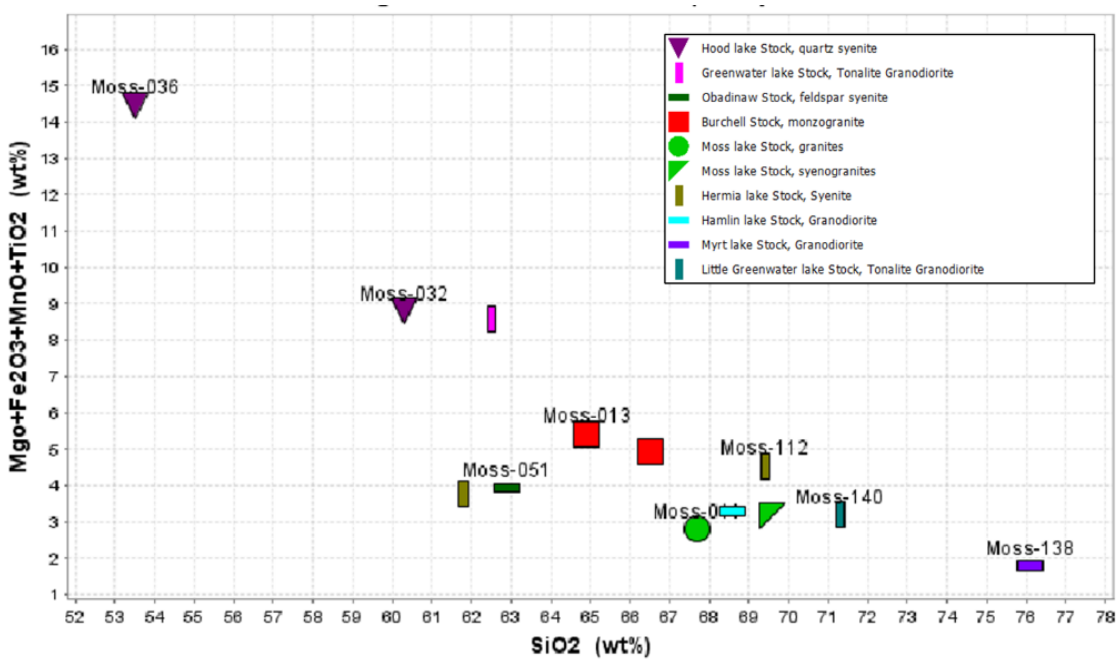

Figure 5.13. Diagram, sum of "mafic" oxides (FeOt+MgO+MnO+TiO_2) vs. SiO_2 (Laurent et al., 2014).

Laurent et al. (2014) proposed that, in general, TTGs can vary according to their geochemical signatures, with bodies with high Y values and low Sr contents corresponding to a "low-pressure" zone and bodies with low Y values and low Sr contents corresponding to a "high-pressure" zone (Fig. 5.14). Furthermore, they argued that late Archean TTGs (<3.0 Ga) are richer in Sr and poorer in Y than older TTGs (Champion & Smithies, 2007; Martin and Moyen, 2002 in

Laurent et al., 2014), which would correspond to a "high-pressure" formation zone. However, Hamlin and Myrt Lakes stocks present higher HREE (Fig. 4.58) and lower Sr values (Fig. 5.14), suggesting that these bodies correspond to Archean hybrid granites (Laurent et al., 2014).

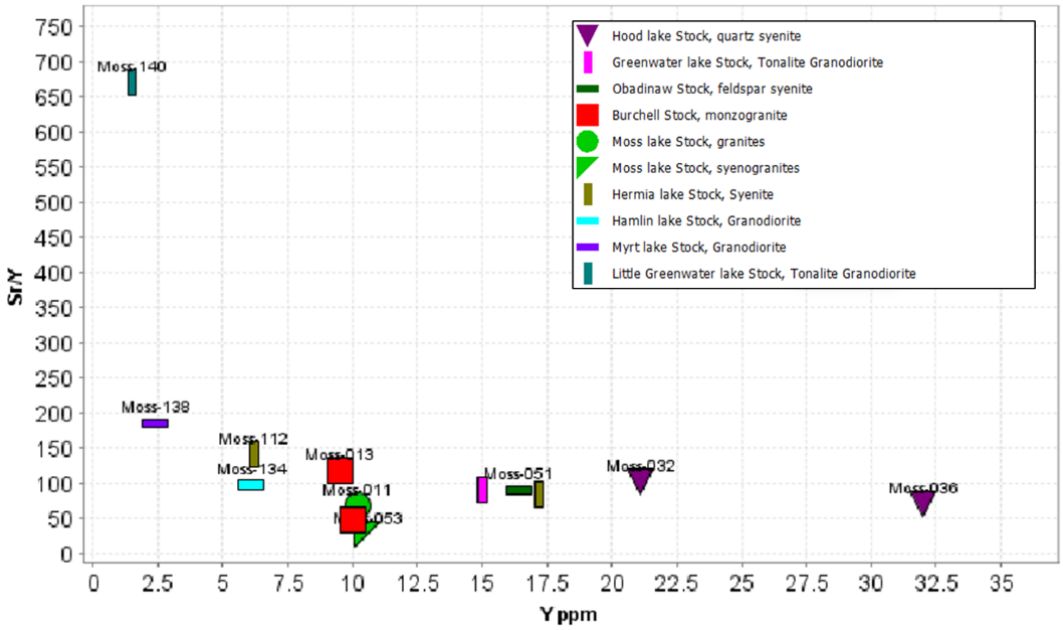

Figure 5.14. Sr/Y versus Y diagram for intrusive felsic bodies from the study area.

The second group corresponds to granitic rocks, syenogranites, monzogranites and syenites. They are represented by samples of the Hood Lake (Moss-32 and Moss-36) and Greenwater Lake stocks (Moss-100). These samples present higher REE abundances than the first group of intrusive felsic rocks (TTG series), marking a clear differentiation (Fig. 5.10). They exhibit metaluminous to slightly peraluminous affinity (Fig. 5.11) and significant enrichment in Cr and Ni (>200 ppm) (Fig. 5.15), which is typical of rocks with sanukitoid affinity (Martin et al., 2005). Sanukitoids are typically syn- to post-tectonic intrusions, which vary in size from well-foliated to undeformed rocks (Laurent et al., 2014). In the Superior Province, they occur as

individual monogenetic stocks (Sage et al., 1996; Stevenson et al., 1999 in Laurent et al., 2014), often containing large (1–6 cm) K-feldspar phenocrysts within a medium-grained (0.1–1 cm) matrix composed of plagioclase (Laurent et al., 2014). These features were observed in the Hood Lake and Greenwater Lake stocks (Appendix A). Geochronologically, the age obtained for the Greenwater Lake stock is consistent with a tectonic activity of 2707.35 ± 0.14 Ma. Additionally, several authors (Williams et al., 1991; Osmani, 1997) describe these rocks as late tectonic to post-tectonic intrusions, consistent with what has been discussed in this thesis.

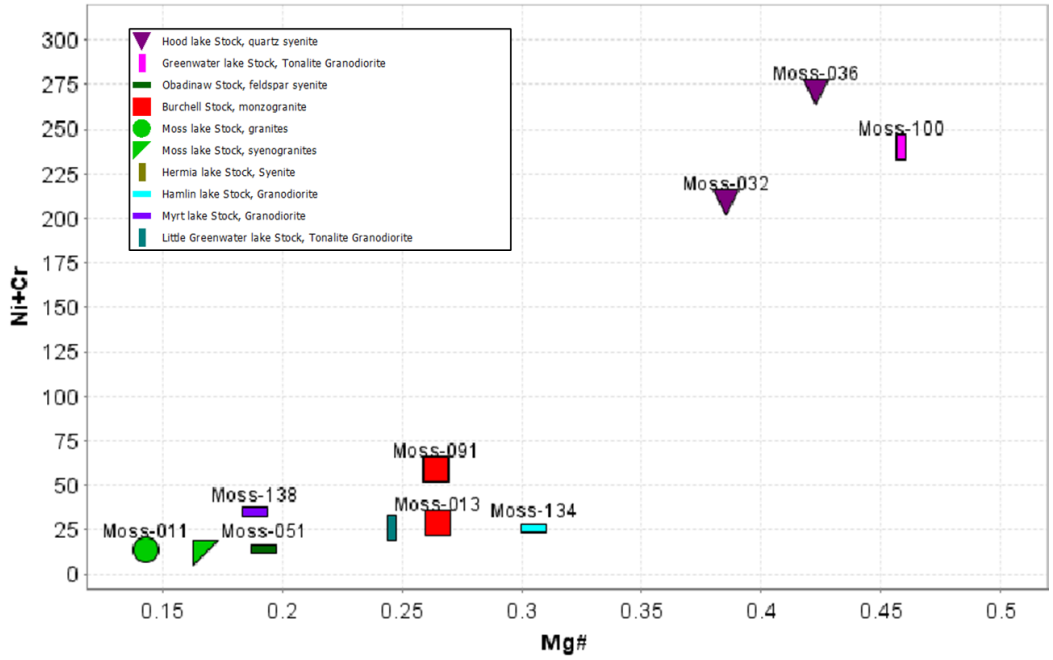

Figure 5.15. Diagram Cr + Ni (ppm) versus Mg (MgO/MgO + FeO) of Perez et al. (2024).

Finally, the third group of felsic intrusive rocks, contains samples classified as Archean hybrid granites (Laurent et al., 2014) including the Hermia Lake (Moss-112 and Moss-114), Burchell Lake (Moss-13 and Moss-91), Moss Lake (Moss-11 and Moss-53), Hamlin Lake (Moss-134), Myrt Lake (Moss-134) and Obadinawa stocks (Moss-51). Generally, the hybrid granitoids

are formed by the interaction of several magmas or sources (metasomatism, mixing), forming a heterogeneous group that cannot be defined solely by geochemical parameters due to the various constituents involved in their formation exhibiting significant variability across different cratonic regions (Lunde et al., 2014). Generally, the Archean hybrid granites, like the sanukitoids, are rich in REE (Fig. 4.57) compared to the TTG granites. However, the Archean hybrid granites have lower Ni + Cr, like TTG granites, showing characteristics more like sanukitoid rocks (Fig. 5.15). These hybrid geochemical characteristics between the TTG and sanukitoid granites infer that these intrusive bodies would correspond to Archean hybrid granites, as proposed by Laurent et al. (2014).

5.4 Tectonic setting

Tectonic assemblage refers to volcanic and/or sedimentary rock packages formed within a specific depositional or volcanic setting during a defined time interval (Anhaeusser, 2014). These units commonly share lithofacies but may exhibit consistent structural, metamorphic, geochemical, and geophysical traits (Thurston, 1991). Faults, unconformities, or intrusions typically bound assemblages and may comprise multiple formations or groups (Thurston, 1991; Stott et al., 2010). In the Shebandowan Greenstone Belt, Williams et al. (1991) initially defined three tectonic assemblages: the Greenwater and Burchell, characterized by mafic-to-felsic volcanic successions, and the overlying Shebandowan assemblage. Later, Corfu and Stott (1998) reclassified these into the Greenwater-Burchell, Kashabowie, and Auto Road assemblages based on new age constraints and stratigraphic reinterpretation. However, geochemical, isotopic, and petrographic data from this study better align with the original model of Williams et al. (1991) and

Lodge (2016), which distinguishes the Burchell and Greenwater assemblages as separate entities. Lodge (2016), working in the same area, documented structural breaks and distinct geochemical trends, including komatiites and U-Pb age data, supporting the earlier subdivision. This approach refines the stratigraphy of the western Wawa Subprovince and strengthens correlations with volcanic sequences in the Abitibi Subprovince.

The rocks in the study area have a complex tectonic history, given the complexities in the structural and stratigraphic maps, and the quantity and quality of the geochronological data (Williams et al., 1991; Corfu and Stott.,1998; Lodge, 2016; Lodge & Chartland, 2013). However, new data from this study allows us to refine the model for the tectonic environment. The rocks of the Greenwater assemblage comprise, tholeiitic and calc-alkaline volcanism (Fig 4.43), evolving from a mantle plume, into a magmatic arc environment, with granitic to granodioritic felsic bodies. In contrast, the Burchell assemblage comprises calc-alkaline volcanism evolving from primitive arc with juvenile source of mantle-derived magmas into more evolved magmatic arc environments, which includes contemporary to synvolcanic plutonism with granitic felsic bodies (Fig. 4.43).

Previous work proposed an arc environment with evidence for combined arc/back-arc volcanism for the Greenwater and Burchell assemblages (Williams et al., 1991; Corfu and Stott.,1998). Integrated structural, geochronological, and geochemical evidence was used to argue that the Shebandowan greenstone belt was part of an active Neoarchean arc–back-arc system that evolved through multiple tectonic stages (Williams et al., 1991; Corfu and Stott.,1998; Percival et al., 2012; Lodge, 2016). However, there is controversy regarding the repeated volcanic successions in the Shebandowan greenstone belt. Williams (1991) initially proposed that repeated volcanic successions result from structural repetition, including recumbent folding followed by vertical

folding and imbrication structures. More recently, Lodge (2016) proposed a geodynamic and tectonic model for these repetitions in the Shebandowan greenstone belt, separating them into two stages. The first stage (~2722–2720 Ma) corresponds to rifting of older crust driven by plumes, generating mafic tholeiitic rocks, komatiites, and rift-related felsic units (Lodge et al., 2015; Lodge, 2016). A second stage (~2718–2716 Ma) is dominated by arcs, producing intermediate calc-alkaline volcanic rocks, magnesian andesites, and adakites. This second stage could reflect rapid changes in plate interactions, analogous to modern microplate dynamics (Hannington et al., 2006; Tsuchiya et al., 2005; Tatsumi, 2006). This interpretation supports the coexistence of plume- and subduction-related processes in different regions of the Archean Earth (Bédard, 2006; Bédard et al., 2013; Polat and Hoffman, 2003).

The geochemical, petrographic, and geochronological evidence obtained in this thesis shows that the formation environment in the study area is related to a mantle plume that evolved to a subduction environment, which supports Lodge (2016). Hollings et al. (1999) support one type of model, which includes mantle plume magmatism adjacent to a subduction zone to explain the intercalation of ultramafic rocks with arc-type felsic volcanic rocks in the Lumby Lake greenstone belt. This model could explain the existence of komatiite rocks reported east of the study area (Williams, 1991), which were not sampled in this thesis, but belong to the Greenwater assemblage. It would also explain the positive values of εNd(t) (Fig. 5.4) related to a juvenile mantle and the geochemical signatures with enrichment in LREE patterns characteristic of a subduction environment (Fig. 5.8).

Back-arc magmas are produced through partial melting of a normal MORB (N-MORB) source (Woodhead et al., 1993; Taylor & Martinez, 2003), whereas magmas associated with arcs

emanate from a more depleted mantle source as a consequence of melt extraction (Ewart et al., 1977) or as a result of aqueous fluids originating from the subducting plate (Tollstrup et al., 2010). The mafic rocks of the Greenwater assemblage are characterized by flat HREE with enriched LREE and negative Nb anomalies (Fig. 5.5) and belong to the tholeiitic series (Fig. 4.44). They show a slight tendency away from the MORB field towards higher Th/Yb values (Fig. 5.6), with positive εNd(t) values between +1.6 to +2.7 (Fig. 5.4), which are within the limits of the range of depleted mantle values at this time but could also indicate minor contamination by older, slightly enriched crustal components (Pearce, 2008; Tomlinson et al., 2004; Fig. 5.4). However, the presence of pillow lavas (Figs. 4.3 and 4.6) and komatiites within the Greenwater assemblage suggests involvement of a mantle plume (Williams et al., 1991; Osmani, 1997; Corfu et al., 1998) and is more consistent with an oceanic plateau setting for the mafic rocks of assemblage (Pearce, 2008; Tomlinson et al., 2004; Hollings, 1999; Hollings et al., 1998; Fig. 5.16B). In contrast, the mafic rocks of the Burchell assemblage have moderate slopes in the LREE and relatively flat HREE, with negative Nb and Ti anomalies (Fig. 5.7) and belong to the calc-alkaline series (Fig. 4.44), with positive εNd(t) values between +1.5 and +3.2 (Fig. 5.4), suggesting a strong juvenile magma character in a primitive arc environment, possibly a low-angle, hot subduction zone as argued by Lodge et al. (2015; Fig. 5.16A).

Felsic and intermediate metavolcanic rocks are present in both assemblages, and similar geochemical signatures were observed, with significant enrichment of LREE and HREE, consistent with a subduction magmatic environment (Figs. 4.48a and 4.48B). However, the geochemical signatures of the intermediate felsic and metavolcanic rocks allowed for discrimination between assemblages (Figs. 4.48A; 4.48B; 4.49 and 4.50).

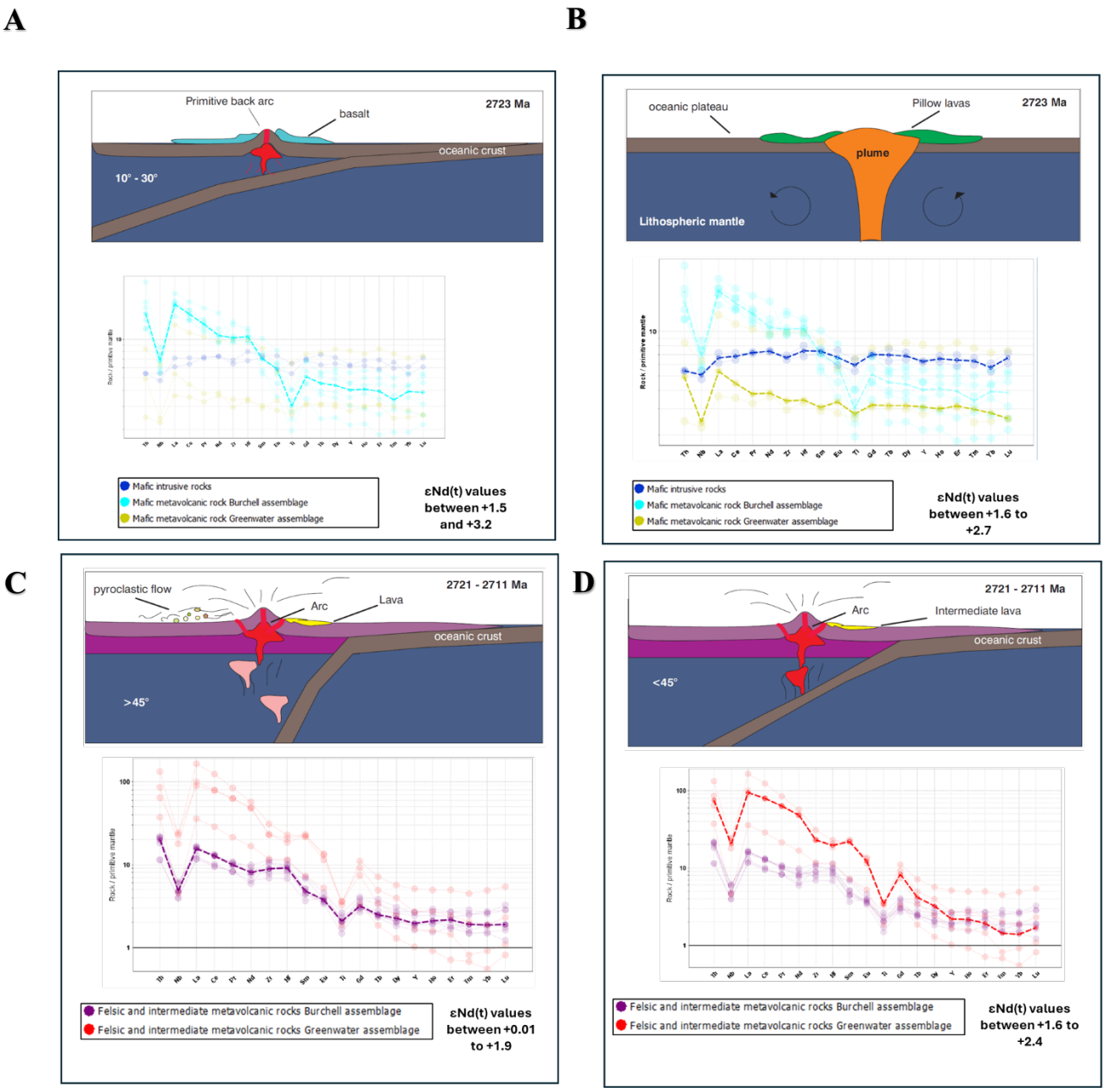

Figure. 5.16. Schematic illustration of the possible tectonic evolution of the study area, with spider diagrams and εNd(t) values. ***A.*** *Tectonic setting <2723 Ma, early phase for the Burchell assemblage, primitive arc environment, with a low subduction angle (10°–30°). Spider diagrams and εNd(t) values for mafic rocks.* ***B****. Tectonic setting <2723 Ma, early phase for the Greenwater assemblage, oceanic plateau environment produced by a mantle plume. Spider diagrams and εNd(t) values for ultramafic and mafic rocks.* ***C.*** *Tectonic setting 2721 to 2711 Ma, for the Burchell assemblage, a calc-alkaline arc environment, with a high subduction angle (>45°) and spider diagrams and εNd(t) values for felsic to intermediate rocks.* ***D****. Tectonic setting 2721 to 2711 Ma, for the Greenwater assemblage, a calc-alkaline arc environment, with a low subduction angle (<45°) and spider diagrams and εNd(t) values for felsic to intermediate rocks.*

The felsic and intermediate metavolcanic rocks located in the Greenwater assemblage display enriched LREE, with negative Ti anomalies and flat HREE (Fig. 5.16C and 5.1D), with εNd (t) values between +1.6 to +2.4 (Fig. 5.4). The felsic and intermediate metavolcanic rocks located in the Burchell Assemblage, display less enriched LREE, with smaller negative Ti anomalies than the Greenwater assemblage, and flat HREE (Fig. 5.12), with εNd (t) values between +0.01 to +1.9 (Fig. 5.4). The above suggests that this group of rocks experienced varying degrees of partial melting or different degrees of crustal assimilation (Figs. 5.16C and 5.16D) in contemporaneous and spatially separated geodynamic settings within the same terrane (Smith et al., 1997; Pearce & Stern, 2006).

Although the similar geochemical and petrographic characteristics of the Burchell and Greenwater assemblage intrusive rocks are consistent with a subduction environment, there are sufficient to suggest an independent magmatic history for each assemblage. The Little Greenwater Lake stock located in the Greenwater assemblage (Fig. 2.4), has calc-alkaline characteristics and slightly peraluminous features (Fig. 5.11), exhibits enrichment in light rare earth elements (LREE), fractionated heavy rare earth elements (HREE), and a low europium content (<0.5 ppm), consistent with the typical TTG signature (Moyen, 2011). Laurent et al. (2014) proposed that, in general, TTGs can vary according to their geochemical signatures, with bodies with high Y values and low Sr contents corresponding to a "low-pressure" zone (Fig. 5.14) and bodies with low Y values and low Sr contents corresponding to a "high-pressure" zone (Fig. 5.14). Furthermore, they argued that late Archean TTGs (<3.0 Ga) are richer in Sr and poorer in Y than older TTGs (Champion & Smithies, 2007; Martin and Moyen, 2002 in Laurent et al., 2014), which would correspond to a "high-pressure" formation zone. For these reasons, the Little Greenwater Lake stock likely formed

under high-pressure conditions, possibly in the early Archean, an age also proposed by Osmani (1991) for this body.

The Hood Lake and Greenwater Lake stocks, located in the Greenwater assemblage (Fig. 2.4), exhibit significantly higher REE concentrations than the TTG assemblage, with metaluminous to slightly peraluminous compositions strongly enriched in Cr and Ni (>200 ppm). These bodies are interpreted as sanukitoid granites, syn-post-tectonic to post-tectonic intrusions. Petrographically, they contain large K-feldspar phenocrysts and medium-grained plagioclase-rich matrices. The Greenwater Lake stock has been dated at 2707.35 ± 0.14 Ma and +2.34 εNd(t) values (Fig. 5.4). This confirms a post-tectonic emplacement and juvenile mantle source, associated with the late stages of arc evolution. The stocks from Lake Hermia, Obadinawa, Moss, Hamlin, and Burchell, located in the Burchell Assemblage (Fig. 2.4), exhibit rare earth element (REE) enrichment similar to the sanukitoids but exhibit Ni + Cr ratios similar to those of the TTGs. These hybrid geochemical characteristics between the TTG and sanukitoid granites suggest that these intrusive bodies correspond to Archean hybrid granites, as proposed by Laurent et al. (2014). Hybrid granitoids have been interpreted as formed by the interaction of several magmas or sources (metasomatism, mixing), forming a heterogeneous group that cannot be defined solely by geochemical parameters because the various constituents involved in their formation exhibit significant variability across different cratonic regions (Lunde et al., 2014). Within this group of Archean hybrid granites, two magmatic pulses can be distinguished, the first represented by the Obadinaw (2718.34 ± 0.14 Ma) and Moss Lake (2716.09 ± 0.45 Ma) stocks, which would represent an initial pulse in the Burchell assemblage (Fig. 5.11), which infers a significant synvolcanic plutonism for this time. A second, younger magmatic pulse is represented by the Hermia (2684 Ma) and Burchell (2683.7 Ma) stocks (Fig. 5.11), which exhibit less +1 εNd(t) values (Fig. 5.4),

which correspond to the latest stage of volcanism in the study area and greater influence of older crustal material likely formed during a post-arc stage.

6. Conclusions

The tholeiitic and calc-alkaline volcanism of the Greenwater assemblage is consistent with an oceanic plateau environment that evolved to a primitive arc environment with both intrusive and volcanic mafic rocks. Positive εNd(t) values between +1.0 to +2.7, suggest derivation from depleted mantle sources with minimal participation of older continental crust. That transitioned to a calc-alkaline subduction zone comprising felsic and intermediate rocks with approximate ages of ~2723 Ma. These rocks show evidence of more significant fractionation forming the andesite-diorites with strongly fractionated rare earth patterns. This fractional crystallization continued until the generation of felsic ash tuffs. The subduction environment would generate syn-post-tectonic sanukitoid bodies represented by the Hood Lake stock and the Greenwater Lake stock with an age of ~2707.35 Ma and the Hood Lake stock.

The Burchell assemblage comprises calc-alkaline volcanism formed in a subduction environment, which comprises basaltic rocks formed in a low-angle "hot" subduction environment, that subsequently transitioned to felsic and intermediate-type volcanic rocks, mainly andesite-diorites, which show fractionated rare-earth element patterns, generated from a juvenile magma with slight partial mixing with older, slightly enriched crustal components, represented by values from +0.01 to +3.3 εNd(t). The fractional crystallization process would continue until ash tuffs and pyroclastic flows (~ 2716 Ma) of rhyolitic composition. The subduction environment would generate syn to post-tectonic intrusions classified as hybrid granitoids with two subduction-related intrusive events: the first at ~2717–2718 Ma (Moss Lake and Obadinaw stocks) and the second at ~2683–2684 Ma (Lake Hermia and Burchell Lake stocks).

The research area exhibits geochemical indicators supporting the existence of tonalitic-trondhjemitic-granodioritic (TTG), sanukitoids granites and Archean hybrid granites. The geochemistry data, together with newly acquired and previously existing geochronological and isotopic data, suggest a protracted crustal evolution, confirming distinctive magmatic events in the Burchell and Greenwater assemblages. This began in the early Archean (Little Greenwater Lake stock), with juvenile mantle-produced magmas generated from a subduction zone. Subsequently, processes or interactions between metasomatized rocks may have facilitated the formation of the first group of hybrid granites (Obadinaw and Moss Lake stocks) located in the Burchell assemblage with ages between 2716.09 and 2718.34 Ma. Later on, forming syn-post-tectonic to post-tectonic sanukitoid bodies (Greenwater Lake and Hodd Lake stocks), located in the Greenwater assemblage, with an age around ~2707 Ma, and εNd(t) values of +2.34, confirms a juvenile mantle source, associated with the late stages of arc evolution. Finally, the second group of hybrid granites (Hermia Lake and Burchell Lake stocks) located in the Burchell assemblage with ages between 2684 and 2683 Ma, and less +1 εNd(t) values. This would correspond to the latest stage of volcanism in the study area and a greater influence of older crustal material, which likely formed during a post-arc stage.

References

ALS (2023). Complete characterization packages ALS Laboratory. https://www.alsglobal.com/en/geochemistry/rock-characterisation/complete-characterisation-packages

Anhaeusser, C. R. (2014). Archaean greenstone belts and associated granitic rocks–a review. Journal of African Earth Sciences, 100, 684-732.

Arndt, N. T., Lesher, C. M., & Barnes, S. J. (2008). Komatiite. Cambridge University Press.

Ayer, J. A., Thurston, P. C., Bateman, R., Dube, B., Gibson, H. L., Hamilton, M. A., & Trowell, N. (2002). Evolution of the Abitibi greenstone belt based on U-Pb geochronology: Autochthonous volcanic construction followed by plutonism, regional deformation and sedimentation. Precambrian Research, 115(1-4), 63–95. https://doi.org/10.1016/S0301-9268(02)00006-0

Beakhouse, G. P., Stott, G. M., Blackburn, C. E., Breaks, F. W., Ayer, J., Stone, D., Farrow, C., Corfu, F. (1996). Western Superior Province, Field Trips A5 and B6. Geological Association of Canada, Winnipeg.

Bédard, J.H., Brouillette, P., Madore, L. and Berclaz, A., (2003). Archaean cratonization and deformation in the northern Superior Province, Canada: an evaluation of plate tectonic versus vertical tectonic models, Precambrian Research, vol. 127, p.61-87.

Carleton University. (2025). *Analytical procedures*. Institute for Integrated Gravimetry and Geochronology Research Centre. Retrieved April 23, 2025, from https://iggrc.carleton.ca/analytical-procedures

Campbell, I., Franklin, J., Gorton, M., Hart, T., and Scott, S., (1981). The role of subvolcanic sills in the generation of massive sulfide deposits. Economic Geology, vol. 76, p. 2248-2253.

Card, K.D. and Ciesielski, A., (1986). DNAG#1, Subdivisions of the Superior Province of the Canadian Shield, Geoscience Canada, vol. 13, p.5-13.

Chorlton, L., (1987). Geological setting of gold mineralization in the western part of the Shebandowan Greenstone Belt, District of Thunder Bay, northwestern Ontario. Ontario Geological Survey, Open File Report 5636, 348 p

Chown, E. H., Daigneault, R., Mueller, W., & Mortensen, J. K. (2002). Tectonic evolution of the northern volcanic zone, Abitibi belt, Quebec. Economic Geology, 97(7), 1521–1549. https://doi.org/10.2113/gsecongeo.97.7.1521

Condie, K. C., (1976). Trace-element geochemistry of Archean greenstone belts. Earth-Science Reviews, vol. 12, p. 393-417.

Condie, K. C., (1993). Chemical composition and evolution of the upper continental crust: contrasting results from surface samples and shales. Chemical Geology, vol. 104, p. 1-37.

Corfu, F., Stott, G.M., (1986). U–Pb ages for late magmatism and regional deformation in the Shebandowan Belt, Superior Province, Canada. Can. J. Earth Sci. 23,1075–1082

Corfu, F. and Stott, G.M., (1998). Shebandowan greenstone belt, western Superior Province: U-Pb ages, tectonic implications, and correlations, GSA Bulletin, vol. 110, p.1467-1484.

DePaolo, D. J. (1981). Neodymium isotopes in the Colorado Front Range and crust–mantle evolution in the Proterozoic. Nature, 291(5812), 193–196. https://doi.org/10.1038/291193a0

Ducea, M. N., Saleeby, J. B., and Bergantz, G., (2015). The architecture, chemistry, and evolution of continental magmatic arcs. Annual Review of Earth and Planetary Sciences, vol. 43, p. 299-331

Ewart, A., Brothers, R., and Mateen, A., (1977). An outline of the geology and geochemistry, and the possible petrogenetic evolution of the volcanic rocks of the Tonga-Kermadec-New Zealand island arc. Journal of Volcanology and Geothermal Research, vol. 2, p. 205-250.

Fisher, R.V., (1966). Rocks composed of volcanic fragments. Earth Science Reviews. International Magazine for Geo-Scientists. Amsterdam. Vol.1, p.287–298.

Frost, B. R., & Frost, C. D. (2008). A geochemical classification for feldspathic igneous rocks. Journal of Petrology, 49(11), 1955-1969.

Jensen, L. S. (1976). A new cation plot for classifying subalkalic volcanic rocks. Ontario Division of Mines Miscellaneous Paper, 66.

Jones, D.L., Howell, D.G., Coney, P.J., Monger, H.W.H., 1983. Recognition, character and analysis of tectonostratigraphic terranes in western North America. J. Geol. Educ. 31 (4), 295–303.

Hannington, M. D., de Ronde, C. E. J., & Petersen, S. (1999). Modern seafloor tectonics and submarine hydrothermal systems: A review of mineral deposits and their genesis. Economic Geology, 94(7), 1197–1214. https://doi.org/10.2113/gsecongeo.94.7.1197

Harley, S. L., Kelly, N. M., & Möller, A. (2007). Zircon behaviour and the thermal histories of moutain chains. Elements, 3(1), 25–30. https://doi.org/10.2113/gselements.3.1.25

Harris, F. R., (1970). Geology of the Moss Lake Area, District of Thunder Bay. Ontario Department of Mines, Geological Report 85, 61p.

Hart, T.R., (2007). 9. Project Unit 06-003. Geochronology of the Hamlin and Wye Lakes Area, Shebandowan Greenstone Belt, Thunder Bay District in Summary of Field Work and Other Activities 2007, Ontario Geological Survey, Open File Report 6213, pp.9-1 to 9-8.

Hart, T., Gibson, H., and Lesher, C., (2004). Trace element geochemistry and petrogenesis of felsic volcanic rocks associated with volcanogenic massive Cu-Zn-Pb sulfide deposits. Economic Geology, vol. 99, p. 1003-1013.

Hoffman, P.F., (1991). On accretion of granite-greenstone terranes. In: Robert, F., Sheahan. P.A., Green, S.B. (Eds). Nuna Conf. Greenstone Gold and Crustal Evolution, Val d' Or. Geol. Assoc. Can., p.32-45.

Hollings, P., (1998). Geochemistry of the Uchi Subprovince, Nothern Superior Province: An Evaluation of the Geodynamic Evolution of the Nothern Margin of the Superior Province Ocean Basin. In Saskatchewan, U. o., ed.: Saskatoon, 309 p.

Hollings, P., Wyman, D. and Kerrich, R., (1999). Komatiite-basalt-rhyolite volcanic associations in Northern Superior Province greenstone belts: significance of plume-arc interaction in the generation of the proto continental Superior Province, Lithos, vol. 46, p.137-161.

Howell, D.G., (1989). Tectonics of suspect terranes. Mountain building and continental growth; Chapman and Hall, London, 232p.

Hodgkinson, J.M., (1968). Geology of the Kashabowie Area, District of Thunder Bay; Ontario Department of Mines, Geological Report 53, 35p.

Hunt, D S, February (2010). Report on the Diamond Drilling Program, Burchell Lake Project, Shebandowan Area, Province of Ontario. For Mengold Resources inc. Assessment file number 20000004544

Kelemen, P. B., Hanghøj, K., & Greene, A. R. (2003). One view of the geochemistry of subduction-related magmatic arcs, with an emphasis on primitive andesite and lower crust. In H. D. Holland & K. K. Turekian (Eds.), Treatise on geochemistry

Kerr, A., (2003). 3.16 Oceanic Plateaus. Treatise on Geochemistry, vol. 3, p. 537-565.

Laurent, O., Martin, H., Moyen, J.F., Doucelance, R., 2014. The diversity and evolution of late-Archean granitoids: Evidence for the onset of ‘‘modern-style” plate tectonics between 3.0 and 2.5 Ga. Lithos 205, 208–235. https://doi.org/10.1016/j.lithos.2014.06.012.

Le Maitre, R. W. (1989). A classification of igneous rocks and glossary of terms : recommendations of the International Union of Geological Sciences, Subcommission on the Systematics of Igneous Rocks. Blackwell.

Lodge, R.W.D. and Chartrand, J.E. (2013). Establishing regional geodynamic settings and the metallogeny of volcanogenic massive sulphide mineralization of greenstone belt assemblages (circa 2720 Ma) of the Wawa Subprovince via geochemical comparisons; Ontario Geological Survey, Miscellaneous Release—Data 306.

Lodge, R. W. D., Gibson, H. L., Stott, G. M., Franklin, J. M., & Hudak, G. J. (2015). Geodynamic setting, crustal architecture, and VMS metallogeny of ca. 2720 Ma greenstone belt assemblages of the northern Wawa subprovince, Superior Province. Canadian Journal of Earth Sciences, 52(3), 196-214.

Lodge RWD, Gibson HL, Stott GM, Franklin JM, Hudak GJ (2015) Geodyamic setting, crustal architecture, and VMS metallogeny of ca. 2720 Ma greenstone belt assemblages of the northern Wawa subprovince, Superior Province. Canadian Journal of Earth Sciences 52:196-214.

Lodge, R. W. (2016). Petrogenesis of intermediate volcanic assemblages from the Shebandowan greenstone belt, Superior Province: Evidence for subduction during the Neoarchean. Precambrian Research, 272, 150-167.

MacLean, W. H., & Barrett, T. J. (1993). Lithogeochemical techniques using immobile elements. Journal of geochemical exploration, 48(2), 109-133.

Martin, H., Moyen, J.F., (2002). Secular changes in TTG composition as markers of the progressive cooling of the Earth. Geology 30 (4), 319–322.

Martin, H., Smithies, R.H., Rapp, R., Moyen, J.F., Champion, D., (2005). An overview of adakite, tonalite–trondhjemite–granodiorite (TTG), and sanukitoid:relationships and some implications for crustal evolution. Lithos 79 (1–2), 1–24. https://doi.org/10.1016/j.lithos.2004.04.048.

Mattinson, J.M., (2005). Zircon U-Pb chemical abrasion ("CA-TIMS") method: Combined annealing and multi-step partial dissolution analysis for improved precision and accuracy of zircon ages: Chemical Geology, v. 220, p. 47–66.

Middlemost, E. A. (1994). Naming materials in the magma/igneous rock system. Earth-science reviews, 37(3-4), 215-224.

Morton, P. (1982). Archean volcanic stratigraphy, petrology, and chemistry of mafic and ultramafic rocks, chromite, and the Shebandowan Ni-Cu mine, Shebandowan, northwestern Ontario; unpublished PhD thesis, Carleton University, Ottawa, Ontario, 346p.

Moyen, J.F., (2011). The composite Archaean grey gneisses: petrological significance, and evidence for a non-unique tectonic setting for Archaean crustal growth. Lithos 123 (1–4), 21–36.

Nwakanma, M. U. (2024). Characterization of alteration and mineralization of the Moss gold deposit, Shebandowan greenstone belt, Northwestern Ontario.

Nymoen, K. G., Mole, D. R., Thurston, P. C., Tinkham, D. K., Marsh, J. H., & Stern, R. A. (2025). Crustal evolution and architecture of the Wawa Subprovince, Superior Province: Insights from zircon U-Pb-Hf-O isotopes and geochemistry. Precambrian Research, 418, 107705.

Osmani, I.A., (1997). Geology and mineral potential: Greenwater Lake area, West-Central Shebandowan Greenstone Belt; Ontario Geological Survey, Report 296, 135p.

Osmani, I.A. (1997a). Precambrian geology, Burchell-Greenwater lakes area, East half. Ontario Geological Survey, Map 2623, 1:20,000.

Osmani, I.A. (1997b). Precambrian geology, Burchell-Greenwater lakes area, West half. Ontario Geological Survey, Map 2622, 1:20,000.

Osmani, I.A. (1997c). Precambrian geology, Burchell-Greenwater lakes area, West half. Ontario Geological Survey, Map 2624, 1:20,000.

Parrish, R., Roddick, J.C., Loveridge, W.D., and Sullivan, R.W., (1987). Uranium-lead analytical techniques at the geochronology laboratory, Geological Survey of Canada: Geological Survey of Canada Paper 87-2, p. 3–7.

PCIGR (2023). Geochronology U-P Dating. Pacific Centre for Isotopic and Geochemical Research Department of Earth, Ocean and Atmospheric Sciences, The University of British Columbia. https://pcigr.eos.ubc.ca/services/geochronology

Pedreira Pérez, R., Tremblay, A., & Stevenson, R. K. (2024). Archean crustal growth and reworking in the Superior Province, Canada: Insights from whole-rock geochemistry and Nd isotopic data of the La Grande, Nemiscau and Opatica subprovinces. Gondwana Research, 135, 151–179. https://doi.org/10.1016/j.gr.2024.04.006

Pearce, J. A., (2008). Geochemical fingerprinting of oceanic basalts with applications to ophiolite classification and the search for Archean oceanic crust. Lithos, vol. 100, p. 14-48.

Pearce, J. A., & Stern, R. J. (2006). Origin of back-arc basin magmas: Trace element and isotope perspectives. Back-arc spreading systems: Geological, biological, chemical, and physical interactions, 166, 63-86.

Pearce, J. A. (1996). A user's guide to basalt discrimination diagrams. Trace element geochemistry of volcanic rocks: applications for massive sulphide exploration. Geological Association of Canada, Short Course Notes, 12, 79-113.

Pearce, J. A., Harris, N. B., & Tindle, A. G. (1984). Trace element discrimination diagrams for the tectonic interpretation of granitic rocks. Journal of petrology, 25(4), 956-983.

Percival, J. A., Skulski, T., Sanborn-Barrie, M., Stott, G. M., Leclair, A. D., Corkery, M. T., & Boily, M. (2012). Geology and tectonic evolution of the Superior Province, Canada. In Tectonic styles in Canada: The LITHOPROBE perspective (Vol. 49, pp. 321–378). Saint-John's, Newfoundland: Geological Association of Canada.

Percival, J. A., Sanborn-Barrie, M., Skulski, T., Stott, G. M., Helmstaedt, H., and White, D. J., (2006). Tectonic evolution of the western Superior Province from NATMAP and Lithoprobe studies. Canadian Journal of Earth Sciences, vol. 43, p. 1085-1117.

Percival, J.A., Stern, R.A. and Skulski, T., (2001). Crustal growth through successive arc magmatism: reconnaissance U-Pb SHRIMP data from the northeastern Superior Province, Canada, Precambrian Res., vol. 109, p.203-238.

Percival, J. A. & Sullivan, R.W. (1988). Age constraints on the evolution of the Quetico Belt, Superior Province, Ontario; *in* Radiogenic and isotopic studies: report 2; Geological Survey of Canada, Paper 88-2, p.97-107.

Pettijohn, F.J. (1975) Sedimentary Rocks. 3rd Edition, Harper and Row, New York, 628 .

Poirier S., Poirier S., Patrick G., Richard P., Palich J.,2013. InnovExplor – Consulting Firm Mines & Exploration., 2013: Technical Report and Preliminary Economic Assessment for the Moss Lake Project (compliant with Regulation 43-101 / NI 43-101 and Form 43-101F1) 178 pages.

Polat, A and Kerrich, R., (2001). Magnesian andesites, Nb-enriched basaltandesites, and adakites from late-Archean 2.7 Ga Wawa greenstone belts, Superior Province, Canada: implications for late Archean subduction zone petrogenetic processes, Contrib. Mineral Petrol., vol. 141, p.36-52.

Rapp, R. P., & Watson, E. B. (1995). Dehydration melting of metabasalt at 8–32 kbar: implications for continental growth and crust-mantle recycling. Journal of petrology, 36(4), 891-931.

Rasband W., NIH National Institutes of Health of USA (2024). ImageJ (Vertion 1.54d) [Software] IamgeJ imagen processing and anaysis in Java. http://https://imagej.net/ij/index.htm

Reynold N, & Fiel M, (2022). NI 43-101 Technical report mineral resource estimate for the Moss Lake project, Ontario, Canada. report No. R407.2022. 164 pg.

Richards, B (2024). Goldshore Announces an Indicated Mineral Resource Estimate of 1,535Koz Contained Gold at 1.23 g/t Au and an Inferred Mineral Resource Estimate of

5,198Koz Contained Gold at 1.11 g/t Au at the Moss Gold Project. https://goldshoreresources.com/goldshore-announces-an-indicated-mineral-resource-estimate-of-1535koz-contained-gold-at-1-23-g-t-au/

Rogers, N., McNicoll, V., van Staal, C. R., & Tomlinson, K. Y. (2000). Lithogeochemical studies in the Uchi-Confederation greenstone belt, northwestern Ontario: implications for Archean tectonics (pp. 1-11). Natural Resources Canada, Geological Survey of Canada.

Rollinson, H. R., & Pease, V. (2021). Using geochemical data: to understand geological processes. Cambridge University Press.

Ross, P.-S., and Bédard, J. H., (2009). Magmatic affinity of modern and ancient subalkaline volcanic rocks determined from trace-element discriminant diagrams. Canadian Journal of Earth Sciences, vol. 46, p. 823-839.

Santaguida, F. (2001). Precambrian geology compilation series–Quetico sheet; Ontario Geological Survey, Map 2663, scale 1:250 000.

Saunders, A. D., and Tarney, J., (1984). Geochemical characteristics of basaltic volcanism within back-arc basins. Geological Society, London, Special Publications, vol. 16, p. 59-76.

Schmidt, M., and Jagoutz, O., (2017). The global systematics of primitive arc melts. Geochemistry, Geophysics, Geosystems, 38 p

Scoates, J. S., & Jon Scoates, R. F. (2013). Age of the Bird River Sill, Southeastern Manitoba, Canada, with implications for the secular variation of layered intrusion-hosted stratiform chromite mineralization. Economic Geology, 108(4), 895-907.

Smith, I. E. M., Worthington, T. J., Price, R. C., and Gamble, J. A., (1997). Primitive magmas in arc-type volcanic associations; examples from the Southwest Pacific. The Canadian Mineralogist, vol. 35, p. 257-273

Shute, A.L., (2009). Geology and alteration associated with the Hamlin Lake VMS system, Shebandowan Greenstone belt, Northwestern Ontario, Canada. Unpublished M.Sc thesis, Lakehead University, 213p.

Stephan, T., Phillips, N., Tiitto, H., Perez, A., Nwakanma, Creaser, R., and Hollings, P.: "Going with the fl ow - Changes of Vorticity Control Gold Enrichment in Archean Shear Zones (Shebandowan Greenstone Belt, Superior Province, Canada)", under review in Structural Geology.

Stott, G. M., Corkery, M. T., Percival, J. A., Simard, M., & Goutier, J. (2010). 20. Project Units 98-006 and 98-007. A Revised Terrane Subdivision of the Superior Province.

Stott, G.M., Corkery, T., Leclair, A., Boily, M. and Percival, J., (2007). A revised terrane map for the Superior Province as interpreted from aeromagnetic data [abstract]; Institute on Lake Superior Geology Proceedings, 53rd Annual Meeting, Lutsen, MN, vol. 53, part1, p.74-75.

Stott, G.M. and Schnieders, B.R., (1983). Gold mineralization in the Shebandowan Belt and its relation to regional deformation patterns; in The Geology of Gold in Ontario, Ontario Geological Survey, Miscellaneous Paper 110, p.181-193.

Streckeisen, A. (1976). To each plutonic rock its proper name. Earth Science Reviews. International Magazine for Geo-Scientists. Amsterdam. Vol.12, p.1–33.

Streckeisen, A. (1978). IUGS Subcommission on the Systematics of Igneous Rocks. Classification and Nomenclature of Volcanic Rocks, Lamprophyres, Carbonatites and Melilite Rocks. Recommendations and Suggestions. Neues Jahrbuch fur Mineralogie. Stuttgart. Abhandlungen, 143, 1-14.

Sun, S. S., & McDonough, W. F. (1989). Chemical and isotopic systematics of oceanic basalts: implications for mantle composition and processes. Geological Society, London, Special Publications, 42(1), 313-345.

Taylor, B., and Martinez, F., (2003). Back-arc basin basalt systematics. Earth and Planetary Science Letters, vol. 210, p. 481-497.

Thurston, P. C., (2015). Greenstone Belts and Granite-Greenstone Terranes: Constrains on the Nature of the Archean World. Geoscience Canada, vol. 42, p. 437-484.

Thurston, P.C., Williams, H.R., Sutcliffe, R.H., Stott, G.M. (Eds.), (1991). Geology of Ontario. Ontario Geological Survey Special Volume 4, Part 1, 709 pp.

Tollstrup, D., Gill, J., Kent, A., Prinkey, D., Williams, R., Tamura, Y., and Ishizuka, O., (2010). Across-arc geochemical trends in the Izu-Bonin arc: Contributions from the subducting slab, revisited. Geochemistry, Geophysics, Geosystems, vol. 11, 27 p.

Tomlinson, K. Y., Stott, G. M., Percival, J. A., & Stone, D. (2004). Basement terrane correlations and crustal recycling in the western Superior Province: Nd isotopic character of

granitoid and felsic volcanic rocks in the Wabigoon subprovince, N. Ontario, Canada. Precambrian Research, 132(3), 245-274

Vermeesch, P. (2018). IsoplotR: A free and open toolbox for geochronology. Geoscience Frontiers, 9(5), 1479–1493. https://doi.org/10.1016/j.gsf.2018.04.001

Walker, J. D., Tikoff, B., Newman, J., Clark, R., Ash, J., Good, J., Bunse, E. G., Möller, A., Kahn, M., Williams, R. T., Michels, Z., Andrew, J. E., & Rufledt, C. (2019). StraboSpot data system for structural geology. In Geosphere (Boulder, Colo.); (Vol. 15, Issue 2, pp. 533–547). Geological Society of America. https://doi.org/10.1130/GES02039.1

Whalen, J.B., Percival, J.A., McNicoll, V.J. and Longstaffe, F.J., (2002). A Mainly Crustal Origin for Tonalitic Granitoid Rocks, Superior Province, Canada: Implications for Late Archean Tectonomagmatic Processes, Jour. Petrology, vol. 43, p.1551-1570.

Woodhead, J., Eggins, S., and Gamble, J., (1993). High field strength and transition element systematics in island arc and back-arc basin basalts: evidence for multi-phase melt extraction and a depleted mantle wedge. Earth and Planetary Science Letters, vol. 114, p. 491-504.

Wentworth, C. K. (1922). A Scale of Grade and Class Terms for Clastic Sediments". The Journal of Geology. 30 (5): 377–392.

Williams, H.R., Stott, G.M., Heather, K.B., Muir, T.L. and Sage, R.P., (1991). Wawa Subprovince; in Geology of Ontario, Ontario Geological Survey, spec. vol. 4, pt.1, p.485-539.

Wyman, D. A., Hollings, P., & Richards, J. P. (1999). Archean subduction processes: Evidence from greenstone belt volcanic geochemistry. Precambrian Research, 97(3-4), 223–242. https://doi.org/10.1016/S0301-9268(99)00034-8

Appendix A. Thin Section Descriptions

This appendix shows the results of the petrographic analyses on 40 thin sections. All the samples present a degree of metamorphism; for this reason, the adjective meta is omitted in their classification. Mode classification diagrams were used as appropriate for the classification of the samples. For samples of plutonic protolith, Streckeisen (1976) was used; samples with volcanic protoliths used Streckeisen (1978); samples with volcanic sedimentary protoliths used Schmid (1981). For the metasedimentary samples, Pettijohn et al. (1987) were used.

Table of thin sections

Sample: Moss-03

Latitude	48.54259°	**Longitude**	-90.71199°
Map unit.	Mafic and ultramafic intrusive rocks - Diorite		
Rock type	Intermediate metavolcanic rock		
Texture	Aphyric holocrystalline with microlithic texture		
General description	The sample is an intermediate metavolcanic rock with aphyric and microlithic holocrystalline texture. The sample is characterized by feldspars (55%) of anhedral to subhedral crystals, which are altered to carbonates. Quartz (25%) is restricted to sizes less than 1900 µm and monocrystalline; plagioclase (5%) is mostly andesine (Michel-Levy method). Alteration minerals, including Alunite (5%), are pervasive and distributed in feldspar crystals. Chlorite (5%) and sericite (1%) in the laminar form are located in the veinlets. Calcite (1%) presents well-developed prismoid crystals at the veinlets' edges. The presence of opaque minerals (3%) in the cubic form of pyrite and chalcopyrite is distributed throughout the sample.		
Alteration	Sericite, Chlorite; Carbonates; Alunite		

Mineralogical composition

Mineral	Modal (%)	Shape	Grain size (µm)	Observation
Feldspars	55	Anhedral	800 - 3100	Alteration to alunite
Quartz	25	Euhedral	180 - 1900	Monocrystalline
Plagioclase	5	Euhedral	500 - 900	Andesine Michel-Levy Method
Chlorite	5	Anhedral	350	Alteration minerals in veins
Sericite	1	Flaky	50	Alteration mineral
Alunite	5	N/A	< 4	Association with Plagioclases
Calcite	1	Euhedral	900	In veins
Opaques	3	Cubic	80 - 1400	Pyrite - calcopyrite

Sample: Moss-10

Latitude	48.53079°	**Longitude**	-90.71929°
Map unit.	Intermediate to felsic hypabyssal rocks - feldspar porphyry		
Rock type	Felsic metavolcanic rock		
Texture	Schist texture		
General description	The sample corresponds to an intermediate metavolcanic rock apparent lamination. Some sectors have oriented polycrystalline quartz, with spherulitic quartz structures, but they are deformed. Strongly altered by chlorite; sericite and carbonates. With opaques (pyrite) associated with chlorite.		
Alteration	Chlorite - Sericite - Carbonates		

Mineralogical composition

Mineral	Modal (%)	Shape	Grain size (mm)	Observation
Plagioclase	55	Anhedral	5	
Sanidine	25	Anhedral	10	Polycrystalline
Quartz	5	N/A	75	
Carbonates	5	N/A	5	Alteration
Sericite	8	Micro-tabular	4	Alteration
Chlorite	<1	Irregular	< 1	Alteration
Opaques	<1		< 1	

Sample: Moss-11

Latitude	48.55098°	**Longitude**	-90.71744°
Map unit.	Late felsic to mafic intrusive rocks - Moss Lake stock		
Rock type	Felsic intrusive rock		
Texture	Inequigranular holocrystalline texture		
General description	The sample corresponds to a Felsic intrusive rock with inequigranular holocrystalline texture. The sample is characterized by orthoclase (70%) and sanidine (1%), of anhedral-type shape crystal. The quartz (15%) is restricted to 100 - 190 sizes polycrystalline; plagioclase (3 %) which exhibits polysynthetic twinning, biotite (1%) and amphiboles such as hornblende (1%). Alteration minerals included actinolite-tremolite (1%) and epidote (1%). Additionally, sericite (1%) and minerals clays (1%) are preferentially located where there is orthoclase. The presence of opaque (5%) minerals is generally associated with hornblende and biotite.		
Alteration	Actinolite-Tremolite, Sericite, Epidote, Clays		

Mineralogical composition

Mineral	Modal (%)	Shape	Grain size (µm)	Observation
Orthoclase	70	Anhedral	1000 -1300	Exsolution- perthitic
Sanidine	<1	Anhedral	500	
Quartz	15	Subhedral	100 - 190	Polycrystalline
Plagioclase	3	Euhedral	300	Polysynthetic twinning
Biotite	<1	Tabular	320	Associated with Opaques
Hornblende	<1	Anhedral	120	Preferably where there is biotite
Actinolite-Tremolite	<1	Tabular	< 16	Alteration mineral
Sericite	<1	Flaky	< 16	Alteration mineral
Epidote	<1	Anhedral	100	Alteration mineral
Opaques	5	Cubic	60	Magnetite – pyrite associated with biotite.

Clays	<1		< 16	Alteration mineral in orthoclase–sanidine.

Sample: Moss-13

Latitude	48.61045°	**Longitude**	-90.62377°
Map unit.	Late felsic to mafic intrusive rocks – Burchell Lake stock.		
Rock type	Felsic intrusive rock		
Texture	Inequigranular holocrystalline texture		
General description	The sample corresponds to a felsic intrusive rock with an inequigranular holocrystalline texture. The sample is characterized by plagioclase (40%), which was classified as labradorite (Michel-Levy Method). Shadows are observed in the plagioclases due to alteration, possibly clay minerals. Orthoclase (20%) and microcline (5%), with a subhedral- - anhedral crystalline form in zoned phenocrysts with inclusions of hornblende and plagioclase crystals, which could indicate an overgrowth of these crystals quartz (20%) is restricted to sizes <4 mm monocrystalline; biotite (1%) and amphiboles such as hornblende (1%) are both associated with each other. Alteration minerals, including chlorite (1%) and clay minerals (1%), the latter are preferentially located where orthoclase and plagioclase exist. The presence of opaque minerals (1%) is mainly pyrite and is generally associated with hornblende and biotite.		
Alteration	Chlorite; clays minerals		

Mineralogical composition

Mineral	Modal (%)	Shape	Grain size (mm)	Observation
Plagioclase	40	Euhedral - Subhedral	0.5 -2.5	Labradorite (Michel-Levy Method) with alteration minerals
Orthoclase	20	Anhedral	1 - 4	Alteration to carbonates
Microcline	5	Anhedral	0.5 – 2.6	Exsolution - perthitic
Quartz	20	Subhedral	0.5 - 4	Polycrystalline and monocrystalline
Hornblende	10	Subhedral - Euhedral	0.7 - 1	Preferably where there is biotite.
Biotite	<1	Tabular	1	Associated with horblende

Zircon	<1	Euhedral	0.2	
Chlorite	<1	Anhedral	0.5	Alteration mineral
Opaques	1	Cubic	< 0.5	Pyrite Magnetite
Clays	<1	N/A	N/A	Alteration mineral in orthoclase

Sample: Moss-14

Latitude	48.60464°	**Longitude**	-90.58906°
Map unit.	Felsic metavolcanic rocks		
Rock type	Felsic metavolcanic rock		
Texture	Schist texture		
General description	The sample corresponds to an intermediate metavolcanic rock (Wall Rock) intruded by a quartz vein (100%) with a granular texture and anhedral crystals with chlorite veins. The wall rock with deformed layers, some layers with polycrystalline quartz. Between the layers, some epidote crystals of irregular and tabular habit are observed, as granular aggregates filling fractures and associated with opaque minerals. some sectors with tremolite-actinolite of high relief and prismatic habit oriented toward lamination. The sample has a black groundmass.		
Alteration	Chlorite – epidote - tremolite-actinolite.		

Mineralogical composition

Mineral	Modal (%)	Shape	Grain size (µm)	Observation
Plagioclase	55	Micro-tabular	< 4	
Quartz 1	5		< 4	In wall rock
Groundmass	20		< 4	
Tremolite-actinolite	10		< 4	Alteration
Epidote	10		30	Alteration
Quartz 2	100	Anhedral	60	In veins, polycrystalline Undulose extinction

Chlorite	<1	Micro-tabular	< 4	In veins alteration

Sample: Moss-16

Latitude	48.60599°	**Longitude**	-90.58110°
Map unit.	Felsic metavolcanic rocks		
Rock type	Felsic metavolcanic rock		
Texture	Porphyritic with hyalocrystalline groundmass.		
General description	The sample corresponds to an intermediate metavolcanic rock. Composed of plagioclase (55%); subhedral to euhedral crystals, predominantly andesine (measured by the Michel-Lévy method); potassium feldspar albite - sanidine (25%); quartz (5%) with crystals anhedral. Opaques <1% of the sample with magnetite and pyrite were also observed mainly. Minerals of alteration, mainly sericite, replace some phenocrysts of feldspar, creating shadows. Chlorites in the contacts between the veinlets and the host rock. In the groundmass, crystals smaller than 0.1 mm are observed; these comprise 20% of the sample and are composed mainly of plagioclase and small sericite crystals. The sample is crossed by two families of veins. The first family of carbonates with the development of calcite, which is cut at somewhere between 60-70 degrees by a second family of veinlets, these of polycrystalline quartz.		
Alteration	Sericite – Chlorite - Carbonates		

Mineralogical composition

Mineral	Modal (%)	Shape	Grain size (mm)	Observation
Plagioclase	55	Subhedral	1	some phenocrystals of feldspar, creating shadows in the old crystals (Alteration)
Sanidine	25	Subhedral	1.5	Measured by the Michel-Lévy method
Quartz	5	Anhedral	1.5	Some rounded crystals
Calcite	5	Tabular	0.5	In veins
Sericite	8	Tabular	<0.031	Alteration

Chlorite	<1	N/A	0.1	
Opaques	<1	Euhedral	0.125	

Sample: Moss-17

Latitude	48.60599°	**Longitude**	-90.58110°
Map unit.	Intermediate to felsic hypabyssal rock - feldspar porphyry		
Rock type	Felsic metavolcanic rock		
Texture	Schist texture		
General description	The sample corresponds to an intermediate metavolcanic rock apparent lamination. The sample can be divided into two domains: a) cryptocrystalline matrix (67%). b) Particles between 0.2 - 0.8 mm floating quartz crystals (7%) of subangular to angular and subspherical to sub-elongated shape oriented. Likewise, feldspar crystals (10%) of the elongated shape of 0.2 - 1.5 mm size altered to sericite (10%). Additionally, microfractures with an alteration microhalo. The microfractures contain alteration minerals such as chlorite (3%) and carbonates (<1%). Opaque minerals are present with (2%), mainly of galena - pyrite of euhedral-cubic shape.		
Alteration	Chlorite - Sericite - Carbonates		

Mineralogical composition

Mineral	Modal (%)	Shape	Grain size (mm)	Observation
Plagioclase	10	Subhedral	1 – 1.5	
Quartz	7	Subhedral	0.2 – 0.8	Monocrystalline
Carbonates	<1	Micro-tabular	0.8	Alteration
Sericite	10	Micro-tabular	0.6	Alteration
Chlorite	3	Irregular	0.6	Alteration
Opaques	2	Euhedral - cubic	0.31	
Groundmass	67	N/A	0.0040	

Sample: Moss-19

Latitude	48.56876°	**Longitude**	-90.65775°
Map unit.	Mafic metavolcanic rock - chlorite epidote actinolite schist		
Rock type	Meta-Ultramafic Rock		
Texture	Schist texture		
General description	The sample corresponds to a quartz sericite schist with veins. It is predominantly composed of quartz 1 (30%) in rock with 0.1 mm crystals, plagioclase (10%) and feldspar (25%) altered to sericite (15%), giving a sugary appearance to the feldspar crystals with sizes less than 0.5 mm. Crystals of actinolite tremolite (10%) were also observed throughout the rock. The veins contain quartz 2 (5%) monocrystalline, calcite (3%) in well-developed crystals with their characteristic twinning, and chlorite (1%) associated with the edges of the veins. The opaque minerals (<1%) correspond to pyrite developed in cubic crystals.		
Alteration	Actinolite, chlorite; sericite; calcite		

Mineralogical composition

Mineral	Modal (%)	Shape	Grain size (mm)	Observation
Quartz 1	30	Subhedral - Anhedral	0.1	In wall rock
Quartz 2	5	Subhedral	0.2 – 0.3	In veins monocrystalline
Actinolite tremolite	10	Fibrous	< 0.5	Distributed throughout the groundmass
Plagioclase	10	Subhedral	0.1	Altered to sericite
Feldspar	25	Anhedral	<0 .5 -1	In the groundmass alteration
Sericite	15	Flaky	N/A	Association with veins and opaques
Chlorite	1	Subhedral	< 0.5	Association with veins
Calcite	3	Euhedral	0.2 -0.5	In veins with well-developed crystals
Opaques	<1	Cubic	0.1	Pyrite in crystal cubic

Sample: Moss-20

Latitude	48.56497°	**Longitude**	-90.59602°
Map unit.	Mafic metavolcanic rocks - chlorite epidote actinolite schist		
Rock type	Meta-ultramafic rock		
Texture	Schist texture		
General description	The sample corresponds to a meta ultramafic rock. Predominantly hornblende phenocrysts between 80-90%, 0.50 mm, crystals from euhedral to subhedral; the matrix is actinolite with pyroxenes (augite). Some sectors are observed with carbonates resulting from rock alteration and with a percentage of less than 1% of opaques (chalcopyrite-pyrite).		
Alteration	Actinolite, Carbonates.		

Mineralogical composition

Mineral	Modal (%)	Shape	Grain size (mm)	Observation
Hornblende	80	Euhedral Subhedral	0.5	Occurring as skeletal phenocrysts
Actinolite tremolite	10	Fibrous	0.02	Occurring between the hornblende crystals in elongated shapes and bordered grains
Augite	2	Subhedral	0.02	Pyroxene
Carbonates	8	N/A	< 0.003	Observed among the skeletal of the hornblendes.
Opaques	<1	Fibrous	0.1	Restricted to the matrix of the rock.

Sample: Moss-21

Latitude	48.56497°	**Longitude**	-90.59602°
Map unit.	Mafic metavolcanic rocks - chlorite epidote actinolite schist		
Rock type	Meta-Ultramafic Rock		
Texture	Schist texture		
General description	The sample corresponds to an ultramafic rock with a strong penetrating alteration. The rock was originally ultramafic with hornblende phenocrysts (25%) of anhedral to subhedral crystals. The hornblendes are associated with epidotes (50%), possibly produced by alteration of plagioclase. However, no traces or signs of plagioclase were observed in the sample. Some sectors with actinolite (20%) are between the hornblende crystals in elongated shapes and bordered grains. Sericite (4%) and chlorite (1%) appear to fill microfracture and are among the skeletons of the hornblendes		
Alteration	Actinolite - sericite		

Mineralogical composition

Mineral	Modal (%)	Shape	Grain size (mm)	Observation
Hornblende	25	Anhedral Subhedral	0.3 – 0.8	Occurring as skeletal phenocrysts
Actinolite	20	Fibrous	0.02	Occurring between the hornblende crystals in elongated shapes and bordered grains.
Epidote	50	Anhedral	1.5	Alteration
Sericite	4	Subhedral	0.2	Observed among the skeletal hornblendes and veins
Chlorite	1	Subhedral	0.5	Vein

Sample: Moss-22

Latitude	48.56819°	**Longitude**	-90.57891°
Map unit.	Mafic metavolcanic rocks; massive flow, fine to medium-grained		
Rock type	Felsic metavolcanic rock		
Texture	Schist texture		
General description	The sample corresponds to a layered felsic metavolcanic rock with a groundmass of 43 - 50% black, with 50 µm deformed plagioclase (20%) and quartz (10%) crystals, with some 200 µm polycrystalline quartz crystals (5%) in spherules. As secondary minerals, sericite (15%) with a flaky texture and carbonates.		
Alteration	Sericite - carbonates		

Mineralogical composition

Mineral	Modal (%)	Shape	Grain size (µm)	Observation
Plagioclase	20	Micro-tabular	50	
Quartz	5	Spherulite	200	
Quartz	10	Anhedral	50	
Sericite	15	Flaky	< 4	Alteration
Carbonates	7	Micro-tabular	< 4	In veins alteration
Groundmass	43	N/A	< 4	

Sample: Moss-24

Latitude	48.58650°	**Longitude**	-90.55314°
Map unit.	Mafic metavolcanic rocks		
Rock type	Meta felsic intrusive rock		
Texture	Holocrystalline texture		
General description	The sample corresponds to a felsic intrusive rock with a strong pervasive alteration; intruded for a quartz vein. The wall rock is characterized by feldspar - orthoclase (20%) of subhedral anhedral-shaped crystal with relict textures with orientation. The quartz 1 (15%) is a polycrystalline and subhedral, between 0.2 - and 0.5 mm in size, and is restricted to the wall rock. Alteration minerals included actinolite-tremolite (30%) and epidote (1%). The presence of opaque (6%) pyrite and magnetite is restricted to the wall rock. The vein is composed mainly of quartz 2 (20%) anhedral and polycrystalline, and quartz 3 (7%) the 0.2 size and subhedral in aggregates. Additional anhedral epidote (1%) associated with quartz 3.		
Alteration	Actinolite-tremolite, chlorite, epidote.		

Mineralogical composition

Mineral	Modal (%)	Shape	Grain size (mm)	Observation
Feldspar Orthoclase	20	Subhedral Anhedral	0.5 – 1.5	Relict textures
Quartz 1	15	Subhedral	02 – 0.5	Wall rock
Quartz 2	20	Anhedral	0.5 – 1.6	Vein polycrystalline
Quartz 3	7	Subhedral	0.1 – 0.3	Vein association aggregates.
Actinolite-Tremolite	30	Tabular	0.1 – 0.5	Alteration mineral
Epidote	1	Anhedral	0.1 – 0.04	Preferably with quartz 3.
Chlorite	1	Anhedral	0.04	Alteration mineral
Opaques	6	Cubic	250 µm	Pyrite associated magnetite

Sample: Moss-25

Latitude	48.60544°	**Longitude**	-90.579928°
Map unit.	Felsic metavolcanic rocks		
Rock type	Intermediate metavolcanic rock		
Texture	Inequigranular holocrystalline texture		
General description	The sample corresponds to an Intermediate metavolcanic rock with aphanitic inequigranular holocrystalline texture. The sample is characterized by orthoclase (45%) and sanidine (20%) of anhedral to subhedral type shape crystal. The quartz (1%) is restricted to 0.2 mm sizes and monocrystalline shape; plagioclase (20 %) exhibits polysynthetic twinning. Alteration minerals, including chlorite (5%) of 0.3 mm, sericite (3%) of < 0.08 mm size in Fflaky shape and both minerals located in the veinlets. The Calcite (3%) with well-developed prismoid-shaped crystals. The presence of opaque (3%) minerals is generally associated with hornblende and biotite.		
Alteration	Chlorite; Sericite, Carbonates		

Mineralogical composition

Mineral	Modal (%)	Shape	Grain size (mm)	Observation
Orthoclase	45	Anhedral	0.3	Deformed association plagioclase
Sanidine	20	Subhedral	0.1 -0.5	Deformed association plagioclase
Quartz	1	Subhedral	0.1 -0.3	Monocrystalline
Plagioclase	20	Euhedral	300	Polysynthetic twinning
Chlorite	5	Subhedral	0.3	Alteration in vein
Sericite	3	Flaky	< 0.08	Alteration mineral
Carbonates	3	prismoid	0.8	Alteration mineral calcite in vein
Opaques	3	Cubic	60	Magnetite – pyrite

Sample: Moss-26

Latitude	48.60544°	**Longitude**	-90.57992°
Map unit.	Felsic metavolcanic rock		
Rock type	Intermediate metavolcanic rock		
Texture	Hyalocrystalline texture		
General description	The sample corresponds to an intermediate metavolcanic rock. Composed mainly of plagioclase (70%); subhedral to euhedral crystals, predominantly albite (measured by the Michel-Lévy method); some crystals with a porphyritic texture but altered. Quartz (10%) occurring as a subhedral crystal wall rock. Carbonates (10%) as alteration products. Sericite between 3 – 5% and pyrite (<1%) in veins. The sample is cut by two families of veins. The first family of carbonates developed calcite (2%), and the second family of quartz veins (5%) equigranular polycrystalline quartz.		
Alteration	Carbonates - sericite		

Mineralogical composition

Mineral	Modal (%)	Shape	Grain size (mm)	Observation
Plagioclase	70	Subhedral	0.5 – 0.1	Phenocrystals of feldspar, altered.
Quartz	10	Subhedral	0.2 – 0.1	In wall rock
Carbonate	10	Anhedral	<0.031	Alteration of some areas of the sample
Sericite	3	Tabular	<0.031	Restricted to the matrix of the groundmass
Opaques	<1	Cubic	<0.031	Pyrite location in veins
Quartz	5	N/A	1 – 1.5	In polycrystalline veins with undulose extinction
Calcite	2	Tabular	0.3	In veins

Sample: Moss-27

Latitude	48.59394°	**Longitude**	-90.54543°
Map unit.	Mafic and ultramafic intrusive rocks - Gabbro, leucogabbro		
Rock type	Meta- ultramafic intrusive Rock		
Texture	Schist		
General description	The sample corresponds to a meta ultramafic rock. Predominantly of hornblendes phenocrysts between 65 - 70%, 0.4 - 1.5 mm, crystals from euhedral to subhedral; with plagioclase crystals of 10%, possibly albite; with quartz 10% (granophyric texture), 0.8 - 2 mm; a second family of quartz 5% euhedral - subhedral crystals. Chlorite 4% and carbonates 5% are accessory minerals.		
Alteration	Carbonates – Chlorite.		

Mineralogical composition

Mineral	Modal (%)	Shape	Grain size (mm)	Observation
Hornblende	65	Anhedral Subhedral	0.4 – 1.7	Amphibole
Plagioclase	10	Fibrous	0.020	
Quartz 1	10	Euhedra - Subhedral	0.8 - 2	Graphic texture
Quartz 2	5	Subhedral	0.3 – 0.5	
Carbonates	5	N/A	< 0.003	
Chlorite	4	Fibrous	0.07	
Opaques (pyrite)	<1	Cubic	0.07	

Sample: Moss-28

Latitude	48.56819°	**Longitude**	-90.57891°
Map unit.	Mafic metavolcanic Rocks; massive flow, fine to medium-grained		
Rock type	Felsic metavolcanic rock		
Texture	Phyllite texture		
General description	The sample corresponds to a felsic metavolcanic rock with a groundmass of 10% black; plagioclase crystals (45 %) size 8 µm oriented with the layers. A second type of plagioclase 2 (10 %) is observed in tabular shape and 60 µm. Quartz (5%) crystals are observed in aggregates forming lithophysae structures with central openings. These aggregates are aligned and surrounded by the rock groundmass. Some quartz and plagioclase 2 crystals are surrounded by sericite (5%) and actinolite–tremolite (25%).		
Alteration	Sericite - actinolite – tremolite		

Mineralogical composition

Mineral	Modal (%)	Shape	Grain size (µm)	Observation
Plagioclase 1	45	Micro-tabular	8	
Plagioclase 2	10	Tabular	60	
Quartz	5	spherulite	65	Spherulite
Groundmass	10	N/A	< 4	Minerals cannot be identified
Sericite	5		< 4	
Actinolite – tremolite	25	N/A	9	Fibrous

Sample: Moss-30

Latitude	48.51835°	**Longitude**	-90.58952°
Map unit.	Mafic and ultramafic intrusive rocks		
Rock type	Schist		
Texture	Lepidoblastic.		
General description	The sample corresponds to a schist with a lepidoblastic. texture with aligned and parallel minerals with actinolite (75%) of greenish-yellow colour, tremolite (2%), biotite (2%), and muscovite (3%) aligned with each other and quartz crystals (2%) with anhedral shape. Chlorite (13%), epidote (1%), carbonates (1%) and hematite (< 1%) are products of alteration and fractures.		
Alteration	Carbonates - Sericite		

Mineralogical composition

Mineral	Modal (%)	Shape	Grain size (mm)	Observation
Actinolite	75	Flakes - tabular	0.1 - 1	
Tremolite	2	Tabular	0.4	
Biotite	2	Tabular	0.5	
Muscovite	3	Tabular	0.5	
Quartz	2	Anhedral	0.4	
Chlorite	13	Tabular l	0.7	
Carbonates	< 1	Anhedral	0.3 – 0.6	
Epidote	< 1	Tabular	0.4	
Hematite	< 1	N/A	N/A	Alteration

Sample: Moss-32

Latitude	48.51331°	**Longitude**	-90.59850°
Map unit.	Late felsic to mafic intrusive rocks - Feldspar porphyritic rocks Hood Lake stock		
Rock type	Felsic intrusive rock		
Texture	Inequigranular holocrystalline texture		
General description	The sample corresponds to a felsic intrusive rock with inequigranular holocrystalline texture with orientation in the crystals. The sample is characterized by orthoclase (56%), sanidine (2%), and microcline (2). These minerals with sizes between 0.5 to 15 mm are oriented and have well-developed crystalline. The quartz (5%) of monocrystalline type is restricted to sizes between 0.2 - 0.7 mm and preferentially located between the orthoclase crystals and clusters of hornblendes. The euhedral hornblende (20%) associated with clinopyroxenes (8%), biotite (3%) and epidota (1%). zircons of sizes less than 0.6 mm among clinopyroxenes and opaque minerals (1%) in cubic shape.		
Alteration	Epidote		

Mineralogical composition

Mineral	Modal (%)	Shape	Grain size (mm)	Observation
Orthoclase	56	Euhedral	7 - 15	Exsolution- perthitic in phenocrysts
Sanidine	2	Anhedral	2 – 3.5	Associated with orthoclase and microcline
Microcline	2	Anhedral	0.5 – 1.5	Observed in transitional contact with orthoclase
Quartz	5	Subhedral	0.2 – 0.7	Monocrystalline
Clinopyroxenes	8	Subhedral - euhedral	1 – 1.5	In clusters
Biotite	3	Tabular	0.25 – 0.5	slightly oriented
Hornblende	20	Euhedral	0.5 – 1.7	Associated with biotite and opaque hornblende
Epidote	<1	Subhedral	0.6	Alteration mineral
Opaques	<1	Cubic	0.1	Magnetite – pyrite

Zircon	<1	Euhedral	< 0.6	Associated with clinopyroxenes

Sample: Moss-33

Latitude	48.51369°	**Longitude**	-90.61742°
Map unit.	Late felsic to mafic intrusive rocks - Hood Lake stock.		
Rock type	Felsic intrusive rock		
Texture	Porphyry holocrystalline texture		
General description	The sample corresponds to a felsic intrusive rock with inequigranular holocrystalline texture, deformed which is evidenced by the orientation of sanidine, orthoclase and hornblende crystals. The sample is formed by orthoclase (20%) and sanidine (41%) of tabular - euhedral type shape crystal, with phenocrysts of 6 - 10 mm size. These minerals present antiperthitic exsolution textures (exsolution of plagioclase (albite?) from orthoclase and sanidine). Additionally, microcline (10%) with crystal sizes between 7 - 10 mm is observed. The quartz (5%) is restricted to < 0.3 mm sizes polycrystalline; plagioclase (10 %) which exhibits polysynthetic twinning (albite?), biotite (5%); amphiboles such as hornblende (5%); Pyroxenes (2%); opaques (1%) and rutile (1%) possibly a product of alteration or product of metamorphism.		
Alteration	Rutile		

Mineralogical composition

Mineral	Modal (%)	Shape	Grain size (mm)	Observation
Orthoclase	20	Tabular - euhedral	6 - 8	Porphyry exsolution - perthitic
Microcline	10	Tabular	4	Porphyry
Sanidine	41	Tabular - euhedral	7 - 10	Porphyry exsolution - perthitic
Quartz	5	Subhedral	0.3	Polycrystalline between the spaces of phenocrystals.
Plagioclase	10	Tabular	0.1 – 0.3	Polysynthetic twinning
Biotite	5	Flaky - tabular	0.5	Associated with Opaques
Hornblende	5	Subhedral	1.2	Preferably where there is biotite.

Rutile	1	Euhedral	0.5	Alteration mineral or product of metamorphism
Pyroxenes	2	Anhedral	1.1	
Opaques	1	Subhedral	0.2	

Sample: Moss-36

Latitude	48.51245°	**Longitude**	-90.70646°
Map unit.	Late felsic to mafic intrusive rocks - pegmatite		
Rock type	Meta felsic intrusive rock		
Texture	Gneissic texture		
General description	The sample corresponds to a gneiss with orientations of sanidine phenocrystals and with well-defined domains in the sample. Orthoclase crystals (20%) of subhedral shape and sizes of 1 - 2 mm, which are being altered to clay minerals; sanidine (8%) of tabular shape, oriented and sizes of 8 - 10 mm. The quartz (34%) polycrystalline subhedral and plagioclase (10%) that presents polysynthetic twinning, biotite (1%) located in microfractures and amphiboles such as hornblende (22%) in clusters and in well-defined domains, clay minerals (1%) as a product of orthoclase alteration and opaque minerals (2%) located in microfractures.		
Alteration	Actinolite-Tremolite, Sericite, Epidote, Clays		

Mineralogical composition

Mineral	Modal (%)	Shape	Grain size (mm)	Observation
Orthoclase	20	Subhedral	1 - 2	With clay mineral alterations
Sanidine	8	Tabular	8 - 12	Phenocryst
Quartz	34	Subhedral	1 - 4	Polycrystalline
Plagioclase	10	Euhedral	0.3 - 1.4	with twinning
Biotite	1	Tabular	0.1	Associated with microfractures
Hornblende	24	Subhedral	1.5 - 2	In clusters
Opaques	2	Subhedral	0.2	Magnetite in microfractures
Clay	< 1	N/A	N/A	Alteration

Sample: Moss-37

Latitude	48.51245°	**Longitude**	-90.70646°
Map unit.	Mafic and ultramafic intrusive rock		
Rock type	Schist		
Texture	Schistose texture		
General description	The sample corresponds to a actinolite schist intruded by alkali feldspar vein. The schist shows a well-developed foliation characterized by the alignment of chlorite and actinolite. Chlorite appears as green, flaky crystals, with gray interference colors and located mainly in the between ctinolite schist and alkali feldspar vein. Actinolite is present as elongated green needles with moderate birefringence and a lepidoblastic texture in several directions. Epidotes appear as yellowish prismatic crystals. Zoisite crystals (<1%) with a bluish colour and a tabular crystalline habit are observed. The intrusive rock of potassium feldspar and plagioclase (for this last mineral, relict textures of polysynthetic twins are locally observed) is strongly altered to clay minerals. Both rocks (igneous and metamorphic) are cut by microfractures, which serve as fluid circulation channels and receptors for minerals such as chlorite and epidote; later, opaque minerals (pyrite and chalcopyrite) are formed.		
Alteration	Chlorite – carbonates		

Mineralogical composition

Mineral	Modal (%)	Shape	Grain size (µm)	Observation
Epidote	4	Tabular	400	Lepidoblastic
Actinolite	55	Tabular	200	Lepidoblastic
Chlorite	40	Tabular	100	Alteration
Zoisite	<1	Tabular	400	Lepidoblastic
Opaques	<1	Cuboid	30	
Alkali feldspar	N/A	Subangular	500	Holocrystalline
Carbonate	N/A	N/A	< 4	Alteration

Sample: Moss-38a

Latitude	48.51245°	**Longitude**	-90.70646°
Map unit.	Late felsic intrusive rocks - Feldspar porphyritic rocks - Hood Lake stock		
Rock type	Felsic intrusive rock		
Texture	Porphyritic texture		
General description	The sample corresponds to meta-felsic intrusive rock with a porphyritic texture. However, foliation is observed with the orientation of the orthoclase (62%) and pyroxene (10%) phenocrysts. A perthitic texture can be observed in orthoclase crystals. Quartz (8 - 10%) of anhedral type and between the interstices between the feldspar crystals. Horblendes (3%) and rutile (1%) also occur. Opaque minerals (magnetite 2%) are associated with pyroxenes and biotite (7%).		
Alteration			

Mineralogical composition

Mineral	Modal (%)	Shape	Grain size (mm)	Observation
Orthoclase	62	Euhedral	15	Phenocrystal perthitic texture
Microcline	7	Anhedral	2.5	Intergrowths orthoclase/microcline
Quartz	8	Anhedral	0.3	Anhedral and between the interstices between the feldspar crystals.
Rutile	1	Anhedral	0.5	
Biotite	7	Tabular	0.6	Anhedral - flakes.
Hornblende	3	Subhedral	1	Concentrated in sectors of the sample and is associated with pyroxenes and rutile
Pyroxene	10	Subhedral	1	
Opaque minerals	2	Anhedral	0.2	Magnetite

Sample: Moss-38b

Latitude	48.51245°	**Longitude**	-90.70646°
Map unit.	Late felsic intrusive rocks - Feldspar porphyritic rocks - Hood Lake stock		
Rock type	Felsic intrusive rock		
Texture	Gneiss texture		
General description	The sample corresponds to a felsic intrusive rock with two well-differentiated bands that can be distinguished. A light-colored one composed mainly of feldspar and a dark band of ferromagnesian mineral. The total sample with orthoclase phenocrysts (45%) and microclines (5%). Additionally, plagioclase (5%) and quartz (8 - 10%) occur, both as anhedral-type minerals in the interstices between the feldspar crystals. Within the ferromagnesian minerals, hornblende (20%) and rutile (1%) and pyroxenes (10%) are present. Biotite (12%) orients in bands and opaque minerals (magnetite 2%).		
Alteration			

Mineralogical composition

Mineral	Modal (%)	Shape	Grain size (mm)	Observation
Orthoclase	45	Euhedral	4-10	Phenocrystal perthitic texture
Microcline	5	Anhedral	3	Intergrowths with orthoclase
Quartz	8	Anhedral	0.3	Anhedral and between the interstices of the feldspar crystals.
Rutile	1	Anhedral	0.5	
Biotite	12	Tabular	0.5 - 1	Flakes and two directions aligned
Hornblende	20	Subhedral	1	It is concentrated in a thick layer associated with associated with pyroxenes, biotite and rutile
Plagioclase	5	Anhedral	03	Between the interstices of the feldspar crystals.
Pyroxene	10	Subhedral	1	
Opaque minerals	2	Anhedral	0.2	Magnetite

Sample: Moss-44

Latitude	48.52640°	**Longitude**	-90.79595°
Map unit.	Mafic and ultramafic intrusive rocks - Gabbro, leucogabbro		
Rock type	Meta- ultramafic intrusive rock		
Texture	Medium to coarse-grained crystalline texture		
General description	Ultramafic rock with 50% phenocrysts; predominantly composed of 5% hornblende crystals; 25% plagioclase 2, and 20% clinopyroxenes (augite). The groundmass is 38% plagioclase with 8% pyroxene. The alteration minerals present 3% chlorite and opaques, mainly pyrite, less than 1%.		
Alteration	Chlorite - opaques		

Mineralogical composition

Mineral	Modal (%)	Shape	Grain size (mm)	Observation
Plagioclase 1	25	Euhedral	1.5	With twinning
Plagioclase 2	38	N/A	< 0.0039	Groundmass
Pyroxene	8	Anhedral	< 0.0039	Groundmass
Clinopyroxene	20	Tabular	2 - 3	Phenocrysts high relief
Hornblende	5	Euhedral	2	Phenocrysts with twinning
Chlorite	3	N/A	0.25	Alteration
Opaques (Piryte)	<1	Euhedral	1	

Sample: Moss-47

Latitude	48.53220°	**Longitude**	-90.80005°
Map unit.	Intermediate to felsic hypabyssal rocks		
Rock type	Intermediate metavolcanic rock		
Texture	Schist		
General description	The sample corresponds to intermediate metavolcanic rock. Composed of plagioclase 1 in phenocrysts (10%) with subhedral to euhedral crystals, predominantly andesine (measured by the Michel-Lévy method); plagioclase 2 (60%) restricted to the groundmass with sizes of 0.1 mm or smaller. Quartz (5%) with monocrystalline anhedral crystals and with irregular border alteration minerals include carbonates (5%) are associated with feldspar phenocrystals and sericite (9%) and associated with plagioclase of the fundamental mass. Chlorite (8%) with orientation associated with chalcopyrite. Opaque minerals of 0.25 to 0.30 mm of pyrite, chalcopyrite, galena and sphalerite and cubic -euhedral shapes.		
Alteration	Sericite – Chlorite - Carbonates		

Mineralogical composition

Mineral	Modal (%)	Shape	Grain size (mm)	Observation
Plagioclase 1	10	Subhedral	0.8 - 1.5	In feldspar phenocrysts, mainly andesine (Michel-Levy Method) with shadows on the crystals (Alteration)
Plagioclase 2	60	Anhedral	0.1	In groundmass
Quartz	8	Anhedral	0.3 – 0.5	Monocrystalline and with irregular edges
Carbonates	5	N/A	N/A	Alteration and association with plagioclase 1 phenocrysts.
Sericite	7	Tabular	< 0.004	Alteration
Chlorite	8	N/A	N/A	Alteration product and orientation of the crystal's association with chalcopyrite.

Opaques	2	Cubic - Euhedral	0.25 – 0.30	Pyrite, chalcopyrite, galena and sphalerite

Sample: Moss-50

Latitude	48.53446°	**Longitude**	-90.80623°
Map unit.	Intermediate to mafic metavolcanic rocks - massive flow, fine to medium grained		
Rock type	Metasedimentary rock		
Texture	Schist texture		
General description	The sample corresponds to a metasedimentary rock. With a framework of quartz particles between 25 - 30% angular to subrounded in shape. quartz fragments of two types, monocrystalline and polycrystalline; with 5% angular plagioclase grains. Matrix mainly of quartz grains 10% silt size, forming subrounded amalgamated and compact, plagioclase crystals 20% with tabular in shape. Secondary minerals, the opaque minerals are chalcopyrite - pyrite <1%, and hematite 4%, the latter located at the intersections of the structural crystals. The rock has 20% carbonates, possibly a product of alteration, and sericite 10% crystals.		
Alteration	Sericite – Hematite- Carbonates		

Mineralogical composition

Mineral	Modal (%)	Shape	Grain size (mm)	Observation
Quartz 1	30	Angular to surrounded	0.25	Framework
Quartz 2	10	surrounded	0.01	Matrix
Plagioclase 1	5	Anhedral	0.12	Framework
Plagioclase 2	20	Tabular	< 0.004	Matrix
Carbonates	20	N/A	< 0.004	Alteration
Sericite	10	N/A	< 0.004	Metamorphism
Hematite	4	N/A	< 0.004	Alteration
Pyrite - chalcopyrite	<1	Cubic	0.12	

Sample: Moss-51

Latitude	48. .59055°	**Longitude**	-90.73760°
Map unit.	Late felsic to mafic intrusive rocks - hornblende +/- pyroxene syenite, monzonite - Obadinaw stock		
Rock type	Felsic intrusive rock		
Texture	Inequigranular holocrystalline texture		
General description	The sample corresponds to a felsic intrusive rock with an inequigranular holocrystalline texture. The sample is characterized by phenocrystals of orthoclase (80%) with perthitic texture and anhedral crystals. The polycrystalline quartz (10%) is located between the orthoclase crystals with sizes between 02 - 0.7 mm. Plagioclase (3%) presents polysynthetic twinning; like quartz, the crystals are located between the orthoclase crystals. Biotite (2%) is associated with carbonates, possibly due to alteration. Amphiboles such as hornblende (3%) aligned with the biotites. Alteration minerals such as carbonates are associated with biotite and calcite (2%), with a well-developed crystalline habit with its characteristic twinning; opaque minerals (1%), include magnetite and pyrite, with a size equal to or less than 0.01 mm.		
Alteration	Carbonates, calcite		

Mineralogical composition

Mineral	Modal (%)	Shape	Grain size (mm)	Observation
Orthoclase	80	Anhedral	2 – 4.5	Exsolution- perthitic in phenocrysts
Quartz	10	Euhedral subhedral	0.2 -0.7	Polycrystalline
Plagioclase	3	Euhedral	0.2 – 0.5	Polysynthetic twinning
Biotite	2	Tabular	0.2 – 1.5	Associated with carbonates
Hornblende	3	Euhedral subhedral	0.6 – 1.7	Preferably where there is biotite.
Carbonates - calcite	2	Euhedral subhedral	0.8 - 2	Alteration minerals in biotite in some sectors of calcite are observed
Opaques	< 1	Euhedral	0.01	Magnetite – pyrite

Sample: Moss-53

Latitude	48.56476°	**Longitude**	-90.71276°
Map unit.	Late felsic to mafic intrusive rock - hornblende +/- pyroxene syenite, monzonite - Moss Lake stock		
Rock type	Felsic intrusive rock		
Texture	Inequigranular holocrystalline texture		
General description	The sample corresponds to a felsic intrusive rock with inequigranular holocrystalline texture. The sample is characterized by orthoclase (62%) and microcline (3%), of anhedral-type shape crystal. The quartz (15%) is polycrystalline; plagioclase may be oligoclase (8 %). hornblende (7%). The minerals accessories included titanita <1%, Opaques; Magnetite - hematite (<1%)		
Alteration	Sericite		

Mineralogical composition

Mineral	Modal (%)	Shape	Grain size (mm)	Observation
Orthoclase	62	Anhedral	1.5 - 3	Exsolution- perthitic
Quartz	15	Subhedral	0.3 – 1.2	Polycrystalline
Microcline	3	Anhedral	2.5 – 0.8	Red twinning
Plagioclase	8	Subhedral	0.5	Polysynthetic twinning oligoclase??
Hornblende	7	Subhedral	0.6 – 1.4	Green in PPL
Pyroxenes	3	Euhedral	0.8 – 0.8	Brown, green in PPL (aegirine) extinction >80° in XPL.
Titanite	<1	prismoid	0.4 – 0.5	
Opaque	<1	Cubic	0.1	Magnetite - hematite
Sericite	< 1	N/A		Alteration mineral

Sample: Moss-57

Latitude	48.53639°	**Longitude**	-90.72133°
Map unit.	Intermediate to felsic hypabyssal rocks - feldspar porphyry		
Rock type	Intermediate metavolcanic rock		
Texture	Schist		
General description	The sample corresponds to a strongly chloridized intermediate metavolcanic rock. It is composed of plagioclase phenocrystals (20%), subhedral crystals with shadows, and actinolite tremolite within the crystals. A second family of plagioclase 2 (40%) of sizes 0.06 mm in the groundmass, which is chloritized. Quartz (10%) of subhedral form is also a constituent of the groundmass. Actinolite tremolite (15%) is distributed throughout the sample but is located mainly with the plagioclase 1 and horblende phenocrysts (5%). Alteration minerals include, calcite (5%), sericite (2%), and chlorite (2%) which are present throughout the sample. Opaque minerals are magnetite (1%), which is 0.1 mm or smaller.		
Alteration	Sericite – calcite - chlorite		

Mineralogical composition

Mineral	Modal (%)	Shape	Grain size (mm)	Observation
Plagioclase 1	20	Subhedral	2.3 – 4.5	In phenocrysts with shadows an strong alteration chlorite
Plagioclase 2	40	Anhedral	0.06	In groundmass.
Actinolite tremolite	15	Anhedral	0.1	In groundmass and same crystal of plagioclase 1.
Quartz	10	Subhedral	0.1	In groundmass.
Calcite	5	Tabular	0.2 - 0.5	Alteration
Sericite	2	Tabular	0.1	Alteration
Chlorite	2	N/A	N/A	All sample is chloritized
Horblende	5	Subhedral	0.3	Alteration to chlorite
Opaques	<1	Euhedral	0.1	Magnetite

Sample: Moss-59

Latitude	48.59503°	**Longitude**	-90.73920°
Map unit.	Clastic metasedimentary rocks (Quetico type)		
Rock type	Metasedimentary rock		
Texture	Schist texture		
General description	The sample corresponds to a metasedimentary rock. With a framework of quartz particles (40%), angular to sub-rounded in shape. Quartz fragments of two types, monocrystalline and polycrystalline; with 5% angular grains of plagioclase. Quartz matrix mainly of silt particle size of amalgamated and compact subrounded grains. Secondary minerals, opaque minerals (magnetite 2%) and biotite (13%) are present.		
Alteration	Hematite - magnetite		

Mineralogical composition

Mineral	Modal (%)	Shape	Grain size	Observation
Quartz	40	Angular to surrounded	Medium sand	Framework
Plagioclase	5	Tabular	Fine sand	Framework
Quartz	40	surrounded	Silt	Matrix
Biotite	13	Tabular	Silt	Produced metamorphism
Opaque (Hematite - magnetite)	2	Tabular	Silt	Matrix

Sample: Moss-85

Latitude	48.61206°	**Longitude**	-90.64042°
Map unit.	Late felsic to mafic intrusive rocks - Burchell Stock		
Rock type	Mafic metavolcanic rock		
Texture	Schist texture		
General description	The sample corresponds to a schist. It is mainly composed of feldspar (75%) in subhedral crystals with a size equal to or less than 0.06 mm; quartz (3%) in veins primarily; biotite (5%) in flaky with a preferential direction (aligned). Alteration minerals include chlorite (15%) and carbonates (1%). The opaque minerals, chalcopyrite (1%), and are in tabular and elongated include.		
Alteration	Chlorite; carbonate		

Mineralogical composition

Mineral	Modal (%)	Shape	Grain size (mm)	Observation
feldspars	75	Subhedral	< 0.06	In groundmass.
Quartz	3	Subhedral	0.2	In veins with crystal subhedral,
Carbonate	1	N/A	< 0.06	Alteration of some areas of the sample
Biotita	5	Flaky	0.1 -0.3	In clusters and oriented
Chlorite	15	Tabular	0.1	Oriented
Opaques	1	Tabular	0.25	Chalcopyrites

Sample: Moss-90

Latitude	48.61927°	**Longitude**	-90.63634°
Map unit.	Late felsic intrusive rocks - Burchell Lake stock		
Rock type	Felsic volcanic rock		
Texture	Aphanitic - inequigranular holocrystalline texture		
General description	The sample corresponds to a meta-felsic volcanic rock with inequigranular holocrystalline texture. The sample is characterized by orthoclase (45%) of anhedral-type shape crystal, these exhibit an earthy appearance, suggesting the presence of clay minerals as alteration products. The quartz (35%) is restricted to 0.1 - 0.5 mm sizes polycrystalline; plagioclase (25 %) which exhibits polysynthetic twinning, muscovite (1%) Associated with some veinlets and accessory minerals, hornblende (<1%) and pyrite (2%). Additionally, mineral clays (1%).		
Alteration	Clays		

Mineralogical composition

Mineral	Modal (%)	Shape	Grain size (mm)	Observation
Orthoclase	45	Anhedral	0.4 - 1	Clay mineral alterations
Quartz	35	Subhedral	0.1 – 0.5	Polycrystalline
Plagioclase	25	Subhedral	0.3	Polysynthetic twinning
Muscovite	1	Tabular	0.1	Associated with veinlets
Horblende	< 1	Euhedral	0.4	
Opaques	2	Cubic	0.4	Pyrite
Clays	< 1	N/A		Alteration

Sample: Moss-91

Latitude	48.61927°	**Longitude**	-90.63634°
Map unit.	Late felsic to mafic intrusive rocks - Burchell Lake stock - pegmatite		
Rock type	Felsic rock		
Texture	Porphyritic - holocrystalline texture.		
General description	The sample presents two types of rocks. A pyroclastic rock that is intruded by a felsic volcanic rock. Orthoclase phenocrysts (41%), with sanidine crystals (15%) with phanerocrystalline texture; plagioclase (15%) of smaller size 0.1 - 0.6 mm. and quartz (15%) of size 0.5 – 0.3. As accessory minerals, there are opaque minerals (7%) and biotite (7%). The pyroclastic rock is composed of epidote (50%) and a cryptocrystalline groundmass (50%), which is not identifiable due to the size of the grains (<0.031 mm).		
Alteration	Epidote		

Mineralogical composition

Mineral	Modal (%)	Shape	Grain size (mm)	Observation
Quartz	15	Subhedral	0.3 - 0.5	In cryptocrystalline groundmass
Plagioclase	15	Subhedral	0.5 - 2	Crystals and groundmass holocrystalline texture
Sanidine	15	Euhedral	0.1 - 0.6	Phenocrystals
Orthoclase	41	Euhedral	8	Phenocrystals
Opaques	7	Anhedral	<0.031	Pyrite
Biotite	7	Tabular	0.3 - 0.7	
Epidote	50	Euhedral	0.4	Alteration
Groundmass cryptocrystalline	50	N/A	<0.031	

Sample: Moss-98

Latitude	48.54174°	**Longitude**	-90.60434°
Map unit.	Mafic and ultramafic intrusive rocks		
Rock type	Meta-mafic rock		
Texture	Schist texture.		
General description	The sample corresponds to an ultramafic rock with alteration. The sample comprises plagioclase (80%) with an average size of 0.5 mm, with pyroxenes (1%), possibly augite. But, due to the size of the crystals (0.1 mm), it is not easily identifiable. Carbonates (15%), a product of alteration, and opaques (4%), mainly magnetite, chalcopyrite, bornite and pyrite.		
Alteration	Carbonates		

Mineralogical composition

Mineral	Modal (%)	Shape	Grain size (mm)	Observation
Plagioclase	80	Subhedral - Anhedral	0.5	In groundmass and alteration
Carbonates	15	N/A	< 0.06	Alteration
Pyroxene	1	Subhedral	0.1	Augite
Opaques	4	Subhedral	0.06 – 0.1	Magnetite, chalcopyrite, bornite, pyrite

Sample: Moss-100

Latitude	48.55483°	**Longitude**	-90.52454°
Map unit.	Felsic to mafic intrusive rocks - Greenwater Lake stock.		
Rock type	Felsic intrusive rock		
Texture	Schist texture		
General description	The sample corresponds to a felsic intrusive rock with crystal alignment. It is composed of two types of quartz: quartz 1 (10%) of monocrystalline 0.5 – 1 mm size, quartz 2 (30%) of anhedral shape with a size between 0.1 – 0.2 mm. plagioclase (10%) and microcline (5%). Additionally, amphiboles are observed, mainly hornblende (2%) and amphiboles (4%), possibly diopside and augite. The sample presents a well-differentiated layer of biotites (25%), a sector where the presence of quartz 2 is most marked and where the highest amount of chlorite (13%) of the sample is observed, showing a schistose-type texture. Accessory minerals are titanite, zircons and opaque minerals (<1%), mainly magnetite.		
Alteration	Chlorite		

Mineralogical composition

Mineral	Modal (%)	Shape	Grain size (mm)	Observation
Quartz 1	10	Subhedral	0.5 - 1	Monocrystalline
Quartz 2	30	Anhedral	0.1 – 0.2	Monocrystalline
Plagioclase	10	Subhedral	1 - 2	
Microcline	5	Anhedral	2.5	Association with plagioclase
Amphibolite	2	Anhedral	03 -06	Hornblende
Clinopyroxene	4	Subhedral	0.4 - 1	Diopside/augite
Biotite	25	Tabular	0.2 -0.5	Associated with the most metamorphosed sector aligned in one direction.
Chlorite	13	Flaky	0.1	Produced alteration association whit biotite
Titanite	< 1	Tabular	0.5	Trace
Opaques	< 1	Subhedral	0.08	Magnetite

Sample: Moss-107

Latitude	48.61442°	**Longitude**	-90.53245°
Map unit.	Mafic and ultramafic intrusive rock		
Rock type	Meta-mafic volcanic Rock		
Texture	Schist texture		
General description	The sample corresponds to a ultramafic rock with alteration. Plagioclase phenocrystals (5%) deformation with skeletal textures and altered to carbonates (10%) of amorphous forms. Biotite (10%) of tabular form and aligned. The sample presents a dark groundmass (60%) altered to sericite (5%) and crystals of actinolite tremolite (8%); opaque minerals (2%) are observed, mainly pyrite.		
Alteration	Actinolite; tremolite; Sericite		

Mineralogical composition

Mineral	Modal (%)	Shape	Grain size (mm)	Observation
Plagioclase 1	5	Anhedral	0.65 – 1.5	Occurring as skeletal phenocrysts and deformation
Biotite	10	Tabular	0.6 - 1	Aligned
Actinolite - tremolite	8	Subhedral	< 0.06	Distributed throughout the sample
Sericite	5	Tabular	< 0.06	Alteration of groundmass
Carbonates	10	Amorphous	N/A	Alteration of plagioclases
Opaques	2	Subhedral	0.1	Pyrite
Groundmass	60	N/A	N/A	Dark and altered to sericite, it presents actinolite tremolite.

Sample: Moss-108

Latitude	48.62031°	**Longitude**	-90.53899°
Map unit.	Mafic volcanic rock - Pillowed flows		
Rock type	Pillow lava rock		
Texture			
General description	The rock is pillow lava with vesicles and rounded masses of quartz; the groundmass of fine-grained plagioclase crystals and pyroxene.		
Alteration	Actinolite - tremolite - Chlorite		

Mineralogical composition

Mineral	Modal (%)	Shape	Grain size (mm)	Observation
Quartz	7	Subhedral	0.08	In bulbous and rounded masses. Polycrystalline.
Plagioclase	80	Subhedral - Anhedral	0.006	Groundmass with skeletal texture.
Pyroxene	10	Tabular	< 0.003	Interstitial
Actinolite tremolite	2	Fibrous	< 0.003	
Chlorite	1	Tabular	0.006	Alteration

Sample: Moss-114

Latitude	48.57303°	**Longitude**	-90.61374°
Map unit.	Late felsic to mafic intrusive rocks - Hermia Lake stock.		
Rock type	Felsic intrusive rock		
Texture	Inequigranular holocrystalline porphyritic texture		
General description	The sample corresponds to a felsic intrusive rock with inequigranular holocrystalline porphyritic texture The sample is characterized by orthoclase (92%) with exsolution-perthitic and sizes between 8 - 22 mm. sanidine (1%), subhedral in contact with orthoclase. Quartz (0.5%) is restricted to sizes 0.2, with some rounded crystals. Plagioclase (0.5%) presents polysynthetic twinning, biotite (0.5%) and amphiboles such as hornblende (2%). Pyroxenes (1%), possibly clinopyroxene, these last three are associated with each other. Zircon of sizes 0.2 mm or smaller. The alteration minerals are calcite (1%) with well-developed crystals and a characteristic twinning. Opaque minerals (1%), as magnetite and pyrite are observed in cubic crystals and are associated with zircon.		
Alteration	Calcite		

Mineralogical composition

Mineral	Modal (%)	Shape	Grain size (mm)	Observation
Orthoclase	92	Euhedral Subhedral	8 - 22	Phenocrysts with exsolution-perthitic
Sanidine	1	Subhedral	4	Association with orthoclase
Quartz	0.5	Subhedral	0.2	Less than 1%
Plagioclase	0.5	Euhedral	0.3 - 4	Less than 1%
Hornblende	2	Anhedral	2.2	Preferably where there is biotite.
Biotite	0.5	Euhedral	0.7	Less than 1%
calcite	1	Euhedral	0.6	Alteration
Zircon	0.5	Euhedral	0.2	Less than 1%
Pyroxene	1	Subhedral	0.8	Association with hornblende
Opaques	1	Cubic	0.5	Magnetite

Sample: Moss-121

Latitude	48.64876°	**Longitude**	-90.52799°
Map unit.	Mafic volcanic rocks		
Rock type	Meta-ultramafic rock		
Texture	Phyllite texture		
General description	The sample corresponds to a ultramafic rock, with aphanitic texture of plagioclase crystals (10%) of subhedral form. Quartz (5%) in crystals floating in the groundmass. Pyroxenes (5%) associated with plagioclase. Alteration minerals such as sericite (4%), carbonates (2%) of amorphous forms and chlorite (3%) are located around the quartz crystals. Accessory minerals such as ilmenite (1%) are tabular and of size less than 0.06 mm. Opaque minerals (5%), mainly magnetite in triangular form and pyrite.		
Alteration	Actinolite, sericite, chlorite, carbonates.		

Mineralogical composition

Mineral	Modal (%)	Shape	Grain size (mm)	Observation
Plagioclase	5	Subhedral	0.2	In the groundmass
Quartz	5	Subhedral	0.7	Isolated crystals floating in the groundmass
Pyroxene	5	Subhedral - tabular	0.2	Associated with plagioclase
Sericite	4	Subhedral	< 0.06	Alteration in groundmass
Carbonates	2	Amorpho us	0.3	Alteration
Chlorite	3	Subhedral	0.2	Alteration
Ilmenite	1	Tabular	< 0.06	
Groundmass	70	N/A	N/A	Dark
Opaques	5	Triangular - cubic	0.1 – 0.5	Magnetite, pyrite

Sample: Moss-134

Latitude	48.46203°	**Longitude**	-90.82953°
Map unit.	Granodiorite - Hamlin Lake stock		
Rock type	Felsic intrusive rock		
Texture	Equigranular panidomorphic texture.		
General description	The sample corresponds to a felsic intrusive rock with inequigranular panidomorphic texture of quartz (25%) is mainly monocrystalline. Plagioclase (50%) has shadows inside due to sericite alteration. Feldspars (10%) were altered to clay minerals and sericite. Accessory minerals are biotite (1%) of tabular form, hornblende (0.5%), apatite (1%) and zircons (<1%). Additionally, alteration minerals are represented by carbonates (0.5%) located only in one sector of the sample and sericite (5%) associated with plagioclase and feldspars. Opaque minerals (1%), mainly pyrite and magnetite.		
Alteration	Sericite, Carbonates, Clays		

Mineralogical composition

Mineral	Modal (%)	Shape	Grain size (mm)	Observation
Quartz	25	Euhedral	0.4 - 1	Monocrystalline
Plagioclase	50	Euhedral	2.5 - 1	Albite – oligoclase (Michel-Levy Method)
Feldspar	10	Euhedral - Subhedral	1 – 1.5	Associated with clay minerals
Biotite	1	Tabular	0.3 – 2.6	
Hornblende	0.5	Subhedral	0.5	Preferably where there is biotite.
Carbonates	0.5	Subhedral	01	
Sericite	5	Flaky	< 0.06	Altering plagioclase
Apatite	<1	Anhedral	0.1	Accessory mineral
Zircon	<1	Anhedral	0.1	Accessory mineral
Clays	<1	N/A	N/A	Alteration mineral in feldspar

Opaques	1	Cubic	0.1	Pyrite – magnetite.

Appendix B. Geochemical data

	ME-ICP06 %														
SAMPLE	**SiO2**	**Al2O3**	**Fe2O3**	**CaO**	**MgO**	**Na2O**	**K2O**	**Cr2O3**	**TiO2**	**MnO**	**P2O5**	**SrO**	**BaO**	**LOI**	**Total**
Moss-006a	70.6	15.65	2.47	1.77	1.76	4.2	1.98	0.005	0.3	0.02	0.07	0.03	0.02	2.9	101.78
Moss-007	57.3	16.1	7.04	2.97	4.56	3.46	2	0.026	0.49	0.06	0.1	0.03	0.04	5.3	99.48
Moss-008	51.6	17.35	9.11	4.32	3.74	6.33	1.01	<0.002	0.67	0.16	1.42	0.11	0.18	4.67	100.67
Moss-009	63.7	13.8	6.13	2.43	3.71	3.04	1.06	0.005	0.45	0.04	0.08	0.02	0.01	3.56	98.04
Moss-016	70.8	14.95	2.27	2.26	1.21	5.36	1.44	0.004	0.23	0.04	0.05	0.03	0.03	2.93	101.6
Moss-029	42.4	10.4	25.5	9.89	2.67	0.5	1.44	<0.002	0.71	0.95	0.35	0.02	0.03	4.08	98.94
Moss-039	59.3	14	12.4	0.93	0.7	5.58	1.35	<0.002	0.54	<0.01	0.07	0.02	0.01	6.83	101.73
Moss-040	62.8	15.6	4.88	4.19	2.68	2.97	2.02	0.015	0.37	0.12	0.13	0.02	0.03	5.56	101.39
Moss-041	66.1	15.15	3.01	2.61	1.37	4.2	1.64	0.003	0.29	0.08	0.08	0.02	0.03	3.69	98.27
Moss-043	62	17.9	4.59	4.19	2.7	4.81	2.06	0.007	0.42	0.06	0.12	0.06	0.04	1.66	100.62
Moss-054	68.6	14.95	2.64	2.75	1.09	5.19	1.2	0.002	0.26	0.03	0.06	0.04	0.03	2.47	99.31
Moss-055	70.1	15.2	2.46	3.03	1.09	4.49	1.36	0.002	0.27	0.02	0.08	0.04	0.03	1.87	100.04
Moss-089	52.1	15.05	13.45	5.37	4.22	1.36	1.83	0.019	0.72	0.3	0.17	0.02	0.02	4.26	98.89
Moss-100	62.5	16.4	4.36	5.01	3.69	5.59	1.68	0.019	0.45	0.06	0.24	0.16	0.1	0.88	101.14
Moss-102	45.1	16.65	10.6	9.39	9.3	2.02	0.33	0.069	0.6	0.14	0.05	0.01	0.01	3.89	98.16
Moss-104	75.7	10.65	4.92	1.26	1.92	4.86	0.05	0.003	0.41	0.05	0.08	<0.01	<0.01	1.9	101.8
Moss-105	67.6	15.3	2.43	1.53	0.47	5.21	2.45	<0.002	0.4	0.03	0.14	0.08	0.09	2.29	98.02
Moss-107	65.1	15.3	3.27	2.37	0.92	4.7	2.67	<0.002	0.77	0.04	0.39	0.07	0.14	2.84	98.58
Moss-108	46.9	15.55	12.45	10.05	7.21	0.76	0.58	0.05	0.87	0.21	0.13	0.04	0.01	3.37	98.18
Moss-112	69.4	15.95	3.05	2.61	0.99	5.11	3.32	<0.002	0.46	0.03	0.18	0.11	0.12	0.55	101.88
Moss-113	39.5	15.35	14.6	6.3	7.74	4.62	0.05	0.014	1.42	0.2	0.14	0.01	0.01	8.83	98.78
Moss-114	61.8	16.5	2.77	2.33	0.74	6.01	6.33	<0.002	0.2	0.06	0.24	0.16	0.14	1.32	98.6
Moss-119	49.7	13	13.95	9.48	6.14	2.67	0.14	0.008	1.17	0.2	0.09	0.02	<0.01	1.93	98.5
Moss-124	73.8	13.3	1.38	0.43	0.37	3.55	4.8	<0.002	0.05	0.04	0.1	0.02	0.05	0.68	98.57
Moss-127	60.6	15.9	6.11	5.46	2.89	4.45	0.43	0.011	0.52	0.11	0.14	0.07	0.01	2.37	99.07
Moss-130	67.6	11.95	8.35	1.52	1.91	0.39	3.62	<0.002	0.15	0.11	0.01	0.01	0.03	4.21	99.86
Moss-131	61.4	11.95	14.1	1.15	2.87	3.11	2.27	0.002	0.31	0.7	0.05	0.01	0.03	1.98	99.93
Moss-134	68.6	15.45	2.12	2.58	0.93	5.46	2	<0.002	0.21	0.03	0.06	0.07	0.06	1.71	99.28
Moss-138	76.1	12.9	1.38	0.79	0.32	3.51	4.35	0.003	0.08	0.01	0.02	0.05	0.14	0.48	100.13
Moss-140	71.3	15.35	2.18	3.17	0.71	5.44	0.9	<0.002	0.28	0.02	0.06	0.12	0.03	0.58	100.14
Moss-03	66.9	15.7	3.24	2.83	1.88	4.47	2.47	0.007	0.32	0.03	0.11	0.04	0.04	3.23	101.27
Moss-10	60.9	15.05	6.9	2.2	3.74	2.24	2.25	0.006	0.52	0.03	0.1	0.01	0.04	4.19	98.18
Moss-11	67.7	15.4	2.16	0.88	0.36	5.3	5.57	<0.002	0.23	0.04	0.07	0.08	0.12	0.41	98.32
Moss-13	64.9	16	3.55	2.78	1.28	5.26	3.01	0.003	0.53	0.05	0.21	0.12	0.16	0.87	98.72
Moss-14	58.9	15.8	6.86	2.12	4.95	5.1	1.36	0.021	0.57	0.1	0.16	0.03	0.05	4	100.02
Moss-17	68.4	14.35	2.71	2.21	1.52	4.62	1.32	0.004	0.2	0.04	0.05	0.04	0.03	2.78	98.27
Moss-19	69.1	14.65	2.73	1.26	1.16	4.41	2.25	0.005	0.31	0.06	0.07	0.01	0.04	2.15	98.21
Moss-20	46.9	18.4	10.3	9.27	9.79	2.04	1.34	0.097	0.56	0.15	0.05	0.02	0.01	2.91	101.84
Moss-22	75.9	12.75	1	1.22	0.86	2.44	4.12	<0.002	0.04	0.05	0.01	<0.01	0.02	2.14	100.55
Moss-25	58.9	16	5.26	4.24	2.99	5.7	0.73	0.013	0.78	0.06	0.4	0.04	0.05	5	100.16
Moss-26	70.6	14.15	2.69	3.13	1.24	4.06	1.41	0.005	0.28	0.04	0.06	0.02	0.03	3.86	101.58
Moss-27	49.5	12.55	16.55	9.69	5.38	1.62	0.16	0.003	1.4	0.22	0.11	0.01	<0.01	1.92	99.11
Moss-28	76.4	12.2	0.82	0.78	0.89	1.68	4.34	<0.002	0.04	0.07	0.01	<0.01	0.01	1.8	99.04
Moss-32	60.3	15.55	5.03	4.06	3.15	5.62	5.23	0.02	0.52	0.09	0.4	0.24	0.21	0.41	100.83

Moss-36	53.5	15.1	7.79	7.54	5.7	5.44	0.75	0.024	0.83	0.14	0.71	0.28	0.06	1.04	98.9
Moss-37	42.3	11.8	11	7.36	19.35	0.8	1.41	0.084	0.23	0.17	0.02	<0.01	0.02	4.51	99.05
Moss-44	48.1	16.2	9.36	8.89	6.56	4.33	0.35	0.023	0.88	0.13	0.26	0.05	0.01	3.37	98.51
Moss-47	63.4	14.3	4.35	3	2.55	5.18	1.09	0.002	0.59	0.08	0.11	0.02	0.03	3.7	98.4
Moss-50	63.1	15.85	6.44	0.68	3.05	3.79	2.01	0.023	0.57	0.06	0.16	0.03	0.07	2.84	98.67
Moss-51	62.9	17.85	2.77	1.22	0.66	6.29	5.7	<0.002	0.44	0.05	0.17	0.16	0.16	0.53	98.9
Moss-53	69.6	15.5	2.33	1.32	0.47	6.35	5	0.002	0.31	0.05	0.12	0.04	0.11	0.34	101.54
Moss-56	62.3	16.6	5.27	5.08	3.6	4.49	0.51	0.023	0.44	0.08	0.11	0.07	0.04	2.97	101.58
Moss-57	61.4	16.7	5.26	4.73	3.66	4.46	0.62	0.025	0.44	0.08	0.09	0.07	0.04	2.76	100.34
Moss-59	63	12.85	7.16	6.6	3.16	2.12	1.32	0.025	0.54	0.19	0.13	0.03	0.03	1.28	98.44
Moss-90	76.2	13.2	1.03	0.43	0.13	6.73	0.96	0.002	0.06	0.01	0.01	0.02	0.01	0.38	99.17
Moss-91	66.5	15	3.29	2.02	1.18	4.67	4.11	0.005	0.4	0.05	0.15	0.05	0.07	0.59	98.09
	C-IR07 %	**S-IR08 %**	**ME-MS81 ppm**												
SAMPLE	**C**	**S**	**Ba**	**Ce**	**Cr**	**Cs**	**Dy**	**Er**	**Eu**	**Ga**	**Gd**	**Ge**	**Hf**	**Ho**	**La**
Moss-006a	0.35	0.02	215	19.1	36	1.26	0.88	0.4	0.5	19.8	1.25	0.8	3.13	0.2	9.4
Moss-007	0.61	0.03	411	16.6	212	2.33	1.77	0.88	0.67	19.9	1.59	1.4	2.1	0.35	8
Moss-008	0.58	0.06	1710	421	8	1.22	12.15	4.89	8.58	20.3	22.9	1.9	15.1	1.95	190
Moss-009	0.35	0.48	120	23.5	37	0.74	2.01	1.28	0.6	14.7	2.31	1	3.03	0.44	11
Moss-016	0.45	0.03	283	8.2	28	2.45	0.61	0.37	0.31	17.8	0.79	0.7	2.37	0.15	3.7
Moss-029	1.23	0.18	299	139	5	3.34	4.17	2.38	2.27	12.3	6.56	1.2	5.73	0.81	61.4
Moss-039	0.05	8.39	122	4.7	19	0.66	1.4	1.09	0.38	12.5	1.23	0.5	3.9	0.3	1.7
Moss-040	0.93	0.02	236	23.2	125	1.64	1.47	1.06	0.65	19.1	1.94	1	2.72	0.31	11
Moss-041	0.62	0.03	237	18.7	29	1.13	0.75	0.4	0.52	19.3	1.15	0.7	2.8	0.15	8.9
Moss-043	0.09	0.05	367	25	75	2.76	1.81	0.87	0.6	22.2	2.06	1.1	3.25	0.36	12.2
Moss-054	0.37	0.04	304	14.7	28	1.3	0.65	0.38	0.35	19.8	0.94	0.8	3.08	0.15	6.7
Moss-055	0.25	0.03	307	15.8	28	1.44	0.77	0.38	0.4	19.7	0.96	0.7	3.03	0.15	7.6
Moss-089	0.4	0.04	169.5	30	162	2.65	4.3	2.71	1.1	18.9	4.1	1.4	3.56	0.93	13.3
Moss-100	0.03	0.02	952	90	156	0.75	3.23	1.2	1.68	21.4	5.8	1.1	4.67	0.5	38.4
Moss-102	0.17	0.04	58.4	6.3	546	0.28	2.32	1.5	0.56	15.6	1.83	1.4	1.06	0.49	2.5
Moss-104	0.26	0.17	6.7	36.6	24	0.05	2.53	1.78	0.76	10.3	2.67	1.1	4.22	0.54	18.8
Moss-105	0.33	0.06	866	51	12	1.6	0.95	0.34	0.88	20.1	1.99	0.7	3.53	0.15	24.6
Moss-107	0.47	0.13	1365	219	10	1.92	1.8	0.69	1.92	19.9	4.41	1.1	7.09	0.26	113
Moss-108	0.06	0.01	145.5	24.8	391	1.45	3.61	2.14	1.07	18.7	3.35	1.4	2.9	0.72	10.4
Moss-112	0.06	0.02	1110	80	17	1.22	1.18	0.63	1.04	18.8	2.65	0.7	3.62	0.22	39.3
Moss-113	1.38	0.08	79.4	19.9	99	0.25	6.16	4.03	0.94	19.2	4.58	0.8	3.05	1.26	8.9
Moss-114	0.29	0.03	1330	157.5	7	1.65	3.37	1.39	2.6	26.5	7.09	0.9	14.85	0.57	68
Moss-119	0.03	0.03	24.7	12.7	72	0.09	4.76	2.81	0.99	19.9	4.09	1.7	2.1	1.02	4.9
Moss-124	0.03	0.02	467	47.7	9	2.01	1.62	1.16	0.56	16.8	2.27	1.1	3.63	0.32	22.9
Moss-127	0.13	0.02	142.5	29.6	100	0.26	2.57	1.25	0.9	20.5	2.67	1.1	3.03	0.47	13.6
Moss-130	0.38	2.36	286	58.7	<5	1.92	7.16	4.77	1.1	18	6.83	1.1	7.35	1.59	27.2
Moss-131	0.2	0.21	269	52.6	27	7.93	7.31	4.84	1.15	19.4	6.57	1.4	7.66	1.64	23.1
Moss-134	0.22	0.03	550	22.2	18	1.5	1.24	0.57	0.52	21.3	1.38	1	2.56	0.2	10.5
Moss-138	0.03	0.02	1360	24.6	34	2.06	0.37	0.16	0.27	15.9	0.67	0.6	2.41	0.08	12.5
Moss-140	0.03	0.05	339	16	19	0.49	0.3	0.13	0.37	19.7	0.63	0.5	2.83	0.05	7.7
Moss-03	0.49	0.66	424	22.3	46	1.63	1.52	0.81	0.56	19.6	1.79	1.5	3.1	0.34	11.5
Moss-10	0.33	0.17	372	17.2	36	1.41	1.91	1.12	0.59	16.6	1.74	1.1	2.9	0.4	8.8
Moss-11	0.02	0.03	1125	139	12	3.52	2.29	0.88	1.65	17.8	4.32	0.8	6.07	0.34	70.2
Moss-13	0.04	0.02	1520	100	18	1.78	1.99	0.89	1.56	22.8	4.26	0.9	5.94	0.35	48.5
Moss-14	0.29	0.03	436	22.9	156	1.61	2.26	1.29	0.77	20.7	2.4	0.7	3.46	0.48	10.4
Moss-17	0.44	0.03	305	7.5	29	2.7	0.79	0.43	0.34	19.5	0.94	1	2.33	0.12	3.4

Moss-19	0.22	0.1	321	13.6	41	1.36	0.91	0.56	0.53	21.4	1.07	1.1	2.99	0.19	7.1
Moss-20	0.05	0.05	126	7.9	723	3.16	2.2	1.47	0.47	16	1.89	1.2	1.02	0.49	3.7
Moss-22	0.27	0.02	157	20.1	7	1.4	11.05	6.37	0.35	18	10.1	1.9	4.11	2.21	7.4
Moss-25	0.76	0.02	421	141.5	95	2.85	2.91	1.16	2.19	21.3	5.46	0.9	6.38	0.45	68.4
Moss-26	0.65	0.02	282	15.8	35	2.96	0.92	0.44	0.4	20.3	1	0.6	3.03	0.12	9.3
Moss-27	0.06	0.25	16.4	11.4	20	0.15	5.31	3.32	1.25	20.6	4.21	1.7	2.48	1.12	4.2
Moss-28	0.18	0.01	139.5	21.4	<5	1.43	10.15	6.07	0.35	18.4	8.91	2.2	3.8	2.08	7.8
Moss-32	0.03	0.02	1970	190	148	3.45	4.83	1.9	3.44	23.1	9.41	1.1	8.44	0.8	93.9
Moss-36	0.04	0.06	559	340	167	0.99	7.21	2.54	5.84	16.1	15.95	1.4	17.55	1.1	138.5
Moss-37	0.03	0.01	182.5	7.7	635	13.95	0.97	0.78	0.33	10.1	0.99	1.2	0.63	0.24	3.4
Moss-44	0.42	0.05	64.5	34.6	169	0.34	4.01	2.39	1.38	19.9	4	1.4	3.21	0.82	15.6
Moss-47	0.58	0.45	274	25.8	16	1.01	2.86	1.65	0.76	16.6	2.73	0.8	3.75	0.62	12.4
Moss-50	0.13	0.1	687	49.1	175	2.76	2.51	1.3	1.09	20.4	3.06	1.1	3.99	0.52	24.9
Moss-51	0.06	0.04	1490	132	9	6.52	3.66	1.48	2.49	22.5	6.15	0.8	9.95	0.61	55.2
Moss-53	0.06	0.02	1020	127	9	1.74	2.25	0.87	1.82	20.7	4.85	1	4.84	0.37	47.9
Moss-56	0.28	0.01	312	18	169	0.77	1.34	0.83	0.62	21.4	1.82	0.9	2.58	0.25	8
Moss-57	0.22	0.01	404	22.7	181	0.87	1.55	1.02	0.65	21.6	2.14	1	2.45	0.32	11.1
Moss-59	0.32	0.39	281	67.3	179	2.64	2.8	1.64	1.2	17.6	3.76	1.5	4.92	0.62	36.2
Moss-90	0.03	0.03	113	24.8	17	0.31	0.52	0.39	0.36	22.1	0.86	0.8	7.73	0.09	13.9
Moss-91	0.02	0.04	629	100.5	42	2.87	1.99	0.87	1.07	21.6	3.37	0.9	6.06	0.35	57.8
	ME-MS81 ppm														
SAMPLE	**Lu**	**Nb**	**Nd**	**Pr**	**Rb**	**Sm**	**Sn**	**Sr**	**Ta**	**Tb**	**Th**	**Tm**	**U**	**V**	**W**
Moss-006a	0.07	1.92	8.1	2.39	76.9	1.47	0.5	232	<0.1	0.15	0.62	0.07	0.2	47	2.4
Moss-007	0.13	2.79	8.7	2.29	80.5	1.62	1.1	250	<0.1	0.27	0.96	0.14	0.28	145	7.6
Moss-008	0.47	20.4	209	52.7	27.8	35.3	2	938	0.6	2.54	25.7	0.58	7.06	121	2.8
Moss-009	0.21	4.18	10.6	2.8	29.4	2.28	1.6	156.5	0.1	0.36	1.65	0.19	0.64	108	1.3
Moss-016	0.06	1.16	4.4	0.98	24.8	0.78	0.8	275	<0.1	0.11	0.6	0.05	0.26	36	0.7
Moss-029	0.4	17.3	64.4	17.55	54	9.86	1.3	163	0.6	0.77	5.46	0.33	1.42	65	1
Moss-039	0.2	5.14	3.8	0.66	42.7	1.02	1.1	168	0.3	0.18	1.75	0.16	0.73	75	5.9
Moss-040	0.14	3.36	11.1	2.69	60.3	2.02	0.9	140.5	0.1	0.27	1.54	0.12	0.63	106	5.2
Moss-041	0.06	2.35	8.3	2.14	48.3	1.3	0.5	199.5	<0.1	0.16	0.6	0.05	0.22	41	1.3
Moss-043	0.16	4.27	12.9	3.12	65.6	2.54	1.1	534	0.1	0.26	1.2	0.14	0.39	86	1.4
Moss-054	0.06	1.82	6.2	1.66	27.1	1.16	1	369	<0.1	0.11	0.59	0.06	0.21	41	1
Moss-055	0.05	1.58	7.4	1.69	25.1	1.3	0.6	361	<0.1	0.13	0.54	0.05	0.22	39	<0.5
Moss-089	0.4	6.17	15	3.77	100	3.43	1.3	218	0.2	0.58	1.04	0.37	0.26	209	1.7
Moss-100	0.16	8.14	44.5	11	36.6	7.83	0.9	1355	0.5	0.62	3.31	0.16	0.85	77	0.7
Moss-102	0.19	1.6	4.9	0.9	9.1	1.29	0.6	117.5	<0.1	0.34	0.21	0.22	0.05	231	0.7
Moss-104	0.27	5.89	16	4.2	0.6	2.78	0.8	38.7	0.2	0.45	2.11	0.23	0.55	43	0.8
Moss-105	0.06	3.27	22.6	5.91	62	3.25	0.9	635	0.1	0.2	3.16	0.05	0.95	39	1.5
Moss-107	0.08	16.3	77.6	23.3	114	9.58	1	578	0.5	0.37	11.25	0.06	2.06	49	3.3
Moss-108	0.38	5.33	14	3.29	24.9	3.19	1.1	345	0.2	0.55	1.02	0.32	0.24	217	0.6
Moss-112	0.05	5.15	33.7	8.92	85	4.52	0.7	871	0.1	0.27	6.16	0.07	0.83	50	0.7
Moss-113	0.55	4.51	13	2.87	1	3.78	1	106.5	0.1	0.85	0.71	0.57	0.22	288	4.3
Moss-114	0.17	17.15	75.8	19.55	154.5	11.9	0.9	1460	1.1	0.74	13	0.21	3.55	28	1.3
Moss-119	0.45	3.39	10	1.96	2.2	3.18	0.5	140	0.1	0.68	0.46	0.49	0.12	413	1.6
Moss-124	0.17	2.86	17.9	5.27	123.5	3.36	1	131	0.1	0.37	11.3	0.17	4.6	14	1.7
Moss-127	0.19	4.02	16.4	3.92	11.2	3.08	0.8	635	0.1	0.4	1.65	0.21	0.46	132	4.3
Moss-130	0.72	9.56	28.2	7.27	88.6	6.43	2.8	62.5	0.6	1.09	5.78	0.71	1.28	9	3.9
Moss-131	0.67	10.9	26.7	6.81	95.6	6.92	2	129	0.7	1.12	3.55	0.73	0.96	29	11.6
Moss-134	0.1	4.78	10.1	2.66	58.6	1.96	0.6	595	0.1	0.19	2.03	0.07	0.42	39	3.4

Moss-138	0.04	2.29	8.3	2.3	118	1.14	<0.5	445	<0.1	0.1	6.2	0.03	1.4	14	1
Moss-140	0.01	0.69	5.9	1.73	20.1	0.98	<0.5	1005	<0.1	0.05	0.97	0.03	0.23	34	0.5
Moss-03	0.14	3.44	11.4	2.91	74.3	2.24	0.9	377	0.3	0.26	1.76	0.14	0.64	70	4.6
Moss-10	0.21	4.43	8	2.29	61.2	1.94	1.1	110	0.3	0.3	1.82	0.18	0.46	128	1.8
Moss-11	0.12	16.4	49.8	15.9	197	7.9	1.1	684	1.1	0.45	20.7	0.13	3.82	17	0.7
Moss-13	0.11	7.55	45.2	11.65	82.8	6.76	1	1120	0.4	0.52	7.53	0.09	1.27	52	<0.5
Moss-14	0.24	4.23	13.4	2.84	38.8	3.12	0.9	314	0.3	0.41	1.8	0.21	0.52	145	1.9
Moss-17	0.07	1.2	3.9	0.95	30	0.74	0.5	333	0.1	0.12	0.55	0.06	0.22	36	0.8
Moss-19	0.08	1.79	6.2	1.68	53.2	1.35	0.5	196.5	0.1	0.15	0.59	0.06	0.26	53	3.6
Moss-20	0.19	1.73	5.2	1.04	60	1.36	<0.5	250	0.1	0.33	0.42	0.18	0.07	206	1.4
Moss-22	1.02	33.2	14.5	3.26	146	7.67	3.2	36.7	2.5	1.68	9.06	0.97	4.53	<5	1.1
Moss-25	0.17	12.7	66.4	17.25	20.7	10.25	1.1	395	0.6	0.53	7.31	0.15	1.7	99	1.5
Moss-26	0.07	1.9	7.7	1.76	36.1	1.18	<0.5	237	0.1	0.12	0.59	0.06	0.57	48	0.6
Moss-27	0.53	3.86	9.9	2	2.3	3.32	0.8	119.5	0.2	0.82	0.46	0.44	0.14	468	0.9
Moss-28	0.93	29.3	14.9	3.49	153.5	7.04	3.4	30.7	2.2	1.5	8.28	0.89	4	<5	1.4
Moss-32	0.21	5.98	89.8	22.9	152	14.75	1.7	2170	0.2	1.07	7.65	0.19	1.16	98	0.9
Moss-36	0.31	23	152	42.9	17.6	27.2	1.9	2280	1.2	1.6	15.5	0.34	2.43	147	4.5
Moss-37	0.1	1.92	3.5	0.93	55	0.77	<0.5	46.1	0.1	0.15	1.48	0.09	0.53	92	0.6
Moss-44	0.34	3.88	21.6	4.81	4.7	4.49	1.1	547	0.2	0.6	1.5	0.27	0.4	251	1.7
Moss-47	0.23	5.33	12.6	3.49	27.3	2.38	0.6	222	0.4	0.43	2.37	0.23	0.69	135	2.4
Moss-50	0.16	5.81	22.1	5.71	64	3.99	0.7	345	0.5	0.45	6.42	0.19	1.94	125	1.8
Moss-51	0.17	16.05	63.4	16.8	118.5	9.67	1.7	1470	0.8	0.75	11.15	0.19	2.5	50	2.7
Moss-53	0.09	19.15	62.2	18.15	155.5	9.76	1.2	282	1.1	0.5	15.85	0.11	2.12	25	0.8
Moss-56	0.09	2.85	10.2	2.25	11	1.96	0.5	607	0.2	0.25	0.98	0.11	0.29	109	0.7
Moss-57	0.12	3.26	12.5	3.01	12	3.02	0.6	625	0.2	0.26	1.86	0.11	0.28	117	0.9
Moss-59	0.3	6.02	27.6	7.56	46	5.14	1.8	344	0.5	0.56	11.05	0.21	3.09	116	1.8
Moss-90	0.11	4.99	8.4	2.37	53.2	1.32	<0.5	198	0.3	0.11	47.9	0.05	8.02	15	1.8
Moss-91	0.14	10.05	36.1	10.45	136.5	4.67	0.8	485	0.4	0.4	14.55	0.1	2.31	52	0.7
	ME-MS81 ppm			**ME-MS42 ppm**											
SAMPLE	**Y**	**Yb**	**Zr**	**As**	**Bi**	**Hg**	**In**	**Re**	**Sb**	**Se**	**Te**	**Tl**			
Moss-006a	4.6	0.4	112	0.2	0.04	0.005	<0.005	<0.001	<0.05	<0.2	0.04	0.03			
Moss-007	8.4	0.94	77	0.3	0.1	0.008	0.047	<0.001	0.05	<0.2	0.04	0.06			
Moss-008	53.2	3.47	696	0.4	0.19	0.005	0.029	<0.001	0.12	0.2	0.06	0.02			
Moss-009	12.1	1.25	120	1.2	0.28	<0.005	0.018	<0.001	0.06	1.1	0.17	<0.02			
Moss-016	3.5	0.29	80	1	0.03	<0.005	<0.005	<0.001	<0.05	<0.2	0.03	<0.02			
Moss-029	23.3	2.41	260	0.1	0.04	<0.005	0.016	<0.001	<0.05	<0.2	0.01	0.3			
Moss-039	9.3	1.31	151	5.4	2.42	0.014	<0.005	<0.001	0.14	7.4	3.82	0.04			
Moss-040	8.4	0.91	100	0.6	0.31	<0.005	0.012	<0.001	0.05	0.8	0.36	<0.02			
Moss-041	4.1	0.3	111	0.2	0.12	<0.005	0.01	<0.001	<0.05	<0.2	0.01	<0.02			
Moss-043	9.8	0.93	118	0.5	0.09	<0.005	0.006	<0.001	0.11	<0.2	0.01	0.11			
Moss-054	4.1	0.4	114	0.1	0.02	<0.005	<0.005	<0.001	<0.05	<0.2	<0.01	<0.02			
Moss-055	3.9	0.32	104	0.3	0.01	<0.005	<0.005	<0.001	<0.05	<0.2	<0.01	0.03			
Moss-089	25	2.69	153	0.3	0.04	<0.005	0.023	<0.001	0.18	<0.2	0.02	0.06			
Moss-100	15	1.04	193	<0.1	0.01	<0.005	0.005	<0.001	<0.05	<0.2	<0.01	0.03			
Moss-102	14	1.38	38	0.4	<0.01	<0.005	<0.005	<0.001	<0.05	0.2	0.02	<0.02			
Moss-104	15.4	1.97	173	0.3	0.02	<0.005	0.026	<0.001	<0.05	0.2	0.01	<0.02			
Moss-105	4.6	0.27	131	0.1	0.06	<0.005	0.007	<0.001	<0.05	<0.2	0.07	0.02			
Moss-107	7.6	0.45	346	<0.1	0.1	<0.005	<0.005	<0.001	0.05	<0.2	0.05	0.09			
Moss-108	20.6	2.12	112	0.3	0.01	0.007	0.006	<0.001	0.11	<0.2	0.01	0.04			
Moss-112	6.2	0.42	149	0.3	0.05	<0.005	0.005	<0.001	<0.05	<0.2	<0.01	0.21			

Moss-113	37	3.53	110	<0.1	0.02	0.006	0.075	<0.001	<0.05	<0.2	<0.01	<0.02			
Moss-114	17.2	1.27	762	<0.1	0.08	<0.005	0.009	<0.001	<0.05	<0.2	<0.01	0.1			
Moss-119	28.1	2.63	72	0.4	<0.01	<0.005	0.013	<0.001	0.1	0.2	<0.01	<0.02			
Moss-124	9.5	1.19	104	<0.1	0.1	<0.005	0.005	<0.001	<0.05	<0.2	<0.01	<0.02			
Moss-127	13.8	1.34	107	0.6	0.02	<0.005	0.007	<0.001	0.06	<0.2	0.01	<0.02			
Moss-130	46.7	4.7	232	2	0.49	0.005	0.009	<0.001	0.07	0.3	0.28	<0.02			
Moss-131	47.2	4.54	296	0.3	0.11	<0.005	0.062	<0.001	<0.05	0.2	0.26	0.33			
Moss-134	6.1	0.56	90	0.1	0.02	<0.005	0.008	<0.001	<0.05	<0.2	0.02	0.03			
Moss-138	2.4	0.24	85	0.1	0.02	<0.005	<0.005	<0.001	<0.05	<0.2	0.01	0.04			
Moss-140	1.5	0.19	107	<0.1	<0.01	0.007	<0.005	<0.001	<0.05	<0.2	<0.01	0.06			
Moss-03	9	0.88	100	0.7	0.29	<0.005	0.007	0.001	0.06	0.7	1	0.04			
Moss-10	11	1.33	116	0.9	0.65	0.005	0.02	<0.001	<0.05	<0.2	1.43	0.03			
Moss-11	10.2	0.84	265	0.7	0.13	<0.005	0.006	<0.001	<0.05	<0.2	0.01	0.04			
Moss-13	9.5	0.79	234	0.6	0.05	<0.005	0.006	<0.001	<0.05	0.2	<0.01	0.15			
Moss-14	12	1.3	127	0.5	0.02	<0.005	0.019	<0.001	0.05	<0.2	0.01	<0.02			
Moss-17	3.6	0.4	78	0.2	0.02	<0.005	<0.005	<0.001	<0.05	<0.2	<0.01	<0.02			
Moss-19	4.8	0.59	110	<0.1	0.08	<0.005	0.006	<0.001	<0.05	<0.2	0.09	0.03			
Moss-20	12.6	1.22	33	<0.1	0.01	<0.005	0.006	<0.001	<0.05	0.2	0.02	0.02			
Moss-22	67.3	6.78	56	0.2	0.52	<0.005	0.009	0.001	<0.05	0.2	<0.01	0.05			
Moss-25	12.2	0.92	256	0.8	0.03	<0.005	0.022	<0.001	0.05	0.2	<0.01	0.02			
Moss-26	3.9	0.39	101	<0.1	<0.01	<0.005	0.006	<0.001	<0.05	<0.2	<0.01	0.02			
Moss-27	28.7	3	77	0.4	0.01	<0.005	0.011	0.001	0.08	0.8	0.01	0.04			
Moss-28	61.1	5.93	53	<0.1	0.81	<0.005	0.008	<0.001	<0.05	<0.2	<0.01	0.04			
Moss-32	21.1	1.36	298	1.5	0.05	<0.005	<0.005	<0.001	<0.05	0.2	0.01	0.32			
Moss-36	32	2.12	1020	0.2	0.07	<0.005	0.009	<0.001	<0.05	0.2	0.01	0.05			
Moss-37	5.6	0.6	20	<0.1	0.01	<0.005	<0.005	<0.001	<0.05	<0.2	<0.01	0.33			
Moss-44	20.8	2.18	106	0.7	0.03	<0.005	0.011	<0.001	0.1	0.4	0.03	<0.02			
Moss-47	16	1.74	145	0.2	0.06	<0.005	0.014	<0.001	<0.05	0.5	0.23	<0.02			
Moss-50	12.6	1.16	142	0.9	0.16	<0.005	0.01	0.001	0.19	0.2	0.05	0.06			
Moss-51	16.4	1.28	517	1.3	3.43	<0.005	0.011	<0.001	<0.05	0.2	0.01	0.13			
Moss-53	10.6	0.67	218	<0.1	0.07	<0.005	<0.005	<0.001	<0.05	0.2	<0.01	0.03			
Moss-56	7.4	0.73	91	0.6	0.01	<0.005	0.006	<0.001	0.07	0.2	<0.01	<0.02			
Moss-57	8.7	0.75	86	0.6	0.02	<0.005	0.006	<0.001	0.09	<0.2	<0.01	<0.02			
Moss-59	16.3	1.54	181	0.1	0.2	<0.005	0.018	<0.001	<0.05	0.4	0.03	0.17			
Moss-90	4.5	0.46	229	0.2	0.04	<0.005	<0.005	<0.001	0.07	<0.2	<0.01	<0.02			
Moss-91	10	0.91	268	0.5	0.02	<0.005	0.011	<0.001	<0.05	0.2	<0.01	0.2			
	ME-4ACD81 ppm										**Au-AA25 ppm**				
SAMPLE	**Ag**	**Cd**	**Co**	**Cu**	**Li**	**Mo**	**Ni**	**Pb**	**Sc**	**Zn**	**Au**				
Moss-006a	<0.5	<0.5	7	4	10	<1	26	3	5	19	0.01				
Moss-007	<0.5	<0.5	20	29	30	<1	55	5	12	61	0.01				
Moss-008	<0.5	<0.5	21	31	20	<1	18	17	9	151	<0.01				
Moss-009	<0.5	<0.5	40	189	20	<1	49	5	14	43	0.04				
Moss-016	<0.5	<0.5	6	4	40	<1	14	2	5	45	<0.01				
Moss-029	<0.5	<0.5	10	12	10	1	4	9	12	91	0.01				
Moss-039	1.2	<0.5	220	20	<10	4	35	7	8	6	0.08				
Moss-040	<0.5	<0.5	11	1	40	<1	38	2	11	96	0.01				
Moss-041	<0.5	<0.5	8	170	20	<1	19	<2	5	64	0.01				
Moss-043	<0.5	<0.5	14	13	50	2	36	10	6	76	0.01				

Moss-054	<0.5	<0.5	7	14	20	<1	19	4	4	48	<0.01				
Moss-055	<0.5	<0.5	6	12	20	<1	14	4	4	48	<0.01				
Moss-089	<0.5	<0.5	41	39	90	<1	215	8	27	203	0.01				
Moss-100	<0.5	<0.5	16	6	20	<1	84	12	8	74	0.01				
Moss-102	<0.5	<0.5	52	50	20	<1	276	3	26	72	0.02				
Moss-104	<0.5	<0.5	17	27	10	<1	17	3	8	35	0.02				
Moss-105	<0.5	<0.5	5	7	10	<1	5	10	3	40	<0.01				
Moss-107	<0.5	<0.5	6	11	20	2	7	12	3	95	<0.01				
Moss-108	<0.5	<0.5	46	30	30	<1	185	7	28	110	0.01				
Moss-112	<0.5	<0.5	6	5	30	<1	7	17	4	63	<0.01				
Moss-113	<0.5	<0.5	37	41	50	<1	77	6	40	195	<0.01				
Moss-114	<0.5	<0.5	3	5	10	<1	3	17	1	60	<0.01				
Moss-119	<0.5	<0.5	42	38	10	<1	65	6	44	98	<0.01				
Moss-124	<0.5	<0.5	1	1	10	<1	5	27	5	14	0.01				
Moss-127	<0.5	<0.5	18	13	20	<1	30	5	14	76	<0.01				
Moss-130	<0.5	<0.5	8	17	20	2	7	5	4	60	0.04				
Moss-131	<0.5	<0.5	5	20	20	2	30	2	8	77	0.01				
Moss-134	<0.5	<0.5	4	2	20	<1	8	6	3	35	0.01				
Moss-138	<0.5	<0.5	2	3	20	<1	1	22	<1	26	<0.01				
Moss-140	<0.5	<0.5	4	33	20	<1	7	6	2	39	<0.01				
Moss-03	2	<0.5	13	593	10	2	15	<2	7	33					
Moss-10	1.4	<0.5	43	14	30	<1	36	<2	17	54					
Moss-11	<0.5	<0.5	2	6	10	<1	2	39	1	74					
Moss-13	<0.5	<0.5	8	9	30	<1	11	15	5	69					
Moss-14	<0.5	<0.5	23	3	80	<1	38	<2	18	128					
Moss-17	<0.5	<0.5	8	5	50	<1	19	<2	5	77					
Moss-19	<0.5	<0.5	7	3	20	<1	23	3	6	67					
Moss-20	<0.5	<0.5	54	68	50	<1	300	<2	34	71					
Moss-22	<0.5	<0.5	<1	2	30	<1	<1	15	8	38					
Moss-25	<0.5	<0.5	17	21	110	<1	48	4	9	126					
Moss-26	<0.5	<0.5	8	4	40	<1	24	2	5	72					
Moss-27	<0.5	<0.5	53	172	10	<1	37	<2	49	108					
Moss-28	<0.5	<0.5	<1	1	30	<1	<1	9	8	55					
Moss-32	<0.5	<0.5	15	76	40	1	61	24	8	96					
Moss-36	<0.5	<0.5	32	31	10	1	104	21	13	102					
Moss-37	<0.5	<0.5	90	14	80	<1	764	<2	16	100					
Moss-44	<0.5	<0.5	30	31	20	<1	43	<2	25	61					
Moss-47	<0.5	<0.5	48	118	20	1	83	3	14	54					
Moss-50	<0.5	<0.5	23	64	30	1	64	11	16	75					
Moss-51	<0.5	<0.5	3	3	10	3	5	29	3	64					
Moss-53	<0.5	<0.5	3	4	20	1	3	20	1	71					
Moss-56	<0.5	<0.5	19	9	40	<1	50	2	14	75					
Moss-57	<0.5	<0.5	19	9	40	<1	51	<2	13	73					
Moss-59	<0.5	<0.5	24	56	20	1	69	13	14	88					
Moss-90	<0.5	<0.5	1	17	10	<1	4	15	<1	6					
Moss-91	<0.5	<0.5	8	9	40	1	17	21	4	55					

Appendix C. Neodymium isotopes

Sample	$^{147}Sm/^{144}Nd$	$^{143}Nd/^{144}Nd$ (current)	initial 143/144 ratio	uncertainty
Moss-010	**0.1339**	**0.511521**	**0.511346**	**0.000036**
Moss-013	**0.0935**	**0.510834**	**0.510712**	**0.000026**
Moss-019	**0.1152**	**0.511275**	**0.511124**	**0.000032**
Moss-020	**0.1726**	**0.512289**	**0.512063**	**0.000046**
Moss-025	**0.0928**	**0.510859**	**0.510738**	**0.000026**
Moss-027	**0.1968**	**0.512716**	**0.512459**	**0.000052**
Moss-050	**0.1078**	**0.511039**	**0.510898**	**0.000030**
Moss-100	**0.1094**	**0.511185**	**0.511042**	**0.000030**
Moss-102	**0.1913**	**0.512627**	**0.512377**	**0.000051**
Moss-104	**0.1139**	**0.511270**	**0.511121**	**0.000031**
Moss-114	**0.0961**	**0.510871**	**0.510746**	**0.000027**
Moss-119	**0.1877**	**0.512571**	**0.512325**	**0.000050**
Moss-127	**0.1233**	**0.511384**	**0.511223**	**0.000034**

Appendix D. Geochronology data

CA-TIMS U-Pb isotopic data

	Compositional Parameters						Radiogenic Isotope Ratios								Isotopic Ages					
Sample (a)	Th/U (b)	$^{206}Pb^*$ x10^{-13} mol (c)	mol % $^{206}Pb^*$ (c)	Pb^*/Pb_c (c)	Pb_c (pg) (c)	$^{206}Pb/^{204}Pb$ (d)	$^{208}Pb/^{206}Pb$ (e)	$^{207}Pb/^{206}Pb$ (e)	% err (f)	$^{207}Pb/^{235}U$ (e)	% err (f)	$^{206}Pb/^{238}U$ (e)	% err (f)	corr. coef.	$^{207}Pb/^{206}Pb$ (g)	± (f)	$^{207}Pb/^{235}U$ (g)	± (f)	$^{206}Pb/^{238}U$ (g)	± (f)
MOSS-11																				
A	0.511	1.3384	99.80%	162	0.23	8856	0.141	0.18725	0.064	13.527612	0.131	0.524184	0.071	0.970	**2717.5**	**1.06**	2717.22	1.24	2716.90	1.58
B	0.541	0.6279	99.72%	119	0.15	6497	0.150	0.18727	0.066	13.532269	0.135	0.524316	0.075	0.960	**2717.6**	**1.09**	2717.54	1.27	2717.46	1.67
C	0.560	2.0361	99.77%	147	0.38	7982	0.155	0.18731	0.065	13.526975	0.131	0.524009	0.071	0.970	**2717.9**	**1.06**	2717.17	1.24	2716.16	1.57
D	0.572	1.4317	99.68%	106	0.38	5711	0.158	0.18723	0.066	13.522320	0.133	0.524058	0.071	0.968	**2717.2**	**1.09**	2716.85	1.25	2716.37	1.58
E	0.251	2.3893	99.80%	157	0.39	9096	0.069	0.18716	0.064	13.518968	0.131	0.524119	0.071	0.971	**2716.6**	**1.05**	2716.61	1.23	2716.63	1.57
															weighted mean $^{207}Pb/^{206}Pb$ age = 2717.36 ± 0.48 [2.37] Ma (2s); MSWD = 0.88 (n=5) (h)					

(a) **6-3, 7-1** etc. are labels for single zircon grains or fragments annealed and chemically abraded after Mattinson (2005); **bold** indicates results used in weighted mean calculations.
(b) Model Th/U ratio iteratively calculated from the radiogenic 208Pb/206Pb ratio and 206Pb/238U age.
(c) Pb* and Pbc represent radiogenic and common Pb, respectively; mol % $^{206}Pb^*$ with respect to radiogenic, blank and initial common Pb.
(d) Measured ratio corrected for spike and fractionation only. Fractionation calculated from repeated measurements of NBS-982 for Pb ratios and double spike for U ratios.
(e) Corrected for fractionation, spike, and common Pb; all common Pb was assumed to be procedural blank: 206Pb/204Pb = 18.042 ± 0.61%; 207Pb/204Pb = 15.537 ± 0.52%; 208Pb/204Pb = 37.686 ± 0.63% (all uncertainties 1-sigma).
(f) Errors are 2-sigma, propagated using the algorithms of Schmitz and Schoene (2007).
(g) Calculations are based on the decay constants of Jaffey et al. (1971) and 238U/235U = 137.88. 206Pb/238U and 207Pb/206Pb ages corrected for initial disequilibrium in 230Th/238U using Th/U(magma) = 2.8 ± 0.05 (1s).
(h) Age uncertainties reported as ± analytical [+decay constant]; MSWD = mean squared weighted deviation.

CA-TIMS U-Pb isotopic data

	Compositional Parameters						Radiogenic Isotope Ratios						
Sample (a)	Th/U (b)	$^{206}Pb^*$ x10^{-13} mol (c)	mol % $^{206}Pb^*$ (c)	Pb^*/Pb_c (c)	Pb_c (pg) (c)	$^{208}Pb/^{204}Pb$ (d)	$^{208}Pb/^{206}Pb$ (e)	$^{207}Pb/^{206}Pb$ (e)	% err (f)	$^{207}Pb/^{235}U$ (e)	% err (f)	$^{206}Pb/^{238}U$ (e)	% err (f)
MOSS-051													
z5	0.733	10.6772	99.96%	882	0.35	46078	0.203	0.18732	0.021	13.538997	0.049	0.524450	0.034
z10	0.769	12.1109	99.97%	1160	0.30	60109	0.213	0.18735	0.021	13.540956	0.048	0.524443	0.032
z12	0.493	24.3314	99.98%	1799	0.37	98654	0.136	0.18737	0.020	13.540896	0.046	0.524364	0.031
z14	0.751	7.9863	99.98%	1476	0.16	76777	0.208	0.18735	0.021	13.538393	0.046	0.524322	0.030
z15	0.501	10.8162	99.98%	2086	0.14	114179	0.139	0.18737	0.021	13.542725	0.047	0.524436	0.031
z16	0.567	9.6803	99.98%	2222	0.12	119987	0.157	0.18736	0.020	13.539960	0.046	0.524359	0.031
												weighted mean ^{207}P	
MOSS-057													
z8	0.384	12.0143	99.99%	2143	0.15	120362	0.106	0.18661	0.020	13.444070	0.049	0.522752	0.034
z9	0.398	13.0310	99.99%	2157	0.16	120782	0.110	0.18662	0.020	13.442934	0.046	0.522671	0.030
z15	0.381	9.7064	99.97%	1009	0.26	56732	0.105	0.18658	0.020	13.440913	0.046	0.522720	0.030
z19	0.395	9.9174	99.98%	2048	0.13	114727	0.109	0.18662	0.021	13.442548	0.047	0.522667	0.031
z20	0.399	19.8889	99.99%	2338	0.23	130878	0.110	0.18665	0.021	13.442792	0.046	0.522588	0.030
z21	0.378	15.7163	99.98%	1541	0.27	86659	0.105	0.18661	0.020	13.449038	0.048	0.522928	0.034
												weighted mean ^{207}P	
MOSS-100													
z3	0.490	11.8499	99.97%	1138	0.28	62515	0.136	0.18611	0.020	13.386531	0.046	0.521894	0.030
z8	0.542	21.0437	99.98%	1528	0.38	83024	0.150	0.18613	0.021	13.385346	0.052	0.521798	0.039
z9	0.587	9.8427	99.96%	766	0.36	41229	0.162	0.18607	0.020	13.379004	0.055	0.521713	0.042
z10	0.654	11.8269	99.97%	1353	0.25	71820	0.181	0.18613	0.020	13.385106	0.047	0.521804	0.032
z12	0.678	9.7639	99.97%	1359	0.20	71815	0.188	0.18611	0.020	13.384389	0.048	0.521824	0.033
z13	0.548	11.3158	99.98%	1342	0.23	72823	0.152	0.18611	0.020	13.383598	0.050	0.521799	0.036
												weighted mean ^{207}P	

(a) **z1, z2** etc. are labels for single zircon grains or fragments annealed and chemically abraded after Mattinson (2005); **bold** indicates results used in weighted mea
(b) Model Th/U ratio iteratively calculated from the radiogenic 208Pb/206Pb ratio and 206Pb/238U age.
(c) Pb* and Pbc represent radiogenic and common Pb, respectively; mol % $^{206}Pb^*$ with respect to radiogenic, blank and initial common Pb.
(d) Measured ratio corrected for spike and fractionation only. Fractionation calculated from repeated measurements of NBS-982 for Pb ratios and double spike for U
(e) Corrected for fractionation, spike, and common Pb; all common Pb was assumed to be procedural blank: 206Pb/204Pb = 18.042 ± 0.61%; 207Pb/204Pb = 15.5
208Pb/204Pb = 37.686 ± 0.63% (all uncertainties 1-sigma).
(f) Errors are 2-sigma, propagated using the algorithms of Schmitz and Schoene (2007).
(g) Calculations are based on the decay constants of Jaffey et al. (1971) and 238U/235U = 137.818. 206Pb/238U and 207Pb/206Pb ages corrected for initial disequ
using Th/U(magma) = 2.8 ± 0.05 (1s).
(h) Age uncertainties reported as ± analytical [+decay constant]; MSWD = mean squared weighted deviation.

Appendix E. Maps

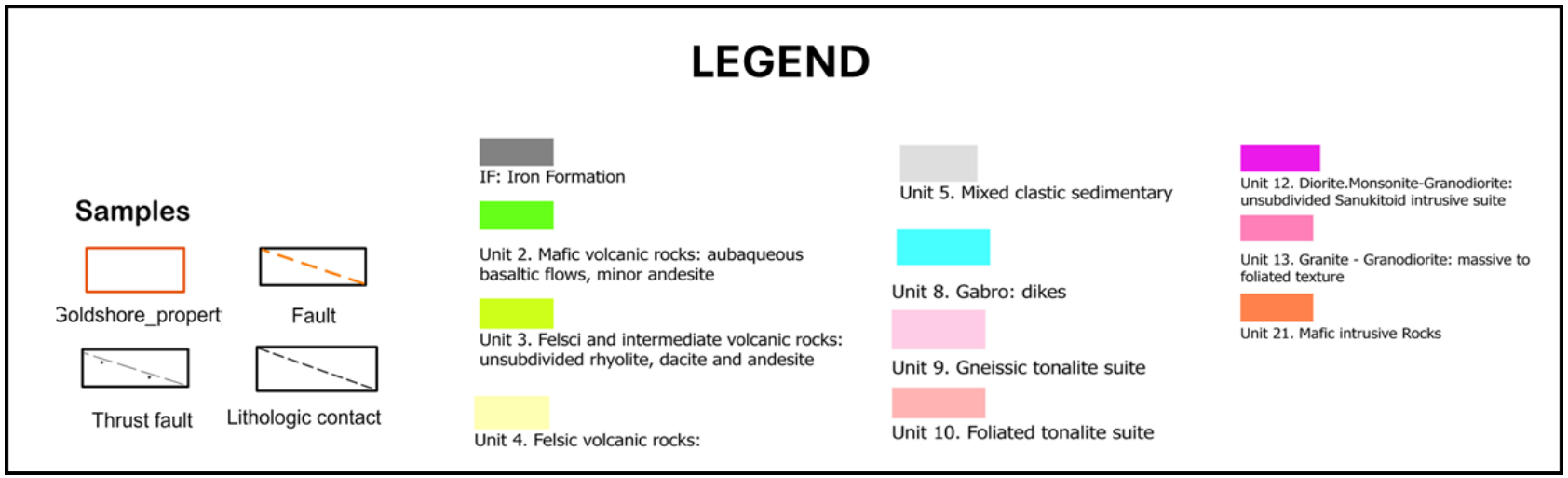

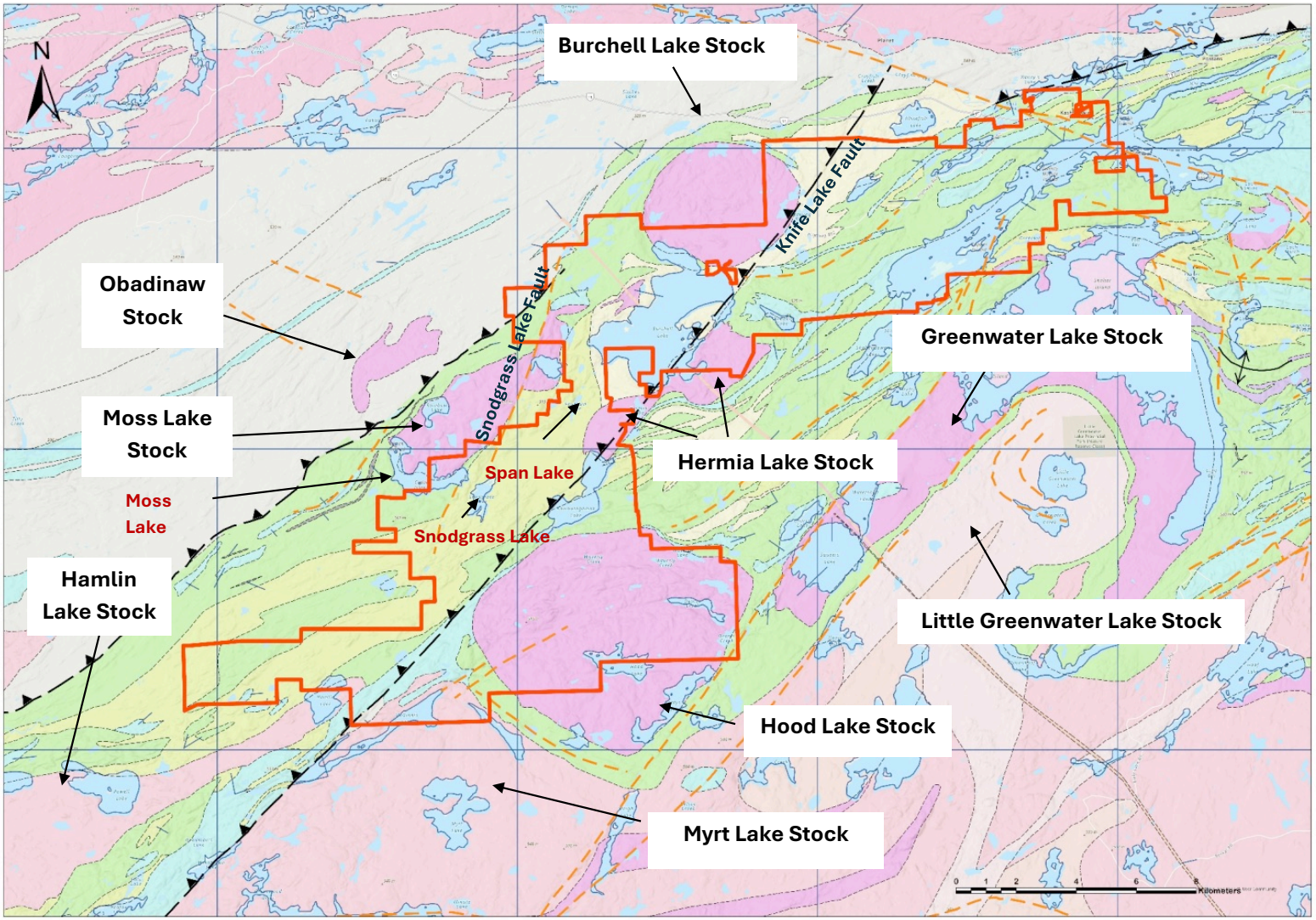

Areas of interest in the geological map

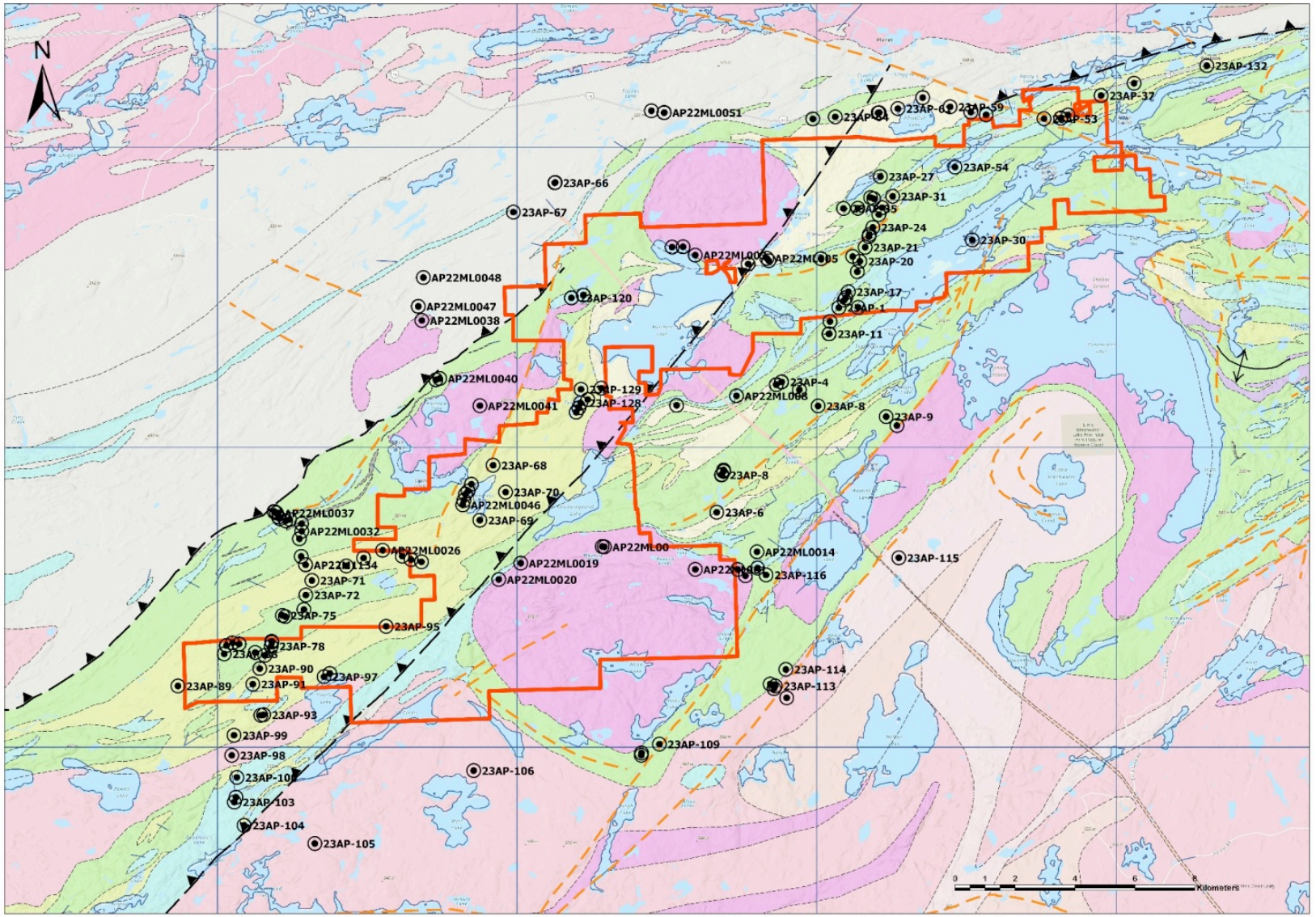
N
AP22ML0051
23AP-66
23AP-67
AP22ML0048
AP22ML0047
AP22ML0038
AP22ML0040
AP22ML0041
23AP-120
23AP-129
23AP-128
23AP-68
23AP-70
AP22ML0046
23AP-69
AP22ML0037
AP22ML0032
AP22ML0026
AP22ML0134
23AP-71
23AP-72
23AP-75
23AP-95
23AP-78
23AP-90
23AP-91
23AP-89
23AP-97
23AP-93
23AP-99
23AP-98
23AP-101
23AP-103
23AP-104
23AP-105
23AP-106
AP22ML0019
AP22ML0020
AP22ML00
23AP-109
23AP-114
23AP-113
AP22ML0014
23AP-116
23AP-115
23AP-6
23AP-8
23AP-4
23AP-9
23AP-11
23AP-17
23AP-1
23AP-20
23AP-21
23AP-24
23AP-30
23AP-31
23AP-27
23AP-54
23AP-53
23AP-59
23AP-32
23AP-132
0 1 2 4 6 8
Kilometers

Total Spots

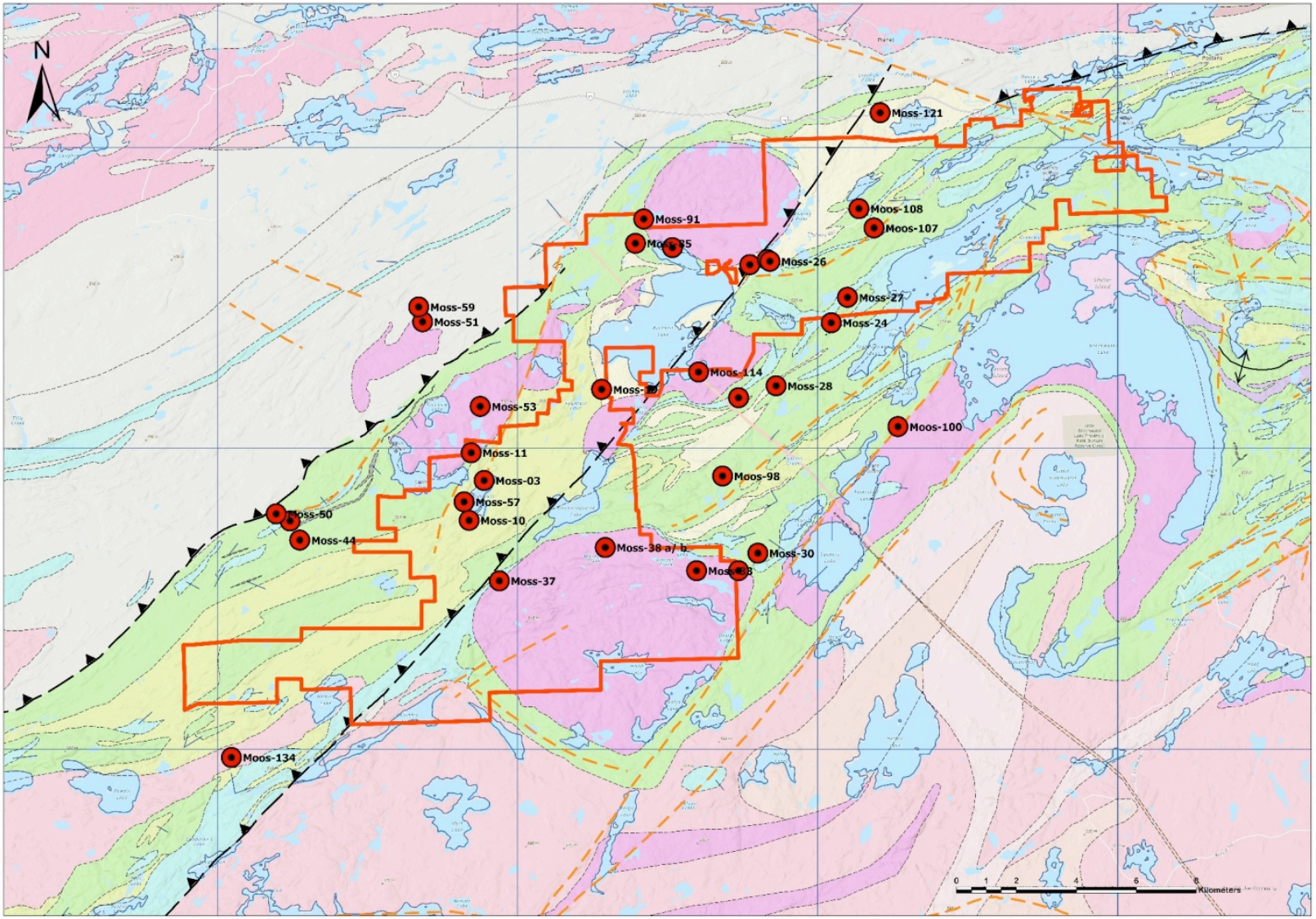

Samples Petrography

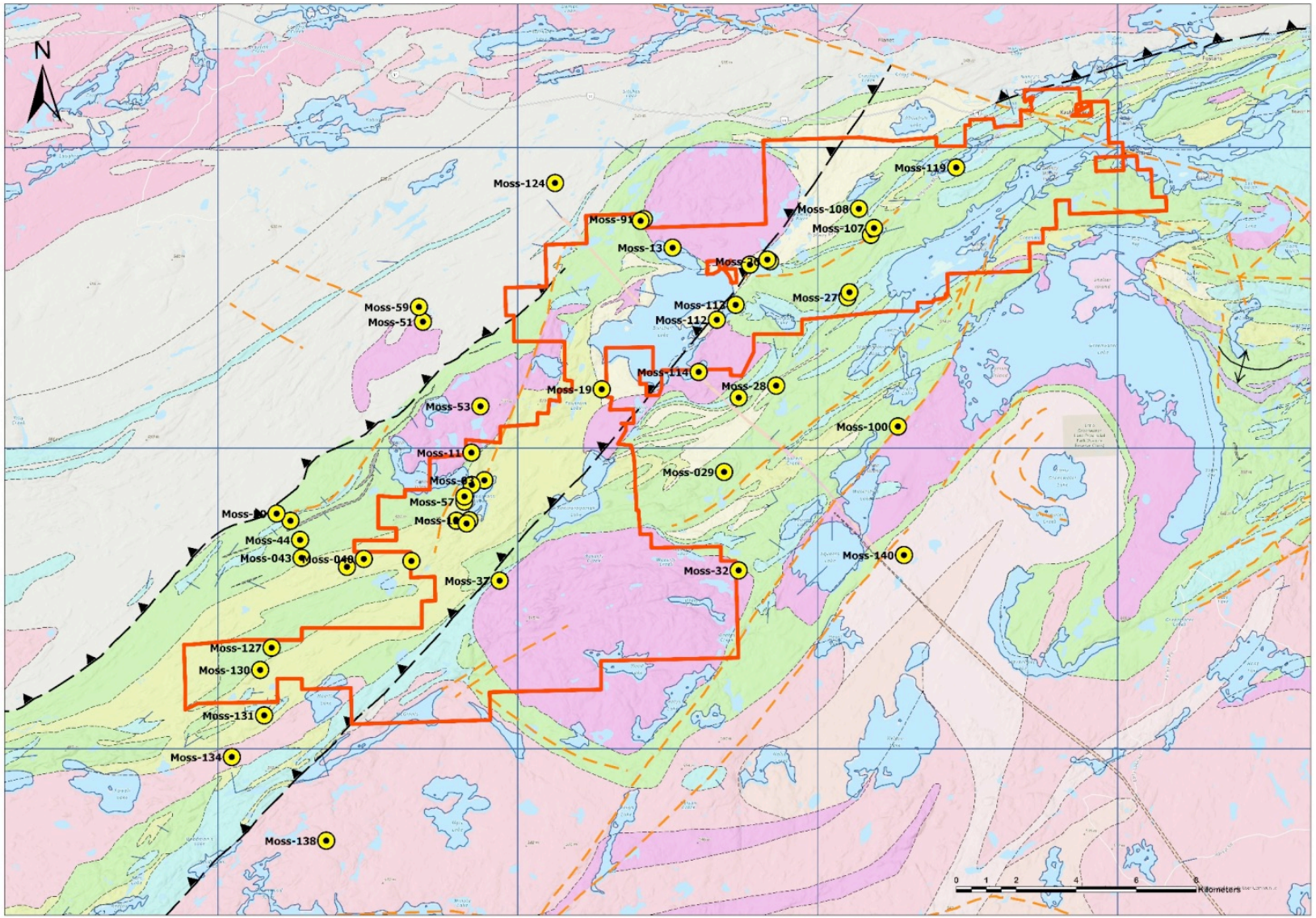

Samples Geochemistry

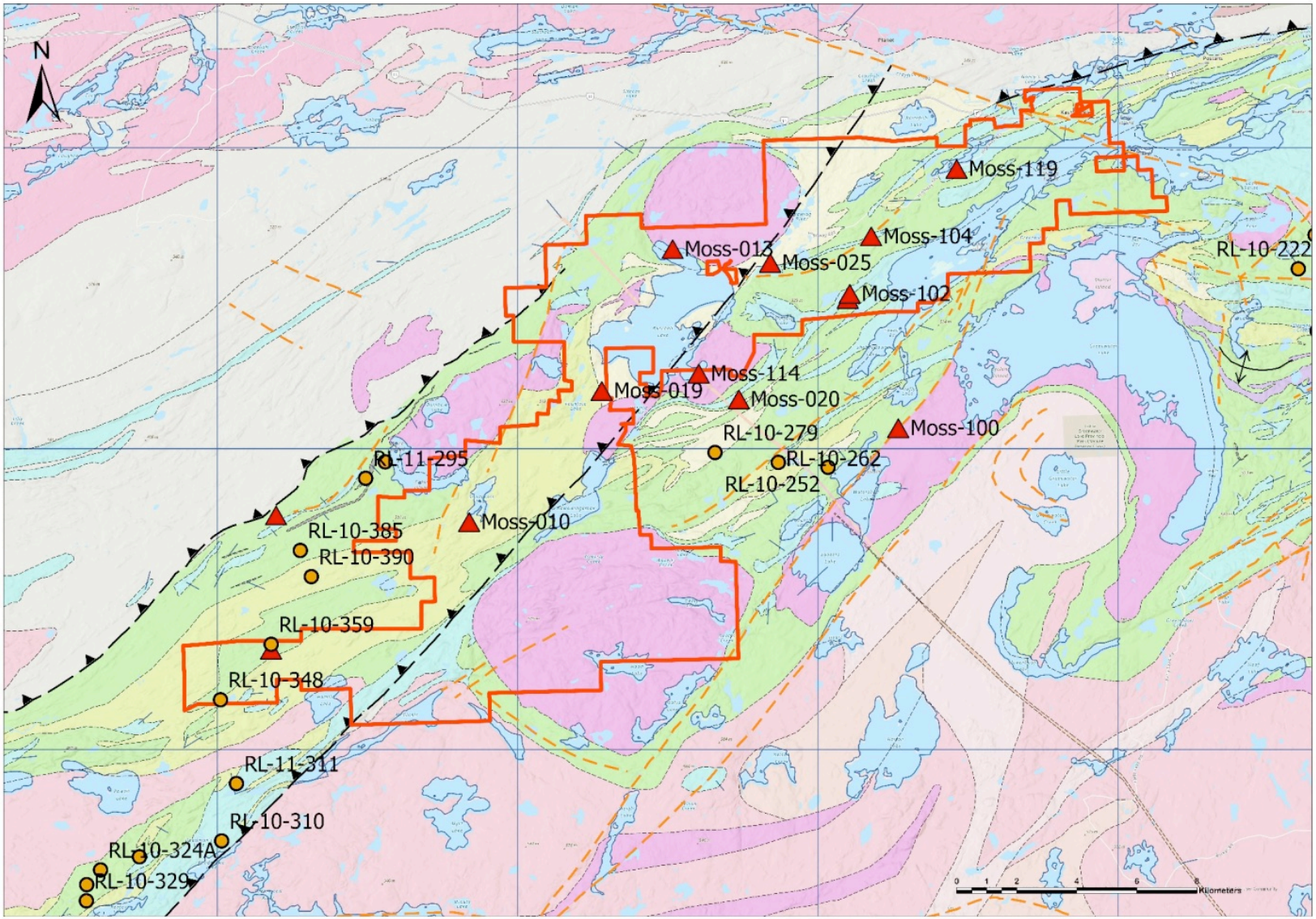

Samples for isotopic Sm – Nd

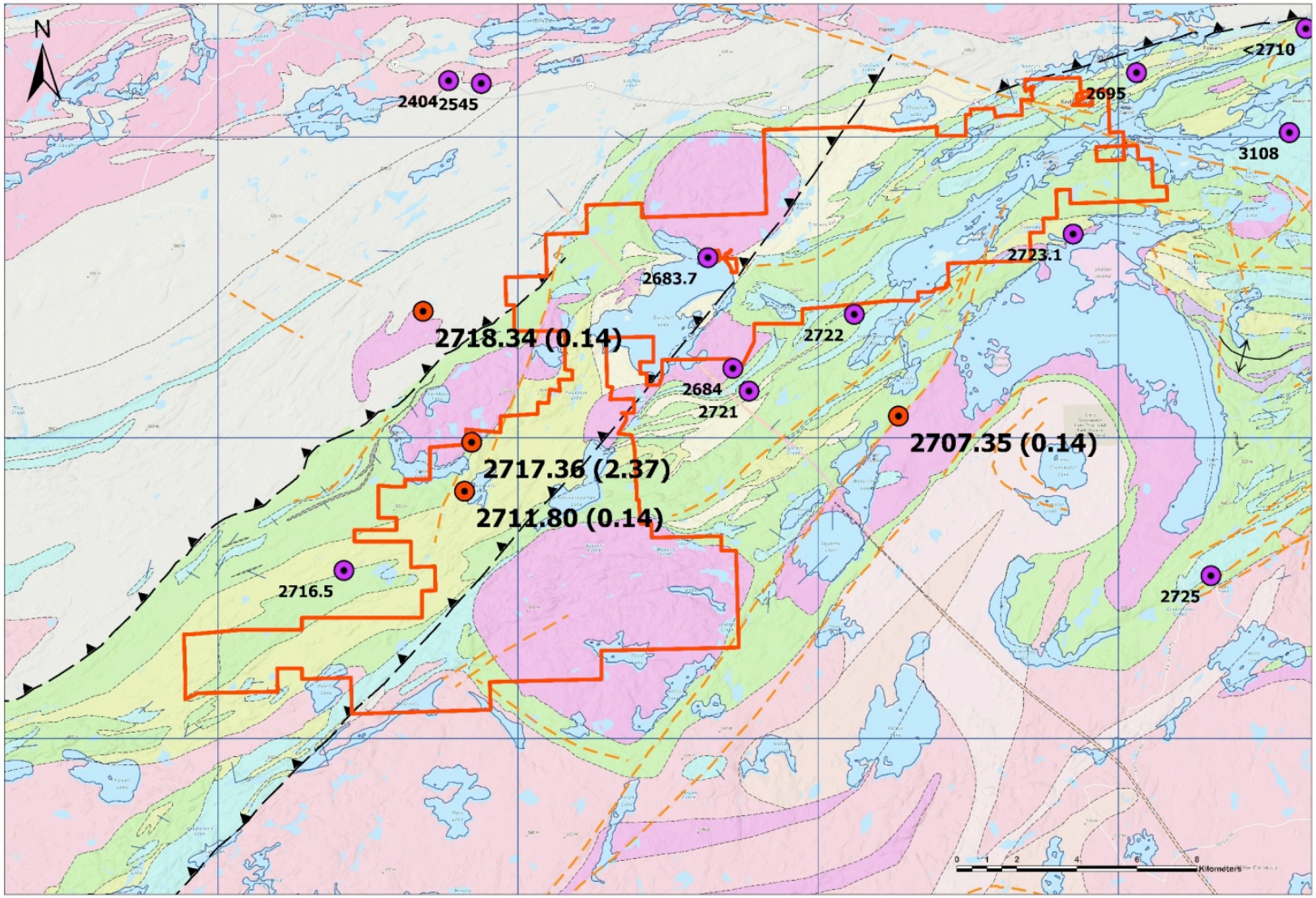

Samples Geochronology

Appendix F. Table of spots

Samples Moss Lake				
Sample	**Spot**	**Longitude**	**Latitude**	**Project**
Moss-001	**22-TS-MOSS-02**	**-90.711997**	**48.5426**	**Moss Lake**
Moss-002	**22-TS-MOSS-02**	**-90.711997**	**48.5426**	**Moss Lake**
Moss-003	**22-TS-MOSS-02**	**-90.711997**	**48.5426**	**Moss Lake**
Moss-004	**22-TS-MOSS-02**	**-90.711997**	**48.5426**	**Moss Lake**
Moss-005	**22-TS-MOSS-02**	**-90.711997**	**48.5426**	**Moss Lake**
Moss-006a	**22-TS-MOSS-06**	**-90.725182**	**48.530759**	**Moss Lake**
Moss-006b	**22-TS-MOSS-03**	**-90.719295**	**48.530793**	**Moss Lake**
Moss-007	**22-TS-MOSS-06**	**-90.725182**	**48.530759**	**Moss Lake**
Moss-008	**22-TS-MOSS-06**	**-90.725182**	**48.530759**	**Moss Lake**
Moss-009	**22-TS-MOSS-07**	**-90.720576**	**48.529833**	**Moss Lake**
Moss-010	**22-TS-MOSS-03**	**-90.719295**	**48.530793**	**Moss Lake**
Moss-011	**22-TS-MOSS-09**	**-90.71745**	**48.550987**	**Moss Lake**
Moss-012	**22-TS-MOSS-10**	**-90.727124**	**48.572956**	**Moss Lake**
Moss-013	**22-TS-MOSS-11**	**-90.623773**	**48.610451**	**Moss Lake**
Moss-014	**22-TS-MOSS-13**	**-90.589061**	**48.604642**	**Moss Lake**
Moss-015	**22-TS-MOSS-13**	**-90.589061**	**48.604642**	**Moss Lake**
Moss-016	**22-TS-MOSS-15**	**-90.581102**	**48.605992**	**Moss Lake**
Moss-017	**22-TS-MOSS-15**	**-90.581102**	**48.605992**	**Moss Lake**

Moss-018	**22-TS-MOSS-16**	**-90.657754**	**48.568761**	**Moss Lake**
Moss-019	**22-TS-MOSS-16**	**-90.657754**	**48.568761**	**Moss Lake**
Moss-020	**22-TS-MOSS-17**	**-90.596025**	**48.564979**	**Moss Lake**
Moss-021	**22-TS-MOSS-17**	**-90.596025**	**48.564979**	**Moss Lake**
Moss-022	**22-TS-MOSS-18**	**-90.578916**	**48.568194**	**Moss Lake**
Moss-023	**22-TS-MOSS-18**	**-90.578916**	**48.568194**	**Moss Lake**
Moss-024	**22-TS-MOSS-19**	**-90.553145**	**48.586501**	**Moss Lake**
Moss-025	**22-TS-MOSS-20**	**-90.579929**	**48.605447**	**Moss Lake**
Moss-026	**22-TS-MOSS-20**	**-90.579929**	**48.605447**	**Moss Lake**
Moss-027	**22-TS-MOSS-21**	**-90.545435**	**48.593943**	**Moss Lake**
Moss-028	**22-TS-MOSS-18**	**-90.578916**	**48.568194**	**Moss Lake**
Moss-029	**22-TS-MOSS-22**	**-90.603661**	**48.542893**	**Moss Lake**
Moss-030	**22-TS-MOSS-23**	**-90.589525**	**48.518354**	**Moss Lake**
Moss-031	**22-TS-MOSS-24**	**-90.589462**	**48.513688**	**Moss Lake**
Moss-032	**22-TS-MOSS-25**	**-90.598503**	**48.513311**	**Moss Lake**
Moss-033	**22-TS-MOSS-26**	**-90.617425**	**48.513691**	**Moss Lake**
Moss-034	**22-TS-MOSS-27**	**-90.696409**	**48.517181**	**Moss Lake**
Moss-035	**22-TS-MOSS-28**	**-90.706469**	**48.512453**	**Moss Lake**
Moss-036	**22-TS-MOSS-28**	**-90.706469**	**48.512453**	**Moss Lake**
Moss-037	**22-TS-MOSS-28**	**-90.706469**	**48.512453**	**Moss Lake**
Moss-038	**22-TS-MOSS-30**	**-90.658248**	**48.521473**	**Moss Lake**
Moss-039	**22-TS-MOSS-31**	**-90.74599**	**48.519113**	**Moss Lake**

Moss-040	**22-TS-MOSS-36**	**-90.767462**	**48.520154**	**Moss Lake**
Moss-041	**22-TS-MOSS-37**	**-90.775171**	**48.517926**	**Moss Lake**
Moss-043	**22-TS-MOSS-39**	**-90.795514**	**48.521018**	**Moss Lake**
Moss-044	**22-TS-MOSS-40**	**-90.795952**	**48.526401**	**Moss Lake**
Moss-045	**22-TS-MOSS-41**	**-90.794701**	**48.530874**	**Moss Lake**
Moss-046	**22-TS-MOSS-41**	**-90.794701**	**48.530874**	**Moss Lake**
Moss-047	**22-TS-MOSS-42**	**-90.80006**	**48.5322**	**Moss Lake**
Moss-048	**22-TS-MOSS-44**	**-90.805248**	**48.533147**	**Moss Lake**
Moss-049	**22-TS-MOSS-45**	**-90.807179**	**48.534734**	**Moss Lake**
Moss-050	**22-TS-MOSS-46**	**-90.806238**	**48.53446**	**Moss Lake**
Moss-051	**22-TS-MOSS-49**	**-90.737609**	**48.590559**	**Moss Lake**
Moss-052	**22-TS-MOSS-50**	**-90.732402**	**48.572795**	**Moss Lake**
Moss-053	**22-TS-MOSS-52**	**-90.712768**	**48.564768**	**Moss Lake**
Moss-054	**22-TS-MOSS-53**	**-90.717748**	**48.541332**	**Moss Lake**
Moss-055	**22-TS-MOSS-55**	**-90.721195**	**48.537929**	**Moss Lake**
Moss-056	**22-TS-MOSS-56**	**-90.721333**	**48.5364**	**Moss Lake**
Moss-057	**22-TS-MOSS-56**	**-90.721333**	**48.5364**	**Moss Lake**
Moss-058	**22-TS-MOSS-57**	**-90.721399**	**48.53511**	**Moss Lake**
Moss-059	**22-TS-MOSS-58**	**-90.739204**	**48.595032**	**Moss Lake**
Moss-060	**22-TS-MOSS-63**	**-90.55812**	**48.647679**	**Moss Lake**
Moss-061	**MMD-22-51**	**-90.71428**	**48.54234**	**Moss Lake**
Moss-062	**MMD-22-51**	**-90.71428**	**48.54234**	**Moss Lake**

Moss-063	**MMD-22-51**	**-90.71428**	**48.54234**	**Moss Lake**
Moss-064	**MMD-22-51**	**-90.71428**	**48.54234**	**Moss Lake**
Moss-065	**MMD-22-51**	**-90.71428**	**48.54234**	**Moss Lake**
Moss-066	**MMD-22-51**	**-90.71428**	**48.54234**	**Moss Lake**
Moss-067	**MMD-22-51**	**-90.71428**	**48.54234**	**Moss Lake**
Moss-068	**MMD-22-51**	**-90.71428**	**48.54234**	**Moss Lake**
Moss-069	**MMD-22-51**	**-90.71428**	**48.54234**	**Moss Lake**
Moss-070	**MMD-22-51**	**-90.71428**	**48.54234**	**Moss Lake**
Moss-071	**MMD-22-51**	**-90.71428**	**48.54234**	**Moss Lake**
Moss-072	**MMD-22-51**	**-90.71428**	**48.54234**	**Moss Lake**
Moss-073	**MMD-22-51**	**-90.71428**	**48.54234**	**Moss Lake**
Moss-074	**MMD-22-51**	**-90.71428**	**48.54234**	**Moss Lake**
Moss-075	**MMD-22-51**	**-90.71428**	**48.54234**	**Moss Lake**
Moss-076	**MMD-22-51**	**-90.71428**	**48.54234**	**Moss Lake**
Moss-077	**MMD-22-51**	**-90.71428**	**48.54234**	**Moss Lake**
Moss-078	**MMD-22-51**	**-90.71428**	**48.54234**	**Moss Lake**
Moss-079	**MMD-22-51**	**-90.71428**	**48.54234**	**Moss Lake**
Moss-080	**MMD-22-51**	**-90.71428**	**48.54234**	**Moss Lake**
Moss-081	**MMD-22-51**	**-90.71428**	**48.54234**	**Moss Lake**
Moss-082	**MMD-22-51**	**-90.71428**	**48.54234**	**Moss Lake**
Moss-083	**MMD-22-51**	**-90.71428**	**48.54234**	**Moss Lake**
Moss-084	**MMD-22-51**	**-90.71428**	**48.54234**	**Moss Lake**

Moss-085	**22-TS-MOSS-71**	**-90.640424**	**48.61207**	**Moss Lake**
Moss-086	**22-TS-MOSS-71**	**-90.640424**	**48.61207**	**Moss Lake**
Moss-087	**22-TS-MOSS-73**	**-90.641421**	**48.615506**	**Moss Lake**
Moss-088	**22-TS-MOSS-74**	**-90.641321**	**48.616278**	**Moss Lake**
Moss-089	**22-TS-MOSS-77**	**-90.637864**	**48.618774**	**Moss Lake**
Moss-090	**22-TS-MOSS-79**	**-90.636347**	**48.619278**	**Moss Lake**
Moss-091	**22-TS-MOSS-79**	**-90.636347**	**48.619278**	**Moss Lake**
Moss-093	**22-TS-MOSS-79**	**-90.636347**	**48.619278**	**Moss Lake**
Moss-094	**22-TS-MOSS-79**	**-90.636347**	**48.619278**	**Moss Lake**
Moss-095	**22-TS-MOSS-84**	**-90.629198**	**48.631356**	**Moss Lake**
Moss-096	**22-TS-MOSS-86**	**-90.619815**	**48.636623**	**Moss Lake**
Moss-097	**23-TS-Moss-3**	**-90.60714802**	**48.530548**	**Moss Lake**
Moss-098	**23-TS-Moss-4**	**-90.60434729**	**48.541746**	**Moss Lake**
Moss-099	**23-TS-Moss-6**	**-90.52907922**	**48.557535**	**Moss Lake**
Moss-100	**23-TS-Moss-7**	**-90.52454143**	**48.554839**	**Moss Lake**
Moss-101	**23-TS-Moss-10**	**-90.54660645**	**48.593011**	**Moss Lake**
Moss-102	**23-TS-Moss-12**	**-90.54449514**	**48.59543**	**Moss Lake**
Moss-103	**23-TS-Moss-12**	**-90.54449514**	**48.59543**	**Moss Lake**
Moss-104	**23-TS-Moss-17**	**-90.53397216**	**48.612405**	**Moss Lake**
Moss-105	**23-TS-Moss-17**	**-90.53397216**	**48.612405**	**Moss Lake**
Moss-106	**23-TS-Moss-18**	**-90.53245042**	**48.614424**	**Moss Lake**
Moss-107	**23-TS-Moss-18**	**-90.53245042**	**48.614424**	**Moss Lake**

Moss-108	**23-TS-Moss-23**	**-90.5389956**	**48.62032**	**Moss Lake**
Moss-109	**23-TS-Moss-25**	**-90.42392431**	**48.652693**	**Moss Lake**
Moss-110	**23-TS-Moss-27**	**-90.44357928**	**48.645875**	**Moss Lake**
Moss-111	**23AP-39**	**-90.60476178**	**48.588482**	**Moss Lake**
Moss-112	**23AP-39**	**-90.60476178**	**48.588482**	**Moss Lake**
Moss-113	**23AP-41**	**-90.59607643**	**48.592769**	**Moss Lake**
Moss-114	**23AP-46**	**-90.61374313**	**48.573032**	**Moss Lake**
Moss-115	**23AP-49**	**-90.62681752**	**48.572032**	**Moss Lake**
Moss-116	**23-TS-Moss-31**	**-90.45532417**	**48.645325**	**Moss Lake**
Moss-117	**23-TS-Moss-30**	**-90.4558607**	**48.645453**	**Moss Lake**
Moss-118	**23-TS-Moss-30**	**-90.4558607**	**48.645453**	**Moss Lake**
Moss-119	**23-TS-Moss-34**	**-90.49440438**	**48.631713**	**Moss Lake**
Moss-120	**23-TS-Moss-41**	**-90.50807187**	**48.652899**	**Moss Lake**
Moss-121	**23-TS-Moss-43**	**-90.52799469**	**48.648764**	**Moss Lake**
Moss-122	**23-TS-Moss-43**	**-90.52799469**	**48.648764**	**Moss Lake**
Moss-123	**23-TS-Moss-43**	**-90.52799469**	**48.648764**	**Moss Lake**
Moss-124	**23-TS-Moss-46**	**-90.67601642**	**48.630868**	**Moss Lake**
Moss-126	**23-TS-Moss-52**	**-90.79395424**	**48.509462**	**Moss Lake**
Moss-127	**23-TS-Moss-58**	**-90.81019853**	**48.494402**	**Moss Lake**
Moss-128	**23-TS-Moss-64**	**-90.83036726**	**48.495107**	**Moss Lake**
Moss-129	**23-TS-Moss-67**	**-90.85283013**	**48.483324**	**Moss Lake**
Moss-130	**23-TS-Moss-68**	**-90.81563118**	**48.48785**	**Moss Lake**

Moss-131	**23-TS-Moss-71**	**-90.81442377**	**48.474208**	**Moss Lake**
Moss-132	**23-TS-Moss-71**	**-90.81442377**	**48.474208**	**Moss Lake**
Moss-133	**23-TS-Moss-72**	**-90.75820182**	**48.499438**	**Moss Lake**
Moss-134	**23-TS-Moss-76**	**-90.82953808**	**48.462031**	**Moss Lake**
Moss-135	**23-TS-Moss-79**	**-90.82845172**	**48.44821**	**Moss Lake**
Moss-136	**23-TS-Moss-80**	**-90.82465354**	**48.441021**	**Moss Lake**
Moss-137	**23-TS-Moss-84**	**-90.63626113**	**48.461707**	**Moss Lake**
Moss-138	**23-TS-Moss-81**	**-90.78807685**	**48.436209**	**Moss Lake**
Moss-139	**23-TS-Moss-89**	**-90.57710912**	**48.483302**	**Moss Lake**
Moss-140	**23-TS-Moss-90**	**-90.52367725**	**48.516311**	**Moss Lake**
Moss-141	**23-TS-Moss-99**	**-90.66837891**	**48.562992**	**Moss Lake**
Moss-142	**23-TS-Moss-99**	**-90.66837891**	**48.562992**	**Moss Lake**